Effect of *Dyrk1a* dose reduction on the transcriptome of the developing mouse cerebral cortex: implications in gliogenesis

Elisa Balducci

DOCTORAL THESIS UPF/2011

Barcelona

Effect of *Dyrk1a* dose reduction on the transcriptome of the developing mouse cerebral cortex: implications in gliogenesis

Memòria presentada per **Elisa Balducci**
per optar al grau de Doctora per l'Universitat Pompeu Fabra

Aquesta tesi ha estat realitzada sota la direcció de la Dra. Maria Lourdes Arbonés de Rafael i la tutoria de la Dra. Cristina Pujades Corbi al Centre de Regulació Genòmica (CRG) i a l'Institut de Biologia Molecular de Barcelona (IBMB-CSIC).

Tesi adscrita al Departament de Ciències Experimentals de la Salut i de la Vida, Universitat Pompeu Fabra, Programa de Biomedicina.

Elisa Balducci **Maria L. Arbonés**

Cristina Pujades Corbi

UNIVERSITAT POMPEU FABRA

Elisa Balducci was supported by an FPU predoctoral fellowship of the Spanish Ministry of Education and Science. This work was supported by grants of the Spanish Ministry of Education and Science (SAF2007-60940 and SAF2010-17004).

«Sempre caro mi fu quest'ermo colle,
e questa siepe, che da tanta parte
dell'ultimo orizzonte il guardo esclude.
Ma sedendo e mirando, interminati
spazi di là da quella, e sovrumani
silenzi, e profondissima quïete
io nel pensier mi fingo, ove per poco
il cor non si spaura. E come il vento
odo stormir tra queste piante, io quello
infinito silenzio a questa voce
vo comparando: e mi sovvien l'eterno,
e le morte stagioni, e la presente
e viva, e il suon di lei. Così tra questa
immensità s'annega il pensier mio:
e il naufragar m'è dolce in questo mare»

“L’infinito”
Giacomo Leopardi

A chi spinge lo sguardo oltre la siepe

Index

Abbreviations

aa, aminoacid
AD, Alzheimer's disease
adj, adjusted
aIPC, astrogliogenic intermediate progenitor cell
BAC, bacterial artificial chromosome
BMP, bone morphogenetic protein
bp, base pairs
BP, biological process
BS, blocking solution
BSA, bovine serum albumine
Btn, biotinylated
CC, cell component
CC, Corpus Callosum
cDNA, complementary DNA
ChIP, chromatin immunoprecipitation
CNS, central nervous system
CNTF, cilliary neurotrophic factor
CP, cortical plate
CREB, cAMP response-element binding
cRNA, complementary RNA
ct, crossing temperature
Cx, cortex
DIV, day(s) *in vitro*
DMEM, Dulbecco's modified Eagle medium
DS, Down syndrome
DSCR, Down syndrome critical region
DYRK, dual specificity tyrosine (Y)-phosphorylation regulated kinase
E, embryonic day
EDTA, ethylendiamintetraacetic acid
EGF, epidhermal grow factor
EGFR, epidhermal grow factor receptor
ERK, extracellular signal regulated kinase
F, forward
FBS, fetal bovine serum
FC, fold change
FGF, fibroblast growth factor
GFAP, glial fibrillary acidic protein
GO, gene ontology
GSK-3, glycogen synthase kinase-3
HDAC, histone deacetylase
hNPC, human neural progenitor cells
HSA, homo sapiens autosome
ICC, immunocitochemistry
IF, immunofluorescence
Ig, immunoglobulin
IHC, immunohistochemistry
IP, immunoprecipitation

IPC, intermediate progenitor cell
IS, incubating solution
IZ, intermediate zone
JAK, janus kinase
kb, kilobase
kDa, kilodalton
LDA, low density array
LGE, lateral ganglion eminence
LIF, leukaemia inhibitory factor
M, mutant
MAPK, mitogen-activated protein kinase
MBD, methyl binding protein
MBP, myelin basic protein
MeCP2, methyl CpG binding protein 2
MF, molecular function
MGE, medial ganglion eminence
miRNA, micro RNA
MMU, Mus musculus chromosome
mnb, minibrain
MR, mental retardation
MZ, medial zone
N, number
n, number
NE, neuroepithelium
NFAT, nuclear factor of activated T-cells
NfI, nuclear factor I
NGF, nerve growth factor
Ngn, neurogenin
NICD, Notch intracellular domain
nIPC, neurogenic intermediate progenitor cell
NLS, nuclear localization signal
NRG, neuregulin
NRSE, neuron-restrictive silencer element
NRSF, neuron-restrictive silencer factor
NSC, neural stem cell
oIPC, oligodendrogenic intermediate progenitor cell
ON, optic nerve
OPC, oligodendroglial progenitor cell
p, passage
P, postnatal
PBS, phosphate-buffered saline
PCA, principal component analysis
PcG, polycomb group
PCR, polymerase chain reaction
PFA, paraformaldehyde
PKA, protein kinase A or cAMP-dependent
PKC, protein kinase C
PLP, proteolipid protein
PNS, peripheral nervous system
POA, preoptic area
qPCR, quantitative polymerase chain reaction
R, reverse

RE1, repressor element 1
REST, repressor element 1
silencing transcription factor
RG, radial glia
RT, retrotranscription
RT, room temperature
RTK, receptor tyrosine kinase
SDS, sodium dodecylsulfate
sem, standard error of the mean
SEP, septum
SGZ, subgranular zone
SHH, sonic hedgehog
siRNA, small interference RNA
SIRT, sirtuin
SPRED, sprouty protein with EVH-1
domain
Spry, sprouty
SS, somatosensory
STAT, signal transducer and
activator of transcription
SVZ, subventricular zone
TEM, transmisson electron
microscopy
TF, transcription factor
Tg, transgenic
TSS, transcription start site
VZ, ventricular zone
W, wild type
YAC, yeast artificial chromosome

Abstract

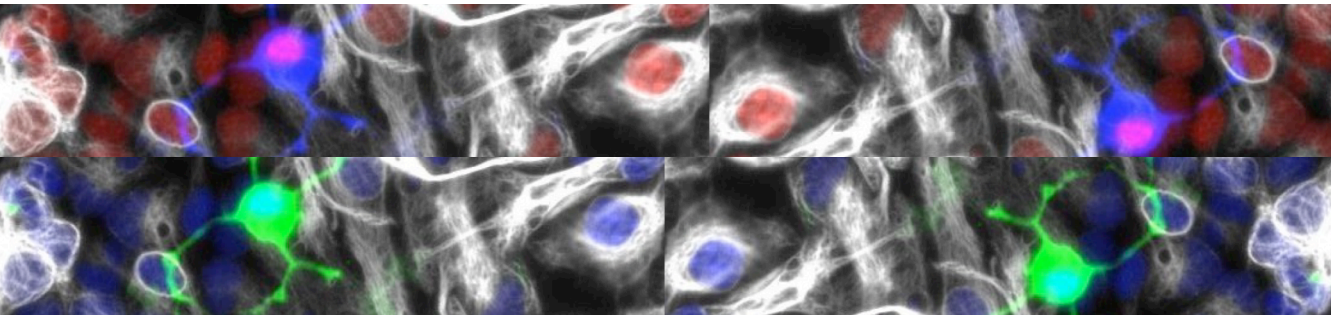

Cerebral cortex is essential to exert the highest functions in mammals. Understanding the developmental processes that underlie the generation and functionality of cortical cell populations represents a mayor issue in neurobiology. *DYRK1A* is a dosage-sensitive gene involved in neurodevelopment with putative roles in corticogenesis.

In the present study, we show that the transcriptome of the cerebral cortex of newborn mice lacking one functional copy of *Dyrk1a* (*Dyrk1a*$^{+/-}$) is substantially altered and is mostly the consequence of a delayed developmental gene expression program. We also show that neural progenitors of *Dyrk1a*$^{+/-}$ mice have a reduced capability to self-renew and to differentiate into oligodendroglial cells *in vitro*. Moreover, we demonstrate that the epigenetic state of *S100b* and *Gfap* glial genes in the cortex of *Dyrk1a*$^{+/-}$ embryos is altered at specific promoter positions before the onset of gliogenesis, suggesting that *Dyrk1a*$^{+/-}$ neural progenitors may have an increased astrogliogenic and a decreased oligodendrogenic potential *in vivo.* In accordance, the number of S100b^{+} oligodendrocytes is reduced in the postnatal cortex of *Dyrk1a*$^{+/-}$ mutants whereas the number of Gfap^{+} astrocytes is increased in the adult. Finally, we show that the myelin thickness of *Corpus Callosum* axons and of axons of the optic and sciatic nerves is significantly decreased in adult *Dyrk1a*$^{+/-}$ mice, indicating a possible role of Dyrk1a in myelination.

Altogether our results indicate that *Dyrk1a* dose reduction alters the differentiation potential of the embryonic cortical progenitors and suggest a new role of Dyrk1a in glial development and function.

L'esorça cerebral és essencial per dur a terme les funcions més complexes en els mamífers. Entendre el procés de desenvolupament involucrat en la generació i el funcionament de les poblacions cel·lulars de l'escorça representa un dels principals camps d'investigació de la neurobiologia. *DYRK1A* és un gen sensible a dosis involucrat en el neurodesenvolupament i molt possiblement en la corticogènesis.

En aquest estudi demostrem que la reducció de la dosi gènica de *Dyrk1a* en ratolí (*Dyrk1a*$^{+/-}$) provoca una alteració substancial del transcriptoma de l'escorça cerebral neonatal que es principalment la conseqüencia de un retard en el l'expresió seqüencial dels gens durant el desenvolupament. També hem demostrat que els progenitors neuronals dels ratolins *Dyrk1a*$^{+/-}$ tenen una menor capacitat d'autorenovació i diferenciació en cèl·lules oligodendroglials *in vitro*. El estat epigenetic dels gens glials *S100b* i *Gfap* es troba alterat en l'escorça d'embrions a posicions especifiques del promotor abans de l'inici de la gliogènesis, suggerint que els progenitors neuronals de ratolins *Dyrk1a*$^{+/-}$ podrien tenir un potencial astrogliogènic incrementat i un potencial oligodendrogènic disminuït *in vivo*. En concordança, l'escorça de ratolins *Dyrk1a*$^{+/-}$ neonatals presenta un major número de progenitors oligodendroglials S100b^{+}, mentres que el número d'astròcits Gfap^{+} es troba incrementat en ratolins *Dyrk1a*$^{+/-}$ adults. Finalment, hem demostrat que la vaina de mielina dels axons del cos callos i del nervi òptic i ciàtic es troba significativament reduïda en els ratolins *Dyrk1a*$^{+/-}$ adults, fet que indica una posible implicació de *Dyrk1a* en mielinització.

En conjunt els nostres resultats indiquen que la baixada de dosi de *Dyrk1a* altera el potencial de diferenciació dels progenitors embrionaris de l'escorça i suggereix un nou paper de Dyrk1a en el desenvolupament i en la funcionalitat glial.

Introduction

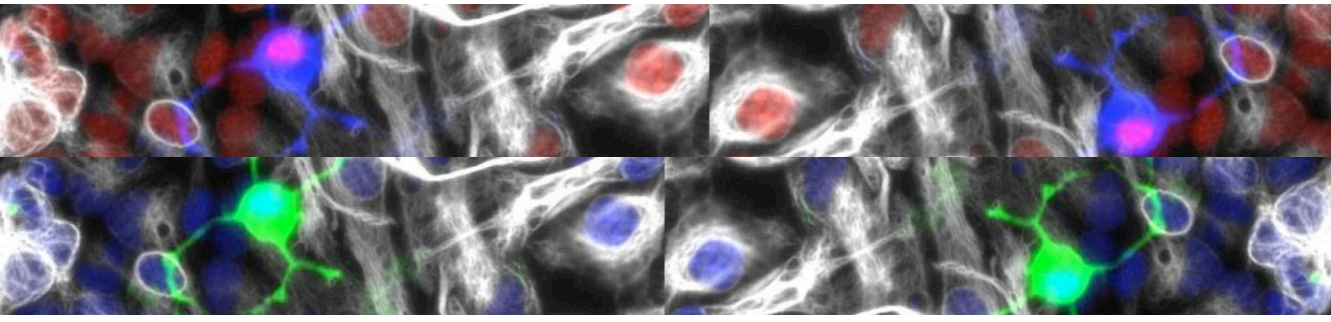

1. Development of the mammalian cerebral cortex

The neocortex represents the major acquisition of mammalian brains, being responsible of the most complex functions. Indeed alterations in cortical physiology in humans cause severe neurological defects with high social impact. For these reasons it has been of major interest among scientists to understand how this brain structure evolved and which are the mechanisms that regulate the development of this structure and its functions.

The development of the mammalian neocortex is quite well known compared to other brain structures and represents a good model to study central nervous system (CNS) development for two main reasons. First, the genesis of different cortical cell populations is temporally segregated: in rodents, neurons are generated from embryonic day 12 (E12) to E18, astrocytes appear at around E18, with their numbers peaking in the neonatal period, and differentiated oligodendrocytes are first seen postnatally (Bayer and Altman, 1991). This sequential occurrence of neurogenesis and gliogenesis is a fundamental feature of vertebrates, given that in lower organisms such as flies, all cell types appear coincidentally. Even more, neurons of the different cortical layers are sequentially generated in an ‘‘inside-out’’ fashion, with the latest-born neurons being the most superficial. Second, this timed genesis also occurs in culture allowing the study of developmental mechanisms *in vitro* (Qian et al., 2000; Morrow et al., 2001).

1.1. Phases of cortical development

1.1.1. The proliferative phase

During the early phases of mammalian brain development, the anterior portion of the neural tube closes to form the vesicles that will give rise to the telencephalon. Fluid filled lateral ventricles characterize the anterior part of the mammalian telencephalon and are rounded by a layer of proliferative neuroepithelial cells: the ventricular zone (VZ) (Boulder Committee, 1970).

At early stages, most neuroepithelial progenitor cells undergo symmetrical divisions and give rise to new proliferative neuroepithelial cells. This mechanism allows the expansion of the pool of founder cells, the neural stem cells (NSC), which will ultimately produce the neocortex (Cai et al., 2002; Noctor et al., 2004). As NSC we refer to the progenitor cells of the VZ that self-renew and are capable to initiate the lineage commitment and give rise to the differentiated cells of the mature brain: atrocytes, oligodendrocytes (together called glia) and neurons. A more detailed description of the cell types here mentioned is given later on in this chapter.

As the pool of progenitors expands and the thickness of the developing brain increases, NSCs elongate and convert in radial glia (RG) that first appear around E12.5 in the mouse telencephalon (reviewed in Guillemot 2005). Radial glia cells have two long processes radially oriented that confer them apical-basal polarity: apically RG contact the ventricle and basally the meninges, basal lamina, and blood vessels (Rakic, 1971a,b; Bentivoglio and Mazzarello, 1999; Gotz et al., 2002) (Fig I1).

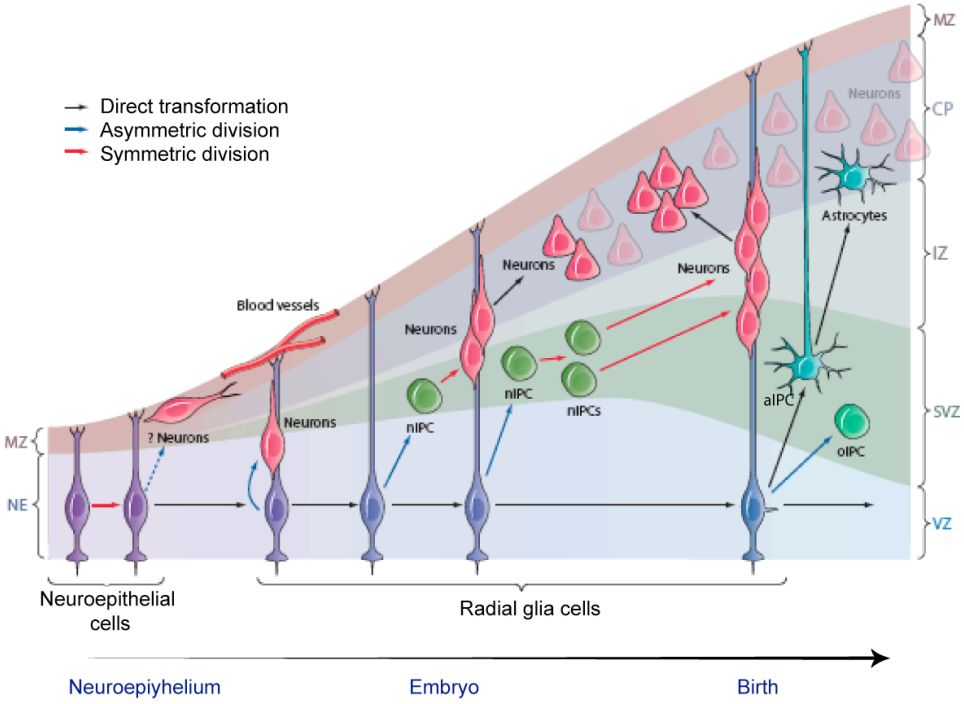

Fig I1: The mammalian cortical development. The Figure represents how neural progenitors generate the cortical cell types from mid-gestation until birth. Solid arrows are supported by experimental evidence; dashed arrows are hypothetical. The colors of the arrows indicate the type of transformation: symmetric (red), asymmetric (blue), or direct (black). IPC, intermediate progenitor cell (nIPC=neurogenic IPC, oIPC=oligodendrogenic IPC, aIPC= astrogliogenic IPC); NE, neuroepithelium; MZ, marginal zone; CP, cortical plate; IZ, intermediate zone; SVZ, subventricular zone; VZ, ventricular zone (Adapted from Kriegstein and Alvarez-Buylla, 2009).

As the name implies, one of the main characteristics of RG is the glial nature of such cell. In fact RG cells, a part of expressing the intermediate filament nestin as neuroepithelial cells do (Frederiksen et al., 1988), express markers such as the glial fibrillary acidic protein (GFAP) and the glutamate aspartate transporter GLAST, which are typical of mature astroglial cells (reviewed in Gotz et al., 2002; Kriegstein

and Alvarez-Buylla, 2009). Due to the astroglial nature of RG, it has long been believed that RG cells are committed progenitors of the astroglial lineage. However compelling evidences have demonstrated that these cells are indeed stem cells that produce most of the cortical neurons (Malatesta et al., 2000; Hartfuss et al., 2001; Miyata et al., 2001; Noctor et al., 2001; Tamamaki et al., 2001) and glial cells (Schmechel and Rakic, 1979; Levitt et al., 1981; Voigt et al., 1989; Choi and Kim, 1985, Hirano and Goldman, 1988).

1.1.2. The neurogenic phase

The onset of neurogenesis is marked by a switch in the mode of division of neural progenitors. During the proliferative phase RG cells divide symmetrically giving rise to two identical RG cells, while in the neurogenic phase RG cells divide asymmetrically generating two daughter cells with different fates (reviewed in Caviness et al., 1995; Rakic, 1995). The result of a RG neurogenic division is another RG cell, which maintains the contact with the ventricle, and a neuron or an intermediate progenitor committed to neurogenesis (nIPC). nIPCs are proliferative cells which do not contact the ventricles, and constitute an additional proliferative region of the developing cortex: the subventricular zone (SVZ) (Magini 1888, Retzius 1894). nIPCs divide symmetrically giving rise to neuronal daughter cells, either directly or after one cycle of nIPC amplification (Haubensak et al. 2004; Miyata et al. 2004; Noctor et al., 2004, 2007; Wu et al. 2005). The intense nIPC proliferation has been suggested to contribute to the enormous cortical expansion observed in primate cortex (Kriegstein et al. 2006).

Newly generated neurons migrate radially out of the proliferative zone using RG processes as migratory guides (Rakic, 1978). As cortical

neurogenesis proceeds, neurons settle in progressively more superficial layers. This “inside-out” process ultimately forms in postnatal stages the six-layered neocortex in which the laminar position of each neuron is determined by its birth date: the deeper cortical layers (VI and V) originate from the VZ after asymmetric division of RG (Chen et al., 2005; Leingartner et al., 2003; Frantz et al., 1994), while the upper ones (IV, III and II) come from the symmetric division of nIPC of the SVZ (Tarabykin et al., 2001; Nieto et al., 2004). The correct lamination of the neocortex is essential for the establishment of neuronal circuitries and ultimately for the proper exertion of brain functions. Thus, the spatio-temporal control of cortical neurogenesis is a complex process that needs to be tightly regulated.

Although neurogenesis in the brain occurs mainly during embryonic and early postnatal development it continues until the adulthood in the SVZ where NSCs, which share characteristics with RG cells, produce neurons that migrate to the olfactory bulb through the rostral migratory stream (reviewed in Kriegstein and Alvarez-Buylla, 2009).

1.1.3. The gliogenic phase

The transition from neurogenesis to gliogenesis, occuring in the late embryonic period, leads to massive postnatal generation of glial cells: astrocytes and oligodendrocytes. Analogously to the expansion of the neuronal population in mammals, the glial population has passed from making up to 10–20% of the cells in the *Drosophila* nervous system to represent at least 50% of the cells in the mammalian brain (reviewed in Rowitch and Kriegstein, 2010). These findings indicate that glial functions are crucial for the increase in brain complexity that has emerged during evolution.

Astrocytes provide structural support, regulate water balance and ion distribution, and maintain the blood–brain barrier. They also participate in cell–cell signaling by regulating calcium flux, producing neuropeptides and modulating synaptic transmission (reviewed in Rowitch and Kriegstein, 2010). Astrogenesis occurs at the terminal phases of radial glial cell function: at the end of embryonic development, most RG detach from the ventricle and convert into astrocytes. This transformation implies morphological changes that lead bipolar RG to become unipolar after ventricle detachment, and finally multipolar (Morest 1970, Choi and Lapham 1978, Schmechel and Rakic 1979, Misson et al. 1991). The appearance of increasing number of astrocytes in the newborn cortex is indeed linked to the progressive disappearance of RG. However the precise timing of astroglial production remains unclear due to the lack of specific markers to distinguish astrocytes precursors from multipotent RG cells. Astrocytes seem to divide symmetrically and locally before terminal differentiation, observation that supports the existence of astrocytic intermediate progenitors (aIPCs) (Mares and Bruckner 1978, Hajós et al. 1981, Ichikawa et al. 1983). Committed astrocytes generated by aIPCs undergo tangential migration, which seems to resemble the inside-out fashion described before for neurons (Ichikawa et al. 1983). Moreover astrocytic migration seems to be restricted into regional domains that depend on the initial position of the RG cell (Rakic 1988). Migration is accompanied by terminal differentiation that gives rise to two different types of astrocytes: fibrous and protoplasmic astrocytes. Fibrous astrocytes populate the white matter and typically have a ‘star-like’ appearance with dense glial filaments, which can be stained with the intermediate filament marker Gfap. Protoplasmic astrocytes are found in the grey matter, have more

irregular processes and typically have few glial filaments. The branched structure that astrocytes acquire during terminal differentiation allows the contact with blood vessels and neuronal synapses required for their functions (reviewed in Rowitch and Kriegstein 2010).

In contrast to oligodendrocytes, which can be generated in the mammalian brain from progenitor cells throughout life, mature astrocytes are mainly produced during postnatal development and are maintained in a quiescent status. However they are able to proliferate in response to injury (Anthony et al., 2004).

Oligodendrocytes are the myelin forming cells that wrap neuronal axons and allow saltatory conduction through the formation of the nodes of Ranvier. In the mammalian brain, oligodendrocyte precursor cells (OPCs) form synapses with neurons, suggesting a high degree of complexity in the interactions between neurons and oligodendroglia (Lin et al., 2004).

Oligodendrocytes originate from RG through intermediate progenitors committed to the oligodendroglial lineage (oIPCs). oIPCs divide symmetrically to originate OPCs, which then migrate during embryogenesis, in a way that by the time of birth they are evenly distributed throughout the brain (Richardson et al., 2006; Kessaris et al., 2006). OPCs generate mature oligodendrocytes mainly during the first two postnatal weeks. However, proliferating OPCs continue to exist in the adult brain, scattered both in the white matter, where they represent 8–9% of total cells, and in the gray matter, where they made up the 2–3% of total cells (Rivers et al. 2008; Dawson et al., 2003). The adult OPC population is maintained relatively stable throughout life because cell proliferation is balance by cell death and differentiation in response to stimuli. More recently it has been shown that neural stem cells of the

adult SVZ, but not of the SGZ, can give rise to oligodendrocytes (Levison and Goldman 1993, Nait-Oumesmar et al. 1999, Menn et al. 2006, Aguirre et al. 2007).

The dynamism of oligodendroglial populations is reflected in the variety of markers expressed by oligodendroglial cells. The expression pattern of these markers, together with cell morphology, characterizes different developmental steps of oligodendrocytes. OPCs are positive for the Platelet-Derived Growth-Factor Receptor-α (PDGFR-α) and the chondroitin sulfate proteoglycan 2 (NG2) markers, while mature myelinating oligodendrocytes, a part from the transcription factors Olig2 and Sox10 that are stably expressed throughout the oligodendroglial lineage, express the myelin basic protein (MBP), the proteolipid protein 1 (PLP1) and the adenomatous polyposis coli protein (APC, or Cc1) (Rivers et al., 2008).

1.2. Fate acquisition of neural progenitors during development

As explained above, it is generally agreed that the different neuronal and glial cells are the progeny of a common progenitor pool. However, understanding at which point fate restriction and lineage commitment occur during cortical development still represents a major issue. Scientists have largely debated about whether separate progenitor cells originate early and coexist during development **("segregating model")** or whether the same common progenitor is able to transform its potential, giving rise to all cell types **("switching model").** During the years, experimental evidences, mainly coming from clonal analysis and fate mapping experiments, alternatively supported both models (refer to Delaunay et al., 2008; Costa et al., 2009; Kriegstein and Alvarez-Buylla, 2009 for a detailed review of existing data on the field). The hypothesis

nowadays accepted is that different kinds of progenitors, with diverse grades of multipotency, coexist in the developing brain. Importantly, direct visualization of retrovirally labeled RG has proven that the same RG cell that produces neurons can then transform into an astroglial cell, thus confirming that the neurogenic to gliogenic transition occurs *in vivo* at least in some individual progenitor cells (Noctor et al., 2008).

1.2.1. Major mechanisms regulating cell fate

For many years scientists believed that glial and neuronal phenotypes were mainly determined by the microenvironment where cells mature. However compelling evidences indicate that the interplay between external cues and intrinsic mechanisms are fundamental in cell fate acquisition. Here, I will describe the major mechanisms underlying cell fate acquisition during neurogenesis and gliogenesis: positional information, Notch mediated cell- cell signaling, cell cycle length, symmetric or asymmetric cell division and epigenetic regulation of gene expression.

1.2.1.1. Positional information

Although the embryonic VZ appears to be a uniform and continuous proliferative zone surrounding the ventricle, in fact it is composed of subdomains existing from the very beginning of the neurogenic process, which differ for the cell type they will generate. The *in vivo* potential of neuroepithelial cells and RG is regionally restricted, from the earliest stages, through the action of morphogens such as sonic hedgehog (SHH), fibroblast growth factors (FGFs), WNTs and bone morphogenetic proteins (BMPs), all of which form gradients that provide positional information to the cells. Neuroepithelial cells and RG interpret the

combination of these gradients unfolding unique programs of transcription factors (TFs) expression, which in turn cross talk and determine specific cell fates (Jessell, 2000; Shirasaki and Pfaff, 2002).

The two main telencephalic subdivisions are the dorsal telencephalon (or pallium), including the dorsal cortex (Cx) and the septum (SEP), and the ventral telencephalon (or subpallium), which includes the lateral and medial ganglion eminences (LGE and MGE) as well as the preoptic area (POA) (Puelles et al., 2000, Fig I2 right half). Each region is defined by a specific set of TF (Fig I2 left side) and generates very different types of cells.

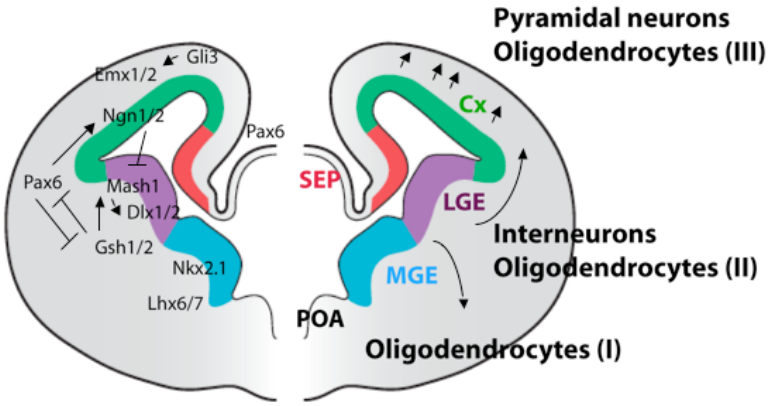

Fig I2: Domains of the embryonic SVZ. Colors indicate the different domains of the SVZ (POA, preoptic area; MGE, medial ganglion eminence, LGE, lateral ganglion eminence; Cx, cortex; SEP, septum). In the left half of the figure are reported the main TFs expressed in each domain. The right half of the figure depicts the cell types generated in each domain, and the direction of their migration (indicated by arrows). Roman numbers I, II and III represent the three waves of oligodendrocyte generation (Adapted from Kriegstein and Alvarez-Buylla, 2009).

As referred to the neuronal lineage, the subpallium generates GABAergic inhibitory interneurons that migrate tangentially to the cortex

(Anderson et al., 1997; Wichterle et al., 2001; for reviews see Marin and Rubenstein, 2001 and 2003). The germinal zone of the pallium instead gives rise to excitatory glutamatergic neurons, which sequentially reach the different layers of the cortex by radial migration in an inside-out fashion as described above (Marin-Padilla, 1971; Rakic, 1974; Wichterle et al. 2001; Marin and Rubenstein, 2003) (Fig I2). The specification of cortical layers also correlates with the acquisition of specific patterns of TFs, such as Fezf2, Ctip2 and Sox5 for the deeper layers and Svet, Satb2, Cux1 and Cux2 for the upper layers (reviewed in Leone et al., 2008).

Analogue regional specification has been observed for the oligodendroglial lineage, whose production occurs in three waves. The first OPCs are produced at E12.5 from Nkx2.1-expressing progenitors of the MGE and the POA. Then they migrate and reach the cerebral cortex around E16.5. The second wave of OPCs production occurs in the Gsh2-positive territories of the LGE around E15.5 and oligodendroglial cells reach the cortex around E18.5. Finally, around birth OPCs are produced by the Emx1-expressing domain of the palium and spread radially in the cortex. Curiously the oligodendrocytes produced in the first wave disappear postnatally and are replaced by the OPCs of the following waves (Kessaris et al., 2006) (Fig I2).

The telencephalic patterning of astrocytes formation has not been described so far. However the existence of a regional specification during astrocytes production has been demonstrated for the spinal cord (Hochstim et al., 2008). The Pax6- and NKx6.1-positive regions of the embryonic spinal cord give rise to three positionally distinct subtypes of white matter astrocytes, which can be distinguished by the combinatorial expression of Reelin and Slit1 (Hochstim et al., 2008).

Positional information is processed in different ways to determine cell fate. Modulation of Notch-mediated cell- cell signaling and cell cycle length are among the main consequences of morphogen gradients.

1.2.1.2. Notch-mediated cell- cell signaling

Diffusible molecules regulate an additional layer of regulation of cell fate acquisition, which consists in signaling between neighboring cells. Notch signaling is the best characterized pathway mediating the communication between adjacent cells. It involves transmembrane receptors (Notch 1-4 in mammals), as well as transmembrane ligands, (Delta-like, Dll, 1, 3, 4 and Jagged, Jag, 1, 2 proteins) (reviewed in Kopan and Ilagan, 2009). Notch has been involved in the maintenance of the neural progenitor pool during neurogenesis (Kawaguchi et al., 2008) by lateral inhibition: cells undergoing neuronal differentiation up-regulate Notch ligands that in turn activate Notch receptors in the neighboring cells and induce the repression of the neurogenic programs, *via* the effectors *Hes1* and *Hes5* (Kageyama et al., 2007).

Recently an exciting finding revealed that the oscillatory expression of *Hes* genes in neural progenitors controls the timing of neurogenic waves, thus maintaining the equilibrium between neural progenitors and committed neurons (Shimojo et al., 2008). Hes oscillations are generated by an auto-regulatory feedback loop (Hirata et al., 2002), and are likely to be influenced by external signals, like the morphogen SHH (Ingram et al., 2008; Solecki et al., 2001; Wall et al., 2009). In addition, Notch signaling at late neurodevelopmental stages has been involved in astrogliogenesis and in the time-dependent regulation of oligodendrogenesis (Fig I3 and reviewed in Pierfelice et al., 2011). The multiple functions of Notch and

the interplay with other pathways make it a key cell fate regulator in the developing cortex.

The multiple functions of Notch and the interplay with other pathways make it a key cell fate regulator in the developing cortex. Morphogens and Notch signaling roles during brain development are summarized in Fig I3 and reviewed in Pierfelice et al., 2011; Freese et al., 2010; Iwata and Hevner 2009; Borello and Pierani, 2010.

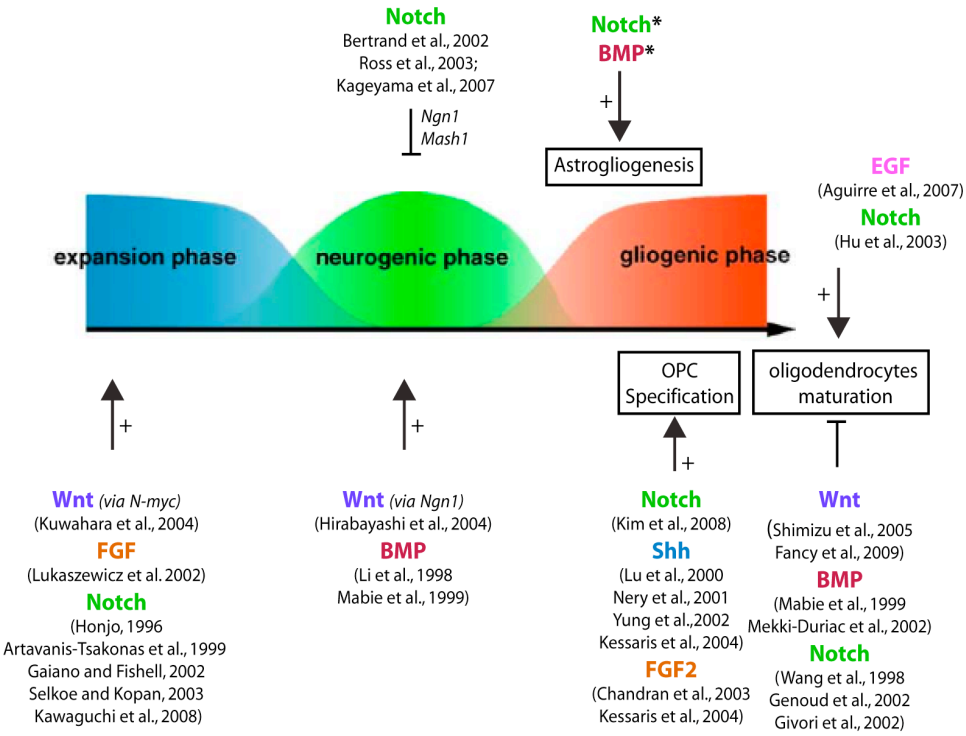

Fig I3: Morphogens and Notch signaling in brain development. The Figure reports the effects of the indicated pathways on each neurodevelopmental stage. Arrows with the "+" symbol indicate a positive effect, while flat headed arrows an inhibitory effect. The main original works showing the reported effects are indicated. Pathways indicated by an asterisk are detailed in the text (Adapted from Hirabayashi and Gotoh, 2005).

1.2.1.3. Cell cycle length

One of the cell functions regulated by morphogen gradients is the cell cycle. The morphogens FGFs, SHH and WNTs decrease the cell cycle duration of neural progenitors by shortening the G1 phase (Lukaszewicz et al., 2002; Yoon et al., 2004; Pierani and Wassef, 2009). Notably, regulation of the cell cycle length has a crucial role in controlling progenitor proliferation and laminar fate: G1 phase becomes longer over time as the neurogenic phase proceeds and cells exit the cell cycle and differentiate (Warren et al., 1999; Zembrzycki et al., 2007).

The time of cell cycle exit has been proven to be fundamental for the proper formation of cortical layers, and in turn, for the correct establishment of neural circuitries (Racik et al., 2009; Takahashi et al., 1999). Likewise, cell cycle regulators control terminal differentiation of oligodendrocytes. In fact, increase in the intracellular concentration of the cdk inhibitor p27/KIP1 is required to induce cell cycle arrest before oligodendrocyte differentiation. Indeed, ectopic expression of p27 results in premature differentiation of oligodendrocytes in the mouse telencephalon (Durand et al., 1997; Ohnuma et al., 1999).

1.2.1.4. Symmetric and asymmetric cell division

Contrarily to morphogens, that are essential from the very beginning of embryo development (Altmann and Brivanlou, 2001), other intrinsic determinants of cell fate are dispensable until the onset of neurogenesis. Those determinants are required for the proper order of symmetric and asymmetric mode of division of progenitors. For this reason they are needed during neurogenesis but not before, when the proliferating neuroepithelium only divides symmetrically (Conlon et a., 1995; Zhong et al., 2000).

In the developing CNS of *Drosophila* the orientation of the cleavage plane during progenitors division can predict the fate of daughter cells (Doe and Skeath, 1996). However, in vertebrates, the cleavage angle of dividing radial glia alone is unlikely to be a cell fate determinant (Morin et al., 2007; Konno et al., 2008). It is likely that cell fate is instead predicted by the inheritance of intrinsic determinants of cell symmetry by daughter cells, like the mammal homologs of the *Drosophila* **Numb** and **Numblike** proteins. Numb and Numblike are membrane-associated proteins essential to maintain the apical adherent junctions of RG and thus the ventricular anchoring (Rasin et al., 2007). Asymmetrical segregation of Numb and Numblike proteins in the daughter cells determines progenitor fate in the cell that inherits Numb or Numblike and neuronal fate in the cell that do not (Zhong et al., 1996, 2000; Petersen et al., 2002). In flies Numb has also been proposed as an antagonist of Notch signaling (Sestan et al., 1999; Shen et al., 2002). However, the role of Numb and Numblike inheritance in neural progenitors, although largely characterized in *Drosophila*, is still uncertain in mammals (Li et al., 2003; Petersen et al., 2002, 2004, 2006; Rasin et al., 2007).

In mammals, another intrinsic determinant of cell fate that exploits its function by segregating asymmetrically during mitosis is the **epidermal growth factor receptor (EGFR)**. The fate of mammalian neural precursor siblings can be determined by the amount of EGFR inherited, and in turn, by the ability to respond to EGF. Asymmetric distribution of EGFR has been observed in one-fifth of EGFR expressing embryonic progenitors in both VZ and SVZ. Cells that inherit high levels of EGFR acquire a RG phenotype and will produce astrocytes later in development, while cells with low levels of EGFR undergo oligodendroglial commitment (Sun et al., 2005a).

1.2.1.5. Epigenetic regulation of gene expression

The epigenetic control of gene expression has emerged in the last years as a key intrinsic determinant of cell fate acquisition during brain development. DNA methylation, histone modifications, and non-coding RNAs mediated processes represent the main epigenetic mechanisms that determine the responsiveness of single cells to external stimuli. The first two mechanisms and their involvement in neurodevelopmental processes will be reviewed here.

DNA methylation is a mechanism of gene silencing that occurs through the addition of a methyl group on cytosines belonging to CpG dinucleotides. The reaction is catalyzed by DNA methyltransferases (DNMTs) that in mammals are three: the "*de novo"* DNMT3a and DNMT3b, which are responsible for the establishment of methylation around the time of embryo implantation, and DNMT1, which ensures that methylation is faithfully copied to daughter cells, *via* what is known as "maintenance" methylation. Compelling evidences emerged in the last years also involved DNMT3b in maintenance of DNA methylation (Walton et al., 2011).

Methylated cytosines in promoter regions inhibit gene expression either by sterically impeding the binding of TFs to DNA (Watt and Molley 1988; Takizawa et al., 2001), or by recruiting transcriptional repressors containing a methyl-CpG binding domain (MBD), like MeCP2 and MBD1 (Lewis et al., 1992; Cross et al., 1997; Nan et al., 1997).

Among the epigenetic mechanisms of gene expression regulation DNA methylation provokes the most stable repression. For this reason DNA methylation seems to be important for constitutively silencing multipotency associated genes (Mohn et al., 2008; Meissner et al., 2008)

as well as for repressing genes associated to alternative fates (Meissner et al., 2008; Setoguchi et al., 2006; Kohyama et al., 2008), as the differentiation of embryonic neural progenitors proceeds and cell fate restriction occurs. Moreover, DNA methylation can mediate short-term repression of lineage specific genes. This is for instance the case of the *Gfap* and *S100b* glial genes that represent one of the best-studied examples of epigenetic regulation during neurodevelopment. Both genes are methylated at specific promoter positions in neurogenic progenitors where they are in fact repressed. Demethylation of *Gfap* and *S100b* promoters occurs in mouse telencephalon around E14.5 and defines the beginning of their expression and the onset of gliogenesis (Takizawa et al., 2001; Namihira et al., 2004).

Covalent modifications on histone tails represent a very dynamic mechanism of gene regulation that is pivotal for the plasticity of progenitor cells and for fate commitment into the different neural lineages. Regulation of gene expression by histone modifications occurs through modulation of chromatin condensation, which in turn renders DNA more or less accessible to the transcriptional machinery. Lysines methylation and acetylation in histones H3 and H4 are pivotal for gene expression regulation. While methylation of lysine residues could be either a repressive or an activating mark depending on the position where it occurs, acetylation is generally an activating mark, which is generally more dynamic than methylation. Among the several histone-modifying enzymes that have been described (reviewed in Hirabayashi and Gotoh, 2010), the most relevant in nervous system development are summarized in Table I1.

The RE1 silencing transcription factor (**REST),** also named neuron restrictive silencing factor **(NRSF**) was initially described as a repressor

of neuronal genes in non-neuronal tissues. Compelling evidences showed later on that REST plays fundamental roles in neuronal commitment within the CNS, where it cooperates with several components of the epigenetic machinery to finely tune neuronal gene expression (see Ballas and Mandel, 2005; Ballas et al., 2005). As very recently described, REST functions are also required for oligodendroglial differentiation (Dewald et al., 2011) and astroglial functions (Prada et al., 2011).

Table I1: Major roles of histone modifications in CNS development

Factor/complex	Catalytic activity	Role in CNS development	Ref
TrxG (Tritorax group of proteins)	H3K4 methylation (+)	The coexistence of both marks maintains the lineage-specific developmental genes in a poised status in uncommitted NPCs. This status, called "bivalent", is resolved during the differentiation process into either gene activat	Mohn et al., 2008
PcG (Policomb group of proteins)	H3K27 methylation (-)	Promotes the neurogenic/astrogliogenic switch of NPCs by repressing *Ngn*	Hirabayashi et al., 2009
		Promotes the neurogenic/oligodendrogenic switch of NPCs	Sher et al., 2008
HDACs (Histone deacetylases)	Histon tails deacetylation (-)	Promote oligodendrocytes maturation	Shen et al., 2005 Shen et al., 2008 Ye et al., 2009 Liu et al., 2009

1.2.2. Cell signaling pathways regulating cell fate

The interplay of intrinsic and extrinsic mechanisms results in complex intracellular pathways that orchestrate the different phases of neurodevelopment. Here are reported two examples of neurodevelopmental processes where cell-signaling pathways are finely regulated: the neurogenic to gliogenic switch and the oligodendrogenesis.

1.2.2.1. The neurogenic to gliogenic switch

The change of NPCs differentiation potential from neurogenic to gliogenic, also called the neurogenic to gliogenic switch, occurs at the end of the neurogenic phase is one of the best characterized mechanisms in brain development. During neurogenesis (around E13.5), the canonical Wnt pathway promotes the expression of *Neurogenin 1* (*Ngn1*) in NPCs (Hirabayashi et al., 2004, Zhou et al., 2006). This transcription factor promotes neuronal differentiation in two synergic ways: by its transcriptional activity that positively regulates neuronal genes (Nieto et al., 2001; Powell and Jarman, 2008), and by sequestering the transcriptional co-activator p300 required for the janus kinase (JAK)-signal transducer and activator of transcription (STAT) astroglial signaling pathway (Sun et al., 2001, Bonni et al., 1998). In addition, DNA methylation of glial promoters by Dnmt1 impedes the STAT-dependent activation of glial genes during the neurogenic phase (Fan et al., 2005; Takizawa et al., 2001; Namihira et al., 2004) (Fig I4).

The switch to gliogenesis, occurring at later embryonic stages, requires the PcG-mediated accumulation of H3K27me3 inhibitory mark at the *Ngn1* loci (Hirabayashi et al., 2009). This intrinsic timer defines the end of NPC response to the neurogenic Wnt signaling and the down-

regulation of *Ngn1*. In addition newly generated neurons induce the astroglial fate of the remaining NPCs through two complementary mechanisms. First they release Cardiotropin1 (CT-1), that together with the leukemia inhibitory factor (LIF) and the ciliary neurotrophic factor (CTNF) cytokines activate the astrogliogenic JAK-STAT pathway (Barnabe-Heider et al., 2005). Second, they express Jag1 and Dll ligands that activate Notch signaling in the neighboring NPCs and induce the expression of Nuclear Factor-Ia (*Nfia)* (Namihira et al., 2009). Nfia TF, a key activator of astrogliogenesis (Deneen et al., 2006), induces Dnmt1 dissociation from glial genes promoters, thus allowing their demethylation and STAT binding (Namihira et al., 2009) (Fig I4).

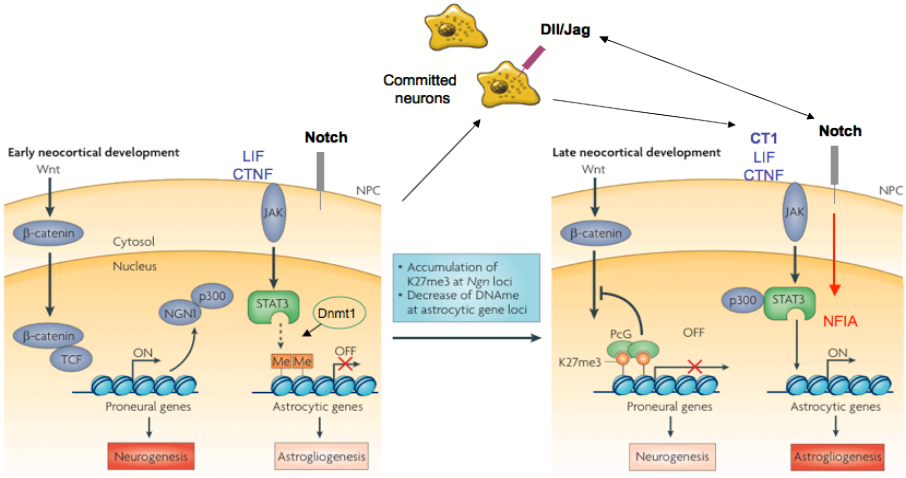

Fig I4: The neurogenic to gliogenic switch. Major signaling pathways and epigenetic changes involved in the neurogenic to gliogenic switch of embryonic neural progenitors (Adapted from Hirabayashi and Gotoh, 2010).

Nfia is also involved in the transcriptional repression of the Notch effector Hes1 (Piper et al., 2010), which is responsible for the

maintenance of the self-renewing neural progenitor identity at early neurodevelopmental stages, during the proliferative phase of RG (Schmid et al., 2003; Anthony et al., 2005). Thus, Nfla uncouples the proliferative and astrogliogenic output of Notch signaling and represents a master determinant of fate decision in brain development. It is worthy to underline that contrarily to the case of Notch, it remains elusive to date how Wnt pathway can induce proliferation or neurogenesis in a stage dependent manner. Probably a different chromatin state of *Ngn1* promoter accounts for the different Wnt signaling output at different time points.

Notch signaling seems to be necessary to promote astrogliogenesis through the following mechanisms: i) by driving the expression of *Gfap* and other astroglial genes *via* direct binding of its effector CBF1 to their promoters (Anthony et al., 2005; Ge et al., 2002); ii) by repressing pro-neural genes *via* Hes1 (Bertrand et al., 2002; Kato et al., 1997); and iii) by recruiting JAK2 kinase and thus promoting STAT3 phosphorilation and activation (Kamakura et al., 2004). On the other hand the JAK/STAT pathway positively regulates Notch signaling (reviewed in Pierfelice et al., 2011).

BMP2 signaling, although induces neuronal differentiation at early embryonic stages (Li et al., 1998), promotes the neurogenic to gliogenic switch at late developmental stages. It acts synergistically with the JAK/STAT pathway by recruiting p300 to the astrocytic promoters, *via* Smad1 activation (Gross et al., 1996; Nakashima et al., 1999; Nakashima and Taga, 2002). Its gliogenic action is also exerted by the induction of histone acetylation in the *S100b* promoter, an epigenetic modification associated to increased expression of *S100b* (Namihira et al., 2004).

1.2.2.2. Regulation of oligodendrogenesis

Oligodendrogenesis includes well-defined and independent processes occurring from the commitment of NPCs into the oligodendroglial lineage until their acquisition of a mature myelinating phenotype (Fig I5). Even though spinal cord is the best-studied model as referred to oligodendrogenesis, I will focus here on cortical oligodendrogenesis.

OPC specification from NPCs is induced independently by SHH and FGF2 and is inhibited by BMP2 (Mabie et al., 1999, Lu et al., 2000; Yung et al., 2002; Kessaris et al., 2004; Nery et al., 2001). The commitment of NPCs into the oligodendroglial lineage coincides with the up-regulation of *Olig1* and *Olig2* genes that are expressed all along the lineage progression and act at different steps of oligodendrogenesis (reviewed in Ligon et al., 2006). Histone deacetylases (HDACs) are required at this step to down-regulate genes that promote alternative fates, like Sox2 and NeuroD (Hsieh et al. 2004, Lyssiot et l., 2007; Shen and Casaccia-Bonefill, 2008).

Committed OPCs proliferate mainly in response to PDGF (Barres and Raff 1994) and migrate from ventral and dorsal regions of the telencephalon into all parts of the developing forebrain, including the cerebral cortex (reviewed in Richardson et al., 2006), where environmental signals trigger their differentiation.

Cell cycle exit is necessary to start the differentiation process of OPCs (Casaccia-Bonefill et al., 1997; Durand et al., 1998), although not sufficient to trigger it (Tikoo et al., 1998; Tang et al., 1999). Oligodendrocyte differentiation requires in fact a coordinated regulation of gene expression that occurs in a two-step fashion and for which HDACs activity is critical (Marin-Husstege et al., 2002) (Fig I5).

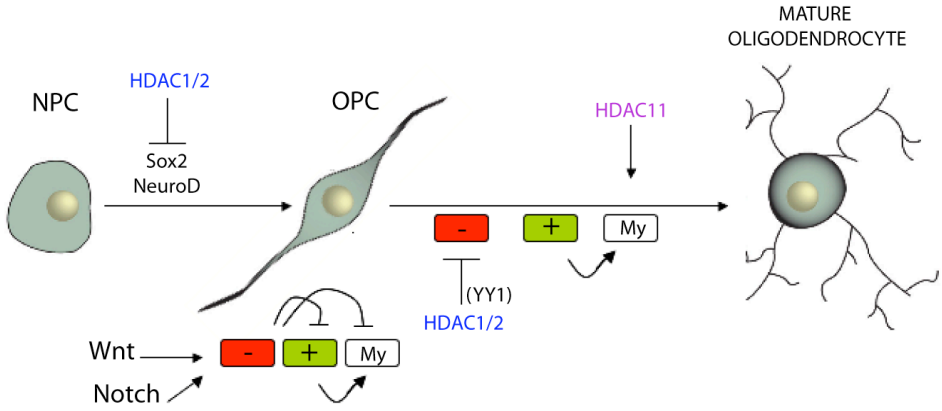

Fig I5: HDACs in oligodendroglial differentiation. During the commitment of NPC to the oligodendroglial lineage, HDAC1 and 2 repress genes promoting other fates. In committed OPCs, myelin-gene repressors (red boxes) inhibit the expression of myelin genes (My, white boxes) either directly or indirectly by inhibiting activators of myelin-genes (green boxes). Wnt and Notch are involved in the maintenance of the OPC pool by activating myelin-gene repressors. YY1 TF promotes oligodendrocyte differentiation by recruiting HDAC1 and 2 to the promoters of myelin-gene repressors. HDAC1 and 2 repress myelin-gene repressors allowing myelin-gene activators to trigger the expression of myelin genes. At this step, HDAC11 is directly involved in the transcriptional activation of myelin genes. More details are given in the text. NPC=neural precursors cells; OPC=oligodendrocyte precursor cells.

OPC differentiation has been regarded as a default program that is constitutively repressed and that requires a “de-repression” mechanism to be activated at specific time points. Repression of OPC differentiation is mediated by TFs that inhibit the expression of myelin genes (as *Mbp* and *Plp*) through HDAC1/2 recruitment to their promoters (He et al., 2007; Shen and Casaccia-Bonnefill, 2008). Meantime, these TFs down-regulate or sequester activators of the transcription of myelin genes, thus conferring an additional level of repression (Liu et al., 2006).

In this context, the role of HDACs in promoting oligodendroglial differentiation consists in repressing the repressors, and in turn allowing

the activators to transcribe myelin genes. It is worthy to underline that among the repressors are Tcf4, a downstream effector of Wnt signaling, and Hes5, a downstream effector of Notch signaling. Although the role of Notch pathway is still controversial, both Notch and Wnt pathways have been described as repressors of the myelination transcriptional program (Wang et al., 1998; Genoud et al., 2002; Shimizu et al., 2005; Fancy et al., 2009). Indeed Notch, in addition to its role in repressing oligodendroglial differentiation *via* Jagged ligand (Wang et al., 1998; Genoud et al., 2002, Givogri et al., 2002), is required for OPCs specification (Park and Appel, 2003, Grandbarbe et al., 2003; Kim et al., 2008). Moreover, Notch signaling promotes axon myelination *via* connexins (Hu et al., 2003).

HDACs modulate oligodendrocyte differentiation through different mechanisms. For example, HDAC1 is recruited by the TF YY1 to the promoters of *Tcf4* and *Id2/4* genes, thus inducing their repression and inhibiting Wnt signaling (He et al., 2007). Wnt signaling is additionally repressed by the competition of HDAC1/2 with the Wnt downstream molecule ß-catenin, for the binding to Tcf4 (Ye et al., 2009). Finally a member of another HDAC family, HDAC11, has been directly involved in the H3K9/K14 deacetylation of myelin genes, which induce their expression (Liu et al., 2009a). The major players in OPCs differentiation, involving both activators and repressors of myelin genes transcription, are listed in Table I2.

The process of oligodendrocyte differentiation here reported, and summarized in Fig I5, is only the first step of the myelination process, which *in vivo* requires axon contact and is mediated by an intense cross-talk between glial and neuronal cells (reviewed in Taveggia et al., 2010).

Table I2: Activators and repressors of myelin genes transcription

TF	Effect	Ref
Hes5	-	Liu et al., 2006
Id2, Id4	-	Samanta and Kessler, 2004
Tcf4	-	Ye et al., 2009; Fancy et al., 2009; He et al., 2007
Olig1, Olig2	+	Lu et al., 2002; Li et al.,2007
Mash1	+	Parras et al., 2007
Sox4/5/6/11	+	Stolt et al., 2006; Chew and Gallo, 2009
Sox8/9/10/17	+	Li et al.,2007; Stolt et al., 2006; Chew and Gallo, 2009; Stolt and Wegner, 2010
Nkx6.1, Nkx6.2	+	Vallstedt et al., 2005
Nkx2.2	+	Qi et al., 2001; Wei et al., 2005
YY1	+	He et al., 2007

(+) activator; (-) repressor.

1.3. Neurodevelopmental diseases

What explained until now should lead to the idea that the timing of differentiation, which is controlled by a complex interplay of intrinsic and extrinsic mechanisms, is key to determine the final number of mature cells and finally the size of the brain regions. It is quite obvious therefore, that an alteration in the correct sequence of events may cause defects in size and functionality of the brain.

One of the major neurodevelopmental human diseases is primary microcephaly that consists in the reduction in brain size at birth, without evident alteration in the overall structure. Among the consequences of

primary microcephaly, mental retardation (MR) is one of the most relevant. However not all forms of microcephaly lead to mental retardation, as in the cases of MOPDII (primordial dwarfism type Majewski II, Willems et al., 2010) and Walcott- Rallison syndrome (reviewed in Shield, 2000).

Notably, *in vivo* studies suggest that many forms of primary microcephaly, result from defects in the control of cell fate: precocious formation of neurons during early developmental stages produces deficiencies in progenitor cells at later stages of neurogenesis, resulting in an overall small cerebral cortex. The most relevant genes related to primary microcephaly and MR, mainly atosomal with recessive inheritance, are reported in Table I3.

While loss of function of microcephaly-related genes triggers a reduction of cortical expansion, native proteins were found involved in cell cycle/checkpoint control, like BRIT1 and CDK5RAP2 (Alderton et al., 2006; Erez et al., 2008; Lin et al., 2005; Xu et al., 2004, Bakircioglu et al.; 2001 and Alkuraya et al., 2011), and/or mitotic spindle dynamics, like CEP152, ASPM, CENPJ (Bond et al., 2005; Pfaff et al., 2007; Zhong et al., 2005, 2006) (Table I3). These data strongly suggest that mechanisms regulating proper cell division are pivotal in the determination of RG cell fate. In the case of *NDE1* mutation, microcephaly is accompanied by lissencephaly, characterized by abnormal organization of the cortical layers (microlissencephaly). This phenotype, confirmed in a *Nde1* knock-out mouse model (Feng and Walsh, 2004), suggests that defects in the mode of division of neural progenitors can affect not only the number of neurons generated, but also their migration, which alters cortical lamination.

Table I3: Genes associated to microcephaly and MR

Gene symbol	Gene description	Other names	Locus	Desease	Ref
BRIT1	BRCT–repeat inhibitor of telomerase I	MCPH1, microcephalyn	8p23	autosomal recessive primary microcephaly (MCPH)	Jackson et al., 2002
WDR62	WD repeat domain 62	MCPH2	19q13.12		Bilguvar et al., 2010; Yu et al., 2010; Bhat et al., 2011; Kousar et al., 2011
CDK5RAP2	cyclin-dependent kinase 5 regulatory associated protein 2	MCPH3	9q33.2		Bond et al., 2005
CEP152	centrosomal protein 152 kDa	MCPH4	15q21.1		Guernsey et al., 2010
ASPM	abnormal spindle-like microcephaly-associated protein	MCPH5	1q31.3		Bond et al., 2002
CENPJ	centromeric protein J	MCPH6	13q12.12		Bond et al., 2005
STIL/SIL	SCL/TAL1 interrupting locus	MCPH7	1p33		Kumar et al., 2009
NDE1	LIS1-interacting protein	NUDE	16p13.11	micro-lissencephaly	Bakircioglu et al., 2011; Alkuraya et al., 2011; Feng and Walsh, 2004(§)
PCNT	pericentrin		21q22.3	Seckel Syndrome	Griffith et al., 2008

Interestingly, alterations in the timing of generation of glial cells causes also MR. This is the case for instance of Noonan Syndrome where a mutation in the *SHP-2* gene, encoding a protein tyrosine phosphatase, leads to a normal neurogenesis but a precocious astrogliogenesis (Gauthier et al., 2007). Notably, the same SHP-2/Ras/MEK/ERK pathway is also affected in Costello syndrome and in the cardio-facial-cutaneous syndrome, suggesting that an altered gliogenesis could underlie the mental retardation that characterizes these syndromes (Bentires-Alj et al., 2006). Similarly, a heterozygous mutation

in *CBP* (*CREB-binding protein*), a transcriptional coactivator of many different transcription factors, and a fundamental player of the neurogenic to gliogenic switch is sufficient to cause MR in Rubinstein-Taybi syndrome (Josselyn et al., 2005).

In conclusion compelling evidences suggest that the right proportion between glial and neuronal populations is fundamental for the correct functionality of the brain. Identification of human mutants and analysis of animal models displaying an imbalance in cortical populations will help identifying the genes and pathways that are relevant in corticogenesis.

2. DYRK1A

2.1. *DYRK1A* dosage imbalance correlates with neurodevelopmental defects

2.1.1. *DYRK1A* loss of function and microcephaly

Human ***DYRK1A*,** located in chromosome 21 (HSA21), (Guimera et al., 1996), has been associated in genotype-phenotype correlation studies performed in rare cases of individuals with partial HSA21 monosomies to developmental delay, microcephaly and mental retardation (Chettouh et al., 1995; Matsumoto et al., 1997). Two recent works strongly indicate the contribution of *DYRK1A* haploinsufficency to the above-described phenotypes of partial HSA21 monosomies. The first one, describes two unrelated patients with a truncating mutation in *DYRK1A* in heterozygosity showing several clinical features including microcephaly and intrauterine growth retardation (Moller et al., 2008). The second one describes one patient with a *de novo* micro-deletion, spanning 52kb within *DYRK1A* gene, showing primary microcephaly and mental retardation (Van Bon et al., 2011). The three patients share, in addition to microcephaly and mental retardation, several other clinical features like motor disfunctions, hypoactivity and facial dismorfisms (Van Bon et al., 2011).

The role of DYRK1A in neurodevelopment has also been suggested by the analysis of mutant animal models. The *Drosophila* ortholog of *DYRK1A* was identified in a genetic screening and was named ***minibrain*** **(*mnb*)** after the phenotype of mutant flies (Tejedor et al., 1995). Disruptions of *mnb* cause a marked reduction in brain size, which is due to a defective proliferation in the neuroepithelial primordial of the larval brain, and specific abnormalities in learning, memory, and visual and

olfactory behaviors (Tejedor et al., 1995). These phenotypes pointed to a key role of *mnb*/*DYRK1A* in neural proliferation and neurogenesis.

A ***Dyrk1a*** knock out mouse model (*Dyrk1a*$^{-/-}$) was generated by gene targeting in our laboratory (Fotaki et al., 2002). The embryonic lethality of *Dyrk1a*$^{-/-}$ mouse, occurring around E10.5, strongly indicates the fundamental role of Dyrk1a in embryo development. Interestingly *Dyrk1a*$^{+/-}$ mice, in which only one *Dyrk1a* functional copy is disrupted, show a general growth delay and body size reduction of around 30% at birth that is maintained until adulthood. Brain weight reduction of *Dyrk1a*$^{+/-}$ mice is proportional to the general decrease in body weight. However, *Dyrk1a* loss of function affects brain size in a region-specific manner: the cerebellum and the mesencephalum show a disproportionate size reduction compared with more anterior structures such as the cerebral cortex and olfactory bulbs. The cerebral cortex of *Dyrk1a*$^{+/-}$ mice, although showing a normal cytoarchitecture, present a structure-specific increase in cellular density, not associated to gross alterations in cell body sizes. As an example of the region specificity of the *Dyrk1a*$^{+/-}$ brain phenotype, a 30% increase in cell density has been observed in the somatosensory and pyriform cortex, whereas no differences in cell density were observed in another laminated structure of the brain, the superior *colliculum* (Fotaki et al., 2002). A detailed analysis of neocortical pyramidal cells revealed important alterations in *Dyrk1a*$^{+/-}$ mice. Pyramidal cells in these mice are considerably smaller, less branched and with less number of spines per branch that in wild type animals (Benavides-Piccione et al., 2005). This result indicates that Dyrk1a influences the complexity of pyramidal cells and thus their capability to integrate information, which is relevant in the context of human and mouse *DYRK1A* haploinsufficiency because of its

involvement in mental retardation. The phenotypic analysis of *Dyrk1a*$^{+/-}$ mice revealed indeed a reduced execution of a spatial learning task and impaired performance in a hippocampal-dependent memory task (Arquè et al., 2008). Another relevant phenotype of mutant mice is the impaired motor phenotype (Fotaki et al., 2004), which could be associated to a reduction in dopaminergic neurons of the *sustancia nigra* (Martinez de Lagran et al, 2007).

2.1.2. *DYRK1A* gain of function and Down syndrome

DYRK1A is triplicated in Down syndrome (DS), which affects around 1 in 800 newborns and represents the most frequent genetic cause of mental retardation, thus having high social impact (Pritchard et al., 2008; Patterson 2009; Wiseman et al., 2009). DS is caused by a complete or partial trisomy of HSA21 (Lejeune at el., 1958, 1959) and despite the high variability of DS phenotype; mental retardation is the invariable feature of the syndrome and the most invalidating aspect. Other hallmarks are hypotonia, altered motor behavior and early onset of Alzeimer's disease as well as heart, bone and immune defects, (reviewed in Roubertoux and Carlier, 2010).

The analysis of partial HSA21 trisomies allowed defining a DS critical region (DSCR) (Rahmani et al., 1990; Ronan et al., 2007; Sato et al., 2008, Fig I6), which is the minimal region whose triplication gives rise to the main DS phenotypes, including MR (Delabar et al., 1993). It means that genes of the DSCR, among which *DYRK1A* is present, that are dose-sensitive might impact on cellular processes that are crucial for brain development and function (Rachidi and Lopes, 2007). The fact that *DYRK1A* haploinsufficiency leads to developmental brain alterations indicates that an extra copy of the gene might also have an impact in

brain development.

The generation of mouse models has been very useful to study the consequence of gene dosage imbalance in DS. Among the DS mouse models the best characterized is the **Ts65Dn**, in which a region of mouse chromosome 16 (MMU16) synthenic to HSA21 is triplicated. This region spans around 120 genes and includes the DSCR (Davisson et al., 1990; 1993). The major brain phenotypes of Ts65Dn mice consist in *i)* impaired spatial and learning memory, *ii)* altered motor behavior, and *iii)* defects in short and long term memory. These behaviour and cognitive impairments resemble those in DS, are also shared by other DS models (depicted in Fig I6 and reviewed in Robertoux and Carlier 2010), and are often associated to altered brain morphology and area-specific cellular density (Baxter et al., 2000, Olson et al., 2004, Belichenko et al., 2004; Insausti et al., 1998; Kurt et al., 2004; Lorenzi and Reeves, 2006, Aldridge et al., 2007, Cox et al., 1984; Coyle et al., 1986; Gearhart et al., 1986, O'Doherty et al., 2005). Altered neuronal branching and synaptogenesis have also been described in diverse brain regions for several DS models, indicating that failure in cerebral connectivity contributes to the neurological DS phenotypes (Benavides-Piccione et al., 2004; Belichenko et al., 2004; Insausti et al., 1998; Kurt et al., 2000, 2004; Lorenzi and Reeves, 2006).

The defects in cellularity in DS mouse models are likely due to defective early neurodevelopmental processes. Indeed, increased cell cycle length and proliferation of NPC as well as impaired neurogenesis have been reported in embryonic and early postnatal Ts65Dn mice (Chakrabarti et al., 2007; Contestabile et al., 2007; 2009). More interestingly, DS fetuses manifest similar defects (Contestabile et al., 2007). Noteworthy, progenitor neurosphere cells obtained from the

embryonic cortex of another DS mouse model, the TsC1je mouse (see the content of triplicated genes related to the Ts65Dn model in Fig I6), show decreased proliferation associated to alterations in the cell cycle (Moldrich et al., 2009).

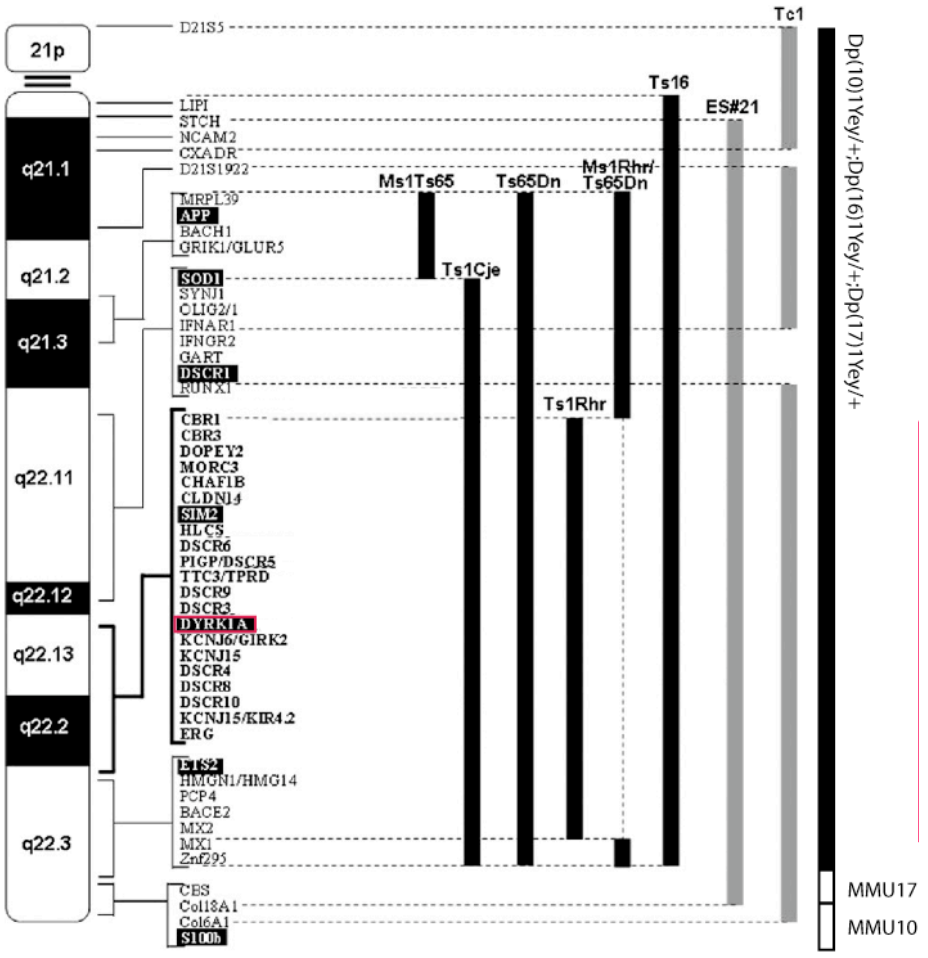

Fig I6: Genetics of segmental trisomic mouse models for Down syndrome. Trisomic mice carrying all or part of HSA21 are indicated in grey vertical lines: Tc1 and ES#21. The regions of MMU16, MMU10 and MMU17 synthenic to HSA21 and present in three copies in DS mouse models are indicated in black (for MMU16) and white (for MMU 10 and 17) vertical lines: Ts16,

Ms1Rhr/Ts65Dn, Ts1Rhr, Ts65Dn, Ts1Cje, Ms1Ts65 and Dp(10)1Yey/+;Dp(16)1Yey/+;Dp(17)1Yey/+. Gene candidates to contribute to DS for which transgenic mice exist are indicated in black boxes. Genes located in the DSCR region of HSA21 are in bold (Adapted from Rachidi and Lopes 2007).

An additional layer of knowledge in the DS field has been provided by the analysis of transgenic (Tg) mouse models, which allow a better understanding of single gene contributions to the DS phenotypes. Different lines of transgenic mice overepressing *DYRK1A*, either alone (Ahn et al., 2006; Altafaj et al., 2001) or in the context of a bigger trisomy (Reeves et al., 1995; Smith et al., 1995), have been generated. Importantly the main phenotype that all these Tg mice share with trisomic DS mouse models is an impaired learning and memory, thus supporting the contribution of *Dyrk1a* overexpression in the neurological defects of DS.

During the course of this work, another *Dyrk1a* overexpression mouse model (hereafter **BAC-*Dyrk1a***) has been generated by the group of Jean Maurice Delabar (Université Paris Diderot) using a bacterial artificial chromosome (BAC) clone that contains the complete mouse *Dyrk1a* genomic sequence including the endogenous promoter (unpublished data). This model presents the following advantages with respect to the transgenic models above mentioned: first, it allows the study of *Dyrk1a* overexpression alone, second only one copy of the gene is integrated into the genome and third transgene expression is driven by its own promoter, thus one would expect it to be spatial and temporally regulated as the endogenous gene. This model has been used in this study and a summary of the methodological aspects of its generation is included in the Methods section.

The observation that both *DYRK1A* gain- and loss- of function correlate with neurological defects, first observed at early developmental stages, indicates that *DYRK1A* is a dose-sensitive gene, which is involved in neurodevelopmental processes.

2.2. DYRK1A protein kinase

DYRK1A is a protein kinase that belongs to an evolutionary conserved family of proteins known as DYRK (Dual-specificity tyrosine (Y) phosphorylation-Regulated Kinases). DYRK kinases show a high grade of homology during evolution (Kentrup et al., 1996) and the phylogenetic analysis of the family allowed the distinction of two groups whose members are more closely related: Dyrk1 and Dyrk2 (see Fig I7). Five DYRK members have been identified in vertebrates: DYRK1A and DYRK1B (belonging to the Dyrk1 group) and DYRK2, DYRK3 and DYRK4 (belonging all to the Dyrk2 group, although DYRK2 and DYRK3 are more closely related that DYRK4) (Fig I7). All DYRK members have been associated to cell homeostasis and differentiation processes. The main functional processes involving DYRK kinases (a part of DYRK1A that is more extensively described along this thesis) are reported, together with their tissue and subcellular localizations, in Fig I7 and have been recently reviewed in Aranda et al. (2011).

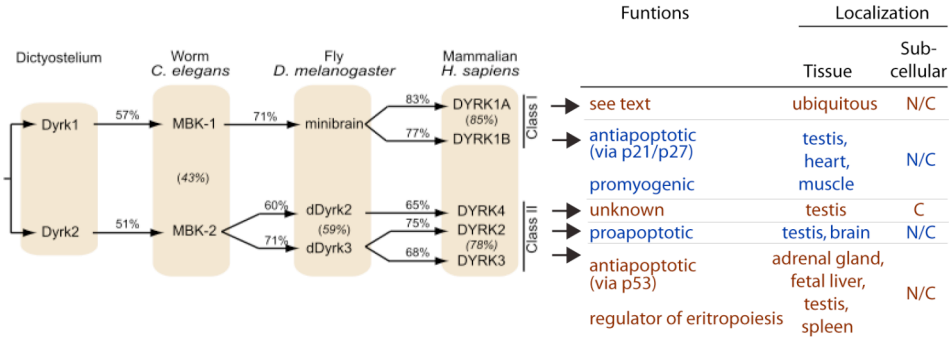

Fig I7: DYRK family of proteins. DYRK subfamily members in the indicated species are here reported. DYRK members can be classified into 2 main groups: class I and class II. The percentage of conservation at the protein level between orthologues is indicated above the arrows and between 2 paralogues is indicated in parentheses within the boxes. For each DYRK protein, the major described functions, the tissue localization and the sub-cellular localization are indicated on the right part of the figure. N=nuclear, C=cytosolic (Adapted from Aranda et al., 2011).

DYRK1A encodes a protein of 763aa with an estimated molecular weight of around 90kDa. Different protein motifs have been defined and a particular function has been associated to some of them (Fig I8). From the amino- to the carboxy- terminal part, the protein contains: a functional nuclear localization signal (NLS1) (Alvarez et al., 2003); a DH-box motif of unknown function; a classical kinase domain (aa 159-479) (reviewed in Becker and Joost, 1999) containing a second functional NLS2, which seems to partially overlap to a predicted nuclear export signal (NES) (Alvarez, 2004; Alvarez et al., 2003); a PEST motif (aa 482-525), which is commonly associated to protein stability although its functionality has not been explored in DYRK1A; a polyhistidine domain (HIS, aa 599-619) that localizes the protein to the nuclear compartment of splicing factors (SFC) or nuclear speckles (Alvarez et al., 2003; Salichs, 2008) and that mediates protein-protein interactions, such the one described with the protein Sprouty2 (Aranda et al., 2008); and, finally, a region rich in serine

and threonine residues (S/T, aa 659-672) with an unknown function. The protein is highly conserved between human and mouse with 99% of homology when aligned with Clustalw2 (EMBL-EBI).

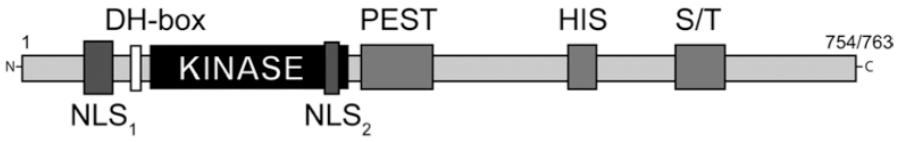

Fig I8: DYRK1A protein structure. Schematic representation of the protein structure where the different protein motifs identified are indicated: NLS, nuclear localization signal; DH-box, DYRK homology box; KINASE, Kinase domain; PEST, motif rich in proline, glutamic acid, serine and threonine residues; HIS; polyhistidine domain; S/T; motif rich in serine and threonine residues. N-, amino-terminal part; C-, carboxy-terminal part.

DYRK1A has been defined as a dual-specificity protein kinase because it has autophosphorylation activity on tyrosine residues as well as serine and threonine phosphorylation activity on itself and on its substrates (Becker and Joost, 1999; Himpel et al., 2000; Kentrup et al., 1996). The canonical DYRK1A phosphorilation consensus sequence is RPx(S/T)P, where x corresponds to all amino acids and S/T are the phosphorylable residues (Himpel et al., 2000).

All the DYRK family members, including DYRK1A, present a conserved Tyr-X-Tyr motif in the activation loop of the catalytic domain (Becker and Joost, 1999). Phosphorylation of the second Tyr-residue of this motif is essential for DYRK1A kinase activity (Himpel et al., 2001). A model for the activation of DYRK family members has been suggested based on studies in *Drosophila* (Lochhead et al., 2005). According to this model, autophosphorylation in the activation loop is an intramolecular event mediated by a transitional intermediate form during translation. The

Tyr-kinase activity is lost once the protein is fully translated, and the mature kinase can only phosphorylate Ser/Thr residues. Therefore, DYRK1A is synthesized as a constitutive active kinase, which implies that other mechanisms that switch kinase activity on/off must exist to regulate its activity.

DYRK1A regulation can occur at both transcriptional and post-translational levels although poor knowledge has been reached to date. *DYRK1A* can be transcribed by three putative promoters (pM, pA and pB, reviewed in Aranda et al., 2011) that show distinct responses to transcription factors, such as E2F1 for pB and CREB for pA (Impey et al., 2004; Maenz et al., 2008). The transcription factor activator protein 4 (AP4) and its corepressor partner geminin have been shown to repress *DYRK1A* transcription outside the CNS through recruiting HDAC3 to the pB and pM *DYRK1A* promoter regions (Kim et al., 2006). Moreover, *DYRK1A* can undergo alternative splice events (reviewed in Aranda et al., 2011) but the products of these events have not been associated yet to different protein activities.

Different posttransductional modifications have been described for DYRK1A. For example, the exogenous phosphorilation in Ser520 of DYRK1A triggers the association with 14-3-3β and induces a conformational change, resulting in increased DYRK1A catalytic activity (Alvarez et al., 2007). Events of competition between substrates have also been described, like for the SPRED1/2 Sprouty-related proteins, whose binding to the DYRK1A kinase domain inhibits DYRK1A-dependent phosphorylation of other substates (Li et al., 2010). Finally, the control of DYRK1A expression *via* let7b and 199b miRNAs has been demonstrated in particular contexts (Buratti et al., 2010; Da Costa et al., 2010).

Another level of DYRK1A regulation is represented by its intracellular localization that is likely to regulate accessibility to its substrates. DYRK1A has been proposed to be a nuclear-cytosolic shuttle protein (Alvarez, 2004); indeed a switch from nuclear to cytoplasmic expression has been described *in vivo* during Purkinje cells differentiation in chicken (Hammerle et al., 2002). Biochemical fractionation experiments indicate that DYRK1A in the adult mouse brain is distributed in both, nuclear and cytosolic fractions. Within the cytosolic fraction, DYRK1A is distributed in a pool associated with the synaptic plasma membrane and a pool associated with the vesicle-containing fractions (Aranda et al., 2008; Murakami et al., 2009). Within the nucleus, DYRK1A accumulates in nuclear speckles through its His-repeat domain (Alvarez et al., 2003; Salichs et al., 2009) suggesting that it could be involved in transcriptional regulation. Nevertheless, in mammalian brains only a small fraction of DYRK1A (around 10%) is detected in the nucleus (unpublished result from Wegiel's lab; Murakami et al., 2009, Martí et al., 2003).

2.3. DYRK1A expression in brain

Although ubiquitously distributed in most mammalian adult tissues (Guimera et al., 1999; Okui et al., 1999), DYRK1A expression is prevalent during brain development, which is consistent with the pivotal role of this kinase in neurodevelopmental processes already mentioned in the Introduction, section 2.1. During development *Dyrk1a* transcripts are detected at early embryonic stages, particularly in the neural tube and otic vesicle of mouse embryos (Fotaki et al., 2002; Okui et al., 1999). Interestingly, mouse and chick *Dyrk1a* mRNAs are expressed in neuroepithelial progenitor cells, and are asymmetrically distributed during

the mitosis of these cells before the first neurogenic division, pointing to a possible role for this kinase in the transition from proliferating to neurogenic divisions of neural precursor cells (Hammerle et al., 2002). The asymmetric segregation of Dyrk1a protein in neural progenitors has been also recently described in the adult SVZ. In adult progenitors the levels of Dyrk1a protein correlates with the levels of EGFR that, in turn, determine the self-renewal capability of these cells (Ferron et al., 2010). In this paper the authors propose that the inheritance of Dyrk1a protein in the cells resulting from the division of a brain adult stem cell determines their fate, opening an exciting field of investigation that could shed light in the current knowledge of the neurogenic processes during development. Indeed, a key role of Dyrk1a in early neurodevelopment is suggested by the stage-dependent expression pattern of *Dyrk1a* transcripts: *Dyrk1a* mRNA expression is transient in pre-neurogenic progenitors; cell-cycle regulated in neurogenic progenitors; down-regulated in post-mitotic neurons as they migrate radially; and persistent in late differentiating neurons (Hammerle et al., 2008). In differentiating neurons Dyrk1a is expressed in growing dendritic trees both in primary neuronal cultures (Aranda et al., 2008) and in the embryonic forebrain (Hammerle 2003).

Although the molecular mechanisms involving Dyrk1a in neurodevelopmental processes remain largely elusive, the requirement of a strict regulation of Dyrk1a levels indicates its critical role in coupling the sequential neurogenic events.

In the adult CNS, DYRK1A expression becomes lower but sustained (Okui et al., 1999; Hammerle et al., 2008), and its regional pattern suggests specific roles of DYRK1A in normal brain functions (Wegiel et al., 2004; Marti et al., 2003). Indeed, Dyrk1a expression is elevated in the olfactory and motor systems of the adult mouse brain, thus supporting its

role in these functions (Martí et al., 2003). Hippocampus and neocortex are also immunopositive for DYRK1A in both human (Wegiel et al., 2004) and mouse (Martí et al., 2003), indicating an involvement in the physiology of high brain functions. In the human neocortex DYRK1A distribution is uneven, with higher expression in the upper layers in both neurons and astrocites (Wegiel et al., 2004). By contrast, DYRK1A has not been detected in adult oligodendrocytes (Wegiel et al., 2004), which is in agreement with the faint immunostaining observed in the white matter of adult mouse brains (Martí et al., 2003). The subcellular localization of human DYRK1A *in vivo* is suggestive of the roles it may exert: in neurons it is expressed in both nucleus (outside the nucleoli), and cytoplasm (mainly in fractions enriched in synaptic buttons), thus indicating that it can regulate nuclear functions and neurotransmission, while in astrocytes it concentrates in cytoplasmic granules (Wegiel et al., 2004).

DYRK1A expression in humans increases with age in both neurons and astrocytes, indicating a role for DYRK1A in the aging process (Wegiel et al., 2004). This indication is in accordance with the increase DYRK1A expression observed in neurofiblilary tangles and ß-amiloid plaques of Alzeimer's Disease (AD) brains (Wegiel et al., 2008; Kimura et al., 2007; Ferrer at el., 2005). In this context, it is worthy to mention that DYRK1A overexpression has been involved in the etiology of early onset AD in DS (reviewed in Wegiel et al., 2011).

2.4. DYRK1A cellular functions

DYRK1A is considered a signaling kinase because of its interaction with components of several cell-signaling cascades. The interaction of DYRK1A with its substrates can occur at both cytosolic and nuclear

compartments, and can involve different mechanisms that go beyond the simple phosphorilation of substrates. A recent review published by Tejedor and Hammerle (2011) reports an updated list of DYRK1A substrates and interactors that may be important for the neurodevelopmental functions of DYR1A. Here I will focus on the main cellular pathways or cellular functions involving DYRK1A, underlying the outcomes that are relevant to the objectives of this thesis.

2.4.1. DYRK1A in cell survival

Two independent groups have defined caspase 9, a key effector in programmed cell death, as a DYRK1A substrate (Laguna et al., 2008; Seifert et al, 2008). Seifert and colleagues demonstrated that in hyperosmotic conditions DYRK1A interacts with and phosphorylates caspase 9 inhibiting its processing and further activation in cells; our group further showed that DYRK1A is the mayor kinase phosphorylating and inactivating caspase 9 during mouse retina development (Laguna et al., 2008). Other anti-apoptotic events triggered by DYRK1A have been reported: i) p53-mediated survival during DNA damage is induced by DYRK1A- (and DYRK3)-mediated phosphorylation and activation of the protein deacetylase SIRT1 (Guo et al., 2010); and ii) the increase in DYRK1A expression levels in human foreskin keratinocytes immortalized by infection with human papillomavirus type 16 appears to favor these cells to escape from apoptosis (Chang et al., 2007). Altogether these findings support a protective role of DYRK1A against apoptosis, in different context; development, stress and cancer, by acting at different levels of the apoptotic response.

2.4.2. DYRK1A in cell cycle

Although DYRK1A protein is expressed throughout the cell cycle, unpublished data from De la Luna's laboratory at the CRG indicate that the levels of DYRK1A vary in a phase dependent manner. Other evidences have linked DYRK1A with cell cycle progression; E2F1, a pivotal TF in the control of cell proliferation, positively regulates DYRK1A transcription *in vitro* (Meanz et al., 2008), and transgenic mice overexpressing *Dyrk1a* present elevated levels of Cyclin B1 (Branchi et al., 2004).

Cell cycle exit of neural progenitors is a key step in neurodevelopmental process (see section 1.2.1.3.). The following evidences suggest a role for DYRK1A in cell cycle control of neural progenitors and neurogenesis: i) *Dyrk1a* overexpression in immortalized rat hippocampal progenitors induces impaired G1-G0/S phase transition (Park et al., 2010); ii) Dyrk1a is transiently co-expressed with p27/kip1, the main cyclin-dependent kinase inhibitor in the mammalian forebrain (Nguyen et al., 2006) and regulates neural progenitors' cell cycle exit and neurogenesis onset (Hammerle et al., 2011); iii) acute overexpression of Dyrk1a in mouse embryonic telencephalon inhibits proliferation and induces premature neuronal differentiation through an unknown mechanism that may involve cyclin D1 nuclear export and degradation (Yabut et al., 2010). All these evidences propose a complex role of DYRK1A in cell cycle regulation for which very little understanding has been reached until now.

2.4.3. DYRK1A in signaling pathways

Notch pathway- DYRK1A has been shown to be a negative regulator of Notch pathway both *in vitro* and *in vivo* (Fernandez-Martinez

et al., 2009). Dyrk1a interacts with the Notch intracellular domain (NICD) and promotes its phosphorylation at multiple sites, which leads to the repression of its transcriptional activity in neural cells. Due the role of Notch in neurogenesis (reviewed in Yoon and Gaiano, 2005; Louvi and Artavanis- Tsakonas, 2006, and in the Introduction, section 1.2.1.2.), it is tempting to speculate that DYRK1A promotes the onset of neurogenesis by inhibiting Notch. If this were the case, an increased Notch activity due to a decreased DYRK1A levels may delay the onset of neurogenesis, thus contributing to the microcephaly associated to *DYRK1A* loss of function mutations. Moreover, an increase in Notch signaling could result in the same phenotype because the precocious neurogenesis could deplete the pool of progenitors.

Notch signaling has been found increased in the cerebral cortex of DS individuals (Dowjat et al., 2007; Lockstone et al., 2007) but decreased in the cerebellum of the Tcj1e DS mouse model (Dauphinot et al., 2005), in which only 85 orthologs of chromosome 21 coding genes are triplicated (Sago et al., 1998). These data indicate that deregulation of Notch signaling in DS is a complex issue involving different triplicated genes in addition to DYRK1A.

No data have been reported until now, involving DYRK1A-mediated regulation of Notch signaling in astrogliogenesis or oligodendrogenesis.

SHH signaling- DYRK1A positively regulates the transcriptional activity of glioma-associated oncogene 1 (Gli1), a major effector of SHH signaling (Mao et al., 2002). DYRK1A retains Gli1 in the nucleus, and enhances the transcriptional activity of full-length Gli1 but not of a natural N-terminally truncated Gli1 variant (Mao et al., 2002; Shimokawa et al., 2008). Both effects rely on DYRK1A-dependent phosphorilation of Gli1 (Mao et al., 2002). Importantly, SHH fails to stimulate DYRK1A kinase

activity, suggesting that this pathway might not directly regulate DYRK1A (Mao et al., 2002). The *in vivo* consequences of DYRK1A regulation of the SHH pathway still unknown.

Receptor tyrosine kinase signaling- Receptor tyrosine kinases (RTKs) are transmembrane proteins that play a critical role in a wide range of biological processes given their involvement in the regulation of cell proliferation, differentiation, migration and survival. The majority of RTKs ligands are soluble peptides like nerve growth factor (NGF), fibroblast growth factor (FGF) and epidermal growth factor (EGF), which induce receptor dimerization and allow signal transduction *via* the RAS-RAF-ERK cascade (for recent review see Lemmon and Schlessinger, 2010). An important class of regulators of RTK-dependent pathways is the Sprouty (Spry1 to 4 in mammals) family of proteins, which interferes with RTK-signaling cascade in a growth-factor and tissue-specific manner (for a recent review see Guy et al., 2009). Another way to fine-tune the output of the signal is through regulated endocytosis of activated RTKs, which then can be recycled to the cell surface or targeted for degradation (reviewed in Sorkin and von Zastrow, 2009).

Dyrk1a has been recently involved in **EGF signaling pathway** by preventing endocytosis-mediated degradation of EGFR. Dyrk1a exerts this role, at least in part, through phosphorylation of Spry2 at residue Thr75 (Ferron et al., 2010). This Dyrk1a effect is important for regulating adult neural stem cells since sustained levels of membrane-bound EGFR is required to maintain the self-renewal potential of these cells (Andreu-Agulló et al, 2009). EGF signaling has also been involved in developmental myelination (Aguirre et al., 2007). A possible role of Dyrk1a in EGF-dependent signaling in the context of myelination remains unknown.

DYRK1A-triggered phosphorylation of Spry2 at residue Thr75 has also been involved in the enhancement of **FGF signaling pathway**. Phosphorylation of Thr75 in Spry2 by DYRK1A abolishes its inhibitory action on FGF-dependent MAPK activation (Aranda et al., 2008). DYRK1A and Spry2 colocalize in growth cones of dissociated cortical neurons and co-purify with the synaptic plasma membrane fraction in mouse brain extracts, pointing to a possible functional interaction of DYRK1A and Spry2 in synaptogenesis (Aranda et al., 2008). Indeed, DYRK1A kinase activity enhances FGF-mediated responses during the differentiation of immortalized hippocampal neurons (Yang et al., 2001).

DYRK1A can also regulate neuronal differentiation *via* activation of **NGF signaling**: DYRK1A potentiates the NGF-dependent differentiation of PC12 cells through its interaction with components of the signaling cascade RAS-BRAF-MEK1 (Kelly and Rahmani, 2005). Given that this effect is independent of DYRK1A kinase activity, a role of DYRK1A as a scaffold protein has been suggested in this case.

Calcineurin- NFAT signaling. Calcineurin is a calcium–calmodulin-activated Ser/Thr protein phosphatase that is activated by sustained elevations of intracellular calcium concentrations. Once activated, calcineurin dephosphorylates NFAT transcription factors within the cytoplasm, promoting their translocation to the nucleus and the subsequent activation of gene expression (reviewed in Hogan et al., 2003). Two independent groups demonstrated that NFAT1 and NFAT3 are targets of DYRK1A kinase activity in the nucleus, where DYRK1A phosphorylation of NFATs primes further phosphorylation of these TFs by GSK3 promoting their translocation to the cytosol (Arron et al., 2006; Gwack et al., 2006). Thus, DYRK1A is a negative regulator of Calcineurin- NFAT signaling.

NFATs are involved, among many other functions, in the control of cardiac hypertrophy (Molkentin et al., 2004) and bone development (Schulz et al., 2004). Indeed, DYRK1A-induced inhibition of NFAT transcription attenuates the hypertrophic response of cardiomyocytes (Kuhn et al., 2009). The phenotypic analysis of NFAT knock out mice reveals cranio-facial abnormalities that resemble those in DS mouse models, suggesting that NFAT increased activity, probably due to *Dyrk1a* triplication, could underlie this DS phenotype (Arron et al., 2006). It is worthy to mention that DSCR1/RCAN1, a negative regulator of calcineurin activity, is also triplicated in DS, thus amplifying the NFAT-dependent effects of HSA21 trisomy (reviewed in Park et al., 2009).

NFATs in the nervous system mediate neurotrophin- and netrin-dependent neuronal differentiation (Graef et al., 2003), as well as Shwann cell differentiation (Kao et al., 2009). In Shwann cells, activation of ErbB receptor by Neuregulin has been shown to promote the NFAT-dependent transcription of the TF Krox20, a key positive regulator of myelin gene expression (Kao et al., 2009).

JAK-STAT signaling pathway- DYRK1A *in vitro* directly phosphorylates the TF STAT3 at Ser727 (Matsuo et al., 2001; Wiechmann et al., 2003; Li et al., 2010). This phosphorylation event requires the phosphorylation of Tyr321 and Gln323 within the DRK1A activation loop, and is prevented by the related Sprouty proteins, SPRED1 and SPRED2 (Wiechmann et al., 2003; Li et al., 2010). This inhibition is the result of a competition event that occurs *via* an interaction between the CRD region of the SPREDs with the kinase domain of DYRK1A that prevents DYRK1A binding to its substrates (Li et al., 2010).

Being STAT3 the main effector of the JAK-STAT pathway and the fundamental role of this pathway in astrogliogenesis (Bonni et al., 1997),

it would be interesting to investigate whether DYRK1A-STAT3 interaction could play a role in the neurogenic-gliogenic switch mentioned in section 1.2.2.1.

2.4.4. DYRK1A in epigenetic regulation of gene expression

Three works published during this thesis suggested a novel role for DYRK1A in NRSF/REST-mediated gene expression regulation (Canzonetta et al, 2008; Lepagnol-Bestel et al. 2009; Lu et al., 2011). In the first paper, Canzonetta and colleagues showed an association between *DYRK1A* triplication and *REST/NRSF* down-regulation in mouse adult brains and in mouse ES cells (Canzonetta et el., 2008). They also showed that *Dyrk1a* dose-reduction has the same effect on *REST/NRSF* mRNA levels than *Dyrk1a* overexpression, indicating that a strict stechiometry governs the REST/NRSF transcriptional complex. In the second paper, Lepagnol-Bestel and colleagues showed that DYRK1A exerts its regulatory function on REST/NRSF transcriptional activity through interaction with the SWI/SNF chromatin remodeling complex, one of the components of the epigenetic apparatus recruited to DNA by REST/NRSF (Ballas et al., 2005). The consequence of this interaction is the regulation of clusters of genes. The authors argue that *Dyrk1a* dosage imbalance affects *REST/NRSF* mRNA levels not persistently, but in a stage and region specific manner. Indeed, in this work, they showed *REST/NRSF* up-regulation in the embryonic cerebral cortex and down-regulation in the adult hippocampus of a DS mouse model. Finally, in the third paper Lu and colleagues showed that REST/NRSF directly induces *DYRK1A* transcription and that DYRK1A-dosage imbalance induces REST/NRSF degradation *via* ubiquitin-proteasome (Lu et al., 2011).

All the evidences above reported suggest that DYRK1A can play a

role in neurodevelopment *via* REST/NRSF-mediated transcriptional regulation. Despite the contradictions of the data, together these three works show that DYRK1A-NRSF functional connections are complex and probably context dependent.

DYRK1A has also been shown to phosphorylate and activate SIRT1, which among other functions is involved in epigenetic regulation of gene expression through deacetylation of histone tails (Guo et al., 2010; for a review on SIRTs: Vaquero 2009). Although a functional interaction between DYRK1A and SIRT1 has only been shown in the context of p53-mediated cell survival (Guo et al., 2010) it is possible that DYRK1A influences SIRT1-mediated epigenetic regulation of gene expression.

Objectives

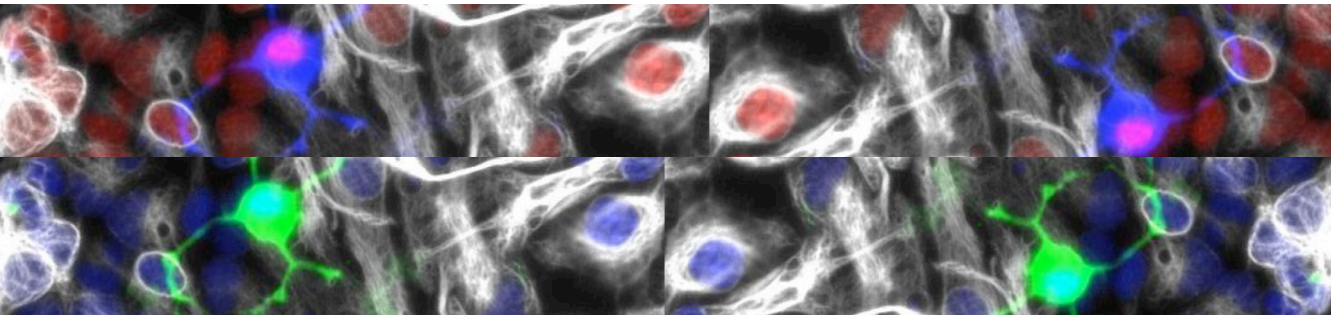

The cerebral cortex is the key structure for highest functions, like cognition and memory, in mammals. Proper establishment of the different cell populations that compose this structure is fundamental for its functionality and occurs in a timely defined manner during development. Despite the progress made in the last two decades, the molecular mechanisms at the basis of this process are still poorly understood.

For this reason, the general aim of this thesis was to provide evidences about the mechanisms that underlie the sequential generation of cells during corticogenesis.

The phenotypes of *DYRK1A* gene-dosage mutations in both human and mouse have revealed the importance of the pleiotropic DYRK1A protein kinase in mammalian brain development and functionality. Alterations in cortical cell densities and in the dendritic tree of cortical pyramidal neurons observed in the brain of adult *Dyrk1a* haploinsufficient mice suggested that DYRK1A may play a role in corticogenesis.

In this work we have further investigated the **role(s) of Dyrk1a in mouse corticogenesis**. The workflow of the study was defined by our own results and data from other laboratories published during the thesis.

The **first objective** we addressed was to determine the effect of *Dyrk1a* dose reduction on gene expression during mouse cortical development. To this end we compared the transcriptomes of the cerebral cortex of *Dyrk1a*$^{+/+}$ and *Dyrk1a*$^{+/-}$ mice at postnatal day 0 and 7.

The differential expression between genotypes of genes involved in self-renewal and differentiation, suggested that Dyrk1a might regulate the behavior of embryonic cortical progenitors. To address this issue the **second objective** of the work was to compare the self-renewal and differentiation potentials of *Dyrk1a*$^{+/+}$ and *Dyrk1a*$^{+/-}$ cortical progenitors by preparing neurosphere cultures from embryos of both genotypes.

The reduced oligodendroglial potential of *Dyrk1a*$^{+/-}$ neurosphere cells and results from a bioinformatic analysis of *Dyrk1a*$^{+/-}$ differentially expressed genes led us to the **third objective** of the thesis, which was to compare, *in vivo*, the epigenetic status of specific *loci* of the gliogenic genes *S100b* and *Gfap* between *Dyrk1a*$^{+/+}$ and *Dyrk1a*$^{+/-}$ developing cerebral cortex.

Based on our *in vivo* and *in vitro* results, we formulated the **fourth objective** of the thesis, which was to evaluate whether the epigenetic and gene expression changes occurring at early developmental stages of *Dyrk1a*$^{+/-}$ cortical differentiation have any consequence at later stages. To this end, we quantified representative glial populations in *Dyrk1a*$^{+/+}$ and *Dyrk1a*$^{+/-}$ postnatal and adult brains.

Cell counts and Mbp (myelin basic protein) expression in the cortex of *Dyrk1a*$^{+/-}$ mice suggested a role of Dyrk1a in myelination. This possibility led us to the **fifth objective** of the thesis, which was to perform an electron microscopy analysis of *Dyrk1a*$^{+/+}$ and *Dyrk1a*$^{+/-}$ nerves from both central and peripheral nervous systems.

Methods

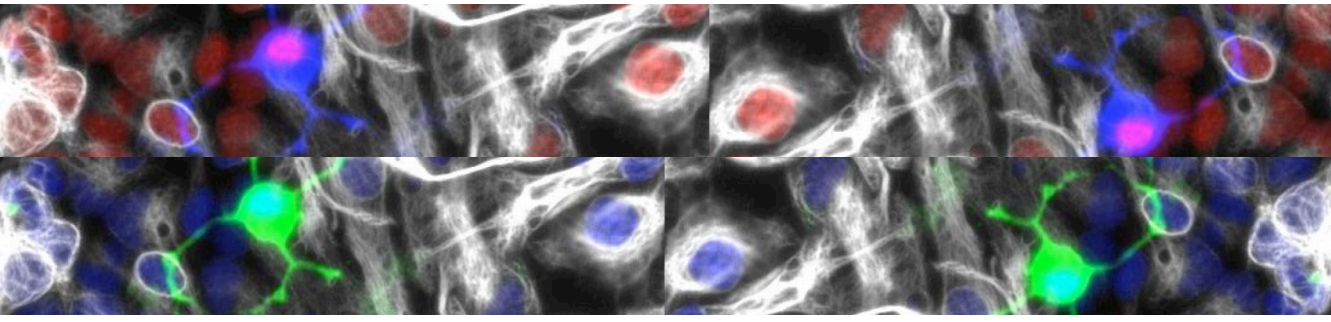

1. Mouse handling

1.1. Mouse models

1.1.1. Breeding

Two mouse models were used along this study to analyze the effects of *Dyrk1a* dosage imbalance on cerebral cortex development; a *Dyrk1a* loss-of-function model, generated in the laboratory by gene targeting (Fotaki et al., 2002), and a *Dyrk1a* overexpressing mouse model, kindly provided by Dr. Jean Maurice Delabar (Université Paris Diderot, Paris, France).

The studies of *Dyrk1a* loss-of-function were performed in mice heterozygous for the deleterious mutation (***Dyrk1a*$^{+/-}$**), because the knockout mice (*Dyrk1a*$^{-/-}$) die at the first stages of brain development, around E11.5 (Fotaki et al., 2002). Mutant *Dyrk1a* mice in a mixed C57BL/6Jx129S2/SvHsd (C57-129) genetic background and in a CD-1 background were used as follows: (i) Gene expression experiments and analysis of *in vivo* phenotypes were done on *Dyrk1a*$^{+/-}$ mice and wild-type (*Dyrk1a*$^{+/+}$) littermates obtained by crossing of F1:C57-129 wild-type females (Harlan Ibérica, S.L.) with C57-129 *Dyrk1a*$^{+/-}$ males and (ii) pyrosequencing and neurospheres experiments were done on siblings from crosses between CD-1 wild-type females (Charles River) and CD-1 *Dyrk1a*$^{+/-}$ males. Some experiments were performed in both C57-129 and CD1 mutant mice and in all cases the results were the same independently of the genetic background.

BAC-*Dyrk1a* expresses the full-length mouse *Dyrk1a* gene under the control of its endogenous promoter. These mice were obtained by microinjection of an ES cell line carrying a BAC that contains the entire *Dyrk1a* gene (Mao et al., 2007) into C57BL/6 blastocysts. The

phenotypes of these mice were analyzed in the F12 progeny resulting from crosses between C57BL/6 wild-type females (Charles River) and BAC-*Dyrk1a* mutant males.

1.1.2. Genotyping

Animal genotyping was performed by polymerase chain reaction (PCR) analysis using genomic DNA obtained from tail samples. DNA was extracted by incubating 2-3 cm of fresh or frozen tissue in 500µl NaOH 50mM at 95ºC for 60'. The solution was then neutralized by adding Tris-HCl 100mM pH8. Samples were centrifuged at maximum speed for 10' and 1 ul of the supernatant, containing DNA, was used for each PCR reaction. Primers and PCR conditions used for genotyping are detailed in Table M1.

Table M1: List of primers and PCR conditions used for genotyping

Usage	Primer	Sequence 5'-3'	T Annealing	N Cycles	Amplicon size (bp)	Ref
Dyrk1a $^{+/-}$	NeoT-F	ATTCGCAGCGCATCGCCTTCTATCGCC	58ºC	35	287 bp	(Fotaki et al., 2002)
	MnbIV-V-R	CGTGATGAGCCCTTACCTATG				
	MnbIV(3)-F	AGAGTGGAGCAAGAATGGGTC	58ºC	35	146 bp	
	MnbIV-V-R	CGTGATGAGCCCTTACCTATG				
BAC - *Dyrk1a*	3'Dyrk-I	TGGGCCAAGCAGTTAGGAGTTT	66ºC	35	200 bp	(Personal communication)
	3' Bac11-r	CCATGATTACGCCAAGCTATTTAGG				
	5' Dyrk-r	ACCCCAGCTAACCAACATCCAT	66ºC	35	200 bp	
	5' Bac11-u	CCGGGGATCCTCTAGAGTCG				

Dyrk1a $^{+/-}$ genotyping includes PCR amplification of two DNA fragments; the recombinant one, amplified with the NeoT-F and MnbIV-V-R primers, and the wild type one amplified with the MnbIV(3)-F and MnbIV-V-R primers. BAC-Dyrk1a genotyping is performed with 3'Dyrk-I and 3'BAC11-r primers or with

5'Dyrk-r and 5'BAC11-u. For each pair of primers the annealing temperature (T), the number (N) of amplification cycles used in the PCR reaction and the amplicone size (in bp) are reported. All primers were used at a final concentration of 10µM; F=Forward primer, R=Reverse primer.

1.1.3. Stabulation

All animals were maintained in the animal facility of the Parc de Recerca Biomèdica de Barcelona (PRBB). The housing conditions were under a 12 hours light/ 12 hours dark schedule (lights on at 8:00 a.m.) in controlled environmental conditions of humidity (60%) and temperature (22ºC ± 2ºC) with food and water *ad libitum*. All experimental procedures were carried out following protocols approved by the Institut Municipal d'Investigació Mèdica (IMIM-Hospital del Mar) or PRBB ethic committees.

Embryos and postnatal animals were obtained from controlled matings. Two to three females (6 weeks to 4 months of age) were placed in the same cage with one male and females were checked for the presence of vaginal plugs. The morning on which the vaginal plug was detected was taken as day 0.5 (E0.5).

1.2. Histology techniques

1.2.1. Sample preparation

To obtain brain sections, mice were deeply anesthetized with Carbon dioxide (CO_2) and transcardially perfused with 4% (w/v) paraformaldehyde (PFA) in 0.1M phosphate buffer saline (PBS) (pH 7.4) at room temperature (RT). Then brains were removed and post-fixed at 4°C in 4% PFA for 24 hours. After rinsing in PBS, fixed brains were processed to obtain either vibratome or criostate sections.

For cryostat sectioning, brains were cryoprotected in 30% (w/v) sucrose in PBS at 4ºC for 1 to 2 days, and frozen at -40ºC in isopentane (Panreac) previously cooled with dry ice. Frozen samples were placed on an OCT-base and 40-50µm coronal sections were cut using a Leica CM3050S cryostat. Sections were collected in 48-well plates filled with a cryoprotective solution (40% v/v gylcerol – 40% v/v etylenglycol in PBS) that allowed long-term storage of the sections at -20ºC.

For vibratome sectioning, brains were stored in PBS at 4ºC until being embedded in 2-6% agarose. Embedded brains were cut in 40-50µm coronal sections in a Leica VT1000S vibratome, placed in 48-well plates filled with the cryoprotective solution and stored at -20ºC. All immunostainings were performed on frozen tissues, with the exception of Dyrk1a immunostainings that were started immediately after vibratome sectioning.

1.2.2. Immunostainings and microscopy

Immunohistochemistry (IHC) was done using the avidin-biotin-peroxidase method (Vectastain ABC kit, Vector Labs). Briefly, after washing the sections in PBS for 15', endogenous peroxidase activity was blocked by incubation with 3% H_2O_2 (v/v) and 10% (v/v) methanol in PBS for 30' at RT. Sections were then permeabilized for 30' to 90' with 0.2% Triton-X100 in PBS and, afterward, incubated 60' at RT in blocking solution (BS): 0.2% Triton-X100 and 10% fetal bovine serum (FBS, Invitrogen) in PBS. Samples incubation with primary antibody was performed overnight (ON) at 4ºC in incubating solution (IS): 0.2% Triton-X100 and 5% FBS in PBS. After washing with 0.2% Triton-X100 in PBS, sections were incubated with the corresponding biotinylated secondary antibody (1:200; Vector Labs) in IS for 60', washed and incubated with an

avidin-biotin-peroxidase solution (Vectastain ABC kit, Vector Labs) according to manufacturer's indications. Peroxidase activity was visualized with 0.03% diaminobenzidine (Sigma) and 0.003% hydrogen peroxide. All samples were counterstained with Nissl (Cresyl violet 0.5%) to visualize nuclei, dehydrated and mounted in Eukitt mounting medium (Sigma). Bright field images were viewed with an *Olympus BX51* microscope.

For immunofluorescence (IF), samples were washed in PBS and then permeabilized as described above. After 60' incubation in BS, sections were incubated ON at 4ºC with the primary antibody (or antibodies in case of double immunofluorescence experiments). After washing, incubation with the secondary antibody (or antibodies) was performed in IS for 60' at RT. Secondary antibodies used for immunofluorescence were: Alexa Fluor 555-conjugated donkey anti-mouse, donkey anti-rabbit, goat anti-guinea pig IgGs; Alexa Fluor 488-conjugated donkey anti-mouse, goat anti-rabbit and donkey anti-rat IgGs (1:1000, Molecular Probes); and biotinylated goat anti-mouse IgM (1:200, Vector Laboratories) followed by 60' incubation with Streptavidin, Alexa fluor-488 conjugated (1:2000, Molecular Probes). Cell nuclei were stained with Hoechst (Sigma). Samples were mounted using Vectashield mounting medium. The described protocols for IF was applied to all primary antibodies listed in Table M2, excluding the membrane protein O4 for which the permeabilizing agent Triton-X100 was excluded from all steps. Vector M.O.M. immunodetection Kit (Vector Laboratories) was used for Cc1 immunostainings to eliminate background. In this case M.O.M. blocking solution and M.O.M. diluent were used instead of BS and IS respectively, and a biotinylated anti-mouse IgG provided in the kit was used as secondary antibody according to manufacturer's

instructions. Immunofluorescence images were viewed under a Zeiss Observer.Z1 microscope, using a Pan-APO 20x objective, and acquired with an AxioCam MRm camera. Confocal images were taken at the Confocal Service Unit of the Centre de Regulaciò Genòmica (CRG, Barcelona, Spain) in a sequential mode with an inverted Leica TCS SP5 confocal microscope, using HCX PI APO 40x 1.32 oil Ph3 CS or HC PL APO 20x 0.70 CS objectives and the Leica Confocal Software (LCS).

In all cases, specificity of the immunoreaction was verified in parallel samples incubated in BS without primary antibody. No immunoreaction was detected in these samples. Samples from animals of different genotypes were processed in parallel to avoid day-to-day variations in the immunostaining.

Table M2: List of primary antibodies used for immunostainings

Antibody	Host	Working dilution	Usage	Source
Cc1	Mouse	1:100	IF	Calbiochem
Dyrk1a	Mouse	1: 250	IF	Abnova
Gfap	Mouse	1:500	IF	Sigma
Gfap	Rabbit	1:1000	IF	DAKO
Glast	Guinea-Pig	1:5000	IF	Millipore
Mbp	Rat	1:500	IF	Chemicon
O4	Mouse (IgM)	1:500	IF	Chemicon
S100b	Rabbit	1:1000	IF, IHC	DAKO
Sox9	Rabbit	1:5000	IF	Stolt et al., 2003
Tuj1	Mouse	1:1000	IF	Covance
Tuj1	Rabbit	1:1000	IF	Sigma

1.2.3. Cell counts

Cell quantification was performed by counting either cell densities (number of cells per mm^3) or cell percentages over total nuclei ($Hoechst^+$ in IF and $Nissl^+$ in IHC). Cell densities were determined using an

Olympus BX51 microscope, with a *JVC* digital color video camera and an interactive computer system consisting of a high-precision motorized microscope stage, a microcator for reading z- positions (Heidenhain MT-12 gauge microcator) and a high resolution video monitor. The interactive test grids and control of the monitorized stage were provided by the *CAST GRID* general stereological software package (Olympus) for PCs running *Microsoft® WindowsTM*. For each stained section, the area of interest was delimited with the "Drawing" tool at 2x magnification and then calculated with the "Area" tool. Afterward, the volume of the selected region was calculated by multiplying the obtained area by the thickness of the section. Within the drawn region the number (N) of immunopositive cells was counted at 40x magnification, moving through all the z-dimension. To determine total cell density the number of $Nissl^+$ nuclei was quantified in the volume selected. In these cases the percentage of immunopositive cells over total nuclei was determined by dividing the N of immunopositive cells (x100) by the N of $Nissl^+$ cells. Differences between genotypes were considered significant for $pValues<0.05$ in a two-tailed Student's t-test.

In the case of IF, between 8 and 10 confocal images at 20x magnification were taken at intervals of 1µm in the region of interest. Confocal projections were obtained using the "z-projection" tool of the Image-J program for image processing (developed and maintained by the National Institutes of Health, Bethesda, MD, Maryland, USA) and were used to count cell numbers and $Hoechst^+$ nuclei. The percentage of immunopositive cells and the statistical significance of the results were determined as described above.

1.2.4. Transmission electron microscopy

The analysis of adult *Corpus Callosum* and optic and sciatic nerves by transmission electron microscopy (TEM) was done at the laboratory of Dr. Eduardo Fernández (Universidad Miguel Hernández, Alicante, Spain). Animals were deeply anesthetized and transcardially perfused with 4% paraformaldehyde and 2% Glutaraldehyde in 0.1 M phosphate buffer (pH 7.4) at RT. Brains and nerves were removed, hemisected and post-fixed in the same fixative, at 4ºC for 24h. The brains were then segmented in the medial sagittal plane with the help of a stainless steel and trimmed to 2-3 mm thick segments. Brain and nerves were washed in 0.1 M phosphate buffer, stained with 1% OsO_4, dehydrated in graded concentrations of ethanol and embedded in Epon 812 (Electron Microscopy Science). Serial 0.5 mm semithin sections were stained with toluidine blue and examined with a Leica DMB Microscope. Thin sections (60 -80 nm thick) were obtained with a Reichert Ultracut ultramicrotome equipped with a diamond knife. Sections were stained with uranyl acetate and lead citrate, and examined with a JEOL JEM-1001 electron microscope. Digital images were acquired with a MegaViewIII camera. The image fields were analyzed using the ImageJ analysis program and a modified version of a software designed to study axonal morphometry (Fernandez et al. 1991). For morphometrical evaluation of axons, fibers taken at magnifications of 11000X were examined. Only fibers with microtubules and neurofilaments sectioned perpendicular to their longitudinal axes were selected for analysis. Because it was difficult to automatically select the boundary between the nerve fibers and the surrounding background for small axons and thinly myelinated fibers using standard image analysis techniques, each image was analyzed using a semiautomatic method. The axonal contour and the external

contour of the myelin sheath (fiber contour) were manually traced on enlarged images. A set of custom macros allowed the calculation of the length of a line, the cross-sectional area, and the lengths of the major and minor axes of the best fitting ellipse. Fiber diameters and axonal diameters were deduced from the fiber and axonal perimeters assuming a cylindrical shape of axons. These basic data were used to derive the form factor, g-ratio and myelin sheath thickness (Fernandez et al. 1991, Branner et al., 2001).

2. Embryonic neurospheres cultures

Pregnant females were sacrificed by cervical dislocation and the embryos removed from the uterus and maintained in PBS in plastic plates on ice until dissection. Whole embryo brains were isolated, the meninges removed and the pallial part of the telencephalon dissected out under a binocular microscope. For each embryo two body pieces were also collected for genotyping, paying attention to wash the chirurgic material in 70% ethanol between sample dissection in order to avoid DNA contamination.

Dissected brain tissues were placed in 6 multi-well plastic plates (1well: 1embryo) containing 2 ml cold PBS and then cut in small pieces with a scalpel. Plates were kept on ice during all the procedure. Cut pieces were then transferred to 15 ml falcon tubes with a plastic Pasteur pipet. After adding fresh cold PBS (10 ml final volume) tubes were centrifuged 5' at 100g, supernatant removed, and an additional wash performed with 5-8 ml of control medium [Dulbecco's Modified Eagle Media (DMEM)/F12 (1:1), 2mM L-glutamine, 0.1% sodium bicarbonate, 5mM Hepes, 1% antibiotic/antimycotic solution (all from Invitrogen), 0.1% primocin (Invivogen) and 0.6% glucose (Sigma)] followed by a

centrifugation (5' at 100g). To obtain single cell suspensions, pellets were then mechanically disgregated with a fire-polished Pasteur pipette in 3 ml control medium. Three to five ml control medium were added to the suspension, and cells were collected by centrifugation (10' at 200g). Pellets were resuspended in 4 ml pre-warmed complete medium [control medium supplemented with 1% N2 (Gibco), 0.4% Bovine Serum Albumin (BSA) (Sigma), 2µg/ml heparin (Sigma), 20ng/ml EGF (Invitrogen), 10ng/ml FGF_2 (Sigma)], transferred to 25ml plastic flasks and incubated at 37ºC, 7.5%CO_2 and 100% humidity. Cells with progenitor properties are able to proliferate giving rise to clonal aggregates of cells, called neurospheres. When the diameter of the neurospheres reached around 50-100µm (between 2 and 5 *days in vitro*, DIV, depending on the conditions) cultures were passaged as follows. Neurospheres were transferred to 15ml falcon tubes and collected by centrifugation (5' at 100g) after addition of 5 ml pre-warmed control medium. To obtain single neurosphere cell suspensions, pellets were mechanically disgregated in 200µl of control medium by passing through a p200 micropipette tip (around 80 strokes). A Neubauer Chamber was used to check the correct disgregation of the neurospheres and to determine the total number of viable cells by Trypan Blue exclusion. After adding 5-8 ml of pre-warmed control medium, single neurosphere cells were collected by centrifugation (10' at 200g). Pellets were accurately resuspended in 1 ml of pre-warmed complete medium and neurosphere cells were then plated at a final density of 10^5 viable cells/ml to generate new neurospheres. In some neurosphere cultures, cells were grown in complete medium containing only the mitogen EGF or the mitogen FGF.

We consider primary neurospheres those directly obtained from the disgregated tissue and secondary neurospheres those obtained after

disgregation, or passage, of cultured neurosphere cells. Passage (p) of primary neurospheres, is called p0 and gives rise to the first generation of secondary neurospheres (p1 secondary neurospheres). These neurospheres generate upon passage the second generation of secondary neurospheres (p2 secondary neurospheres), and so on (Fig M1). All the studies performed in this work were done using p2 or p3 secondary neurospheres.

To generate cumulative cell growth curves, the number of cells counted at each passage was multiplied by the number of cells at the previous passage. All numbers were then normalized by the number of cells counted at p0 in order to avoid bias due to differences in the number of cells recovered from the starting tissue.

To obtain total DNA, RNA or protein, neurosphere cells were collected by centrifugation (10' at 100g) and pellets stored at -80ºC.

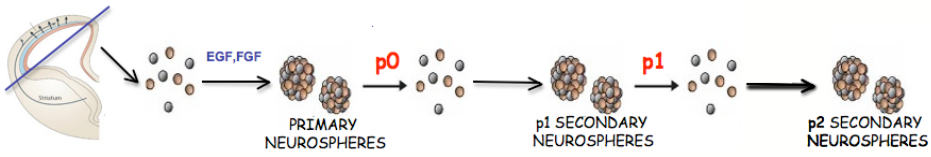

Fig M1: Establishment and passage of neurosphere cultures. Embryonic cortices are disgregated and cultured in the presence of mitogens to allow progenitor cells to generate primary neurospheres. Passage of primary neurospheres (p0) gives rise to p1 secondary neurospheres, which will form p2 secondary neurospheres upon further passaging. (Adapted from Ferron et al., 2007).

2.1. Self-renewal assay

To assess neurosphere self-renewal capability, meaning the capability of single neurosphere cells to originate new neurospheres, we

set up low-density cultures. In these cultures, single neurosphere cells were grown in complete medium at a density of 10^4 cells/ml in 24 multi-well plates (300µl of cell suspension per well), and incubated as described above. In order to avoid drying of the culture, no cells were plated in wells of the plate perimeter that were, instead, filled with control medium. Upon these conditions, small and medium neurospheres, of approximately 30-70 and 70-120 µm respectively, could be observed at 5 DIV together with single cells that did not generate a new neurosphere. Plates were shacked and bright field pictures that include all neurosphere were taken at 5-6 DIV with a Zeiss Observer.Z1, using a Pan-APO 20x objective. Pictures were used to count the number of neurospheres formed (parameter that allowed us to evaluate the self-renewal capability of neurosphere cells) and to determine neurosphere diameter (indicative of the proliferation and survival characteristics of the neurosphere forming cells). Measurements were performed with the ImageJ program: the “cell counter” toll was used to estimate neurosphere numbers and the “measure” tools to measure neurosphere diameters after scale setting. For these quantifications we excluded; (i) doublets, triplets or quartets of cells, probably representing aggregates of individual neurosphere cells without self-renewal capability and (ii) neurospheres bigger than 120-130µm, probably representing neurospheres that were not well disgregated in the previous passage. Differences between genotypes were considered significant for pValues$<$0.05 in a two-tailed Student’s t-test.

2.2. Differentiation assay

To analyze the multipotency of neurosphere cells, a property that allows single neurosphere cells to differentiate into neurons, astrocytes

and oligodendrocytes, we used the following protocol. Single sphere cells were cultured in differentiation medium-I (complete medium without EGF), onto matrigel (BD Biosciences) pre-treated coverslips for two days (37ºC, 7.5% CO_2). Afterwards, medium was replaced with differentiation medium-II (complete medium without neither EGF nor FGF_2 and supplemented with 10% FBS) and cells cultured for 5 more DIV before fixing.

Cultures were fixed 15' with 4% PFA in PBS at RT, then rinsed with PBS and stored at 4ºC until performing IF stainings, following the procedure described in section 1.2.2. Coverslips were mounted with Vectashield or Mowiol mounting mediums and pictures of around 20 fields, evenly distributed within the total coverslip area, were taken with a 40x objective in the Zeiss Observer.Z1, with an AxioCam MRm camera. Cell counts were performed with the "cell counter" tool of the ImageJ program, on pictures taken from at least 2 coverslips per culture. All healthy cultures derived from the same litter and differentiated at the same step and with the same conditions were included in one experiment. Cultures of the same experiment were immunostained in parallel and pictures were taken at the same exposure to reduce technical variability. Total nuclei were then counted in all photographed fields of each culture and the average total cell number per field calculated. Fields with a total number of nuclei outside the range (average nuclei ± 30% average nuclei) were discarded. For the fields included in this range, immunopositive cells for a specific marker were counted and the total number of immunopositive cells in each culture expressed as percentage of the total number of nuclei. Differences between genotypes were considered significant for $pValue<0.05$ in a two-tailed Student's t-test.

3. Gene expression analysis

3.1. RNA extraction

Postnatal P0 and P7 littermate mice were sacrificed by decapitation and total brains extracted. Cerebral cortices (including both the dorsal and ventral parts) were dissected out and stored at -80ºC. Samples were homogenized with a Polytron and total RNA extracted with TriPure Isolation Reagent (Roche). A step of RNA clean-up was performed using RNeasy Mini Kit (Qiagen) and a final step of DNAse treatment was done (DNAse from Ambion). RNA extraction and purification steps were done according to the manufacturers instructions. RNA quality was assessed with an Agilent 2001 Bioanalyzer and RNA was quantified using a NanoDrop (Agilent), before storage at -80ºC.

3.2. Microarray hybridization

Microarray hybridizations were carried out at the Microarray unit of Vall d'Hebron Hospital of Barcelona according to the following experimental design: eight animals per developmental stage, P0 and P7, were collected, half of which were wild types (*Dyrk1a*$^{+/+}$) and the other half mutants (*Dyrk1a*$^{+/-}$). To avoid litter-specific biases, each experimental group was composed in equal parts by animals from 2 different litters. To reduce experimental variability total RNAs from the 16 samples were obtained at the same day. cRNAs were hybridized in Mouse Genome 430.2.0 (Affimetrix) chips in two separated experiments, each including one sample per experimental condition.

3.3. Microarray data analysis

Analysis of the array data was performed by M. Carme Ruiz de Villa, Israel Ortega and Alex Sanchez in the "Statistics and Bioinformatics Research Group" at the Departament d'Estadistica, Universitat de Barcelona. The images obtained from microarray hybridization were processed with the Microarray Analysis Suite 5.0 software (Affymetrix) and raw expression values were analyzed using the RMA method (Irizarry et al., 2003) that allows background correction and normalization of probe values. These normalized values were filtered to increase the statistical power and reduce unnecessary noise. The first filtering step, accounting for the elimination of around 70% of the probes, consisted in keeping only genes that were expressed, defining as "expressed" those genes whose signal reached a minimum threshold that was arbitrary established as the third quartile of all normalized expression values. Among the 12,674 expressed genes left after the first filtering, only genes that showed certain variability among the 4 experimental conditions were kept for further analysis. In our case this meant keeping only those genes for which the standard deviation of the expression was greater than the third quartile of all standard deviations. This second filtering process of the data left a total of 3,169 genes that were further analyzed. To determine the statistical significance of gene expression differences, adjusted p values (adj-pValues here on) were calculated according to Smyth's empirical Bayes moderation of the variance (Smyth, 2004) plus BH's correction (Benjamini and Hochberg, 1995).

A more detailed bioinformatic analysis of the differentially expressed genes was carried out in collaboration with Ionas Erb and Cedric Notredame at the CRG. DNA scanning was performed with the Matscan program (Blanco et al., 2006), while Jaspar and Transfac databases

were used to obtain transcription factors (TF) consensus sequences (Matys et al., 2006; Portales-Casamar et al., 2010). The following public databases were routinely used to integrate information about gene sequences and functions: Ensemble (http://www.ensembl.org) and NCBI (http://www.ncbi.nlm.nih.gov).

3.4. RT-qPCR

Total RNA was extracted from early postnatal and young adult mouse brain tissues as described in section 3.1. In the case of embryonic brain tissues and neurosphere cultures, total RNA extraction was performed with RNeasy Mini Kit (Qiagen) according to the manufacturer's instructions. cDNAs were synthesized from 1µg of total RNA using Superscript II retrotranscriptase (Invitrogen) and random examers. Real-time qPCR was carried out with the Lyghtcycler480 platform (Roche), using SYBR Green I Master kit (Roche). cDNAs were diluted 1:10 and the reagents were mixed according to the manufacturer recommendations. PCR conditions used were the following: one cycle: 95°C 5'; 45 cycles: 95°C 10", 60°C 10", 72°C 10"; one cycle: 95°C 5", and a final cycle: 65°C 1'. Primers for RT-qPCR, listed in table M3, were designed using the "Primer3" free tool (http://frodo.wi.mit.edu/cgi-bin/primer3/primer3) in order to obtain amplicons of 80-130 bp, and optimal annealing temperatures between 59 and 61ºC for each primer pair.

Data were analyzed on the basis of the crossing temperature (ct) values obtained, according to the Pfaffl Method (Pfaffl, 2001) using *Peptidyl-prolyl isomerase a (Ppia)* or *Beta-actin (Actb),* as reference genes for data normalization. Differences were considered significant for pValues<0.05 in a two-tailed Student's t-test.

Table M3: List of primers used for RT-qPCR

Primer	5'-3' sequence
Dyrk1 Ex3-F	ATCCAGCAACTGCTCCTCTG
Dyrk1 Ex4-R	CCGCTCCTTCTTATGACTGG
Rest-F	CGCTGTGGCTACAATACCAA
Rest-R	CAGGTGTTTCCTCCAGTGGT
Actb-F	CAACGGCTCCGGCATGTGC
Actb-R	CTCTTGCTCTGGGCCTCG
Mbp-F	CTTCAAAGACAGGCCCTCAG
Mbp-R	CCAGGTACTTGGATCGCTGT
Gfap-F	GTTACCAGGAGGCACTTGCT
Gfap-R	GTAGGTGGCGATCTCGATGT
Ppia-F	ATGGCAAGACCAGCAAGAAG
Ppia-R	TTACAGGACATTGCGAGCAG
S100b-F	GACTCCAGCAGCAAAGGTGAC
S100b-R	CATCTTCGTCCAGCGTCTCCA
Calb1-F	CCACCTGCAGTCATCTCTGA
Calb1-R	GCTCCTGGATCAAGTTCTGC
Aqp4-F	TTGACATTGACCGTGGAGAA
Aqp4-R	GAGGCCAGGTCTAGGGAGTC

F= Forward primer, R= Reverse primer.

3.5. Low Density Array (LDA)

RNAs were extracted from embryonic and postnatal mouse brain tissues as described in section 3.4. cDNAs were synthesized from 0.5µg of total RNA using MultiScribe retrotranscriptase and random primers (High Capacity cDNA Reverse Transcription Kit, ABI), according to the manufacturer recommendations. For quantitative analysis, the obtained cDNAs were diluted 1:10 in H_2O, added to TaqMan® Universal PCR Master Mix (ABI) in a 1:1 ratio and charged into the LDA, pre-loaded with the TaqMan® Gene Expression Assays chosen by the costumer. The TaqMan Array was then run on the 7900HT system (ABI) following the

manufacturer's instructions. Data were analyzed with SDS software (ABI), based on the Pfaffl Method, as explained in the previous section (Pfaffl, 2001).

4. DNA pyrosequencing

DNA methylation experiments were performed in collaboration with Mario Fraga's laboratory, Centro Nacional Biotecnología (CNB)/ Consejo Superior de Investigaciones Científicas (CSIC). Genomic DNA was obtained from frozen embryonic and newborn mouse cerebral cortices using a phenol/chlorophorm- based extraction method (Hogan, 1986). Genomic DNA from neurosphere cells was extracted from frozen samples with phenol/chlorophorm, after RNase-A treatment and overnight proteinase-K incubation. In all cases total DNA was resuspended in TE buffer and quantified with NanoDrop. Sodium bisulfite modification of 0.5µg genomic DNA was carried out with the EZ DNA Methylation-Gold Kit (Zimo Research) following the manufacturer's protocol. Bisulfite-treated DNA was used for PCR amplification of the genomic regions of interest (3µl bisulfite-treated DNA in 50µl final volume reaction). The set of primers for PCR amplification and sequencing were designed using a specific software pack (PyroMark assay design version 2.0.01.15). Primer sequences, listed in Table M4, were designed to hybridize with CpG-free sites to ensure methylation-independent amplification. PCR was performed with biotinylated primers in 50 cycles amplification. Biotinylated PCR products were isolated by the use of streptavidin sepharose beads and prepared for pyrosequencing, by denaturing and washing steps, using the Vacuum Prep Tool according to manufacturer's instructions (Biotage, Sweden). Pyrosequencing reactions and methylation quantification (expressed as the percentage of

methylated DNA over total DNA) were performed in a PyroMark Q24 System version 2.0.6 (Qiagen). Differences between genotypes in the percentage of methylated DNA were considered significant for pValues<0.01 in a two-tailed Student's t-test.

Table M4: List of primers used for Pyrosequencing

Primer	5'-3' sequence	Annealing temperature	Amplicon size
S100b(-267)-F	AGAAGTTTTTAGTTTTTGGTTGTAGAT	58°C	207bp
S100b(-267)-R	Btn-CACTAAACAACCACAACTAAACTTAAT		
S100b(-267)-seq	GGTTGTAGATTTGTTGTTTAAATTA		
S100b(+59)-F	TGTATGTAGGTTTGGGTGTTTAA	58°C	192bp
S100b(+59)-R	Btn-TCACCTAATCACCTTTACTACTAA		
S100b(+59)-seq	GAAGAATAAGAAGTTGTTTTG		
Gfap(-1502)-F	AGTGATTTATTTTGGTATAGATATAATGG	60°C	153bp
Gfap(-1502)-R	Btn-TTATCCCAAAATACCAAAATATCAACC		
Gfap(-1502)-seq	GTTGTGTTTTAGGTTTT		

Sets of primers designed to study the CpGs of interest. The position with respect to the transcription start site (TSS) is indicated in parenthesis. Bisulfite- converted DNA was amplified with the Forward (F) and Reverse (R) primers. Annealing temperature and amplicon size for each pair of primers is reported. Btn, biotinylated primers; -seq, sequencing primers.

5. Chromatin Immunoprecipitation (ChIP)

Mouse embryonic cerebral cortices were cut in pieces, as described in section 2, to facilitate mechanical disgregation of the tissue. For each sample, pieces were transferred into a 15ml falcon tube, washed by addition of cold PBS up to 5-8ml, and collected by centrifugation (3' at 100g and 4ºC). Pellets were resuspended in 200µl of cold 1% formaldehyde in PBS, and mechanical disgregation was performed in ice using a p200 micropipette (15 strokes). The lysate was transferred to a

2ml Eppendorf tube and 800µl of cold 1% formaldehyde in PBS were added. The sample (or lysate) was left under gentle agitation for 30' in ice to allow cross-linking, and the reaction was then blocked by addition of 100µl glycine 0.125M. After 8' incubation at RT, the cross-linked pellet was collected by centrifugation (10' at 300g and 4ºC) and rinsed twice in PBS (complemented with protease inhibitors, Roche Applied Science) before usage for the following steps or storage at -80ºC. Pellets were resuspended in 1.2ml of IP buffer (0.5% sodium dodecyl sulphate (SDS), 100mM NaCl, 50mM Tris-HCl pH8.1, 5mM EDTA, 5% Triton-X100) complemented with protease inhibitors and sonicated in a Bioruptor device (Diagenode). The following sonication conditions were used to obtain 200-500bp DNA fragments: 6 cycles 30''ON/30''OFF, maximum output at 4ºC. Sheared chromatin was separated from cellular debris by centrifugation (20' maximum speed, 4ºC) and the supernatant was kept for the immunoprecipitation (IP) reaction. Total protein amount in the chromatin sample was determined with Bradford reagent (Sigma), and 200µg of total protein were used for each IP, that was carried out in an Eppendorf tube, overnight under rotation, at 4ºC. Ten percent of the volume used for the IP was stored (input) at 4ºC. All antibodies and the corresponding experimental conditions used in this work are listed in Table M5; IPs obtained with rabbit IgGs were used as negative control and IPs obtained with a histone H3 antibody were used to normalize data (see below).

Table M5: List of antibodies used for ChIP

Antibody	Host	Working condition (per IP reaction)	Source
H4K16Ac	Rabbit	5µg	Active Motif
H3K4me3	Rabbit	5µg	Diagenode
H3K9me3	Rabbit	3µg	Abcam
H3K27me3	Rabbit	5µg	Millipore
H3	Rabbit	3µg	Abcam

The day after the incubation, 30µl of protein A- sepharose beads (GE Healtcare) previously dissolved in IP buffer (complemented with protease inhibitors) were added to each IP reaction and collected by gentle centrifugation (3' at 800g). The immune complexes were rinsed three times in low salt buffer (50mM HEPES pH7.5, 140mM NaCl, 1% Triton-X100) complemented with protease inhibitor and once in high salt buffer (50mM HEPES pH7.5, 500mM NaCl, 1% Triton-X100) complemented with protease inhibitor. Chromatin was finally eluted in 110µl elution buffer (1% SDS, 100mM $NaHCO_3$ in H_2O) by agitation of the tubes in a Thermoblock at 1000 rpm for 3 hours at 65ºC. The elution step was also performed for the inputs. After centrifugation (3' at 800g) 100µl of the eluted chromatin were collected from the supernatant and cleaned with Qiaquick PCR purification Kit (Qiagen) according to the manufacturer's instructions. Purified chromatin was eluted in 100µl water and stored at -20ºC before usage for qPCR. Five µl of chromatin were run in 1% agarose gel to check chromatin fragments size.

Enrichment was assessed by qPCR, performed in triplicate and using 2µl of eluted chromatin, following the procedure described in section 3.4. The primers used for qPCR are reported in Table M6.

Table M6: List of primers used for qPCR in ChIP experiments

S100b(-267)-F: ACAGTCTC CAGCACTCAGCA
S100b(-267)-R: GAGTCAGCTTCTCTGCACCTT
S100b (+59)-F: CCCA CACCCAGTTCT CTCTG
S100b (+59)-R: AAAAAGCAGGTTTTCT CTTGG
Gfap(-1502)-F: TAAGCT GAAGACCTGGCAGTG
Gfap(-1502)-R: GCTGAATAGAGCCTTGTTCTC

Enrichment was estimated according to the Pfaffl Method (Pfaffl, 2001) using the input ct as calibrator. Final values were normalized by the total quantity of Histone H3. Differences between genotypes in the enrichment of specific histone mark over total histone H3 were considered significant for pValues<0.05 in a two-tailed Student's t-test.

6. Protein manipulation techniques

6.1. Sample preparation

Mouse brains were collected after cervical dislocation, in case of young adult animals, or decapitation, in case of embryos or early postnatal animals, and immediately frozen in dry ice. Whole extracts from frozen mouse brain tissues were prepared by resuspending the tissue in SDS-buffer [25mM Tris-HCl pH7.4, 1mM EDTA, 1% (w/v) SDS, 10mM sodium pyrophosphate, 20mM beta-glycerol phosphate, 2mM sodium orthovanadate, 2mM phenylmethylsulphonyl fluoride and a protease inhibitors]. Isolated brains were mechanically homogenized using a Dounze homogenizer (Afora) in 10 volumes of SDS-buffer (1ml buffer/100mg tissue), sonicated with 3 pulses of 15'' each in position 1 of a Branson Sonifier 250, boiled for 15' at 98ºC and centrifuged for 10' at 800g at RT. Protein concentration was determined using a colorimetric

assay (BCA Protein Assay Kit, Pierce) according to the manufacturer's indications.

Neurosphere extracts were prepared in 200µl SDS-buffer from the pellet obtained by centrifugation of 5ml confluent secondary cultures. Samples were boiled for 15' at 98ºC and centrifuged for 5' at 16,000g at RT.

6.2. Western Blot analysis

Protein extracts (30 to 80µg) were mixed with 6X Laemmli buffer (0.5M Tris-HCl pH6.8, 12% (w/v) SDS, 60% (v/v) glycerol, 0.6M dithiothreitol, 0.06% bromophenol blue), heated for 5' at 98ºC and resolved on SDS-PAGE gels of different acrylamide percentage, depending on the molecular weight of the protein, at 30 mA in 1x running buffer (25mM Tris-base, 200mM glycine, 0,1% (w/v) SDS). Proteins were transferred onto a nitrocellulose membrane (Hybond-ECL, Amersham Biosciences) at 400 mA for 60' at 4ºC in 1x transfer buffer (25mM Tris-HCl pH8.3, 200mM glycine, 20% (v/v) methanol) and protein transfer was then checked by staining with Ponceau (Sigma). Transferred membranes were blocked for 60' at RT in 10% (w/v) skimmed milk in TBS-T (10mM Tris-HCl, pH7.5, 100mM NaCl, and 0.1% Tween-20), and then incubated overnight at 4ºC with the corresponding primary antibody diluted in 5% skimmed milk in TBS-T. The list of antibodies used for western blot is reported in Table M7. After two washes of 20' with TBS-T, membranes were incubated for 60' at RT with rabbit anti-mouse (1:2000; Dako), goat anti-rabbit (1:2000; Dako), or goat anti-rat (1:1000; GE Healthcare) IgGs conjugated to horseradish peroxidase diluted in 5% skimmed milk in TBS-T. After two washes of 20' with TBS-T, protein detection was by enhanced chemiluminiscence with ECL or ECL plus Western blotting

detection reagents (Amersham Life Sciences). Chemiluminiscence was determined with a LAS-3000 image analyzer (Fuji Photo Film). Quantifications were done using the Image Gauge software (Version 4.22; Fuji Photo Film) and values were normalized for the levels of glyceraldehyde-3-phosphate dehydrogenase (Gapdh) or Vinculin proteins, or for the intensity of Ponceau staining. Differences between genotypes in protein levels, were considered significant for pValues<0.05 in a two-tailed Student's t-test.

Table M7: List of primary antibodies used for western blot

Antibody	Host	Working dilution	Source
Aqp4	Rabbit	1: 300	Millipore
Dyrk1a	Mouse	1: 250	Abnova
Gapdh	Mouse	1:500	Millipore
Gfap	Rabbit	1:1000	DAKO
Mbp	Rat	1:500	Chemicon
Rest	Rabbit	1:1000	Millipore
Vinculin	Mouse	1: 5000	Sigma

Results

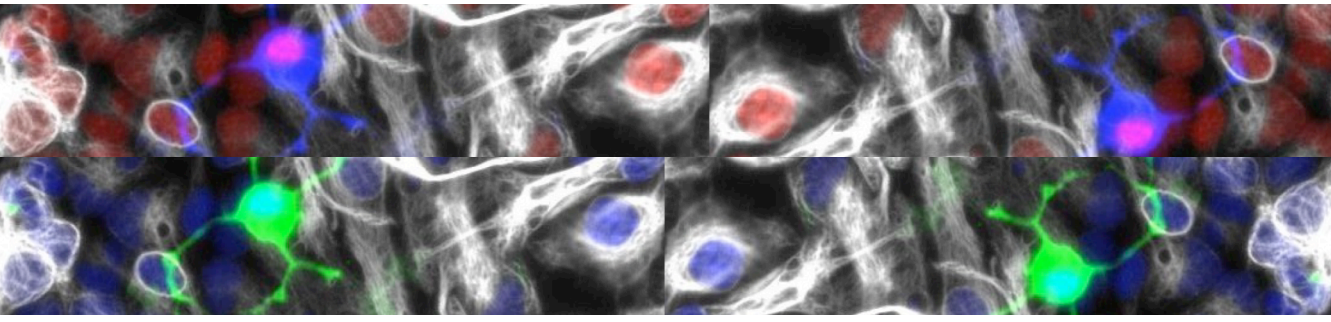

1. Dyrk1a expression in the developing mouse cerebral cortex

The distribution pattern of brain Dyrk1a has been reported (Okui et al., 1999; Martí et al., 2003; Wegiel et al., 2004) but little is known about Dyrk1a protein content and distribution in the developing cerebral cortex. For this reason, we first analyzed the expression of *Dyrk1a* in mouse cerebral cortex at different time points of its development, from E11.5, when the first neurons are generated to P28, when developmental gliogenesis and synaptogenesis are almost complete. The levels of *Dyrk1a* transcripts, determined by qPCR, peaked at late embryonic stages (E16.5) and decreased in the postnatal phase until reaching lower but sustained levels around 1 month after birth. As expected, *Dyrk1a* mRNA levels show a reduction of about 50% in the cerebral cortex of *Dyrk1a*$^{+/-}$ mice at all stages analyzed (Fig R1a).

Western Blot analysis performed on total lysates obtained from postnatal mouse cerebral cortex correlated with the developmental trend observed at the transcriptional level: higher expression of Dyrk1a was observed at P0 compared with the later postnatal stages analyzed, P7 and P28 (Fig R1b).

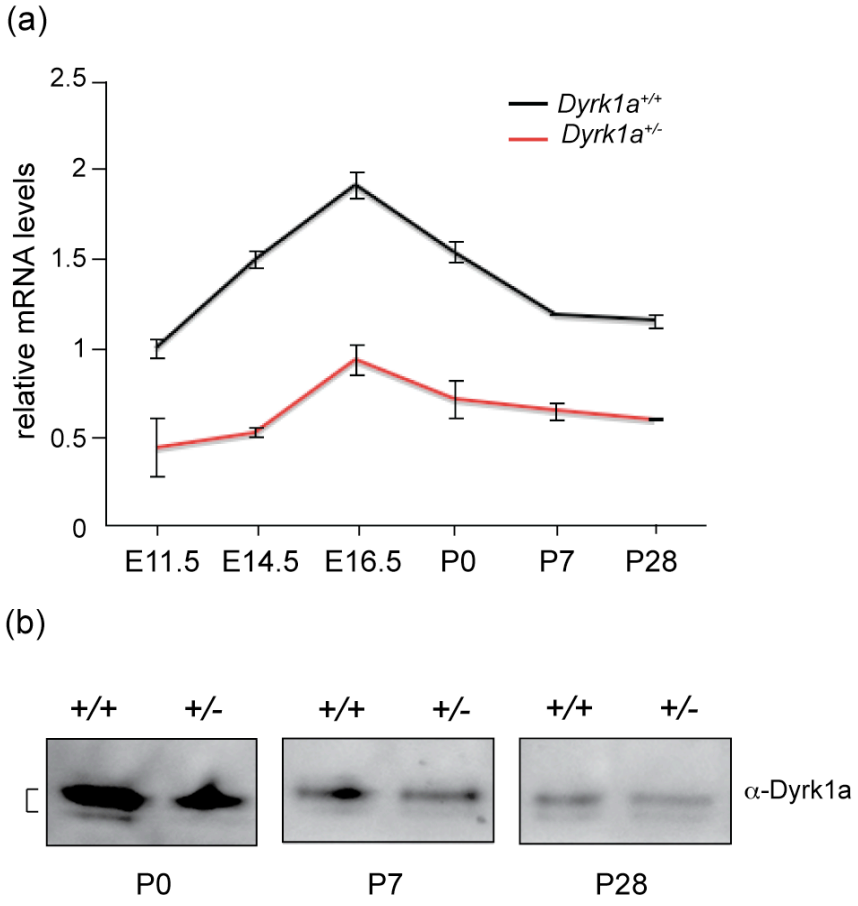

Fig R1: Dyrk1a expression levels in *Dyrk1a*$^{+/+}$ and *Dyrk1a*$^{+/-}$ developing cerebral cortex. (a) *Dyrk1a* mRNA levels in *Dyrk1a*$^{+/+}$ and *Dyrk1a*$^{+/-}$ mouse cerebral cortex were determined by qPCR at different developmental stages. Values correspond to the mean (±sem) of the relative mRNA levels measured in 4 to 6 animals per condition. Differences between genotypes were statistically significant ($p<0.01$ in Student's T-test) at all time points. (b) Dyrk1a protein levels analyzed by Western Blot in one wild type and one mutant cerebral cortex at indicated developmental stage. Equal amounts of protein (80μg) were loaded in the gel. The characteristic doublet of bands of around 90 kDa corresponding to Dyrk1a protein is indicated by a bracket.

Finally the distribution of Dyrk1a protein in the developing telencephalon was evaluated *in vivo* by immunofluorescence (IF) at P1. As shown in Fig R2, Dyrk1a is expressed in the cerebral cortex, both in dorsal and caudal regions. In the somatosensorial cortex most of the cells express Dyrk1a, both in upper and deeper layers (Fig R2a). In the pyriform cortex Dyrk1a was highly expressed in the cytosol of a population of cells with big nuclei while a population of highly compacted cells seem not to express Dyrk1a (Fig R2b and d). Finally in the *Corpus Callosum* (cortical white matter), very few cells express Dyrk1a (Fig R2c).

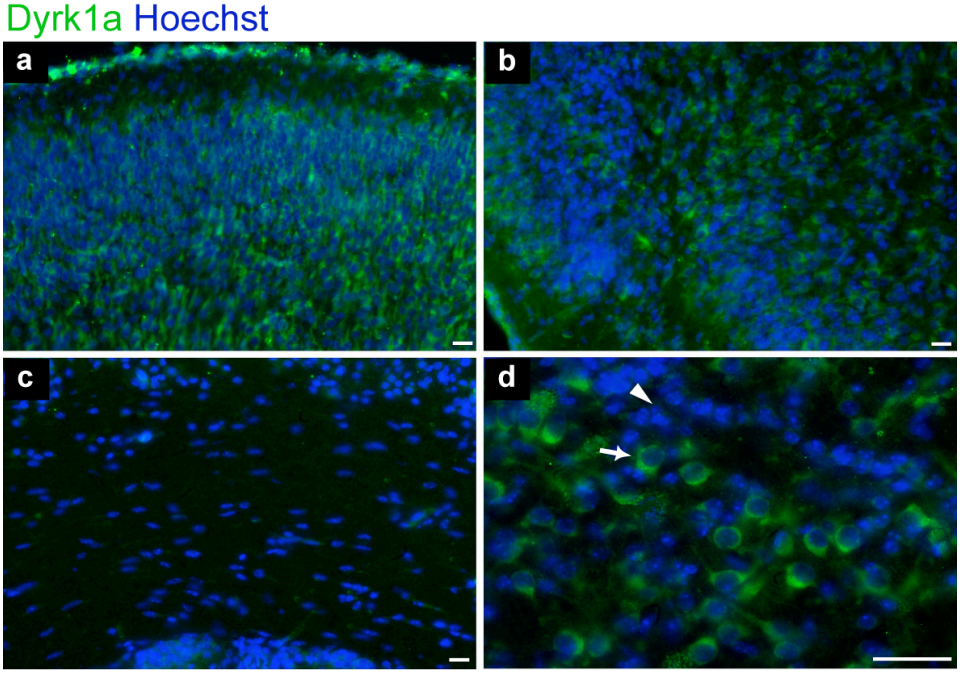

Fig R2: Dyrk1a expression in the developing telencephalon *in vivo*. Dyrk1a immunostaining (green) in coronal brain sections of P1 wild type mice. Sections were counterstained with Hoechst (blue) to label nuclei. (a) Somatosensorial cortex; (b) and (d) Pyriform cortex; (c) *Corpus Callosum*. The arrow in (d) indicates an example of cell with cytosolic Dyrk1a staining, while the arrowhead a cells immunonegative for Dyrk1a. Scale bars: 20μm.

2. Effects of *Dyrk1a* dose reduction on the transcriptome of the developing mouse cerebral cortex

Being Dyrk1a a kinase which is in the cross road of different signaling pathways we hypothesized that it may contribute to cortical development through the interaction with components and/or regulators of intracellular signaling pathways that are relevant for this process. Taking into account that, i) the outcome of intracellular signaling is the modulation of gene expression, ii) some transcription factors are substrates of Dyrk1a, and iii) Dyrk1a is highly expressed during cortical development (see results in Fig R1 and R2) we reasoned that gene expression profiles of the cerebral cortex of *Dyrk1a*$^{+/+}$ and *Dyrk1a*$^{+/-}$ mice could be different.

2.1. Microarray gene expression analysis of *Dyrk1a*$^{+/+}$ and *Dyrk1a*$^{+/-}$ postnatal cerebral cortices

To investigate whether or not *Dyrk1a* dose reduction affects the transcriptome of the cerebral cortex, we used Affymetrix chips and compared the gene expression profiles of *Dyrk1a*$^{+/+}$ and *Dyrk1a*$^{+/-}$ cortices at two developmental stages, P0 and P7. At these stages the cerebral cortex is leaving the neurogenic phase and entering the gliogenic one (Sauvageot and Stiles, 2002).

As summarized in Fig R3, the experiment was designed in order to minimize possible differences intra- and inter-litters, not related to the genotypes.

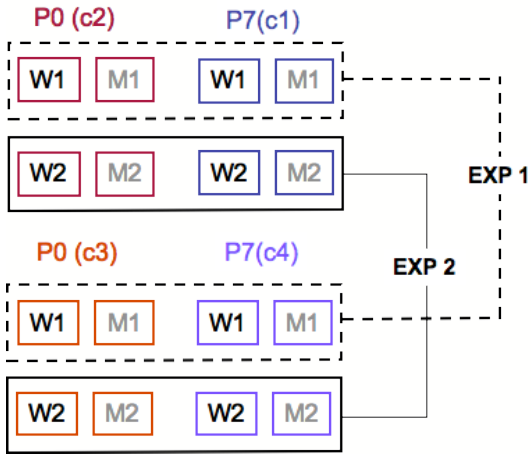

Fig R3: Experimental design of microarray gene expression analysis. Two wild type (W, *Dyrk1a*$^{+/+}$) and 2 mutant (M, *Dyrk1a*$^{+/-}$) animals were collected from 4 different litters at 2 different developmental stages: P0 (litters c2 and c3) and P7 (litters c1 and c4). For each experimental condition (P0W, P0M, P7W and P7M) two samples, one for litter, were included in experiment 1 (EXP 1, dashed line) and two samples in experiment 2 (EXP 2, continuous line). W1 and M1: wild type and mutant samples used for EXP1; W2 and M2: wild type and mutant samples used for EXP2. Additional details on the experiment design and the preparation of the samples can be found in the Methods section.

2.1.1. Bioinformatic analysis of the differentially expressed genes

Microarrays hybridizations produced reliable data, as indicated by the evaluation of quality control parameters recommended by the manufacturer. The first approach we used to analyze row data (signals from the around 45,000 Affymetrix probes) was the Principal Components Analysis (PCA) that allows to globally visualize the distribution of the samples according to their gene expression profile. Given the nature of the PCA method, the first component of the analysis explains more than the second one, that explain more than the third one, and so on. The plot in Fig R4 represents the first two principal components (PC1 and PC2) of the PCA analysis performed on the

obtained microarray data. The clearest evidence that came up by analyzing the overall distribution of the samples was that time is the factor that mainly influences gene expression, as shown by the separation of P0 and P7 clusters along the x-axis, which is the first component of the analysis and accounts for the 65% of the differences between samples. This finding is not surprising given that development implies deep changes in gene expression (Potier et al., 2006). Interestingly the main source of sample clustering within each developmental stage is the genotype. This finding supports the hypothesis that *Dyrk1a* dose reduction has an impact on gene expression in the developing mouse cerebral cortex.

Sample distribution along the Y-axis of the PCA plot, which accounts for 14% of the differences between samples, tells us that experimental variability represents an additional determinant of sample distribution. In fact, within each developmental stage, samples from the same experiment tend to cluster together: all samples included in EXP1 distribute in the upper half of the PCA plot while those included in EXP2 in the lower half (Fig R4). Nevertheless, both experiments reproduced the trend described above, with development being the first and genotype the second determinant of gene expression variability (circles in Fig R4). Circles are more extended at P0 than at P7 indicating a higher variability within each experimental group at P0. In addition, and as indicated by the separation between circles in the plot, differences between wild types and mutants were bigger at P0 than at P7. No litter bias was observed, indicating that the effects of time (developmental stage) and genotype on gene expression programs are robust.

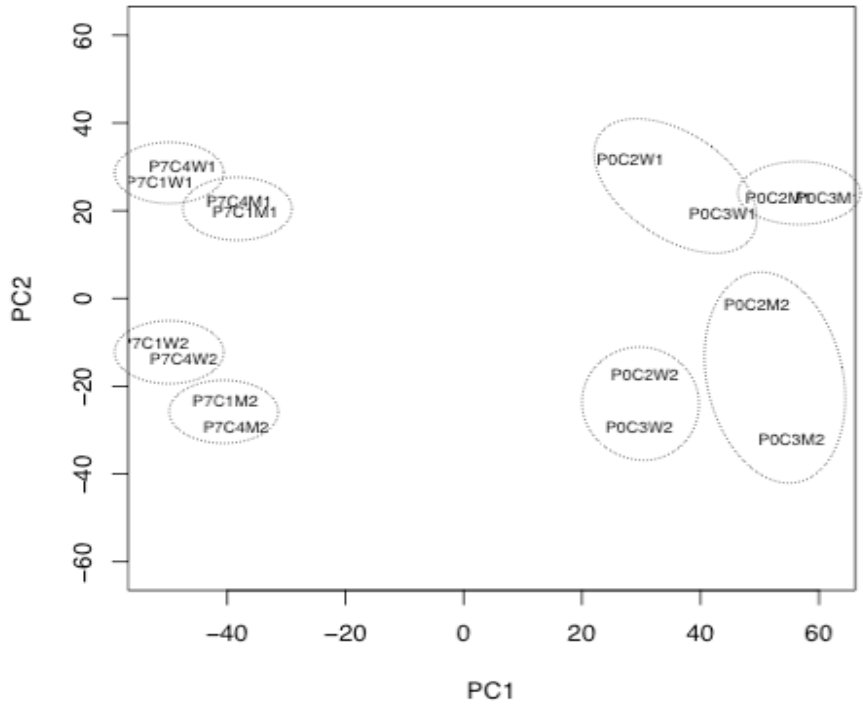

Fig R4: Plot of the first two components of the Principal Component Analysis (PCA) obtained from raw microarray data. Sample distribution is explained by x-axis, representing the first component of the analysis (PC1) and accounting for 65% of the differences between samples, and y-axis, representing the second component of the analysis (PC2) and accounting for 14% of the differences between samples. Sample distribution along the x-axis indicates that sample first clustered according to their developmental stage (P0 and P7) and then, within the same P0 or P7 stage, they clustered according to their genotype, *Dyrk1a*$^{+/+}$ (W) and *Dyrk1a*$^{+/-}$ (M). Sample clustering is also influenced by the experimental condition, EXP1 and EXP2, as further indicated by sample distribution along y-axis. No litter (c1- c2- c3- c4) associated clustering is observed. Circles indicate clustering of the same genotype within each time point (P0 and P7) and experiment (EXP1 or EXP2).

For further analysis of the microarray results only filtered data were used, as detailed in Methods, section 3.3. Considering the 4 experimental situations (P0W, P0M, P7W, P7M) the following comparisons were performed with the 3,169 filtered genes: 1/ mutants *versus* wild types at P0 (P0-MvsW); 2/ mutants *versus* wild types at P7

(P7-MvsW); and 3/ wild types at P7 *versus* wild types at P0 (W-P7vsP0). Comparisons 1 and 2 allowed the identification of genes whose expression is altered due to *Dyrk1a* dose reduction, while comparison 3 defined the developmental trend of the analyzed genes. Setting a threshold of adj-pValues<0.05 (calculated as reported in Methods, section 3.3.), 707 genes, representing 22% of the genes analyzed, showed differential expression between wild type and mutant mice at P0 and 156, representing 5% of the genes, at P7. The majority (87%) of the 3,169 genes analyzed, undergo significant changes in expression between P0 and P7 in the wild type condition (Fig R5a). The complete list of the 3,169 genes can be found in the provided CD, while the 25 genes showing the most significant changes in gene expression in comparisons 1 and 2, are listed in Table A1 in the Appendix.

Most of the changes in gene expression observed in the mutant condition were stage specific and only 61 genes from the 3,169 genes analyzed were found differentially expressed at both P0 and P7 (Fig R5b and Table A2 in the Appendix).

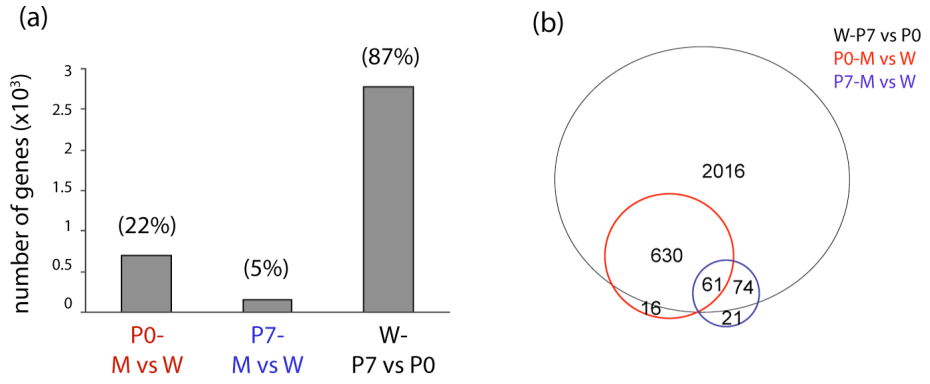

Fig R5: Numbers of the differentially regulated genes. Only genes with an adj-pValue<0.05 were considered for the analysis**.** (a) The histogram shows the number of differentially regulated genes in each comparison: mutant *vs* wild type at P0 (P0-MvsW), mutant *vs* wild type at P7 (P7-MvsW) and wild type at P0 *vs* wild type at P7 (WT-P7vsP0). Numbers in parenthesis are the number of genes expressed as percentage of the 3,169 total genes analyzed. (b) Venn diagram of the same numbers as in (a). The number of genes belonging to each intersection is reported.

Next, we asked how *Dyrk1a* dose reduction influenced the transcriptional program of the postnatal developing cortex. To this end we plotted, in log2 scale, the gene expression fold changes (FC) of the mutant cortices relative to the wild type cortices at one particular developmental stage, P0 or P7; against the gene expression FC obtained for the same set of genes when comparing P0 and P7 wild type cortices (Fig R6). FCs in gene expression due to *Dyrk1a* dose reduction are in most cases between 0.26 and 0.67 (y-axis), which means a difference of gene expression between 20 and 50% between genotypes. The transcriptional changes found in the mutants were slighter than changes provoked on the same genes by the normal developmental process. In fact, gene expression FCs between P0 and P7 in the wild type condition, reported in the x-axis, were in most cases higher than 50%. A further conclusion emerging from this plot is that *Dyrk1a* dose reduction caused both up- and down-regulation of gene expression, as indicated by the even distribution of genes in both positive and negative quadrants of the y-axis. The most evident observation emerging from the analysis of gene distribution was that genes whose expression increased between P0 and P7 in the wild type tissues were found down-regulated in the mutant tissues compared to their wild type controls and *vice-versa* (see Fig R6). This strong anti-correlation suggested that the lack of one functional copy of *Dyrk1a* causes a delay in the transcriptional program that governs

cortical development.

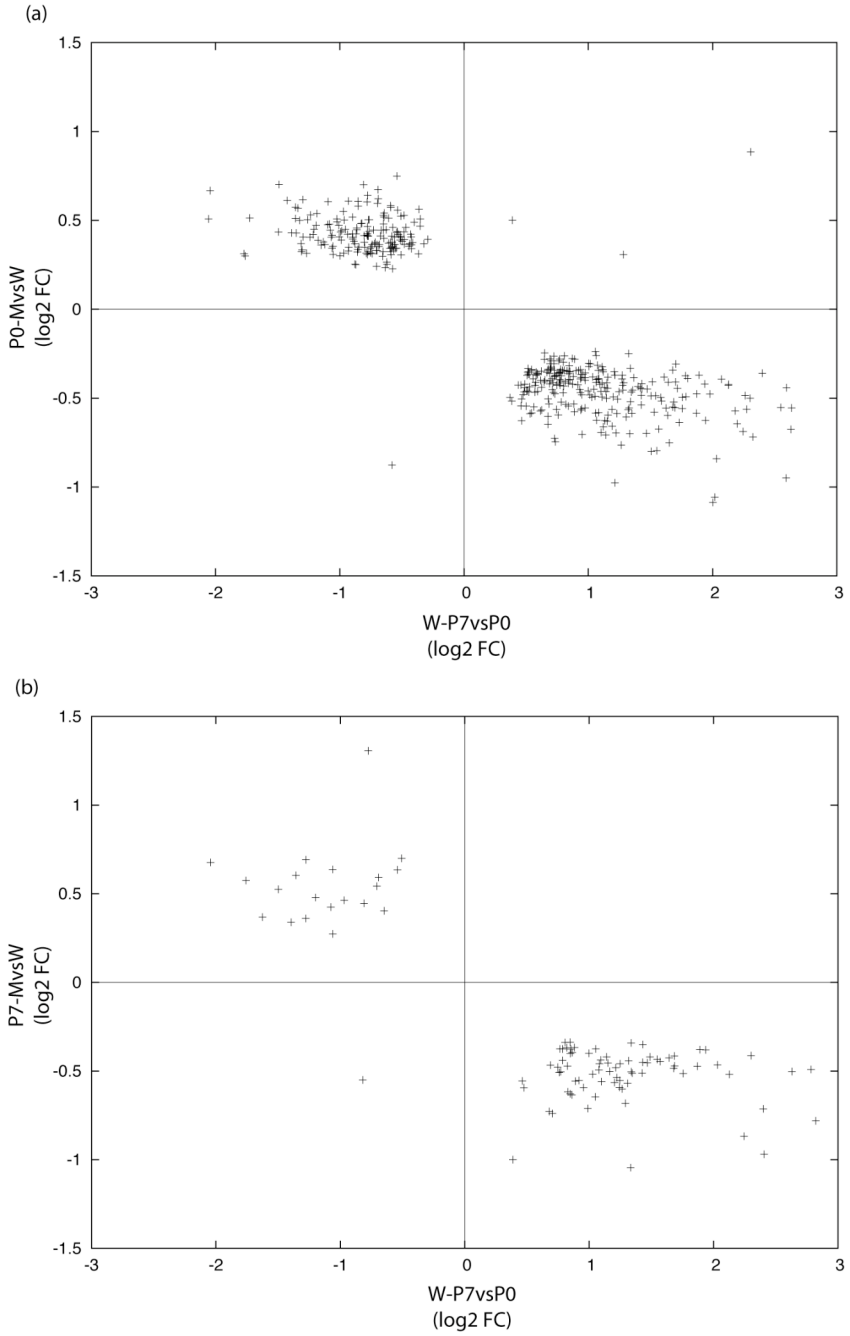

Fig R6: Effect on global gene expression of both development and *Dyrk1a* dose reduction in the cerebral cortex of postnatal mice. Values in y-axes indicate the differences in gene expression (with adj-pValue<0.05) between the cerebral cortex of *Dyrk1a*$^{+/-}$ mutant (M) *and Dyrk1a*$^{+/+}$ wild type (W) animals at P0 (P0-MvsW, upper panel) and at P7 (P7-MvsW, lower panel). The developmental changes that the same genes undergo between P0 and P7 in wild type conditions are reported in the x-axis (W-P7vsP0). Fold changes (FC) in gene expression are reported in log2 scale in each comparison; positive values are up-regulated genes, and negative values are down-regulated genes. Notice that almost the totality of genes is distributed in quadrants that have opposite sign for the two comparisons analyzed.

2.1.2. Biological features of the microarray results

To have some functional information of the genes that were differentially expressed in the *Dyrk1a*$^{+/-}$ cortices we first performed a Gene Ontology (GO) enrichment analysis. GO is a hierarchically organized database containing annotations that describe molecular functions (MF), biological processes (BP) and cellular components (CC) associated with individual genes (Ashburner et al., 2000). Enrichment in specific GO categories was evaluated by comparing the set of differentially expressed genes with an adj-pValue<0.05, with a set of reference genes, which in our case were all the genes present in the array. The most significant GO categories that appeared among the up- and down-regulated genes, at both P0 and P7, are listed in Table A3 in the Appendix. The set of down-regulated transcripts, at P0 and P7, was mainly enriched in genes coding for binding molecules and transporters. Conversely, genes coding for nucleic acid binding molecules were the most represented among the up-regulated genes at both developmental stages.

We next performed the KEGG Pathway analysis with the goal of highlighting cellular pathways and processes involving the differentially expressed genes (adj-pValue<0.05). Genes that were differentially

expressed in the mutants were enriched, at both P0 and P7, in genes coding for components of: i) the glucose metabolism; ii) the JAK-STAT signalling pathway, which plays a pivotal role in immune response and cancer (reviewed in Yu et al., 2009) as well as in developmental neural cell fate (Bonni et al., 1997); and iii) the PPAR signalling, which controls important metabolic pathways involved in lipid and energy metabolism (Chawla et al., 2001; Krey et al., 1997) (see Table R1).

Table R1: KEGG pathway analysis of the differentially expressed genes in *Dyrk1a*$^{+/-}$ cerebral cortices

P0-MvsWT

KEGG ID	P-value	Exp count	Count	Pathway
04080	0.00146	4.93	12	Neuroactive ligand-receptor interaction
00010	0.00148	1.07	5	Glycolysis/Gluconeogenesis
05210	0.0046	1.72	6	Colorectal cancer
04630	0.00511	0.787	4	Jak-STAT signalling
00562	0.00822	0.533	3	Inositol Phosphate metabolism
04620	0.00968	0.501	3	Toll-like receptor signalling
04662	0.0147	0.573	3	B cell receptor signalling
05218	0.0217	1.15	4	Melanoma
05214	0.0395	1.36	4	Glioma
03320	0.0459	1.47	4	PPAR signalling

P7-MvsWT

KEGG ID	P-value	Exp count	Count	Pathway
00710	0.000668	0.501	4	Carbon fixation
00251	0.00306	0.358	3	Glutamate metabolism
00400	0.00499	0.143	2	Phe, Tyr and Thr biosynthesis
05030	0.0143	0.215	2	Amyotrophic lateral sclerosis
00910	0.0143	0.215	2	Nitrogen metabolism
00330	0.0143	0.215	2	Arginine and Proline metabolism
00272	0.0143	0.215	2	Cysteine metabolism
00010	0.0147	0.573	3	Glycolysis/Gluconeogenesis
04630	0.0215	0.241	2	Jak-STAT signalling
00252	0.0273	0.286	2	Alanine and aspartate metabolism
04150	0.0298	0.284	2	mTor signaling
03320	0.0373	0.787	3	PPAR signalling
00601	0.0433	0.0437	1	Glycosphingolipids biosynthesis

Pathways that were over-represented at P0 are in the upper panel, and those over-represented at P7 in the lower panel. The KEGG ID number is shown in the first column. The second column reports the pValue associated to each ID, calculated with a hypergeometric test. The number of expected genes for each pathway was calculated for the total transcripts included in the array and is reported in the third column. The number of genes belonging to each pathway counted in the set of differentially expressed genes with adj-pValue<0.05, are reported in the forth column. Last column includes the description of the pathway.

It is known that certain diseases are associated with genes that cluster together in defined chromosomal positions (Cooper et al., 2010). In order to see if the differentially expressed genes in the mutants are distributed randomly along the 40 mouse chromosomes, we compared the genomic coordinates of the total genes included in the array with the genomic coordinates of the genes that were differentially expressed with an adj-pValue<0.05. The obtained results (not shown) did not reveal any chromosomal region enriched in up- or down-regulated genes in the cerebral cortex of postnatal *Dyrk1a*$^{+/-}$ mice.

Next, we wanted to investigate if the promoter regions of the differentially regulated genes have characteristics in common. For this reason we searched for key regulatory elements in the promoter region of the 328 up- and 370 down-regulated genes in the mutant condition at P0. The reduced size of the set of up- and down- regulated genes at P7 (111 and 45 genes respectively) precluded the analysis at this developmental time point. Among the elements that we considered in the analysis were: the core promoter element TATA-box; the CCAAT-box and the GC-box, which are regulatory consensus sequences located around 100-150bp upstream the TATA-box; the BRE sequences, which are cis-regulatory elements positioned just upstream the TATA box and are required for the binding of TFIIB and the consequent formation of the pre-initiation transcriptional complex; and MED1 (Multiple start site

Element Downstream1) corresponding to the sequence GCTCC(C/G), which is used for transcriptional initiation in TATA less promoters (reviewed in Riethoven et al., 2010). The analysis, performed with the Matscan program and using a hypergeometric test to asses statistical significance, indicated that neither the number of genes containing a specific promoter element nor the position of these promoter elements relative to the transcription start site (TSS), were significantly different between the up- and down-regulated set of genes (Fig A1 in the Appendix).

Several Dyrk1a interacting Transcription factors (TF) have been described in the literature (reviewed in Tejedor and Hammerle, 2011; Aranda et al., 2011; Park et al., 2009). Thus, we considered reasonable looking for the frequency of TF binding sites in the promoters of genes differentially expressed in the mutant tissue. The analysis was done with the Matscan program looking for the presence of the TF consensus sequences available in Jaspar and Transfac databases and then comparing the enrichment of each TF consensus sequence between the groups of genes that were up- or down-regulated in the mutant cerebral cortices at P0. No striking evidences for enrichment of TF binding sites emerged when analyzing the promoter regions of these genes between positions -400 to +100 (data not shown). Similarly, no significant differences were observed between the two sets of genes when the position of the TF binding sites relative to the TSS was analyzed (data not shown). The lack of differences of particular TF consensus sequences is in agreement with the pleiotropic functions described for Dyrk1a and its interaction with multiple signalling pathways.

Three recent papers described a functional interaction between Dyrk1a and the Repressor Element 1 Silencing Transcription factor

(REST), also named Neuron-Restrictive Silencing Factor (NRSF) (Canzonetta et al., 2008; Lepagnol-Bestel et al., 2009; Lu et al., 2011). Although some contradictory results emerge from these 3 works, all of them suggest that Dyrk1a may act as a transcriptional regulator of *REST*. This factor represses the expression of neuronal genes outside the nervous system but also has a role in lineage commitment and in neural plasticity during nervous system development (Ballas et al., 2005). Our Affymetrix array experiment revealed no differences in *Rest* mRNA levels between control and mutant tissues either at P0 or P7 (see in Fig R7a the results of the 3 *Rest* probes included in the array). To exclude the possibility of a false negative result we performed qPCR experiments to compare *Rest* mRNA levels between *Dyrk1a*$^{+/+}$ and *Dyrk1a*$^{+/-}$ cortices at P0 and at P7. As shown in Fig R7b, no differences between genotypes were observed at the two developmental stage analyzed.

Acute down-regulation of *Dyrk1a* by siRNA decreases the stability of REST in human and mouse cell lines (Lu et al, 2011). For this reason we checked by western blot whether there is any difference in the amounts of Rest between *Dyrk1a*$^{+/+}$ and *Dyrk1a*$^{+/-}$ cerebral cortex at P0. As shown in Fig R8 the levels of Rest protein in control and mutant tissues were almost identical.

The above results indicate that *Dyrk1a* dose reduction in the developing mouse cerebral cortex is not likely to have consequences neither in the levels of *Rest* mRNA nor in the levels of Rest protein.

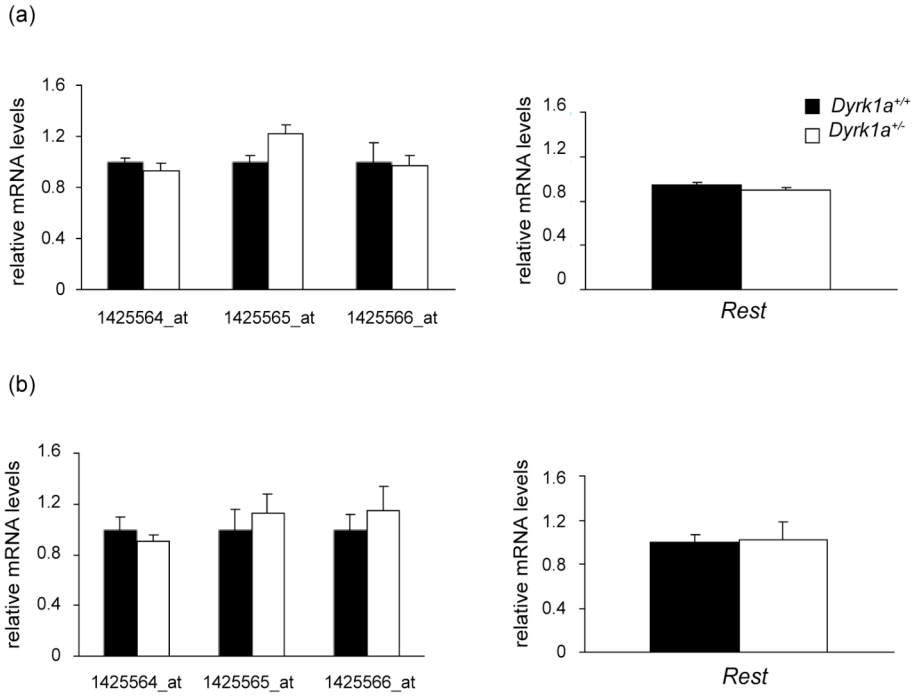

Fig R7: Relative *Rest* mRNA levels in *Dyrk1a*$^{+/+}$ and *Dyrk1a*$^{+/-}$ developing cerebral cortex. Histograms showing *Rest* trascript levels in *Dyrk1a*$^{+/+}$ and *Dyrk1a*$^{+/-}$ mouse cerebral cortex at P0 (a) and P7 (b). Left panels show the hybridization results for the three indicated sets of *Rest* probes included in the Affymetrix array. Differences in *Rest* expression between *Dyrk1a*$^{+/+}$ and *Dyrk1a*$^{+/-}$ cortices have an adj-pValues>0.05 for all *Rest* probes at both P0 and P7. Right panels show the relative *Rest* mRNA levels determined by qPCR. Hostograms values correspond to the mean (±sem) of measurements performed in 6 *Dyrk1a*$^{+/+}$ and 8 *Dyrk1a*$^{+/-}$ mice. p=0.28 at P0 and 0.90 at P7 in a Student's T-test.

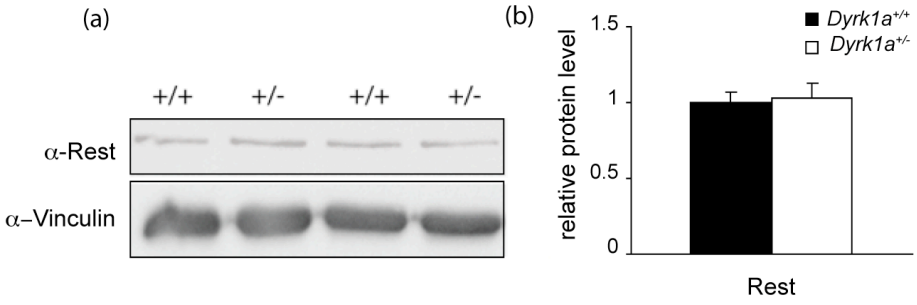

Fig R8: Rest protein levels in the cerebral cortex of newborn *Dyrk1a*$^{+/+}$ and *Dyrk1a*$^{+/-}$ mice. (a) Representative western blot of total lysates prepared from the cerebral cortex of 2 *Dyrk1a*$^{+/+}$ and 2 *Dyrk1a*$^{+/-}$ mice. Rest was detected around 200KDa; immunodetection of Vinculin (130KDa) was used as loading control. (b) Quantification of western blots as the ones shown in (a) does not show differences in Rest protein levels between genotype. Values correspond to the mean (±sem) of 4 determinations per genotype. P=0.92 in a Student's T-test.

We then considered the possibility of *Dyrk1a* dose reduction affecting Rest activity, and looked for Rest target genes in the array data. We checked for the around 35 known REST target genes (Bruce et al., 2004; Ballas et al, 2001; 2005; Otto et al., 2007; Chong et al., 1995; Seth and Majzoub, 2001; Mieda et al., 1997; Mori et al., 1992; Maue et al., 1990; Kraner et al., 1992; Martin et al., 2003) and among them, only the gene coding for *Corticotropin Releasing Hormone (Crh)* and *Calbindin1* (*Calb1*) were found significantly down-regulated in the mutant condition in the array. *Calb1* down-regulation was confirmed by qPCR at P0 and at two earlier developmental stages, E14.5 and E16.5 (Fig R9). It is worthy to mention in this context that, being *Calb1* expressed in differentiated neurons, its down-regulation in the cortex of mutant mice could be the readout of an impaired neurogenesis rather than an altered Rest-dependent transcription.

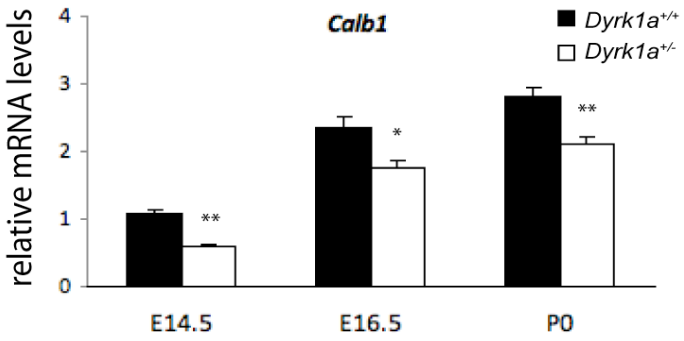

Fig R9: Levels of *Calbindin1* transcripts in *Dyrk1a*$^{+/+}$ and *Dyrk1a*$^{+/-}$ cerebral cortex at different developmental stages. Histogram showing relative *Calbindin1 (Calb1)* mRNA levels, determined by qPCR, in *Dyrk1a*$^{+/+}$ and *Dyrk1a*$^{+/-}$ cerebral cortices at the indicated developmental stage. Values correspond to the mean (±sem) of measurements performed in a minimum of 4 animals per condition. Statistical significance was calculated by Student's T-test (*p<0.05; **p<0.01).

In addition, we used a bioinformatic approach to search for the presence of the REST Repressor Element 1 (RE-1), also known as Neuron-Restrictive Silencing- Element (NRSE), in the promoter regions of the set of differentially expressed genes. The standard RE-1 site is a 21bp consensus sequence (Chong et al., 1995; Schoenherr and Anderson, 1995) whose position in the gene regulatory region is extremely variable, being either upstream or downstream the TSS. The position of RE-1 sites seems to be important for the function of REST on gene expression. For example, when a RE-1 site is far away from the TSS, REST likely acts as an activator rather than a repressor (Johnson et al., 2009). Moreover, a truncated isoform of REST, REST4, which binds to the same RE-1 consensus sequence, acts as a REST dominant-negative (Shimojo et al., 1999). This scenario became even more complicated after the discovery of two low affinity RE-1 motifs, an expanded one, which includes a 3-9bp insertion, and a compressed one of only 20bp, that have been identified in genes involved in lineage specification (Otto et al, 2007; Bruce et al., 2009). The three RE-1 sequences (shown in Fig A2 of the Appendix) were used to scan the regulatory regions of the 707 genes differentially expressed (adj-pValue<0.05) in the cerebral cortex of P0 mutant mice. Using the Matscan program we looked for RE-1 motifs in a region of 4Kb around the TSS of the up- and down- regulated genes. The majority of genes scanned did not contain any RE-1 site, few genes (around 15% of the

total) contain one RE-1 site and almost no genes contained 2 RE-1 sites (Fig R10). Interestingly, the number of the down-regulated genes with one RE-1 site was significantly higher than randomly expected and, conversely, the number of the up-regulated genes with one RE-1 site was significantly lower than expected; indicating that the down-regulated genes are enriched in RE-1 site compared with the up-regulated ones (Fig R10). The up- and down-regulated genes containing one predicted RE-1 site are listed in Table A4 in the Appendix.

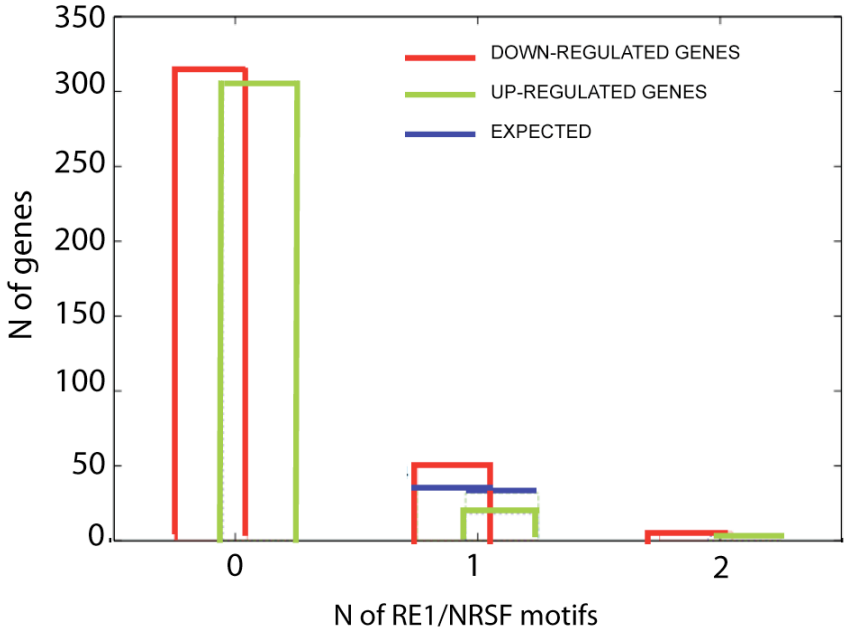

Fig R10: Numbers of RE-1 motifs in the promoter regions of genes that are up- or down-regulated in the cerebral cortex of P0 *Dyrk1a*$^{+/-}$ mice compared with their wild type controls. The chart represents the number (N) of predicted genes that contain respectively 0, 1 or 2 RE-1/NRSE motifs in the 4Kb window around the TSS according to Matscan analysis. The majority of genes do not contain any RE-1 site in the analyzed region, independently of being up- or down-regulated. A significant difference between the number of up- and down-regulated genes with one predicted RE-1 motive was observed: there were more

down-regulated genes than the expected for a random distribution showing one RE-1 site (difference between the red and blue lines, p=2.5e-4), while the opposite occurs for the up-regulated ones (difference between the green and blue lines, p=8.8e-5). Two RE-1 motifs were predicted in very few genes and no difference between the numbers of up- and down-regulated genes was observed. p values were calculated with a hypergeometric test.

REST has been described as a modulator of wide genomic domains, because of its interaction with the chromatin remodeling machinery (Ballas and Mandel, 2005; Ballas et al., 2001; 2005). Indeed, among the genes that emerged differentially expressed in our microarray analysis there are some for which a distal RE-1 site has been predicted in other works. These include the genes coding for *Somatostatin (Sst), Tetraspanin2 (Tspan2), Proenkephalin (Penk),* the *Myelin basic protein* (*Mbp)*, the TFs *Sox4* and *Sox11*, the ion channel *Scn2a1*, and the *solute carrier 12a5 (Slc12a5)* (Sun et al., 2005b; Bergsland et al., 2006; Chong et al., 1995; Lunyak et al., 2002). For this reason we used an additional bioinformatics approach that consists in scanning all mouse chromosomes using a sliding window of 1000Kb. This scanning builds a map of RE-1 sites in the whole mouse genome. The genomic position of the RE-1 sites and the up- and down-regulated genes at P0 was then plotted as shown for mouse chromosome 9 in Fig R11. The analysis of all mouse genome showed 77 down-regulated genes and 22 up-regulated genes in RE-1 enriched regions. This numbers are significantly different from the 53 down-regulated genes and the 46 up-regulated genes expected for a random distribution (p=4.81e-08 and p=1.27e-08 respectively, as determined by a hypergeometric test). This result, together with the result obtained in the previous analysis, predicts that Dyrk1a and Rest functionally interact in the developing mouse cerebral cortex.

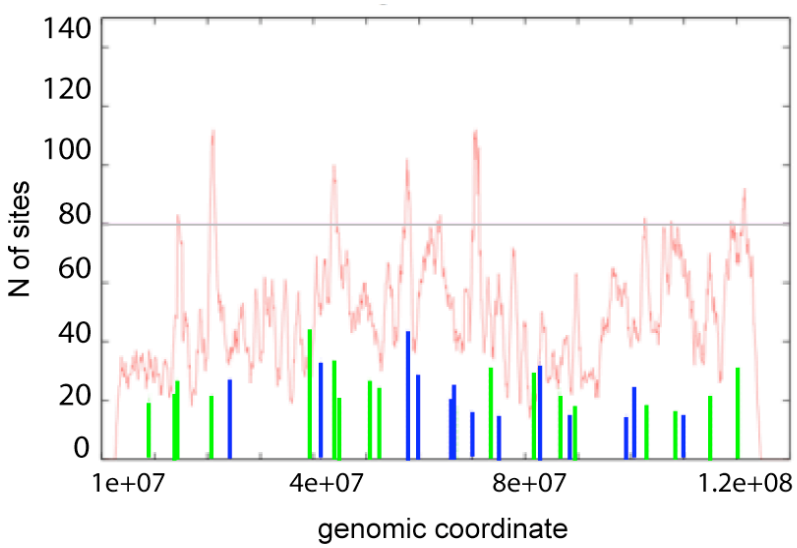

Fig R11: Scanning of the mouse chromosome 9 for RE-1 motifs. A 1000Kb sliding window was used to map RE-1 sites along chromosomes with the Matscan program. Genomic coordinates are indicated in the x-axis and the numbers of predicted RE-1 sites in the y-axis. The red line describes the number of predicted RE-1 sites along chromosome 9. Blue and green bars represent, respectively, the number of up- and down-regulated genes corresponding to specific chromosomal region in *Dyrk1a*$^{+/-}$ mutant cortices at P0. Regions with more than 80 RE-1 sites (above the grey line) were arbitrary considered as RE-1 enriched regions.

Given that the REST complex regulates gene expression in cooperation with the epigenetic machinery (Ballas and Mandel, 2005; Ballas et al., 2001; 2005), the next step was to investigate whether differences in epigenetic modifications could be responsible of the differences on gene expression observed between the cerebral cortices of *Dyrk1a*$^{+/+}$ and *Dyrk1a*$^{+/-}$ mice. Because one of the main epigenetic mechanisms of gene regulation is DNA methylation, which silences gene expression through the addiction of a methyl group to the cytosine of CG dinucleotides (CpGs), we checked for CpGs in the promoter region of the differentially expressed genes at P0. Analyzing 1Kb around the TSS we

found a clear enrichment in CpG content in the set of down-regulated genes when compared to the set of up-regulated ones (Fig R12). It can be therefore argued that increased DNA methylation in the regulatory regions of the down-regulated genes could be at the basis of the decreased expression of this set of genes in *Dyrk1a*$^{+/-}$ cortices.

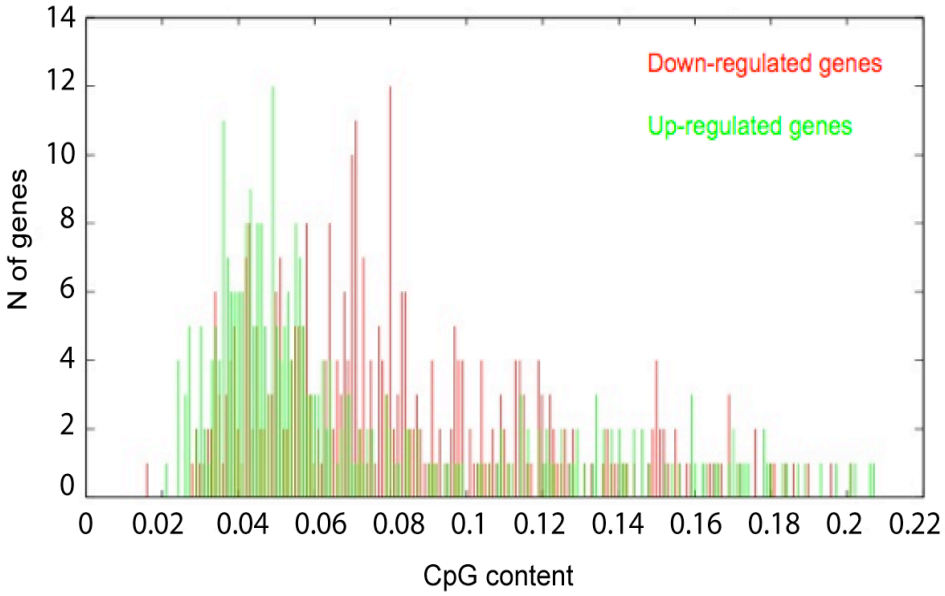

Fig R12: CpG content of the promoter region of the up- and down-regulated genes in *Dyrk1a*$^{+/-}$ cerebral cortex. Genes that were differentially expressed in P0 *Dyrk1a*$^{+/-}$ cerebral cortex compared to *Dyrk1a*$^{+/+}$ are represented according to their CpG content in the 1Kb region around the TSS. Values in the x-axis correspond to the fraction of the 1Kb region analyzed that is represented by the CG dinucleotide. Green bars indicate the number of up-regulated genes and red bars the number of down-regulated ones with a given CpG content.

2.1.3. Validation of microarray results

Microarray results were validated by qPCR taking advantage of the Low Density Array (LDA) platform based on TaqMan chemistry. The main advantage of using LDA is the possibility of analyzing at the same

time a panel of numerous transcripts selected by the customer. For each of them, the corresponding TaqMan probes and primers are spotted by the manufacturer in defined wells of the same LDA card.

To define the best reference genes to normalize our expression data, we used a standard LDA card containing 16 of the most used mouse reference genes (listed in Table A5 in the Appendix). For each experimental condition, 2 of the 4 samples used for the microarray analysis were tested in the reference gene card. Of the 16 reference genes analyzed we discarded those genes showing a crossing temperature (ct) higher than 30 or lower than 15 cycles; or showing differences in expression associated to the genotype. From the remaining 7 genes we chose those displaying the lowest variation in their ct values across samples in all the comparisons analyzed, P0-WsvM, P7-WsvM and W-P7vsP0. Those genes, namely *peptidyl-prolyl isomerase A (Ppia), tata binding protein (Tbp), ubiquitin-c (Ubc)* and *beta-actin (Actb)*, were included as reference genes in the customer LDA card (Table A5 in the Appendix).

The 42 genes included in the customer LDA card for the validation of microarray results were chosen taking into account their difference in gene expression, higher than 20% between *Dyrk1a*$^{+/+}$ and *Dyrk1a*$^{+/-}$ cerebral cortices (adj-pValue<0.05), at least at one developmental stage, P0 or P7, but preferentially at both stages; and their known function in brain development. LDA cards with the selected 42 target genes (listed in Table R2) were used to test three cDNA samples per experimental condition (P0-WsvM, P7-WsvM and W-P7vsP0): two of them were the same used for microarray hybridization, and the third one was an additional sample obtained from and independent animal and litter. This experimental approach allowed us to validate the microarray results both

technically and biologically, thus increasing the robustness of our observations.

Table R2: Comparison of array and LDA results

	Symbols	ARRAY P0	LDA P0	ARRAY P7	LDA P7
cytoskeletal transport and remodelling	Myo9a	1,49	1,26	1,09	1,10
	Myrip	0,65	0,92	0,85	0,92
	Rims2	0,66	ND	1,23	ND
	Kifc2	0,67	0,86	0,86	1,02
	Gpr6	0,50	0,72	0,64	0,84
	Htr7	0,61	0,79	0,79	0,87
	Lin7b	0,60	0,68	0,82	0,96
	Vsnl1	0,65	0,80	0,85	0,93
	Unc13c	0,65	0,72	0,80	0,85
	Rab27b	0,62	0,75	0,73	0,76
	Tspan17	0,65	0,73	0,73	0,84
	Olfm3	0,64	0,71	0,73	0,79
	Thy1	0,62	0,69	0,71	0,79
	Slc32a1	0,72	0,91	0,67	0,74
	Tuba4a	0,66	0,79	0,78	0,76
	Amn	0,81	ND	0,65	ND
	Aplp2 *	1,11	1,17	0,67	1,03
	Chn1	1,06	1,17	0,63	0,82
	Nrn1	0,83	1,04	0,66	0,78
	Syt11	1,04	1,10	0,64	0,86
neural progenitors self renewal and differentiation	Nfib	1,50	1,47	1,60	1,13
	Sox11	1,23	1,47	1,37	1,31
	Sox4	1,42	1,63	1,32	1,42
	Notch2	1,11	1,42	1,67	1,29
	Gfap	0,54	0,82	1,39	1,41
	Aqp4	0,65	0,59	0,74	1,02
	Cnp1	0,64	0,68	0,83	0,91
	Mbp	0,54	0,31	0,58	0,57
	Tspan2	0,75	0,92	0,58	0,76
	S100b	0,95	0,47	0,59	0,68
	Got1	0,88	1,00	0,61	0,86
gabaergic transmission	Gabrb3 *	2,57	1,04	1,14	1,03
	Gabrg1	0,62	0,81	0,86	0,87
	Nts	0,90	1,06	0,59	0,58
	Sst	0,79	0,89	0,50	0,51
	Gabarapl1	0,99	1,17	0,73	0,91
	B3gnt1	0,90	1,07	0,68	0,95
others	Ddit4	1,54	1,90	2,43	1,67
	Itsn1 *	1,14	1,19	2,18	1,16
	Lass5 **	0,47	1,34	0,63	1,23
	Ext1 **	0,16	1,17	3,00	1,09
	Ptger4	0,51	0,55	0,72	0,76

Values in “LDA P0” and “LDA P7” columns correspond to the average FC of gene expression between mutant and wild type cerebral cortices determined by LDA analysis. *Ppia* was used as a reference gene to normalize gene expression levels at both P0 and P7. Values in “ARRAY P0” and “ARRAY P7” columns correspond to the average gene expression fold changes obtained in the Affymetrix array (n=4 per experimental condition). Coloured numbers indicate that the differences in gene expression reach statistical significance ($p<0.05$ in the Student’s T-test in the case of LDA and adj-pValue<0.05 in the microarray); red and green colours indicate respectively down- and up-regulation in mutant mice. **genes for which the array and LDA experiments gave opposite results; *difference in FC between the array and LDA experiments higher than 30%.

We could detect expression of all 42 genes in the LDA cards with the exception of the *Amnionless (Amn)* and the *Regulating Synaptic Membrane exocytosis 2* (*Rims2)* that had ct values higher than 32, indicated a very low level of expression. For the remaining 40 genes, microarray results were confirmed with the exception of two genes; *Exostosin-1 (Ext1)* and the *LAG1 homolog, ceramide synthase 5 (Lass5*) that were found down-regulated in the Affymetrix array and up-regulated in the LDA card. For the remaining 38 genes, with the exception of the *Amyloid beta precursor-like protein 2 (Aplp2)*, the *Gamma-aminobutyric acid (GABA) A receptor, subunit beta 3 (Gabrb3)* and *Intersectin1 (Its1*), the differences in fold changes were less than 0.3 times between the array and the LDA card.

Finally the expression of two genes, the *S100b* gene coding for the S100b Calcium binding protein, and the *Gfap* gene, coding for the Glial fibrillary acidic protein, was additionally analyzed by Sybr-Green qPCR. *S100b* expression was strongly and very significantly reduced (about 50% between mutants and wild types) at P7, according to both the LDA and microarray results, and at P0, according to the LDA results. However, based on microarray data, *S100b* levels were unchanged in mutant cortices at P0, suggesting the possibility of a false negative microarray result in this specific case. Indeed, Sybr-Green qPCR

highlighted a 40% reduction of *S100b* levels in the cerebral cortex of *Dyrk1a*$^{+/-}$ mice at P0, thus confirming the LDA result (Fig R13a). *Gfap* was significantly up-regulated at P7, according to the LDA results, and significantly down-regulated at P0, according to the microarray results. Sybr-Green qPCR performed with cDNA from both P0 and P7 pups showed that *Gfap* expression is similar in the cortex of mutant and wild type animals at P0, but increased in the mutants at P7 (Fig R13b).

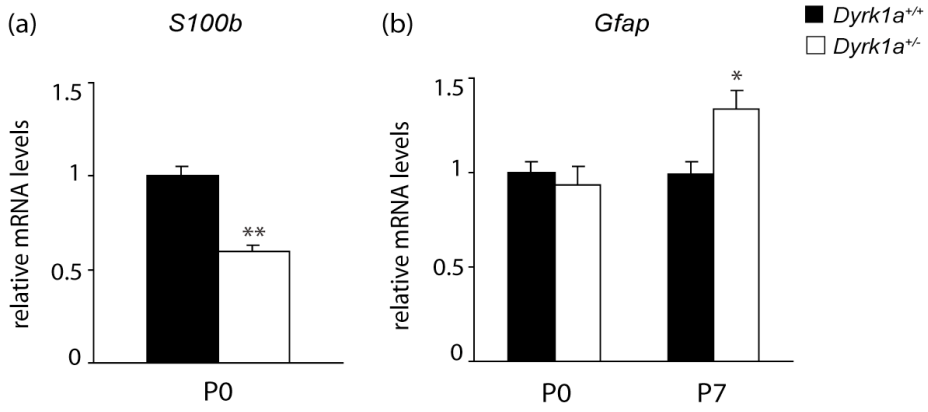

Fig R13: *Gfap* and *S100b* mRNA levels in *Dyrk1a*$^{+/+}$ and *Dyrk1a*$^{+/-}$ early postnatal cerebral cortices. Histograms showing relative *S100b* (a) and *Gfap* (b) mRNA levels, determined by Sybr-Green qPCR, in *Dyrk1a*$^{+/+}$ and *Dyrk1a*$^{+/-}$ cerebral cortices at the indicated developmental stage. Values correspond to the mean (±sem) of measurements performed on a minimum of 14 animals per genotype at P0 and 8 animals per genotype at P7. Statistical significance was calculated by Student's T-test (*p<0.05; **p<0.01).

2.2. Gene expression analysis of late embryonic and postnatal *Dyrk1a*$^{+/-}$ cerebral cortices

Costume LDA cards designed for array validation were also used to investigate; i) how the expression of the selected target genes changes in the cerebral cortex of *Dyrk1a*$^{+/-}$ mutants at additional developmental

time points (E16.5 and P28) and ii) which is the effect of *Dyrk1a* triplication on the expression of this set of genes during cortical development. To answer this last question we took advantage of a transgenic mouse model carrying three copies of the mouse *Dyrk1a* gene, the BAC-*Dyrk1a* mouse.

The gene expression analysis of *Dyrk1a*$^{+/+}$ and *Dyrk1a*$^{+/-}$ cerebral cortex at E16.5 and P28 stages indicated that changes in gene expression are in most cases stage specific. For instance, 11 of the 42 genes analyzed by LDA were differentially expressed between genotypes at E16.5 but only 5 of them were still differentially expressed at P0. These genes were *S100b,* the *2',3'-cyclic nucleotide 3' phosphodiesterase (Cnp1),* the *DNA-damage-inducible transcript 4 (Ddit4),* the member of the *RAS oncogene family Rab27b* and *Visin Like-2 (Vsnl2*). In addition, only 5 of the 42 total genes analyzed; *S100b, Sst,* the *G protein-coupled receptor 6 (Gpr6), Neurotensin (Nts)* and the *Prostaglandin receptor-4 (Ptger4)* were differentially expressed at P28 (Fig R14). These results confirmed what we had previously observed in the microarray data: that in most cases, changes in gene expression are not maintained during development, thus suggesting a role for Dyrk1a in specific and time regulated developmental processes.

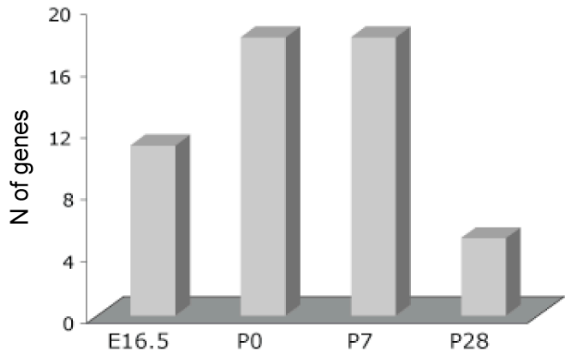

Fig R14: Number of differentially expressed genes in *Dyrk1a*$^{+/-}$ cerebral cortices at different developmental time points. Forty-two target genes were analyzed by custom LDA analysis. Histogram values indicate the numbers (N) of differentially expressed genes between *Dyrk1a*$^{+/+}$ and *Dyrk1a*$^{+/-}$ cerebral cortex at the developmental stage indicated (n=2 animals per genotype at E16.5 and P28; n=3 animals per genotype at p0 and P7). Differences between genotypes were calculated with a Student's T-test.

Custom LDA cards were finally used to investigate if *Dyrk1a* over-expression also affects the cerebral cortex transcriptome, and if so, to what extent. To this end, we compared the cerebral cortex transcriptomes of BAC-*Dyrk1a* and wild type animals at the same time points analyzed before in this study, P0 and P7. As expected, *Dyrk1a* mRNA levels were 50% increased in the cerebral cortex of BAC-*Dyrk1a* at both developmental stages (Fig R15).

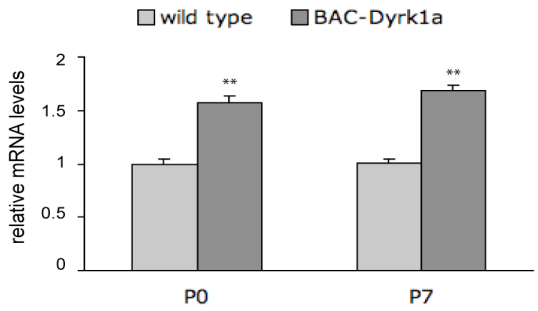

Fig R15: *Dyrk1a* mRNA levels in the cerebral cortex of postnatal BAC-*Dyrk1a* and wild type animals. *Dyrk1a* mRNA levels in wild type and BAC-*Dyrk1a* cerebral cortex were determined by qPCR at P0 and P7. Values correspond to the mean (±sem) of the relative mRNA levels measured in 3 to 6 animals per condition. Statistical significance was determined by Student's T-test (**p<0.01).

The expression analysis highlighted that only a fraction of the genes whose expression was found deregulated in the cerebral cortex of *Dyrk1a*$^{+/-}$ mice were also deregulated in the BAC-*Dyrk1a* model. Interestingly, for these transcripts, the effect of *Dyrk1a* triplication and *Dyrk1a* dose reduction were opposite (Fig R16).

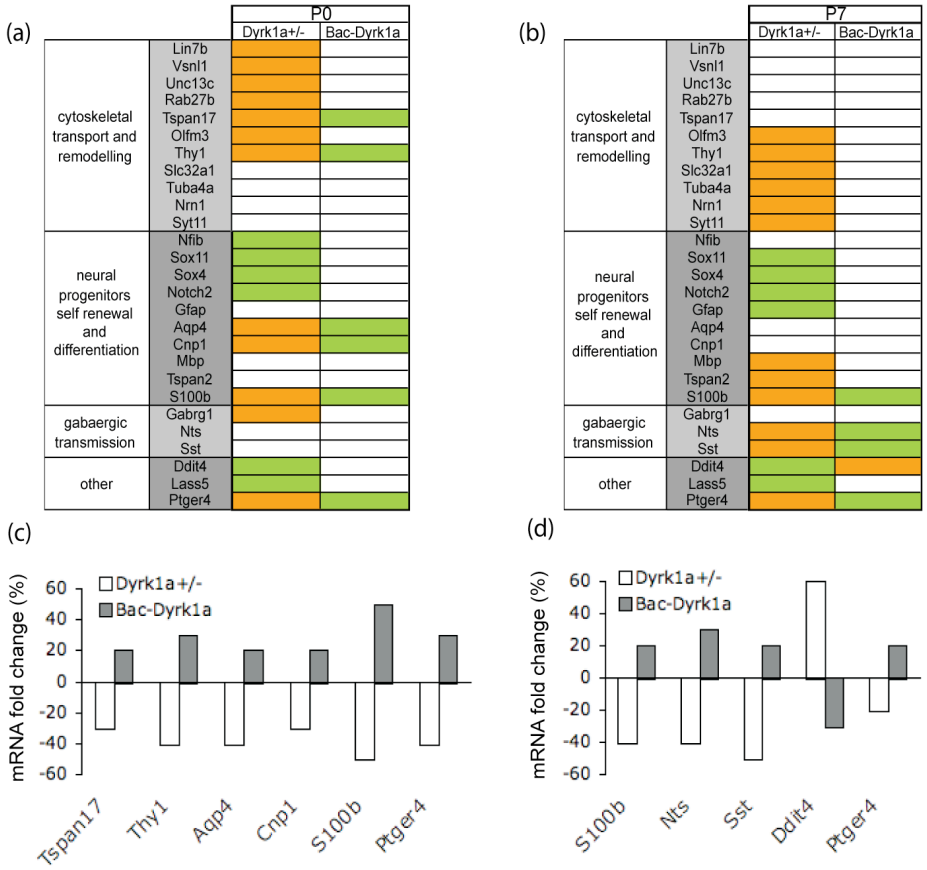

Fig R16: Effects of *Dyrk1a* dose reduction and *Dyrk1a* triplication in cortical gene expression. Forty-two target genes were analyzed by customer LDA in the cerebral cortex of *Dyrk1a*$^{+/-}$ and BAC-*Dyrk1a* mouse models at P0 (a) and P7 (b) (2<n<3 animals per condition). In all cases mRNA levels were normalized by *Ppia* expression levels. Statistically significant up- and down-regulated genes in the mutant condition compared to the wild type condition ($p<0.05$ according to Student's T-test) are represented as green and orange boxes respectively. Among the genes included in the LDA cards, only those significantly deregulated in at least one time point are reported in panels (a) and (b). Genes that are differentially expressed in both *Dyrk1a* models are shown in (c) for P0 and (d) for P7. (c-d) Histogram values represent the averaged fold change, expressed as percentage of the expression in the corresponding wild type control, of individual genes in the cerebral cortex of mutant mice.

Because the analysis in the *Dyrk1a* overexpression model was limited to a pre-selected group of genes we cannot exclude the possibility

of *Dyrk1a* triplication affecting the cerebral cortex development by altering other genes not included in the LDA card. Nevertheless, it is worthy to underline here that changes in gene expression provoked by *Dyrk1a* triplication are usually slighter than those provoked by *Dyrk1a* dose reduction.

3. *In vitro* properties of *Dyrk1a*$^{+/+}$ and *Dyrk1a*$^{+/-}$ embryonic cortical progenitors

Our gene expression analysis highlighted that genes coding for regulators of neural progenitors self-renewal and differentiation were among the most differentially expressed in the cerebral cortex of *Dyrk1a* mutant mice.

This group of genes includes *Notch2* and *Aquaporin-4 (Aqp4)* that are involved in the maintenance of the progenitor state *(*Kong et al., 2008; Kawaguchi et al., 2008). This finding suggests that a relationship between *Dyrk1a* dosage and the self-renewal properties of neural progenitors can exist during development, as already shown in the brain of adult mice (Ferron et al., 2010).

In addition, the altered expression of genes that play a role in lineage commitment and differentiation of neural progenitors, like *Sox4, Sox11, Olig2, Nfla, Nflb, Tcf4* and *S100b*; as well as genes that are markers for differentiated cell types, like *Gfap* (astrocytic marke*r), Thy1* (neuronal marker), *Mbp* and *Cnp1* (oligodendroglial markers), observed in the cortex of *Dyrk1a* mutants opens the possibility of Dyrk1a being involved in the differentiation potential of neural progenitors.

To test whether *Dyrk1a* dosage imbalance affects the self-renewal and differentiation potentials of cortical embryonic neural progenitors we

chose neurosphere cultures as experimental model. Because sphere cells have the unlimited capacity to generate new neurospheres and the capacity to differentiate into neurons, astrocytes and oligodendrocytes (Ferron et al., 2007), this type of cultures allows the study of both self-renewal and differentiation potentials of neural progenitors.

Dyrk1a expression in mouse embryonic neural progenitors has been described *in vivo* by Hammerle and colleagues (Hammerle et al., 2008). To corroborate that Dyrk1a expression is maintained in neurosphere progenitors in culture we used immunocytochemistry (ICC) and qPCR. Dyrk1a was immunodetected in secondary embryonic neurospheres that were incubated *in toto* with a Dyrk1a specific antibody (Fig 17a). *Dyrk1a* expression in secondary embryonic neuropsheres was confirmed by qPCR (Fig R17b). To prove that mutation of one *Dyrk1a* allele leads to a reduction in gene expression we compared *Dyrk1a* mRNA levels between *Dyrk1a*$^{+/+}$ and *Dyrk1a*$^{+/-}$ neurosphere cultures and found the expected 50% reduction in *Dyrk1a*$^{+/-}$ neurospheres (Fig R17b).

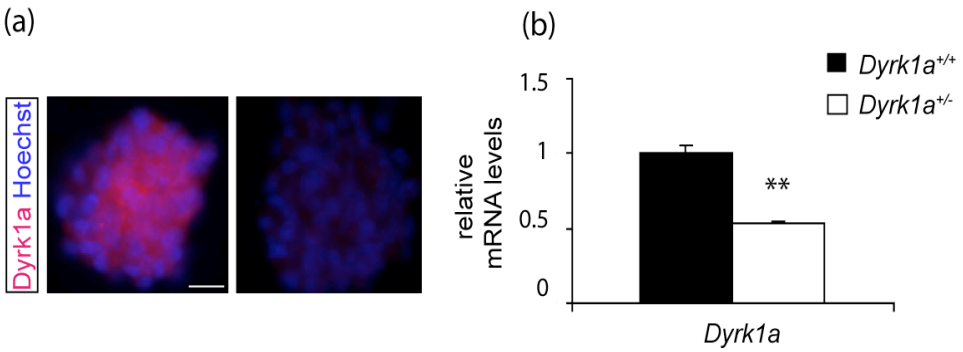

Fig R17: Dyrk1a expression in embryonic cortical neurospheres. (a) Dyrk1a immunodetection (red) in p1 secondary neurospheres obtained from E15.5 wild type embryos (left panel). The lack of signal can be observed in negative controls in which Dyrk1a primary antibody was omitted from the incubation media (right panel). Hoechst (blue) was used to label nuclei. Scale bar: 20µm. (b) Relative *Dyrk1a* mRNA levels in *Dyrk1a*$^{+/+}$ and *Dyrk1a*$^{+/-}$ p1 secondary

neurospheres. Histogram values correspond to the average gene expression levels (±sem) calculated from 8 independent neurospheres cultures per genotype. Statistical significance was determined by Student's T-test (**p<0.01).

Dyrk1a$^{+/+}$ and *Dyrk1a*$^{+/-}$ neurosphere cultures were then used to evaluate the effect of *Dyrk1a* dose reduction on: i) the mitogen-dependent growth and self-renewal potential of embryonic cortical progenitors, ii) the expression of *Aqp4* and *S100b* genes in these progenitors, and iii) their differentiation potential.

3.1. Mitogen-dependent growth and self-renewal potential of neurosphere cells

3.1.1. Neurosphere cells cultured with EGF and FGF

To analyze whether the properties of embryonic neural progenitors are affected by *Dyrk1a* dosage we compared *Dyrk1a*$^{+/+}$ and *Dyrk1a*$^{+/-}$ neurosphere cultures obtained from the cortex of E15.5 embryos.

We were able to establish neurosphere cultures from both genotypes when cells were cultured in the presence of EGF and FGF mitogens. In this condition, the percentage of p1 healthy cultures formed was very similar for both genotypes (Fig R18a) and no major differences in the size or in the number of neurospheres between wild type and mutant p1 cultures were detected by visual inspections.

The phenotypes described for adult *Dyrk1a*$^{+/-}$ neurospheres include an impaired self-renewal capacity in response to EGF and an impaired proliferation after passage 3 and, as a consequence, there is an exhaustion of adult *Dyrk1a*$^{+/-}$ cultures after several passages (Ferron et al, 2010). In order to test whether this is also the case for embryonic *Dyrk1a*$^{+/-}$ neurospheres, we performed cumulative growth curves of embryonic *Dyrk1a*$^{+/+}$ and *Dyrk1a*$^{+/-}$ neurospheres cultures. As represented

in Fig R18b, we found that the average growth rate of *Dyrk1a*$^{+/-}$ embryonic neurospheres, cultured in presence of EGF and FGF, was significantly reduced at p1. In the following passages, mutant cultures maintained the same tendency of growing slower than wild type cultures, although differences did not reach statistical significance probably because of the lower number of cultures analyzed at p2 and at p3.

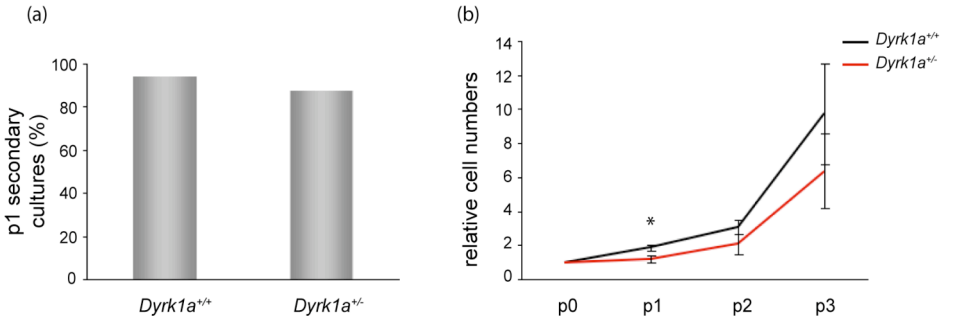

Fig R18: Establishment and cumulative growth curve of *Dyrk1a*$^{+/+}$ and *Dyrk1a*$^{+/-}$ embryonic neurospheres cultures. (a) Histogram values correspond to the percentage of healthy p1 secondary neurosphere cultures obtained from 31 *Dyrk1a*$^{+/+}$ and 31 *Dyrk1a*$^{+/-}$ starting cultures. (b) Cumulative growth curve of *Dyrk1a*$^{+/+}$ and *Dyrk1a*$^{+/-}$ cultures from p0 to p3. At each passage (p) (x-axis) cells were plated at the density of 10^5 cells/ml. When neurospheres reached an average size of about 50-100µm, they were disgregated and the total number of cells obtained was counted. Y-axis indicates the cumulative numbers of single sphere cells obtained in each passage relative to the total number of cells obtained at p0. Each point is the average (±sem) of the number of cells obtained from independent neurosphere cultures. Between 11 and 26 cultures were analyzed per condition. Statistical significance between genotypes was assessed by Student's T-test (*p<0.05).

The following events can explain the reduced growth rate observed in *Dyrk1a*$^{+/-}$ neurosphere cultures: reduced proliferation, increased cell death or reduced self-renewal of secondary neurospheres. Alterations in neurosphere size can be indicative of an altered proliferation and/or cell death of the sphere cells. The averaged diameters of the neurospheres

in *Dyrk1a*$^{+/+}$ and *Dyrk1a*$^{+/-}$ secondary cultures were not significantly different (Fig R19a and b). However, when we analyzed the size distribution of the neurospheres according to their diameter, we observed an enrichment of small neurospheres (30μm<diameter<40μm) in *Dyrk1a*$^{+/-}$ cultures compared to the wild types (Fig R19c). This phenotype indicates that differences in proliferation or cell death, although mild, can exist between *Dyrk1a*$^{+/+}$ and *Dyrk1a*$^{+/-}$ neurospheres.

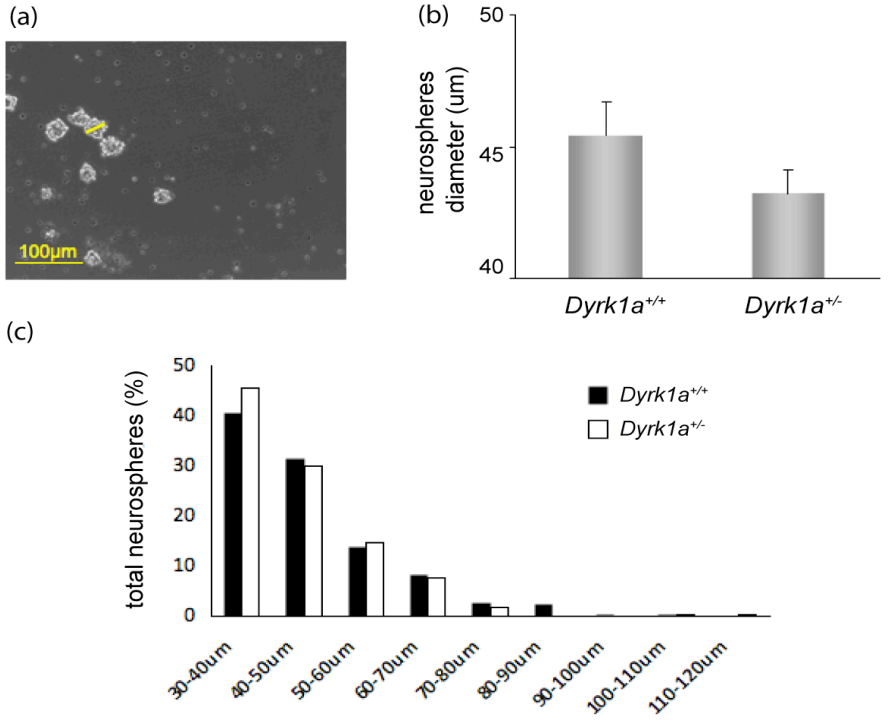

Fig R19: Size of *Dyrk1a*$^{+/+}$ and *Dyrk1a*$^{+/-}$ secondary neurospheres. (a) Phase contrast images (20x field) of low-density secondary neurospheres cultures (10^4 single cells plated in 500μl of complete medium) after 5DIV. The yellow bar is an example of how neurospheres diameter is drawn for ImageJ length measurement. (b) Histogram values correspond to the average diameter (±sem) expressed in μm of *Dyrk1a*$^{+/+}$ and *Dyrk1a*$^{+/-}$ p2 or p3 neurospheres after 5 DIV

(n=24 cultures per genotype). To calculate the average diameter only neurospheres with a size between 30 and 120 μm were taken into account to avoid counting aggregates of more than one neurosphere or small groups of single sphere cells. (c) Histogram shows the size distribution of the same group of neurospheres measured in (b). Neurospheres between 30 and 120 μm of diameter were distributed into bins of 10μm. Histogram values correspond to the number of neurospheres falling into each bin expressed as a percentage of the total number of neurospheres counted.

We then investigated any possible defect in the self-renewal potential of *Dyrk1a*$^{+/-}$ progenitors by counting the neurospheres that were generated from a fixed number of single secondary neurosphere cells 5 days after plating. As for the adult progenitors (Ferron et al., 2010), *Dyrk1a*$^{+/-}$ embryonic neurosphere cells showed a reduced self-renewal potential compared to the wild type ones (Fig R20).

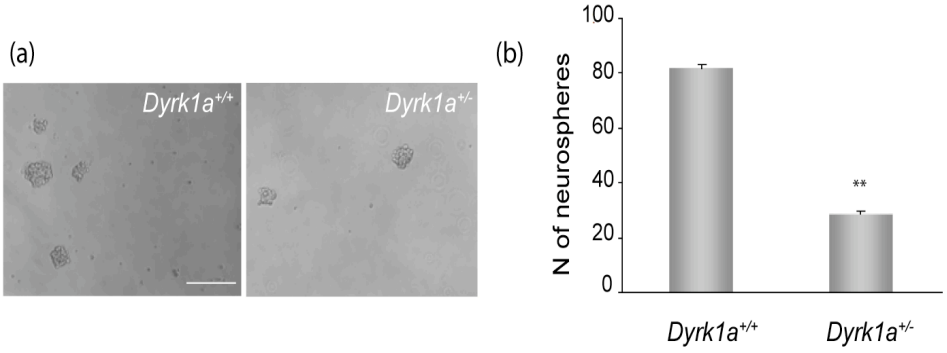

Fig R20: Self-renewal potential of *Dyrk1a*$^{+/+}$ and *Dyrk1a*$^{+/-}$ secondary neurospheres. (a) Representative phase contrast images (20x field) of *Dyrk1a*$^{+/+}$ and *Dyrk1a*$^{+/-}$ low-density cultures at 5DIVs, used for neurosphere quantifications. (b) Histogram showing the total numbers of neurospheres generated by 10^4 *Dyrk1a*$^{+/+}$ and *Dyrk1a*$^{+/-}$ single neurosphere cells after 5DIV. Histogram values correspond to the average number of neurospheres (±sem) quantified in 24 individual cultures per genotype. Significance was determined by Student's T-test (**p<0.01). Scale bar: 100μm.

3.1.2. Neurosphere cells cultured with EGF alone

EGF-dependent self-renewal impairment of adult *Dyrk1a*$^{+/-}$ neurospheres has been associated to a decreased level of EGFR on the membrane of mutant progenitors (Ferron et al., 2010). To test whether the observed self-renewal impairment of *Dyrk1a*$^{+/-}$ embryonic neurospheres is due to a low response of the cells to EGF we cultured E15.5 cortical progenitors in a medium that contained EGF but not FGF. In EGF culture medium neurosphere growth was strongly compromised in both wild type and mutant cultures; probably because FGF represents the main mitogen at this embryonic stage. Indeed at E15.5 neural progenitors just start responding to EGF signaling, that will become the main mitogen of neural progenitors at later developmental stages (Qian et al., 2000). For this reason, we moved to the E17.5 stage, to investigate the effect of EGF signaling on the properties of *Dyrk1a*$^{+/+}$ and *Dyrk1a*$^{+/-}$ neural progenitors. As expected, E17.5 wild type cortical progenitors form healthy neurospheres when cultured with only EGF and these neurospheres formed new neurospheres upon passage (Fig R21a). However, although the cultures could be expanded at least until p3, their net growth was significantly reduced when compared to the growth of E15.5 progenitors cultured in the presence of both EGF and FGF (see cumulative growth curve, in black, in Fig R21b and compare it with Fig R18b). The situation was significantly different for E17.5 *Dyrk1a*$^{+/-}$ cultures because the number of primary neurosphere cultures that form secondary p1 neurosphere was reduced to 60% (Fig R21a) and, more importantly, the net expansion of the culture upon passages was null (Fig R21b). Together, these results show that EGF-dependent growth of *Dyrk1a*$^{+/-}$ cortical progenitors is severely compromised.

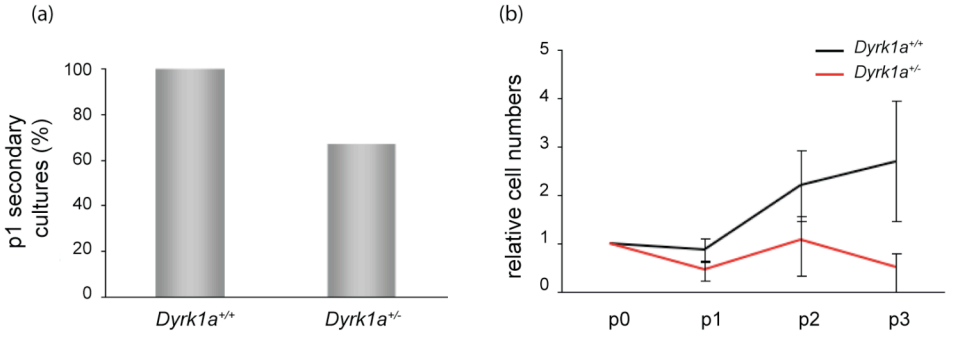

Fig R21: Establishment and cumulative growth curves of *Dyrk1a*$^{+/+}$ and *Dyrk1a*$^{+/-}$ embryonic neurospheres cultured with EGF alone. (a) Histogram values correspond to the percentage of healthy p1 secondary neurosphere cultures obtained from 19 *Dyrk1a*$^{+/+}$ and 19 *Dyrk1a*$^{+/-}$ starting cultures maintained with the EGF mitogen alone. (b) Cumulative growth curve of *Dyrk1a*$^{+/+}$ and *Dyrk1a*$^{+/-}$ cultures from p0 to p3. At each passage (p) (x-axis) cells were plated at the density of 10^5 cells/ml. When neurospheres reached an average size of about 50-100µm, they were disgregated and the total number of cells obtained was counted. Y-axis indicates the cumulative numbers of single sphere cells obtained in each passage relative to the total number of cells obtained at p0. Each point is the average (±sem) of the number of cells obtained from independent neurosphere cultures. Between 5 and 19 cultures were analyzed per condition. Statistical significance between genotypes was assessed by Student's T-test (p=0.28 at p1 and p2; p=0.20 at p3).

To further characterize the EGF-dependent growth defect of E17.5 *Dyrk1a*$^{+/-}$ embryonic progenitors, we measured, as we did before, the diameter and the number of secondary neurospheres generated by single neurospheres in wild type and mutant cultures. The average diameter of 5DIV wild type secondary neurospheres cultured with EGF alone was similar to the diameter of secondary neurospheres cultured in the presence of both EGF and FGF (compare Fig R22a with Fig R19b). However, the average size of *Dyrk1a*$^{+/-}$ secondary neurospheres cultured in EGF alone was significantly reduced (Fig R22a). Moreover, these neurospheres showed reduced EGF-dependent self-renewal potential as indicated by the tendency of *Dyrk1a*$^{+/-}$ single neurosphere cells of

generating less neurospheres than the wild type ones when cultured with EGF alone (Fig R22b).

Our results show that *Dyrk1a*$^{+/-}$ embryonic cortical progenitors respond less to EGF than wild type progenitors and suggest that defects in proliferation and self-renewing of these progenitors account for their null growth expansion when cultured in the absence of FGF.

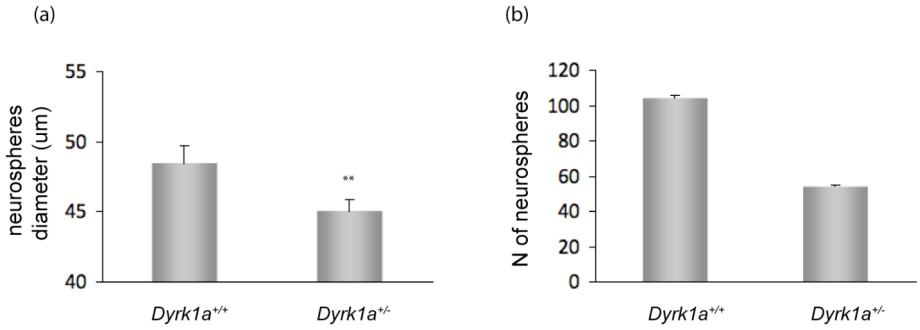

Fig R22: Size and self-renewal potential of *Dyrk1a*$^{+/+}$ and *Dyrk1a*$^{+/-}$ secondary neurospheres cultured with EGF alone. (a) Histogram values correspond to the average diameter (±sem), expressed in μm, of *Dyrk1a*$^{+/+}$ and *Dyrk1a*$^{+/-}$ p2 or p3 neurospheres after 5 DIV (6<n<8 cultures per genotypes). Only neurospheres with a diameter between 30 and 120 μm were taken into account. **p<0.01 in a Student's T-test. (b) Total numbers of secondary neurospheres generated by 10^4 *Dyrk1a*$^{+/+}$ and *Dyrk1a*$^{+/-}$ single neurosphere cells after 5DIV. Histogram values are the average number of neurospheres (±sem) counted on 6 *Dyrk1a*$^{+/+}$ and 8 *Dyrk1a*$^{+/-}$ independent cultures. P=0.08 in a Student's T-test.

3.1.3. Neurosphere cells cultured with FGF alone

Then we wanted to evaluate the effect of *Dyrk1a* dose reduction on FGF-dependent growth and self-renewal potential of cortical embryonic progenitors. To this end, we prepared new neurosphere cultures from E15.5 *Dyrk1a*$^{+/+}$ and *Dyrk1a*$^{+/-}$ cortices and grew them in complete medium without EGF. Both *Dyrk1a*$^{+/+}$ and *Dyrk1a*$^{+/-}$ progenitors formed

healthy neurospheres and these neurospheres were able to form new neurospheres upon passages in almost all cases (Fig R23a).

Like neurospheres that were grown in complete medium (EGF+FGF), no major differences in the sizes of the neurospheres were observed between genotypes (compare Fig R19a with Fig R23b). These observations demonstrate that the main mitogen for expanding E15.5 progenitors in culture is FGF and indicates that FGF-dependent growth and survival of *Dyrk1a*$^{+/-}$ neurosphere cultures is not significantly compromised. However, the number of secondary neurospheres generated by single neurosphere cells was severely reduced in *Dyrk1a*$^{+/-}$ cultures (Fig R23c).

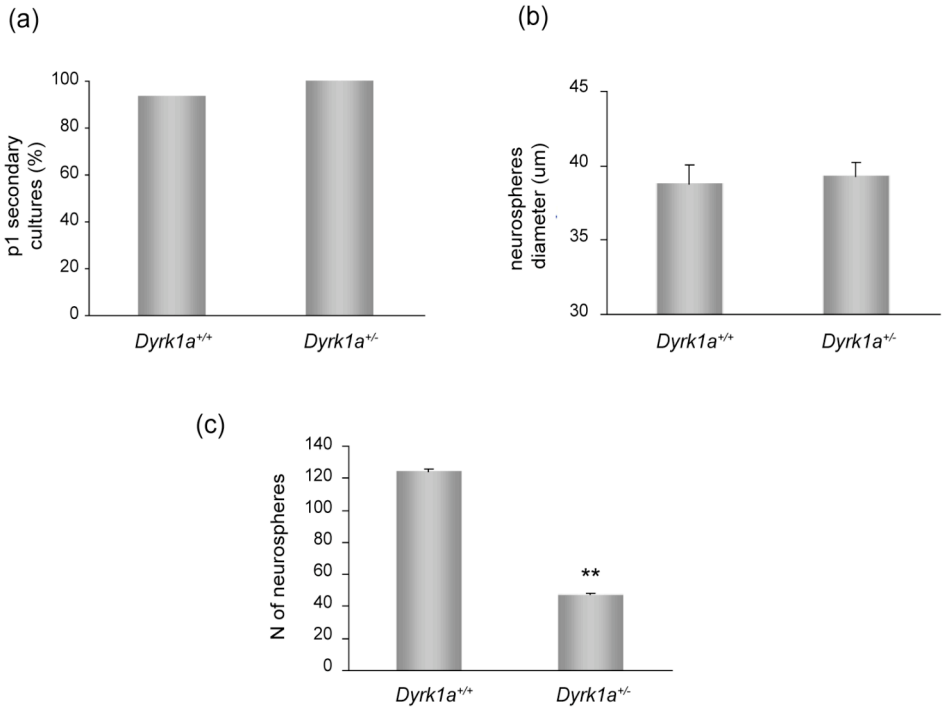

Fig R23: FGF-dependent properties of *Dyrk1a*$^{+/+}$ and *Dyrk1a*$^{+/-}$ cultures. (a) Histogram values correspond to the percentage of healthy p1 secondary

neurosphere cultures obtained from 13 *Dyrk1a*$^{+/+}$ and 19 *Dyrk1a*$^{+/-}$ starting cultures maintained with the FGF mitogen alone. (b) Histogram representing the average diameter (±sem), expressed in μm, of *Dyrk1a*$^{+/+}$ and *Dyrk1a*$^{+/-}$ p1 or p2 secondary neurospheres after 5 DIV (n=7 cultures per genotypes). Only sizes included between 30 and 120 μm are taken into account to calculate the average diameter. (c) Total numbers of secondary neurospheres generated by 10^4 *Dyrk1a*$^{+/+}$ and *Dyrk1a*$^{+/-}$ single neurosphere cells after 5DIV. Histogram values correspond to the average number of neurospheres (±sem) quantified in 7 independent cultures per genotype. Significance was determined by Student's T-test (**p<0.01).

The results here described show that normal amounts of Dyrk1a protein are necessary to preserve FGF-dependent self-renewal potential of embryonic cortical neural progenitors, at least *in vitro.* Because FGF-dependent self-renewal potential of adult *Dyrk1a*$^{+/-}$ progenitors of the brain SVZ is not impaired (Ferron et al, 2010), this result also indicates that Dyrk1a regulates the behavior of brain neuronal progenitors differently in the embryo than in the adult.

3.2. *Aqp4* and *S100b* expression in neurosphere cultures

In our microarray gene expression study, *Aqp4* and *S100b* appeared among the most deregulated genes in the cortex of P0 *Dyrk1a*$^{+/-}$ mice. Both Aqp4 and S100b are expressed in neural progenitors (Kong et al, 2008; Raponi et al., 2007). *Aqp4* codifies for a protein that forms the main water channel of the CNS, and is predominantly expressed by glial cells. Adult neural progenitors of *Aqp4* knockout mice show impaired proliferation, migration and neuronal differentiation (Kong et al., 2008). S100b is a calcium binding protein with several functions in the development and physiology of the nervous system (reviewed in Donato et al., 2009). *S100b* gene in humans is in chromosome-21 and its triplication in DS has been associated to the decreased proliferation and

increased glial phenotype of neural progenitors (Esposito et al., 2008). Interestingly, increased levels of S100b in DS neural progenitors induce *Aqp4* up-regulation (Esposito et al., 2008).

Given the implication of both genes in neural progenitors self-renewal and differentiation, we investigated their expression levels in *Dyrk1a*$^{+/+}$ and *Dyrk1a*$^{+/-}$ neurospheres. We found that the expression of both *Aqp4* and *S100b* were decreased in *Dyrk1a*$^{+/-}$ secondary neurospheres compared to the wild type ones (Fig R24a). The decreased levels of *Aqp4* mRNA correlated with reduced Aqp4 protein levels in embryonic neurosphere cultures (Fig R24b) and in the cerebral cortex of P0 *Dyrk1a*$^{+/-}$ mice (Fig R24c and d). These findings indicate that changes in *S100b* and *Aqp4* levels could contribute to modulate the behavior of *Dyrk1a*$^{+/-}$ neural progenitors.

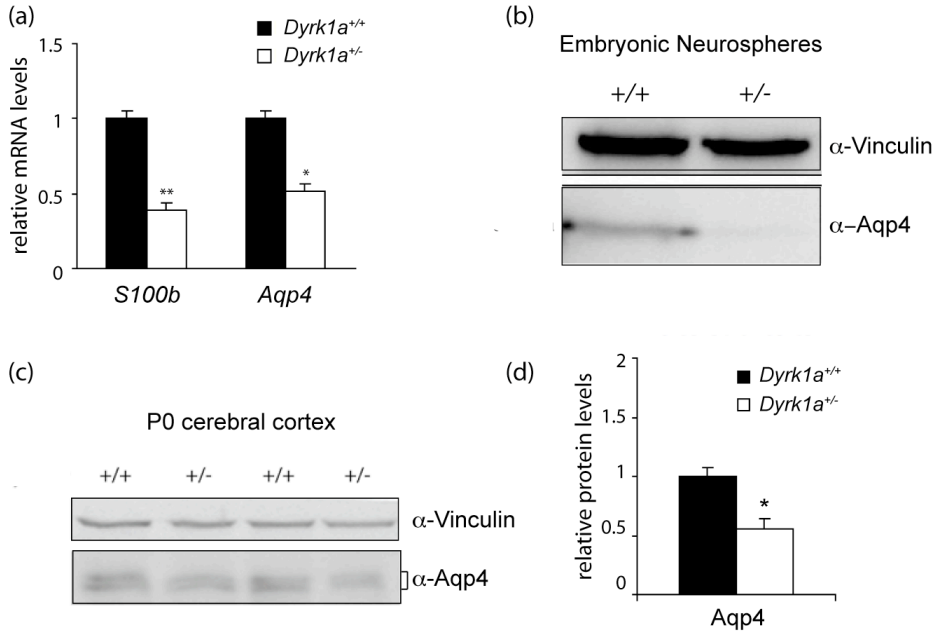

Fig R24: S100b and Aqp4 mRNA and protein levels in *Dyrk1a*$^{+/+}$ and *Dyrk1a*$^{+/-}$ embryonic neurospheres and postnatal cerebral cortex. (a) *S100b* and *Aqp4* mRNA levels, determined by qPCR, in p2 *Dyrk1a*$^{+/+}$ and *Dyrk1a*$^{+/-}$ cortical neurosphere cultures. Histogram values represent the average (±sem) mRNA levels in mutant cultures relative to the levels in the wild type cultures (n=13). Significance was calculated by Student's T-test (*p<0.05; **p<0.01). (b and c) Aqp4 protein immunodetection by western blot in total protein extracts prepared from *Dyrk1a*$^{+/+}$ and *Dyrk1a*$^{+/-}$ p2 neurosphere cultures (b) and from the cerebral cortex of newborn (P0) mice (c). Vinculin was used as loading control. (d) Histogram showing the quantification of western blots like the one shown in panel c. Values correspond to the average (±sem) Aqp4 protein levels in mutant extracts relative to the levels in wild types extracts. Quantifications were performed on tissue extracts prepared from 6 *Dyrk1a*$^{+/+}$ and 7 *Dyrk1a*$^{+/-}$ newborn mice. Significance was determined by Student's T-test (*p<0.05).

3.3. Differentiation potential of neurosphere cells

Once analyzed the growth properties of *Dyrk1a*$^{+/-}$ neural progenitors, we wondered whether their pluripotency is also affected. To answer this question we performed neurosphere differentiation assays, which consist in culturing single neurosphere cells in adhesion and in a medium that allows the progenitors to differentiate into neurons and glial cells (see Methods, section 2.2.). In our differentiating conditions, wild type neurospheres cells grown in the presence of the mitogens EGF and FGF, generated Tuj1^{+} neurons around 3DIV, and glial cells (O4^{+} oligodendrocytes and Gfap^{+} astrocytes) at 5DIV. At 7DIV almost all cells had differentiated into one of the three cell types described. The differentiating conditions we have used favors astrocytic differentiation, as indicated by the high percentage of Gfap^{+} cells obtained. Indeed, at 7DIV 70% of the cells were Gfap^{+} astrocyes while Tuj1^{+} neurons and O4^{+} oligodendrocytes represented less than 10% of total cells each (Fig R25).

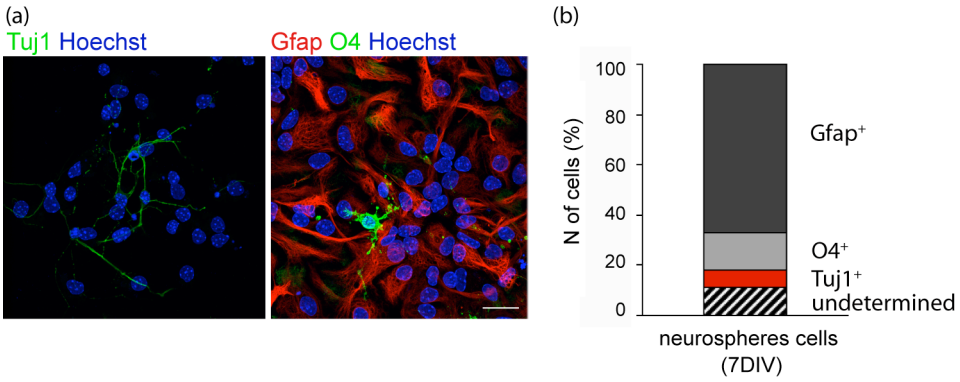

Fig R25: Generation of neuron and glial cells by cortical neurosphere cells. (a) Photographs correspond to 7DIV differentiated wild type progenitors that were immunolabaled with a Tuj1 antibody to label neurons (left panel in green) or with an O4 antibody to label oligodendrocytes and with a polyclonal Gfap antibody to label astrocytes (in green and red, respectively, in the right panel). Nuclei were stained with Hoechst (in blue). Scale bar: 20µm. (b) Histogram showing the percentage of Gfap$^+$ astrocytes, O4$^+$ oligodendrocytes and Tuj1$^+$ neurons in differentiating cultures at 7DIV.

In order to investigate the pluripotency of *Dyrk1a*$^{+/-}$ progenitors, we first evaluated their capability to differentiate into the neuronal and glial lineages. For that, differentiated *Dyrk1a*$^{+/+}$ and *Dyrk1a*$^{+/-}$ neurosphere cells were double immunolabelled at 7DIV with a Tuj1 antibody and an antibody against the glial marker Sox9. Sox9 is expressed by glial progenitors and its expression is maintained in mature astrocytes but not in myelinating mature oligodendrocytes (Stolt et al., 2003). Given that oligodendrocytes *in vitro* do not reach a complete mature phenotype, for which axon contact is required, we can assume that in our cultures oligodendrocytes remained Sox9$^+$ during all their differentiation process. Indeed, O4$^+$ differentiated oligodendrocytes were also Sox9$^+$ in 7DIV cultures (Fig R26a-d). As expected, Sox9 was not expressed by Tuj1$^+$ neurons in these cultures (Fig R26e-h).

Quantification of Sox9$^+$ and Tuj1$^+$ cells in *Dyrk1a*$^{+/+}$ and *Dyrk1a*$^{+/-}$ adherent cultures revealed that, at 7DIVs, around 80% of the cells were

Sox9$^+$ and 10 to 15% were Tuj1$^+$ in the wild type condition, and that these numbers were very similar in *Dyrk1a*$^{+/-}$ cultures (Fig R27).

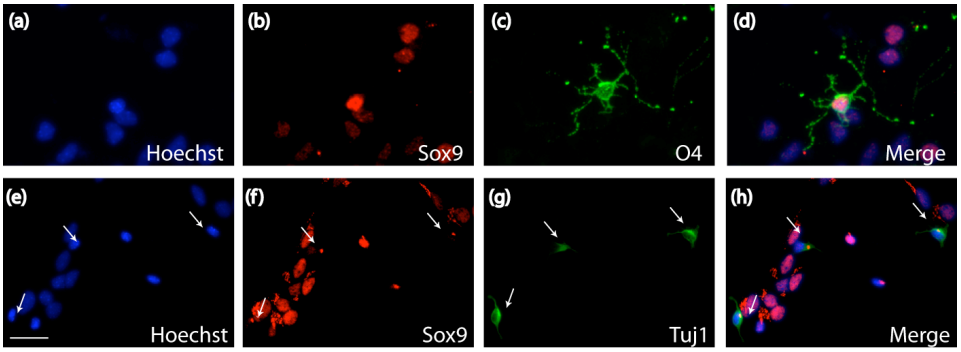

Fig R26: Sox9 expression in differentiating wild type cortical neurosphere cells. (a-d) Representative confocal images of differentiating sphere cells at 7DIV: O4 (green) and Sox9 (red) are coexpressed in oligodendroglial cells. (e-h). Tuj1$^+$ neurons (green, indicated by arrows) are Sox9$^-$ (red). Scale bar: 50µm.

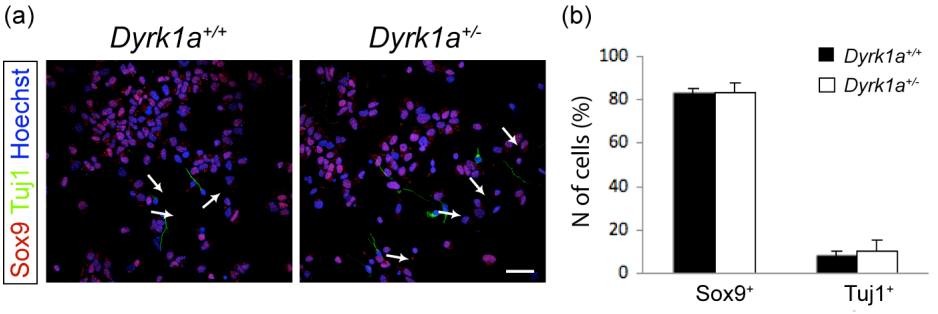

Fig R27: Sox9 and Tuj1 expression in differentiating *Dyrk1a*$^{+/+}$ and *Dyrk1a*$^{+/-}$ neurosphere cells. (a) Representative images showing Sox9$^+$ (red) and Tuj1$^+$ (green) cells in *Dyrk1a*$^{+/+}$ and *Dyrk1a*$^{+/-}$ differentiating cultures at 7DIV. Tuj1$^+$Sox9$^-$ cells are indicated with arrows. Hoechst (in blue) was used to stain nuclei. Scale bar: 20µm (b) Histogram shows the percentage of Sox9 and Tuj1 immunopositive cells over total nuclei at 7DIV. Histogram values correspond to the average percentage of immunopositive cells (±sem) of quantifications performed on 3 independent cultures per genotype. Statistical significance was calculated by Student's T-test.

Given that Sox9 is expressed in different glial subpopulations we used additional cell markers to quantify individual glial populations in *Dyrk1a*$^{+/+}$ and *Dyrk1a*$^{+/-}$ cultures at 7DIV. The high density of Gfap^{+} astrocytes in our cultures together with the nature of the Gfap staining (see Fig R25) made very difficult the quantification of this cell type, and for this reason, we did not count them. Conversely, we quantified the number of cells immunopositive for O4 and S100b glial markers, and found that the number of both O4^{+} and S100b^{+} cells in *Dyrk1a*$^{+/-}$ cultures was significantly lower than in wild type cultures (Fig R28).

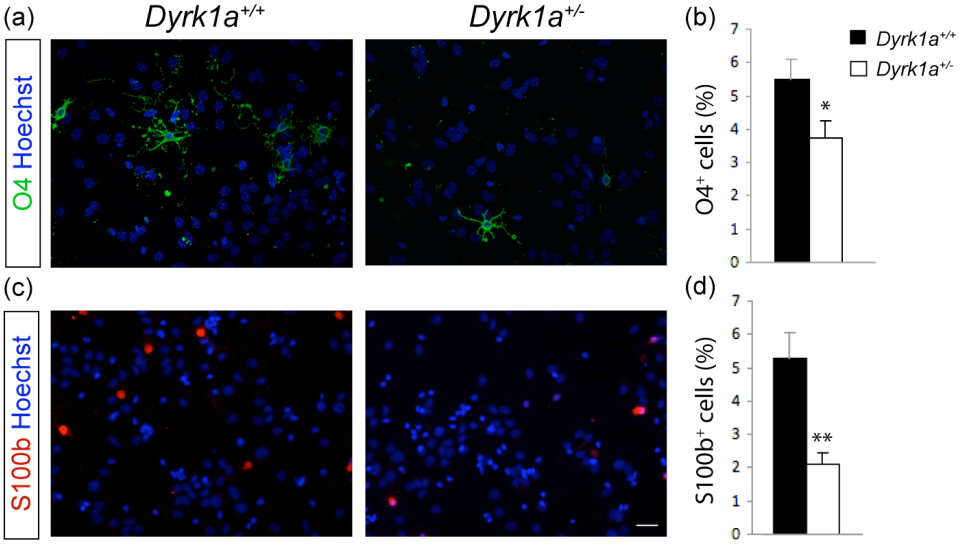

Fig R28: O4 and S100b expression in differentiating *Dyrk1a*$^{+/+}$ and *Dyrk1a*$^{+/-}$ neurosphere cells. *Dyrk1a*$^{+/+}$ and *Dyrk1a*$^{+/-}$ differentiating progenitors were cultured for 7DIV and immunolabelled with O4 (green in a) and S100b (red in c) antibodies. Hoechst staining was used to label nuclei (blue in a and c). Scale bar: 20µm. (c-d) Histogram representing the percentage of O4 (c) and S100b (d) immunopositive cells over total nuclei at 7DIV. Values correspond to the average percentage (±sem) of immunopositive cells obtained from quantifications performed on 13 *Dyrk1a*$^{+/+}$ and 10 *Dyrk1a*$^{+/-}$ independent cultures. Statistical significance was determined by Student's T-test (*p<0.05; **p<0.001).

O4 expression is restricted to the oligodendroglial lineage, while S100b expression can be detected in differentiating oligodendrocytes and in mature astrocytes (Deloulme et al, 2004). In differentiating neurosphere cultures analogous to ours, the expression of S100b becomes evident at 3DIV and only in cells of the oligodendroglial lineage. The number of $S100b^+$ cells in differentiating cultures increases and, after 15DIV approximately, S100b is mainly expressed in $Gfap^+$ astrocytes (Deloulme et al, 2004). In order to evaluate the identity of the $S100b^+$ cells at 7DIV, we double immunolabelled differentiated wild type cultures with a S100b antibody and an antibody against either O4, Mbp, both expressed in oligodendrocytes, or Gfap, expressed in astrocytes. The quantification of immunolabeled cells showed that 67% of the $S100b^+$ cells were $O4^+$, while only 7% of the $S100b^+$ also expressed Gfap. The number of Mbp^+ cells, which represent oligodendrocytes of a more mature state than the $O4^+$ ones, was very low, but in almost all cases, Mbp^+ cells were also immunopositive for S100b (Fig R29). Because S100b is expressed in both $O4^+$ and Mbp^+ oligodendrocytes, it is possible that the remaining $S100b^+$ cells that did not express Gfap were also oligodendrocytes but at different steps of differentiation. Taking all these aspects into account we can conclude that, in our *in vitro* conditions, S100b is mainly expressed in cells of the oligodendroglial lineage.

Altogether, the reduced number of $O4^+$ and $S100b^+$ cells that we observed in *Dyrk1a*$^{+/-}$ cultures at 7DIV, indicates that a normal dosage of *Dyrk1a* is necessary for normal differentiation of the progenitors towards the oligodendroglial lineage, at least *in vitro*. Since the total number of

Sox9^{+} cells did not change between genotypes, our results suggest that astrogliogenesis may be slightly increased in mutant cultures.

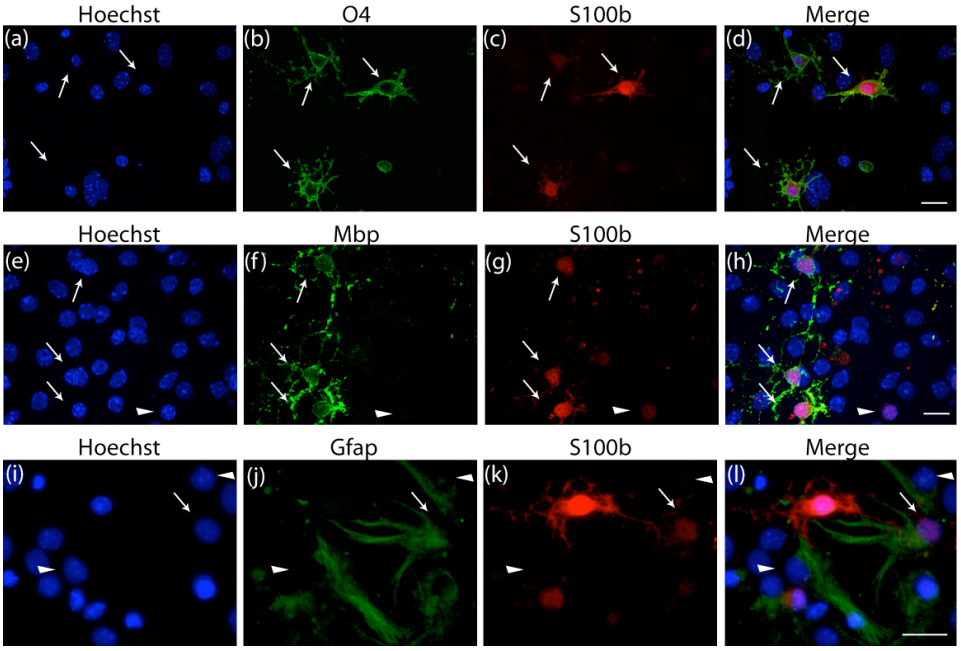

Fig R29: Coexpression of S100b with different glial cell markers in differentiating neurosphere cells. Photographs correspond to differentiating neurosphere cell cultures at 7DIV labeled with S100b antibody (in red) and with O4 (a-d), Mbp (e-h), or Gfap (i-l) antibodies (in green). Nuclei were stained with Hoechst (in blue). Arrows in (a) to (d) indicate cells expressing the oligodendroglial markers S100b and O4. In (e) to (h), arrows point to cells double positives for Mbp and S100b, and the arrowhead to an example of S100b^{+}Mbp^{-} cell. In few cases S100b and Gfap astroglial markers colocalize: the arrow in (i) to (l) is an example of Gfap^{+}S100b^{+} astrocyte while the arrowheads indicate Gfap^{+}S100b^{-} astrocytes. Note that S100b expression in Gfap^{+} cells, when detected, is much lower than S100b expression in Gfap^{-} cells. These Gfap^{-} cells, panels (i) to (l), were strongly labeled with S100b antibodies and have the characteristic morphology of cells of the oligodendroglial lineage expressing O4 shown in panels (a) to (d). Scale bars: 20µm.

4. Epigenetic changes during cortical development of *Dyrk1a*$^{+/+}$ and *Dyrk1a*$^{+/-}$ mice

The defect of *Dyrk1a*$^{+/-}$ neural progenitors in oligodendroglial diferentiation, together with the bioinformatic analysis of the microarray data highlighting that the differentially expressed genes in the cerebral cortex of *Dyrk1a*$^{+/-}$ mice are enriched in genes related to the gliogenic JAK-STAT signalling pathway, suggested that gliogenesis may be altered in the cerebral cortex of *Dyrk1a*$^{+/-}$ mice.

In the developing CNS the neurogenic to gliogenic switch, which allows neural progenitors to generate first neurons and then glial cells (Qian et al., 2000) is tightly controlled by epigenetic mechanisms. Among them, DNA methylation at CpG dinucleotides of glial gene promoters and promoters of essential genes of the JAK/STAT pathway is pivotal in controlling the precise time of the switch (Takizawa 2001, Fan 2005). The promoter regions of genes that were up- or down- regulated in *Dyrk1a*$^{+/-}$ cerebral cortex showed a different CpG content (see Fig R12). This observation suggested that the chromatin state of these progenitors may be different than the chromatin state in wild type progenitors and that this difference may contribute to the altered differentiation potential of *Dyrk1a*$^{+/-}$ progenitors observed *in vitro*. To investigate this hypothesis we focused our study on two glial genes, *S100b* and *Gfap*, whose epigenetic regulation during the neurogenic to gliogenic switch is well documented and whose expression levels were found altered in *Dyrk1a*$^{+/-}$ developing cortices.

4.1. Effect of *Dyrk1a* dose reduction in the methylation state of *S100b* and *Gfap* promoters

The developmental regulation of ***S100b*** promoter methylation in mouse CNS has been described for the following CpGs upstream the TSS: the -9, -152, -267 and -763, according to the Refseq release 5 (Namihira et al., 2004; Fan et al., 2005). These nucleotide positions correspond, respectively to the positions -64, -207, -318 and -818 in the current Refseq release 49. Namihira and colleagues showed that all the four CpGs of *S100b* promoter are highly methylated *in vivo* during the neurogenic phase of the brain, when *S100b* gene is silenced. A specific demethylation of *S100b* promoter at position -267 occurs in the mouse telencephalon between E11.5 and E14.5 and seems to define the beginning of *S100b* expression at late embryonic stages, when gliogenesis occurrs. The same sequential events occur in neural progenitors in culture, suggesting that the epigenetic control of *S100b* expression in neural progenitors contributes to determine their differentiation potential (Namihira et al., 2004).

To investigate our hypothesis we began our analysis comparing the methylation levels of *S100b* promoter at position -267 in E14.5 *Dyrk1a*$^{+/+}$ and *Dyrk1a*$^{+/-}$ cerebral cortices. Our DNA pyrosequencing data, in agreement with the previous published data (Namihira et al., 2004), showed that the level of methylated DNA at this position in the wild type situation is lower than 20%. Interestingly *Dyrk1a*$^{+/-}$ cortices showed significantly higher levels of DNA methylation (Fig R30a). We also investigated at the same time point, the methylation status of CpG(+59) of *S100b* gene, whose regulation has not been described in literature. The methylation frequency of S100b at position +59 was around 50%

and no changes in DNA methylation levels were observed between genotypes (Fig R30b).

The increased methylation of CpG(-267) observed in *Dyrk1a*$^{+/-}$ cortices at E14.5 correlates with the reduced expression of *S100b* gene observed in the cortices of *Dyrk1a*$^{+/-}$ mice at E16.5, when we first detected *S100b* transcripts by qPCR (data not shown). Given that down-regulation of *S100b* in mutant cortices was also found at postnatal stages, we analyzed the methylation status of CpG(-267) in the cerebral cortex of *Dyrk1a*$^{+/+}$ and *Dyrk1a*$^{+/-}$ mice at P0, but no differences between genotypes emerged from this analysis (Fig R30a). At this time point methylated DNA at CpG(-267) represented only 5% of the total DNA, a percentage that is significantly lower than those observed at E14.5 indicating that demethylation at this position continues in cortical cells of both genotypes after this time point of development. Given that cell type diversity increases during corticogenesis and that at P0 most of the cells in the cortex are neurons and the pool of progenitors is significantly depleted, it is possible that the epigenetic status of the remaining neural progenitors is still different in the two genotypes, but this difference can not be appreciated in the whole cortex. It is also possible that demethylation of the *S100b* promoter at CpG(-267) is just delayed in E14.5 mutant cortices and demethylation of this site ends before birth.

The increased methylation of *S100b* promoter at CpG(-267) that we observed in *Dyrk1a*$^{+/-}$ E14.5 cortex, can be due to a defective demethylation or to an increased dafault methylation in the neural progenitors. To test if this could be the case we compared the methylation status of this site in *Dyrk1a*$^{+/+}$ and *Dyrk1a*$^{+/-}$ cortices at E11.5, when *S100b* promoter is highly methylated and the gene repressed (Namihira et al., 2004). At this developmental stage the levels of

methylated DNA at CpG(-267) was higher than at E14.5, around 55%, and not significant differences were observed between genotypes (Fig R30a). This result indicates that in cortical neural progenitors the starting methylation status of this site is independent of *Dyrk1a* dosage.

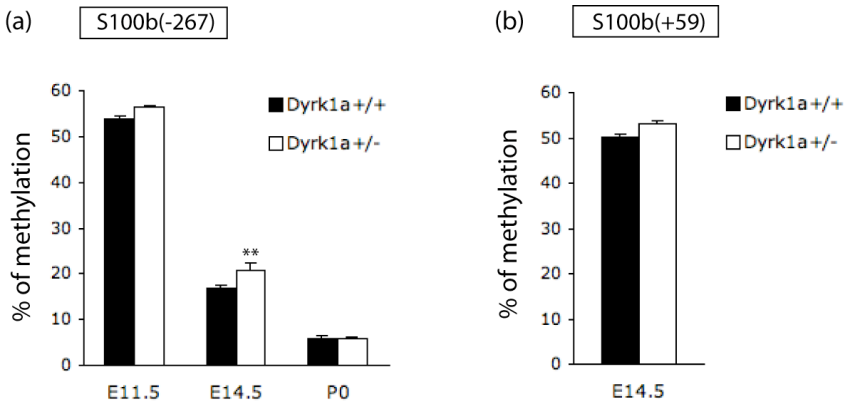

Fig R30: Effect of *Dyrk1a* dose reduction in the methylation state of the *S100b* promoter in the developing cerebral cortex. (a) Histogram showing the methylation frequencies of the CpG(-267) site of *S100b* promoter determined by pyrosequencing analysis of genomic DNA prepared from *Dyrk1a*$^{+/+}$ and *Dyrk1a*$^{+/-}$ mouse cerebral cortices at embryonic (E11.5 and E14.5) and postnatal (P0) stages. (b) Histogram showing the methylation frequency of the CpG(+59) of *S100b* gene at E14.5. Histograms represent the average (±sem) methylation frequencies, expressed as percentage of the total sites analyzed, measured in DNAs obtained from 6 embryos per genotype at E11.5 and E14.5, and from 3-5 animals per genotype at P0. Statistical significance was determined by Student's T-test (**p<0.01).

Gfap expression is undetectable during the neurogenic phase of mouse brain development and becomes significant, in most structures, perinatally upon STAT3 binding to its promoter (Nakashima 1999). It is well established that methylation of *Gfap* promoter at position -1502, which lies within the STAT3 binding site ttcCGagaa, is responsible of *Gfap* gene silencing during neurogenesis. Demethylation of *Gfap* promoter at this position occurs at the end of the neurogenic phase in

neural progenitors, allowing STAT3 binding to the promoter and the transcriptional activation of *Gfap* gene (Takizawa 2001). Demethylated *Gfap* is characteristic of late neural progenitors, which are prone to differentiate into astroglial cells.

We analyzed the methylation status of three CpGs of the *Gfap* promoter: the mentioned CpG(-1502) within the STAT3 binding site, and two other sites, the CpG(-1512) and the CpG(-1466) around the STAT3 binding site. Methylation of the promoter at these sites was around 50% in the wild type situation in E14.5 cerebral cortex but, interestingly, all of them were found less methylated in *Dyrk1a*$^{+/-}$ cortices (Fig R31a). Once more, this result correlates with the up-regulation of *Gfap* expression found in the cortex of mutant mice at P7 (see Table R2 and Fig R13). As in the case of the *S100b* promoter, we did not observe differences between genotypes in the methylation state of *Gfap* promoter when *Dyrk1a*$^{+/+}$ and *Dyrk1a*$^{+/-}$ cortex were compared at P0 (Fig R31b). Curiously, the methylation level of the STAT3 site in the mouse *Gfap* promoter remained almost the same between E14.5 and P0, suggesting that demethylation of this promoter occurs with a different kinetic than the observed for *S100b* promoter.

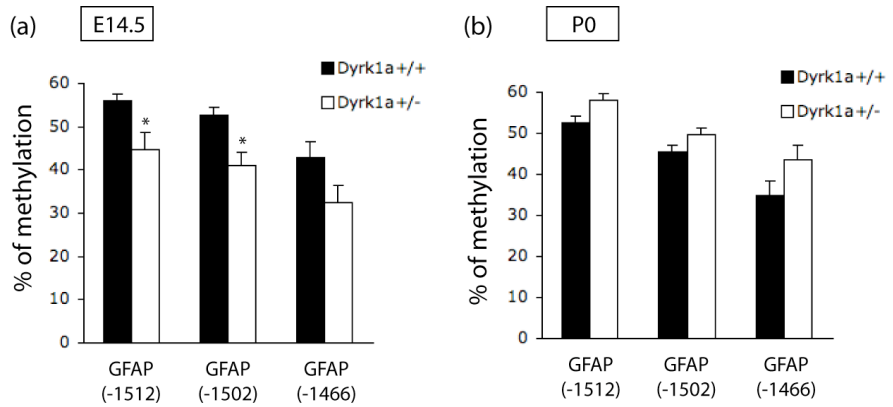

Fig R31: Effect of *Dyrk1a* dose reduction in the methylation state of the *Gfap* promoter in the developing cerebral cortex. Methylation frequencies of the indicated sites within the *Gfap* promoter were determined by pyrosequencing analysis of genomic DNA prepared from *Dyrk1a*$^{+/+}$ and *Dyrk1a*$^{+/-}$ mouse cerebral cortex at embryonic E14.5 (a) and P0 (b). Histogram values correspond to the average (±sem) methylation frequencies, expressed as percentage of the total sites analyzed, measured in DNAs obtained from 6 embryos per genotype at E14.5, and from 3-5 animals per genotype at P0. Statistical significance was determined by Student's T-test (*p<0.05).

With the aim of confirming our *in vivo* results, we studied the methylation status of *S100b* and *Gfap* promoters in embryonic neurosphere cultures obtained from E14.5 *Dyrk1a*$^{+/+}$ and *Dyrk1a*$^{+/-}$ animals. Fig R32a shows that the methylation frequency of CpG(-267) in the *S100b* promoter was very low in neurospheres of both genotypes. Nevertheless, it was significantly higher in *Dyrk1a*$^{+/-}$ neurospheres than in the wild type ones. The methylation frequency of the other site analyzed, CpG(+59), was also lower in neurosphere cells than in E14.5 cortices and, interestingly, DNA methylation was significantly higher in *Dyrk1a*$^{+/-}$ neurospheres than in wild type neurospheres (Fig R32a). These results were in agreement with the decreased *S100b* mRNA levels observed in mutant embryonic neurospheres (Fig R24).

The same CpGs of the *Gfap* promoter analyzed *in vivo* were found almost completely demethylated in embryonic neurospheres of both genotypes (Fig R32b). The differences on the levels of methylated DNA between neurosphere cells and cortical tissue suggest that different epigenetic mechanisms act in neural progenitor cells *in vivo* and *in vitro.*

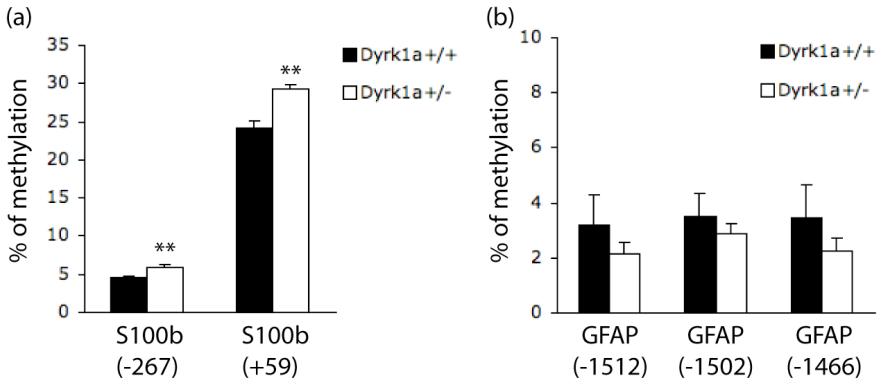

Fig R32: Effect of *Dyrk1a* dose reduction on the methylation state of *S100b* and *Gfap* promoters, in embryonic neurospheres cultures. Methylation frequencies for the indicated positions of *S100b* (a) and *Gfap* (b) promoters were determined by pyrosequencing analysis of genomic DNA prepared from *Dyrk1a*$^{+/+}$ and *Dyrk1a*$^{+/-}$ neurosphere cultures. Histogram values correspond to the average (±sem) methylation frequencies, expressed as percentage of the total sites analyzed, measured in 7 p2 neurosphere cultures per genotype. Statistical significance was determined by Student's T-test (*p<0.05; **p<0.01).

4.2. Effect of *Dyrk1a* dose reduction on histone modifications of the *S100b* and *Gfap* promoters

In addition to DNA methylation, the other major epigenetic changes that modulate the state of the chromatin are covalent modifications of histone tails. There are compelling evidences that an extensive crosstalk exists between these two levels of epigenetic regulation of gene expression (reviewed in Hirabayashi and Gotoh, 2010). For this reason we analyzed whether the changes in DNA methylation detected in the promoter regions of the glial genes *S100b* and *Gfap* in *Dyrk1a*$^{+/-}$ embryonic telencephalon were associated to a different pattern of histone modifications. With this aim we used chromatin immunoprecipitation (ChIP) experiments to study the enrichment of histone modification

marks in the regulatory regions of *S100b*, around CpG(-267) and CpG(+59), and of *Gfap*, around the STAT3 binding site, in the cortex of E14.5 *Dyrk1a*$^{+/+}$ and *Dyrk1a*$^{+/-}$ embryos. We focused our study on two activation marks, which are marks related to an open chromatin state, the trimethylation of lysin4 in histone H3 (H3K4me3) and the acetylation of lysine16 in histone H4 (H4K16Ac), and on two repressive marks, which are associated to a close and trascriptionally inactive chromatin state, the trimetylation of lysin9 and of lysine27 in histone H3, H3K9me3 and H3K27me3, respectively. Our analysis showed that both repressive histone marks as well as the H3K4me3 activation mark were present at very low levels in the promoter regions of *S100b* and *Gfap* analyzed (enrichment values lower than 10% over the total amount of histone H3), with no differences between genotypes (data not shown). On the contrary, we detected higher levels of the H4K16Ac activation mark in both *S100b* and *Gfap* promoter regions in wild type samples, with enrichments around 20-30% over total histone H3 (Fig R33). Increased levels of acetylated histone H4 have been associated to the activation of *S100b* gene in the developing mouse cortex (Nihimira et al., 2004). The comparative analysis between genotypes revealed a significant decreased enrichment of H4K16Ac in the *S100b* promoter of *Dyrk1a*$^{+/-}$ E14.5 cortices in both positions analyzed (Fig R33). This result further supports the finding that the *S100b* promoter in the developing brain of mice lacking one functional copy of *Dyrk1a* is in a more repressed state than in wild type brains. Contrarily to *S100b*, no differences in H4K16Ac enrichment were observed in the *Gfap* promoter (Fig R33).

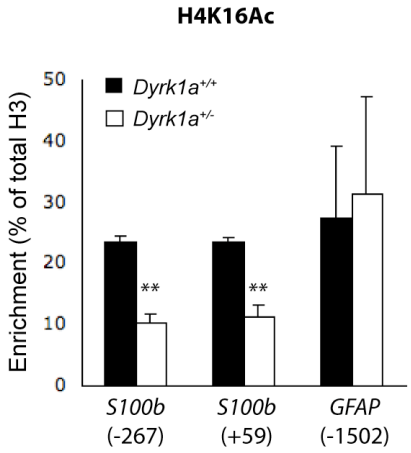

Fig R33: Histone H4 acetylation in *S100b* and *Gfap* promoters of *Dyrk1a*$^{+/+}$ and *Dyrk1a*$^{+/-}$ E14.5 cortex. Histogram showing the enrichment of H4K16Ac at the indicated positions of *S100b* and *Gfap* promoters in E14.5 mouse cerebral cortex, determined by ChIP experiments. Histogram values correspond to the average (±sem) H4K16Ac enrichment, expressed as the percentage of total histone H3, calculated from independent experiments performed with 3 *Dyr1a*$^{+/+}$ and 5 *Dyr1a*$^{+/-}$ animals. Statistical significance was determined by Student's T-test (**p<0.01).

Altogether our results indicate that *Dyrk1a* dose reduction leads to changes in the chromatin state of *S100b* and *Gfap* glial genes during embryonic development *in vivo*. The effects of these changes are gene-specific and correlate with the altered expression of *S100b* and *Gfap* genes in the cerebral cortex of mutant mice detected at later developmental stage. Given the different CpG content of the promoters of the set of up- and down-regulated genes in the cerebral cortex of newborn *Dyrk1a*$^{+/-}$ mice, it is possible that *Dyrk1a* dose reduction affects the chromatin state of other genes and that these changes modify the expression of key developmental genes in a timely defined manner leading to changes in the differentiation process of the cortex.

5. *In vivo* analysis of cortical gliogenesis in *Dyrk1a*$^{+/+}$ and *Dyrk1a*$^{+/-}$ mice

Mouse gliogenesis is mainly a postnatal event starting perinatally and peaking at the first week of life in the case of astrogliogenesis and between the second and third weeks in the case of oligodendrogenesis (reviewed in Wang and Bordey, 2008). Developmental gliogenesis ends after one month, although glial cells can still proliferate in adult CNS, mainly in response to injury.

5.1. Oligodendroglial phenotype of *Dyrk1a*$^{+/-}$ mice

Our *in vitro* studies indicate that *Dyrk1a*$^{+/-}$ neurospheres generate less S100b^{+} oligodendroglial cells upon differentiation (see Fig R28). The increased methylation of the *S100b* promoter and the reduction in *S100b* mRNA levels in *Dyrk1a*$^{+/-}$ developing cerebral cortices (see Fig R30, Table R2 and Fig R13) suggest that the number of S100b^{+} cells may also be altered *in vivo*. To see if this is the case, we decided to count the number of S100b^{+} cells in the somatosensorial (SS) cortex (gray matter) and *Corpus Callosum* (white matter) of *Dyrk1a*$^{+/+}$ and *Dyrk1a*$^{+/-}$ P0 mice. A representative S100b immunolabeling used for cell quantification in the brain regions analyzed is reported in Fig R34a. S100b^{+} cells *in vivo* showed different morphologies in both wild type and mutant mice: from branched big cells in the *Corpus Callosum* to fusiform cells in the cortex (arrows in Fig R34b and d). We also detected dividing S100b^{+} cells in the white matter (arrow in Fig R34c). Because the staining pattern of S100b^{+} cells varies a lot, we decided to include in our quantifications all immunopositive cells. A significant reduction of S100b^{+} cell density in *Dyrk1a*$^{+/-}$ mice compared to the wild type controls, was found in both

structures analyzed, 40% reduction in the *Corpus Callosum* and 25% in the SS cortex (Fig R34e). Because total cell density is increased in the *Corpus Callosum* of *Dyrk1a*$^{+/-}$ mice (Fig R34f), the difference in the percentage of S100b^{+} cells between genotypes increased to 50% in this structure (Fig R34g). Total cell density is also increased in the SS cortex of young adult *Dyrk1a*$^{+/-}$ mice (Fotaki et al. 2002). Although we did not count total cells in the SS cortex of newborn mice, it is reasonable to think that in this structure the difference in the percentage of S100b^{+} cells between genotypes could be greater than 25%.

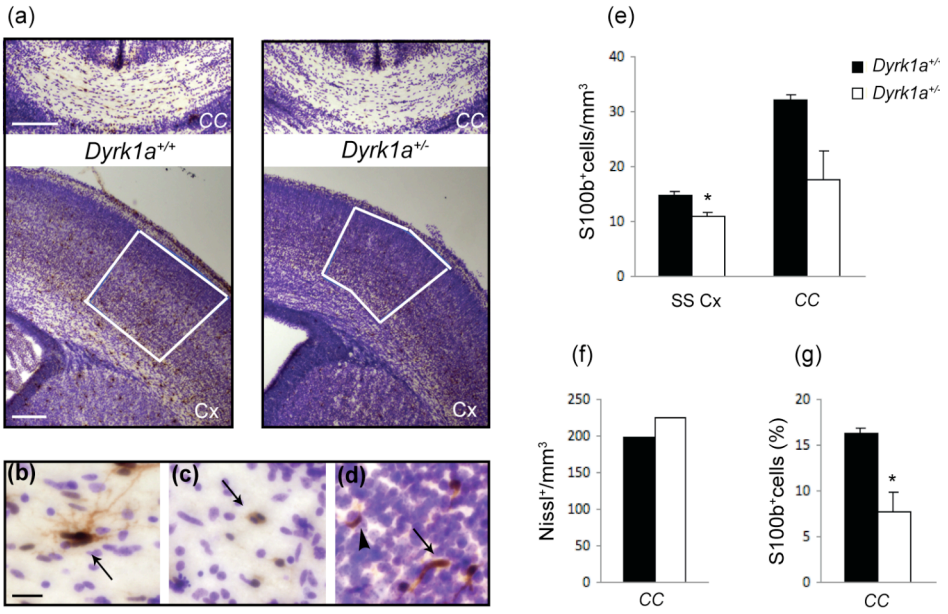

Fig R34: Quantifications of S100b^{+} cells in *Dyrk1a*$^{+/+}$ and *Dyrk1a*$^{+/-}$ cerebral cortex and *Corpus Callosum* of newborn mice. (a-d) Photographs show S100b immunolabelled *Dyrk1a*$^{+/+}$ and *Dyrk1a*$^{+/-}$ brain sections at P0. Cell nuclei are labeled with Nissl. (a) Representative pictures of S100b staining at the level of the *Corpus Callosum (CC)* and cerebral cortex (Cx). White squares delimitate the somatosensorial (SS) cortex where S100b^{+} cells were quantified. (b-d) Photographs showing different morphologies of S100b^{+} cells: a highly branched S100b^{+} cell (b) and dividing S100b^{+} cells (c) of the *CC*, and cells of the SS

cortex with ubiquitous cytoplasmic staining and fusiform morphology (arrow) and perinuclear S100b staining (arrowhead) (d). (e) Histograms show total S100b$^+$ cell densities, expressed as number of cells per mm^3, in the SS Cx and *CC* of *Dyrk1a*$^{+/+}$ and *Dyrk1a*$^{+/-}$ mice. Statistical significance was determined by Student's T-test (*p<0.05 in the SS Cx and p=0.06 in the *CC*). (f, g) Histograms show total numbers of nuclei, stained with Nissl, per mm^3 (f) and the percentage of S100b$^+$ cell over total nuclei (g), in the *CC* of *Dyrk1a*$^{+/+}$ and *Dyrk1a*$^{+/-}$ mice (*p<0.05 as determined by a Student's T-test). Histogram values in (e) to (g) correspond to the average (±sem) numbers obtained in quantifications performed in sections from 3 littermates per genotype. Scale bar: 200µm (a); 20µm (b-d).

S100b is expressed in cells of the oligodendroglial lineage during development and by astrocytes in the adult brain (Deloulme et al, 2004, Vives et al., 2003). By double immunostainings we confirmed that most of the S100b$^+$ cells in the developing brain belong to the oligodendroglial lineage. Indeed, S100b and the oligodendroglial marker O4 were co-expressed in the same cells, both in the *Corpus Callosum* and in the cerebral cortex of P7 mice (Fig R35a-b). Few cells were S100b$^+$O4$^-$ (arrows in a and b), and they usually presented a weak S100b staining (a). In agreement with this we observed few S100b$^+$Gfap$^+$ cells in both the cerebral cortex and the *Corpus Callosum* (Fig R35c-d). These cells corresponded to the cells presenting weak S100b expression (arrowhead in Fig 33d). We never detected S100b$^+$Tuj1$^+$ cells, indicating that S100b expression is excluded from the neuronal lineage (data not shown). Quantification of double positive cells in the *Corpus Callosum* confirmed our observations; 60% of the S100b$^+$ cells were O4$^+$ while only 15% were Gfap$^+$(Fig R35e).

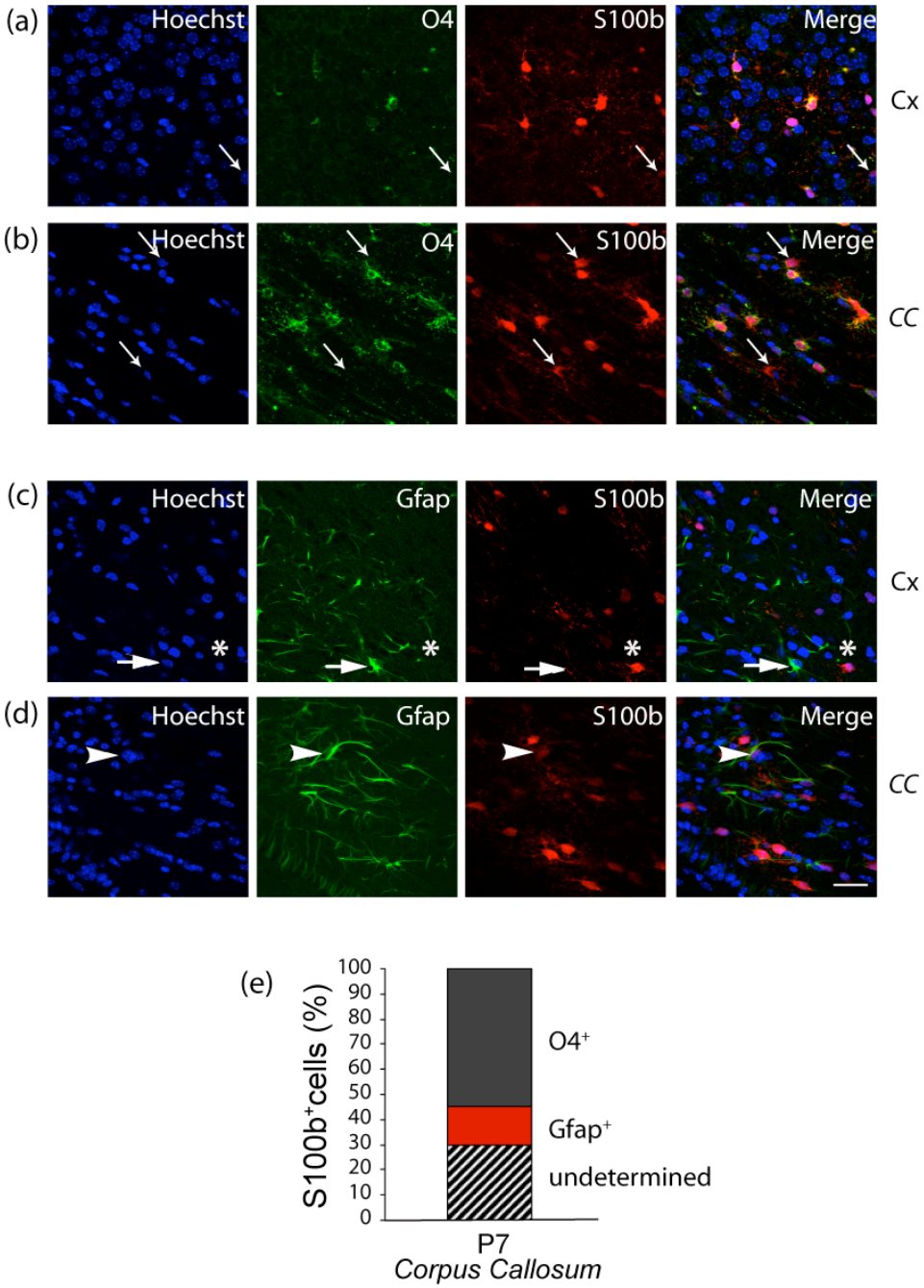
(a)
Hoechst
O4
S100b
Merge
Cx
(b)
Hoechst
O4
S100b
Merge
CC
(c)
Hoechst
Gfap
S100b
Merge
Cx
(d)
Hoechst
Gfap
S100b
Merge
CC
(e)
S100b+cells (%)
100
90
80
70
60
50
40
30
20
10
0
O4+
Gfap+
undetermined
P7
Corpus Callosum

Fig R35: Expression of S100b in the somatosensorial cortex and *Corpus Callosum* of postnatal mice. (a-d) Confocal images of 8μm projections of coronal P7 brain sections labeled with the indicated antibodies; Hoechst was used to stain the nuclei. (a-b) S100b and O4 oligodendroglial markers largely colocalize in the somatosensorial cortex (Cx in a) and the *Corpus Callosum* (*CC* in b). However $S100b^{+}O4^{-}$ cells are also present in both structures (arrows in a and b). S100b and Gfap rarely colocalize. An uncommon case of $S100b^{+}Gfap^{+}$ cell is indicated by the arrowhead in panel (d), while examples of $S100b^{-}Gfap^{+}$ and $S100b^{+}Gfap^{-}$ cells are indicated respectively by the arrow and the asterisk in panel (c). (e) Histogram shows the quantification of $O4^{+}S100b^{+}$ and of $Gfap^{+}S100b^{+}$ cells in the *Corpus Callosum* expressed as percentage of total $S100b^{+}$cells, 80 total $S100b^{+}$ cells were counted. Scale bar: 20μm.

We then asked whether the alterations in gene expression and oligodendroglial cell numbers observed in *Dyrk1a*$^{+/-}$ mice at early postnatal stages have any consequence later in development. For that we analyzed the levels of Myelin Basic Protein (Mbp) in *Dyrk1a*$^{+/+}$ and *Dyrk1a*$^{+/-}$ cortices around 2 weeks after birth, at the peak of the oligodendrogenic process. Mbp represents 30% of total myelin proteins, it is required for the onset of myelinogenesis and is expressed in mature oligodendrocytes (reviewed in Boggs et al., 2006). Given that myelination is a fundamental characteristic of oligodendrocytes, Mbp is often used as a marker of mature functional oligodendrocytes. Western blot analysis showed that Mbp levels were dramatically reduced in mutant cerebral cortices (around 70% compared to the wild types) (Fig R36a-b). Interestingly, this reduction was not associated to a decrease in *Mbp* mRNA levels (Fig R36c), indicating that alterations in post-transcriptional modifications may account for the reduced Mbp protein levels observed in *Dyrk1a*$^{+/-}$ cortex. A significant reduction in the levels of Mbp protein, not associated to a reduction in the levels of mRNA also persisted at 2 months (P60), when oligodendrogenesis has finished (Fig R36d-f).

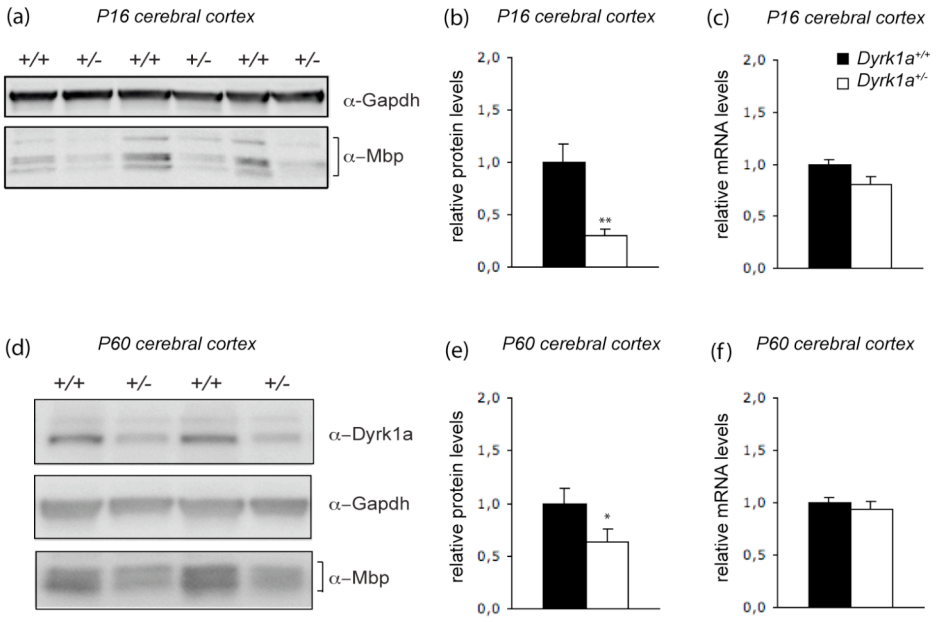

Fig R36: Mbp expression in the telencephalon of *Dyrk1a*$^{+/+}$ and *Dyrk1a*$^{+/-}$ postnatal and adult mice. (a) Western blot immunodetection of Mbp in total protein extracts prepared from the cerebral cortex of P16 *Dyrk1a*$^{+/+}$ and *Dyrk1a*$^{+/-}$ mice. The 4 bands correspond to Mbp isoforms (14, 17, 18, 21 KDa) expressed during development (reviewed in Baron and Hoekstra, 2010). Gapdh was used as loading control. (b) Quantification of the bands in western blots like the one shown in (a), the histogram shows the average values (±sem) of Mbp protein levels measured in 8 animals per genotype. (c) Histogram showing the average (±sem) *Mbp* mRNA levels determined by qPCR in the cerebral cortex of 2 *Dyrk1a*$^{+/+}$ and 3 *Dyrk1a*$^{+/-}$ P16 mice. (d) Western blot immunodetection of Mbp and Dyrk1a in total protein extracts prepared from the cerebral cortex of adult (P60) *Dyrk1a*$^{+/+}$ and *Dyrk1a*$^{+/-}$ mice. The 2 bands in the blot hybridized with the Mbp antibody probably correspond to the 17 and 18 KDa isoforms of Mbp (Baron and Hoekstra, 2010) and the 2 bands in the blot hybridized with the Dyrk1a antibody different phosphorylation forms of Dyrk1a. Gapdh was used as loading control. (e) Quantification of the bands in western blots like the one shown in (d): the histogram represents the average values (±sem) of Mbp protein levels measured in 7 animals per genotype. (f) Histogram showing the average (±sem) *Mbp* mRNA levels, determined by qPCR, in the cerebral cortex of 8 adult *Dyrk1a*$^{+/+}$ and 8 *Dyrk1a*$^{+/-}$ mice. **p<0.01 and *p<0.05 according to Student's T-test.

Because the number of oligodendroglial cells is reduced in the brains of *Dyrk1a*$^{+/-}$ mice at P0, it is possible that the reduced levels of Mbp observed in young and adult mutant brains are due to an impaired generation of mature oligodendrocytes. To test this possibility we counted the number of Cc1^{+} myelinating oligodendrocytes, in the *Corpus Callosum* and pyriform cortex of adult *Dyrk1a*$^{+/+}$ and *Dyrk1a*$^{+/-}$ mice. Cell quantifications did not highlight any difference between genotypes (Fig R37a-b) suggesting that the decreased number of pre-myelinating oligodendroglial cells observed during development is compensated in the adult.

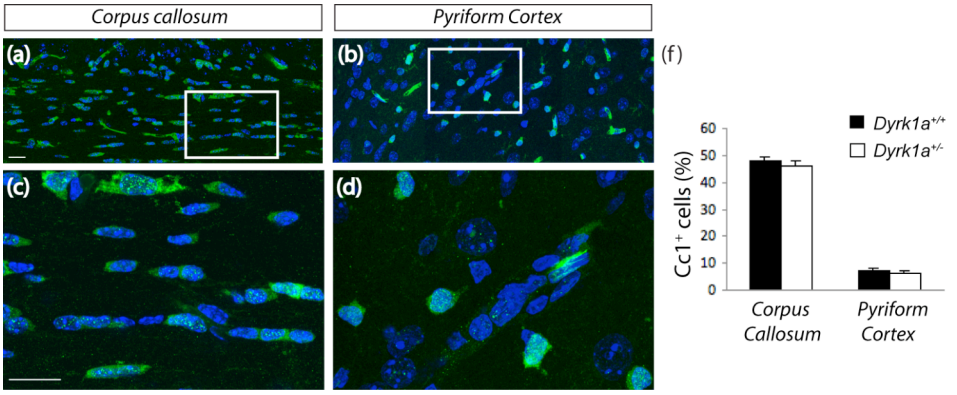

Fig R37: Quantification of Cc1^{+} mature oligodendrocytes in the pyriform cortex and *Corpus Callosum* of adult *Dyrk1a*$^{+/+}$ and *Dyrk1a*$^{+/-}$ mice. (a-d) Representative confocal photographs of coronal brain sections prepared from *Dyrk1a*$^{+/+}$ adult (P60) mice and immunolabelled with an anti-Cc1 antibody. (a, c) correspond to the *Corpus Callosum* and (b, d) to the Pyriform cortex; Cc1 immunostainig is in green and Hoechst staining of the nuclei in blue. Insets in (a) and (b) are, respectively, magnified in (c) and (d). Histograms in (f) show the percentage of total Cc1^{+} cells in the cortex and in *Corpus Callosum* of *Dyrk1a*$^{+/+}$ *and Dyrk1a*$^{+/-}$ adult (P60) mice. Values are the average (±sem) of quantifications performed in sections from 3 different animals per genotype. Statistical significance was determined by Student's T-test ($p>0.05$ in all cases). Scale bar: 20µm.

This negative result opens the possibility that the reduced Mbp protein level in adult *Dyrk1a*$^{+/-}$ brains is the consequence of a defective myelination process rather than of a decreased number of oligodendrocytes. To investigate this possibility we used Transmission Electron Microscopy (TEM) to analyze the myelinic sheaths that wrap axons in the *Corpus Callosum* of young adult *Dyrk1a*$^{+/+}$ and *Dyrk1a*$^{+/-}$ mice.

The *Corpus Callosum* of *Dyrk1a*$^{+/-}$ mice showed a higher density of myelinated axons and a reduced number of big-caliber myelinated axons (Fig R38a). Indeed, we found a significant reduction in the average diameter of myelinated axon in mutant mice with respect to the wild type animals (Fig R38b). Interestingly, the overall myelin thickness was significantly reduced in the mutants (Fig R38c). Taking into account that myelin thickness is proportional to axon diameter (Voyvodic 1989), the reduced number of big-caliber myelinated axons could account for the reduction in the average myelin thickness observed. However, this seems not to be the case because when we reanalyzed the data grouping the axons according to their diameter the myelin thickness was decreased in axons of all sizes (Fig R38d). Differences between genotypes were significant for thin axons but this became less consistent for axon with a diameter higher than 0.8μm, probably because of the reduced number of axons falling into this category.

Importantly, a reduced myelin thickness was also observed in another nerve of the CNS, the optic nerve, in axons of all sizes (Fig R39a), and in the sciatic nerve, which belong to the PNS (Fig R39b). Altogether, these results strongly suggest that *Dyrk1a*$^{+/-}$ mice have a myelination defect that affects both the CNS and the PNS. As

oligodendrogenesis in these mice is delayed, the impaired myelination observed in adult animals may have a developmental origin.

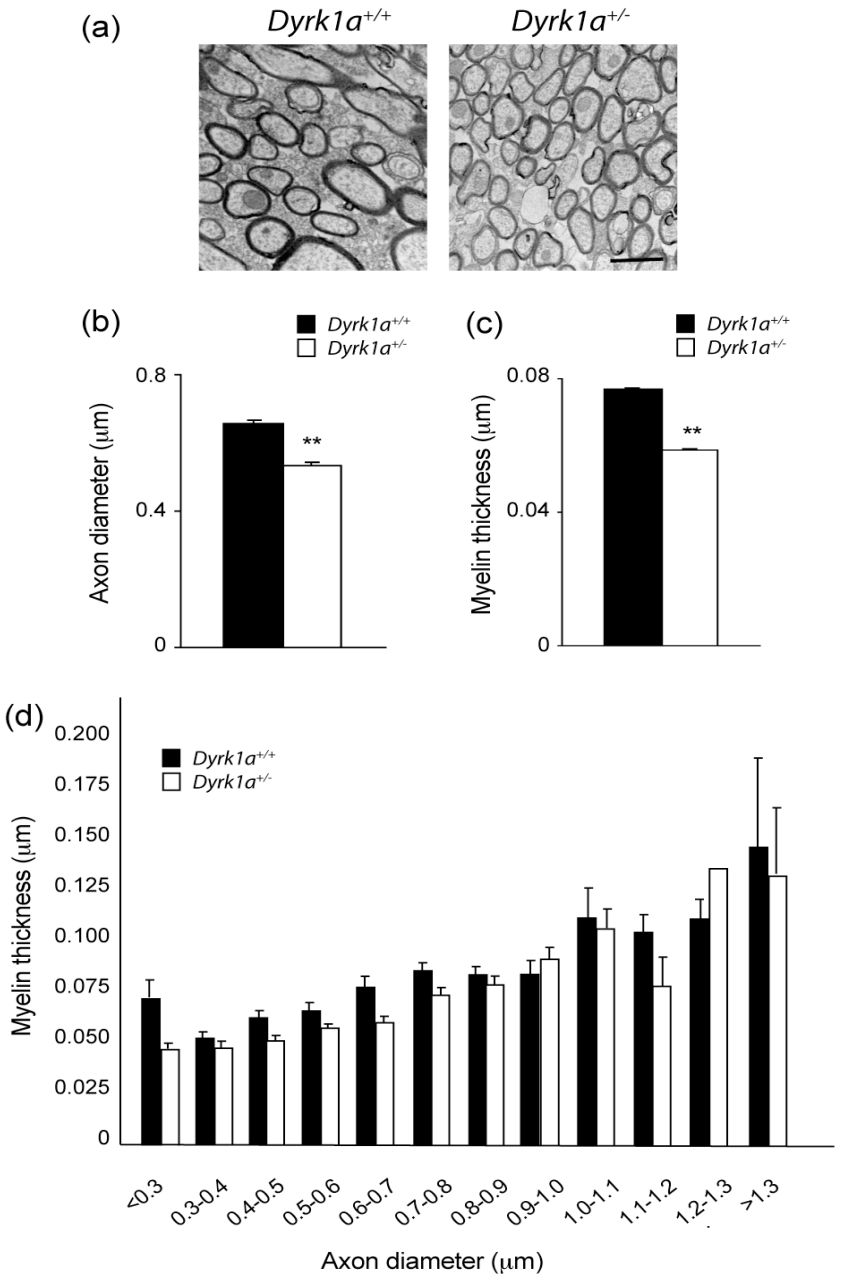

Fig R38: Transmission electron microscopy analysis of the *Corpus Callosum* of adult *Dyrk1a*$^{+/+}$ and *Dyrk1a*$^{+/-}$ mice. (a) Electron micrographs of transverse sections at the body of the *Corpus Callosum* obtained from the brains of adult (P60) littermates of the two genotypes. Scale bar: 1µm. (b-c) Quantifications of the myelinated axon diameter (b) and axonal myelin thickness (c) in callosal transverse sections as the ones represented in (a). Histogram represents the average values (±sem), expressed in µm, obtained by measuring 768 *Dyrk1a*$^{+/+}$ and 1,792 *Dyrk1a*$^{+/-}$ axons in preparations from 2 *Dyrk1a*$^{+/+}$ and 4 *Dyrk1a*$^{+/-}$ littermates, respectively. Statistical significance was determined by Student's T-test (**p<0.001). (d) Histogram representing the average myelin thickness (±sem) of the same axons measured in (c) grouped according to their diameter. Ranges of 0.1µm were used to group the axons

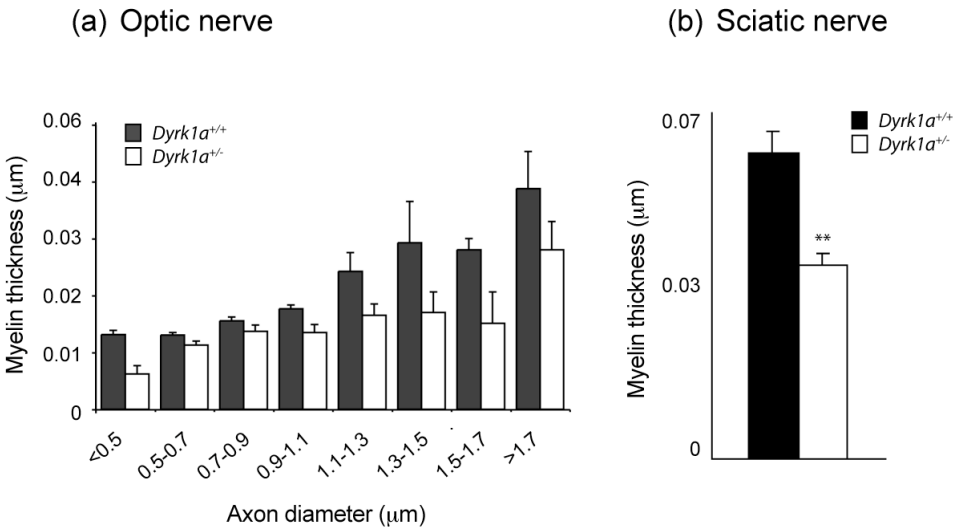

Fig R39: Myelin thickness of optic and sciatic nerves of adult *Dyrk1a*$^{+/+}$ and *Dyrk1a*$^{+/-}$ mice. (a) Quantifications of axonal myelin thickness in transverse sections of *Dyrk1a*$^{+/+}$ and *Dyrk1a*$^{+/-}$ optic nerves. The histogram represents the average myelin thickness (±sem), expressed in µm, of axons grouped according to their diameter (ranges of 0.2µm). Sections from a minimum of three littermates per genotype were used for the quantification. (b) Quantifications of axonal myelin thickness in transverse sections of *Dyrk1a*$^{+/+}$ and *Dyrk1a*$^{+/-}$ sciatic nerves. The histogram represents the average thickness (±sem), expressed in µm, of 158 *Dyrk1a*$^{+/+}$ and 349 *Dyrk1a*$^{+/-}$ axons measured in sections from 2 littermates per genotype. Statistical significance was determined by Student's T-test (**p<0.001).

5.2. Astroglial phenotype of *Dyrk1a*$^{+/-}$ mice

The results so far presented in this work suggest that astrogliogenesis may be increased in the cerebral cortex of *Dyrk1a*$^{+/-}$ mice. These results are the following: i) the decreased methylation of the STAT3 binding site of the *Gfap* promoter in embryonic *Dyrk1a*$^{+/-}$ cortical cells *in vivo* before the onset of astrogliogenesis; ii) the up-regulation of components of signaling pathways, like *Notch2*, and TFs like *Nfia*, *Nfib*, *Sox4* and *Sox11* that positively regulate astrogliogenesis, in postnatal *Dyrk1a*$^{+/-}$ cortices; and iii) the increased levels of *Gfap* mRNA in *Dyrk1a*$^{+/-}$ cerebral cortices at P7, just at the peak of astrogliogenesis. In agreement with these data, our group had previously observed an increase in Gfap immunostaining in some brain regions of *Dyrk1a*$^{+/-}$ mice (Fotaki et al., 2002). To further analyze this phenotype, we first quantified the levels of Gfap mRNA and protein in the telencephalon of young adult *Dyrk1a*$^{+/+}$ and *Dyrk1a*$^{+/-}$ mice. As shown in Fig R40 both mRNA and protein levels where increased in the mutant tissue with respect to the wild type.

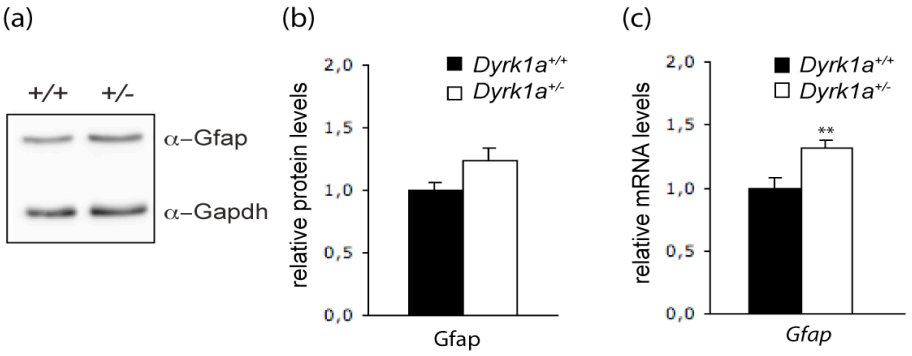

Fig R40: Gfap expression in the telencephalon of adult *Dyrk1a*$^{+/+}$ and *Dyrk1a*$^{+/-}$ mice. (a) Representative western blot immunodetection of Gfap in total protein extracts prepared from the cerebral cortex of adult *Dyrk1a*$^{+/+}$ and *Dyrk1a*$^{+/-}$ mice. Gapdh was used as loading control. (b) Quantification of the

bands in western blots like the one shown in (a): the histogram values correspond to the average (±sem) of relative Gfap protein levels in extracts prepared from 8 animals per genotype. P=0.057 according to Student's T-test. (c) Histogram showing the average (±sem) values of relative *Gfap* mRNA levels determined by qPCR in the cerebral cortex of 8 animals per genotype. (**p<0.01 according to Student's T-test).

We then wondered whether the increased Gfap levels corresponded to an increased number of $Gfap^+$ astrocytes. In the cortical gray matter, astrocytes expressed very low levels of Gfap protein (Emsley and Macklis, 2006 and our results in Fig R41a). For this reason we quantified $Gfap^+$ cells in the CA3 region of the hippocampus, where astrocytes express high levels of this intermediate filament (Emsley and Macklis, 2006). Our data highlighted an increased number of $Gfap^+$ astrocytes in *Dyrk1a*$^{+/-}$ mice compared to the wild type littermates (Fig R41b-c). A global increase in Gfap immunostaining was also observed in other brain regions of *Dyrk1a*$^{+/-}$ mice, like the *Corpus Callosum* (Fig R41d), indicating that the phenotype observed in the hippocampus is not region specific.

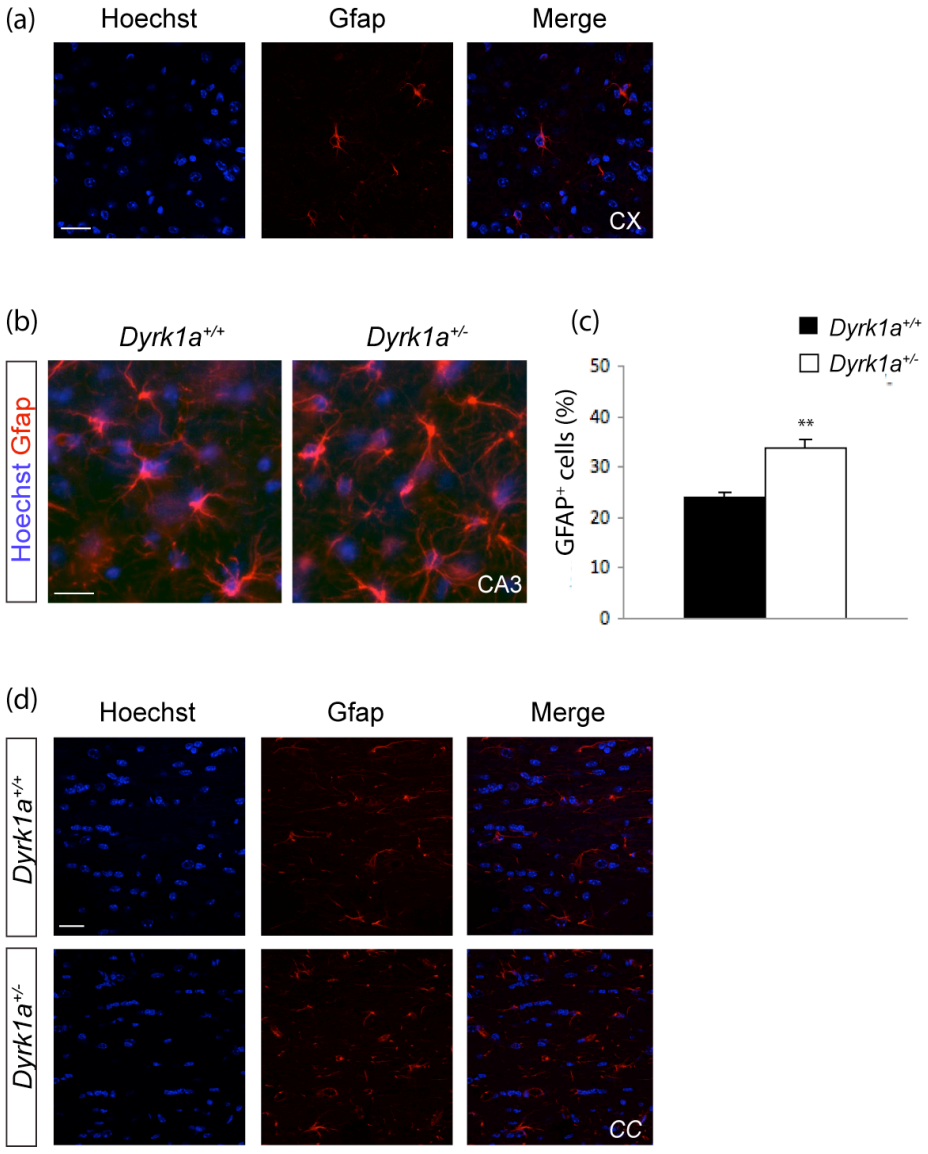

Fig R41: Gfap immunolabelling in *Dyrk1a*$^{+/+}$ and *Dyrk1a*$^{+/-}$ adult brains. (a) Confocal images of wild type coronal brain sections showing Gfap immunolabelling (red) of the pyriform cortex. Notice the reduced number of Gfap^{+} cells. (b) Representative fluorescence images of *Dyrk1a*$^{+/+}$ *and Dyrk1a*$^{+/-}$ coronal brain sections showing Gfap immunolabeled cells (red) in the CA3 region of the hippocampus. (c) Histogram showing the percentage of Gfap^{+} cells over total nuclei in the CA3 region of *Dyrk1a*$^{+/+}$ and *Dyrk1a*$^{+/-}$ brains. Histogram

values correspond to average measurements (±sem) obtained from quantifications in sections from 3 *Dyrk1a*$^{+/+}$ and 3 *Dyrk1a*$^{+/-}$ animals. Statistical significance was determined by Student's T-test (**p<0.01). (d) Representative confocal images of *Dyrk1a*$^{+/+}$ *and Dyrk1a*$^{+/-}$ coronal brain sections showing Gfap immunolabeled cells (red) in the *Corpus Callosum* of *Dyrk1a*$^{+/+}$ and *Dyrk1a*$^{+/-}$ mice. Nuclei in (a), (b) and (d) were stained with Hoechst (blue). Scale bar: 30µm.

Discussion

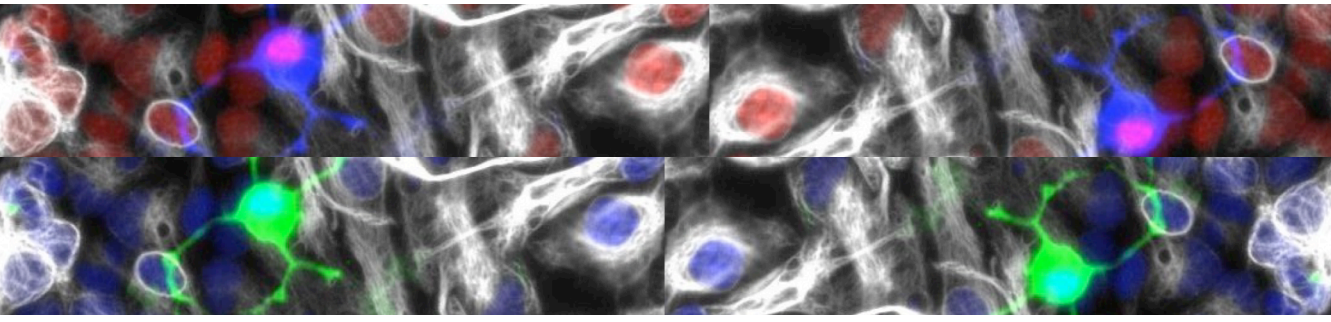

1. *Dyrk1a* and the transcriptome of the developing cerebral cortex

To gain insights into the role of Dyrk1a in the development of the cerebral cortex, we have compared the cerebral cortex transcriptomes of *Dyrk1a*$^{+/+}$ and *Dyrk1a*$^{+/-}$ mice at early postnatal stages.

Our analysis showed that *Dyrk1a* dose reduction leads to changes in the expression of a quite large group of genes, thus pointing to an involvement of Dyrk1a in the developmental processes of this brain structure (Fig R5). These results were in part expected considering the impact of Dyrk1a dose reduction in brain development (Fotaki et al., 2002). Moreover, the analysis showed that almost the totality of genes whose expression is affected by *Dyrk1a* dose reduction undergoes profound changes in their expression during normal cortical development (Fig R5), further supporting a role for Dyrk1a in cerebral cortex development.

One of the most striking evidences emerging from our study is the inverse correlation that exists between the changes in gene expression caused by normal cerebral cortex development ("developmental trend") and those caused by *Dyrk1a* dose reduction ("mutation trend"). In fact, genes that are up-regulated in the wild types between P0 and P7 tend to be down-regulated in the mutants at both developmental stages, and *viceversa* (Fig R6). This result suggests that the transcriptional programs required for cerebral cortex development are delayed in *Dyrk1a*$^{+/-}$ mice, which implies that the differences in gene expression observed in the postnatal mutants are a consequence of the effects of *Dyrk1a* dose reduction at earlier developmental stages. Indeed compelling evidences suggest that Dyrk1a regulates early developmental events: first Dyrk1a

may control the onset and the timing of neurogenesis by modulating the cell cycle exit of embryonic neural progenitors (Yabut et al., 2010; Hammerle et al., 2011) and second, our study on *Dyrk1a*$^{+/-}$ embryonic neurospheres indicates that normal levels of Dyrk1a are necessary for the normal expansion and differentiation of embryonic cortical progenitors, as occurs for adult progenitors (Ferron et al., 2010). Together these findings make plausible the hypothesis that the altered gene expression profile observed in the mutant cortex at postnatal stages is the consequence of earlier developmental defects.

Even thought the “developmental” and the “mutation” trends are inversely correlated, some genes behave differently. Among them, the inhibitory neurotransmitter *Somatostatin (Sst)* and the *Gamma1- subunit of GABA receptor (Gabrg1)* were differentially expressed in the mutant cortex but their expression in the wild types did not change significantly during normal development. Being both genes expressed in inhibitory neurons, their altered expression in the mutants supports a possible role of Dyrk1a in the establishment of inhibitory cortical circuits. Indeed, studies performed in the laboratory using neuron-type specific markers have shown that the number of some GABAergic populations are altered in *Dyrk1a*$^{+/-}$ brains both during development and in the adulthood (Sonia Najas and Elisa Balducci, unpublished results). Another group of genes that does not follow the inverse "developmental" and "mutation" correlation includes *Cyp11a1, Ypel2, Mbnl2, AW551984* and *Rxrg*. The expression of these genes in the mutant cortices changes in the same direction as the changes occurring between P0 and P7 in the wild type cortices. Interestingly for our work (see bellow), *Rxrg* encodes for the gamma subunit of the Retinoic X receptor, which has been shown to be important for myelination (Huang et al., 2011). These exceptions suggest

that the alterations observed in the transcriptome of *Dyrk1a*$^{+/-}$ mice are not simply due to a general neurodevelopmental delay but also to the effect of Dyrk1a dose reduction on specific processes.

The bioinformatics analysis of the promoters of differentially expressed genes did not highlight any enrichment in specific TF binding sites. Dyrk1a has been shown to negatively regulate NFAT transcriptional activity by phosphorylating NFAT members in the nucleus and inducing their export to the cytoplasm (Arron et al., 2006; Gwack et al., 2006). From our data we cannot discard the possibility that regulation of NFAT activity by Dyrk1a is restricted to specific developmental stages not included in our analysis and/or it is affecting, in the cerebral cortex, the expression of very few target genes.

Dyrk1a has also been proposed as a regulator of REST at both transcriptional and post-translational levels and differences in REST expression have been reported in cell lines and mouse tissues with altered levels of Dyrk1a (Canzonetta et al, 2008; Lepagnol-Bestel et al. 2009; Lu et al., 2011). However in our hands, REST mRNA and protein levels are unchanged in *Dyrk1a*$^{+/-}$ postnatal cerebral cortices (Fig R7 and R8). Since the three mentioned works claim that Dyrk1a regulates *REST* in a dosage- and time-dependent manner, we measured *REST* mRNA levels in the following samples which carry reduced or increased amounts of Dyrk1a: in total brain and cortex of *Dyrk1a*$^{+/-}$ adult mice; in *Dyrk1a*$^{+/-}$ embryonic stem (ES) cells; in total brain and cortex of postnatal and adult *BAC-Dyrk1a* mice; and in total brain of adult *Tg-Dyrk1a* mice (same age and model used in Canzonetta an colleagues) (Altafaj et al., 2001; Canzonetta et al., 2008). We did observed some small changes in *REST* expression between mutant and wild type samples but in any of them the differences were statistically significant (data not shown).

Differences in the experimental design; qPCR method used to quantify relative *REST* mRNA, type of sample and number of samples included in the analysis, may account for the differences between the mentioned published results and our results. In agreement with our Rest expression results, only one gene among all differentially expressed genes in *Dyrk1a*$^{+/-}$ cortices has been reported as a bona fide REST target in the CNS (Ballas et al., 2005). However, from our data we cannot exclude the possibility of a functional interaction between Dyrk1a and REST for the following reasons: i) using two different bioinformatics approaches, we predicted an enrichment of RE1 sites in the set of genes that were down-regulated in *Dyrk1a*$^{+/-}$ cortex (Fig R10 and R11); and ii) the epigenetic status of *Gfap* and *S100b* glial genes was altered in *Dyrk1a*$^{+/-}$ neural progenitors, and REST complex is known to interact with the epigenetic machinery to regulate transcription during CNS development (Ballas et al., 2005). Immunoprecipitation experiments could help revealing whether or not and in which context Dyrk1a associates to REST complex *in vivo*.

To investigate whether the effects of Dyrk1a on the transcriptome are dose dependent, a set of 40 genes differentially expressed in *Dyrk1a*$^{+/-}$ cerebral cortex were analyzed in the cerebral cortex of BAC-*Dyrk1a* mice, which carry an additional copy of *Dyrk1a* gene. The comparative analysis showed only 9 genes differentially expressed in both *Dyrk1a* loss- and gain-of function models (Fig R16), suggesting that different pathways are affected by the two mutations. These 9 common genes are: *S100b, Cnp1, Ptger4, Aqp4, Thy1, Tspan17, Nts, Sst* and *Ddit4*. Remarkably, for all these genes the expression in the two types of *Dyrk1a* mutants changed in the opposite direction when compared to their corresponding wild type; meaning that at least for a subset of genes the effects of Dyrk1a on the transcriptome are dose dependent (Fig R16).

Our results also indicate that the differences in expression in this group of genes are more accentuated and reproducible in *Dyrk1a*$^{+/-}$ cortices than in BAC-*Dyrk1a* cortices. This could be the consequence of a stronger biological impact of the loss-of function mutation than the gain of function one, which was in part expected because the phenotypes of *Dyrk1a*$^{+/-}$ mutants are, in general, more severe than the ones in BAC-*Dyrk1a* mice (Fotaki et al., 2002; unpublished data).

To gain insights into the neurodevelopmental pathways that are specifically affected by *Dyrk1a* triplication, a wide gene expression study should be performed. Such analysis would be helpful to unravel the contribution of *Dyrk1a* to DS phenotypes. Indeed, other laboratories have performed global gene expression analysis in the developing brain of the Ts1Cje Down Syndrome mouse model, which presents in trisomy a fragment of mouse chromosome 16 containing around 85 orthologs of chromosome 21 coding genes, including *Dyrk1a* (Sago et al., 1998). Very interestingly, around 5% of the genes appeared differentially expressed in the cerebellum of Ts1Cje mice at P0 (Dauphinot et al., 2005; Potier et al., 2006), while no changes between Ts1Cje and diploid mice were observed when analyzing total brains at the same developmental stage (Amano et al., 2004) (Table D1). These results suggest that brain region-specific effects are an important issue to take into account when designing and analyzing whole genome expression studies.

Comparing whole genome expression studies is not straightforward because of differences in the experimental design and in the statistical analysis adopted. Having this consideration in mind, the comparison of our gene expression analysis with the ones included in Table D1 indicates that the effect of *Dyrk1a* dose reduction in gene expression is comparable to, if not wider than, the effect produced by the triplication of

85 chromosome 21 genes. Although it is possible that some compensatory mechanisms exist in the trisomic condition this comparison highlight the remarkable effect of *Dyrk1a* dose reduction in brain development.

Table D1: Summary of gene expression studies performed on the Ts1Cje Down syndrome mouse model

Tissue	Age	Technique	N of total genes analyzed	Disregulated disomic genes	Ref
Cerebellum	P0 P15 P30	Microarray Affymetrix U74Av2	6902	5% at P0 4% at P15 3% at P30 Enrichment in: Homeobox proteins, Notch pathway genes	Dauphinot et al., 2005
Cerebellum	P0 P15 P30	Microarray Affymetrix U74Av2	8287	5% at P0 4% at P15 3% at P30 Enrichment in: cell development and differentiation genes	Potier et al., 2006
Total brain	P0	Microarray Affymetrix Gene Chip	10602	No changes observed	Amano et al., 2004

2. EGF- and FGF-dependent growth of *Dyrk1a*$^{+/-}$ embryonic neurospheres

The first difference observed when culturing *Dyrk1a*$^{+/-}$ embryonic progenitors with both mitogens, EGF and FGF, or with only one of them was the extremely reduced ability of these progenitors to form healthy primary neurospheres when the mitogen used was EGF. As a result, it

was very difficult to expand these cultures and only few of them were able to form secondary p1 neurospheres (Fig R21, Table D2). Another difference of the cultures grown with EGF with respect to the cultures grown with FGF or the two mitogens together was the reduced average diameter of p1 *Dyrk1a*$^{+/-}$ secondary neurospheres (Fig R22, Table D2). Altogether these results suggest that Dyrk1a is important for EGF-dependent, but not FGF-dependent, growth and/or survival of cortical progenitors. Dyrk1a in CNS development has been involved in both cell proliferation and cell survival (Yabut et al., 2010; Laguna et al., 2008); therefore, defects in both cellular processes may account for the reduced capability of *Dyrk1a*$^{+/-}$ progenitors to grow and form normal sized neurospheres when cultured with EGF alone.

Table D2: Mitogen dependent phenotypes of *Dyrk1a*$^{+/-}$ embryonic neurospheres

Parameter	Biological readout	EGF+FGF	EGF	FGF
survival and health aspect of p1 cultures	capability of generating secondary neurospheres	=	↓	=
diameter of secondary neurospheres	cell death cell proliferation	↓	↓	=
number of secondary neurospheres	self-renewal capability (maintainence of stemness properties)	↓	↓	↓

Black arrows indicate reductions associated to pValues<0.05 as determined by Student's T-test; gray arrows indicate tendencies that do not reach statistical significance according to Student's T-test (p>0.05); = means no change between genotypes. All phenotype were obtained comparing *Dyrk1a*$^{+/-}$ embryonic neurospheres cultures with wild type control cultures.

Another main evidence emerging from the analysis of *Dyrk1a*$^{+/-}$ embryonic neurosphere cells was their decreased self-renewal capability when cultured with EGF and FGF (Fig R20 and Table D2). Recently published data demonstrated that *Dyrk1a*$^{+/-}$ neurospheres obtained from adult brains have a reduced self-renewal capability when cultured in the presence of EGF alone but not when cultured with FGF alone (Ferron et al., 2010). When we cultured *Dyrk1a*$^{+/+}$ and *Dyrk1a*$^{+/-}$ E17.5 neural progenitors in the presence of only EGF, *Dyrk1a*$^{+/-}$ progenitors tended to have a reduced self-renewal potential (Fig R22, Table D2). Although differences between genotypes were not statistically significant, because of the low numbers of cultures that could be analyzed, this result indicates that normal levels of Dyrk1a are required for normal EGF-dependent self-renewal potential of embryonic cortical progenitors. Dyrk1a is an inhibitor of EGFR degradation in neural progenitors. The levels of membrane-bound EGFR in *Dyrk1a*$^{+/-}$ neural stem cells of the adult brain are reduced thus explaining why they respond less to EGF than wild type progenitors (Ferron et al., 2010). Although we still need to measure membrane-bound EGFR in *Dyrk1a*$^{+/-}$ embryonic neurosphere cells, it is reasonable to think that the same mechanism accounts for EGF-dependent self-renewal deficits in adult and embryonic brain progenitors.

An exciting finding emerging from our study is that, in contrast to what has been described by Ferron and colleagues for adult stem cells, FGF-dependent self-renewal potential is also impaired in *Dyrk1a*$^{+/-}$ embryonic neurospheres (Fig R23, Table D2). This result supports the idea that the mechanisms governing the self-renewal potential of neural progenitors are different in the embryo and the adult. An interesting open question is how Dyrk1a regulates FGF-dependent self-renewal of

embryonic progenitors. Dyrk1a is able to interact with all known mammalian Sprouty proteins (Sprouty1 to Sprouty4), which are negative regulators of the FGF-signalling pathway (Mason et al, 2006; Aranda et al., 2008), and Sprouty4 is expressed in the cerebral cortex and ganglion eminences of E14.5 embryos (Ferron et al., 2010). Therefore, it is possible that in cortical embryonic progenitors Dyrk1a positively regulates FGF signaling through phosphorylation and inhibition of Sprouty4 as it as been previously described for Sprouty2 in HEK-293 cells (Aranda et al., 2008).

3. Dyrk1a and the expression of *Aqp4* and *S100b in* neural progenitors

Different reports have shown that the Aqp4 water channel and the S100b calcium binding protein are important for the proliferation and differentiation potentials of neural progenitors (Esposito et al., 2008; Kong et al., 2008). Gene expression analysis of DS fetal neurospheres, which have the chromosome 21 *S100b* gene in trisomy, showed higher levels of *Aqp4* mRNA in trisomic progenitors than in the diploid controls (Esposito et al., 2008, Table D3). Functional studies presented in the same work suggested that *Aqp4* up-regulation in DS neural progenitors is a pro-survival mechanism aimed to compensate the oxidative stress caused by *S100b* triplication (Esposito et al., 2008). The reduced levels of *Aqp4* and *S100b* transcripts that we have observed in *Dyrk1a*$^{+/-}$ embryonic neurospheres opens the intriguing possibility that a novel transcriptional loop involving *Dyrk1a, S100b* (both trisomic in DS) and *Aqp4* could contribute to the phenotypes observed in DS neural progenitors. To test this hypothesis, we determined the levels of *S100b*

and *Aqp4* transcripts in BAC-*Dyrk1a* embryonic neuropsheres, and found up-regulation of *S100b* but not of *Aqp4* gene (data not shown). An intuitive explanation for this finding is that the increased *Aqp4* levels in DS neural progenitors require high levels of *S100b,* which are probably the result of both *S100b* triplication and the up-regulation of *S100b* expression due to *Dyrk1a* triplication. Nevertheless, the following data do not support the existence of such transcriptional loop indicate a much more complex scenario: i) the expression of *S100b* in DS fetal neurospheres was increased only 1.7 times with respect to their control diploid neurospheres (Esposito et al., 2008), value that is very close to the 1.5 increase expected for a gene that is in trisomy (data not shown); ii) in neurosphere cultures derived from Ts1Cje mice (*Aqp4* and *S100b* in disomy, and *Dyrk1a* in trisomy) *Aqp4* mRNA levels were increased but *S100b* and -unexpectedly- *Dyrk1a* mRNA levels were normal (Moldrich et al., 2009) and iii) the levels of *S100b* and *Aqp4* mRNAs in Ts65Dn P0 cerebral cortices (*Aqp4* and *S100b* in disomy, and *Dyrk1a* in trisomy) were the same as control diploid tissues (data not shown).

Remarkably, both DS and Ts1Cje neurospheres displayed an impaired proliferation (Moldrich et al., 2009; Esposito et al., 2008) and, in both cases, the authors of the work explained *Aqp4* up-regulation as an attempt of the cells to overcome the proliferation defect. Similarly, and in view of the effect of *Dyrk1a* dose reduction in neurosphere growth, one can speculate that a moderate up-regulation of *Dyrk1a* due to the increased dosage of the gene may be beneficial, limiting the proliferative defects of trisomic progenitor cells. If this were the case, one will expect an increased proliferation of progenitors cells when only *Dyrk1a* is in trisomy. We have cultured cortical neurosphere cells obtained from BAC-*Dyrk1a* and wild type littermate embryos but the growth curves of these

two types of cultures were very similar (data non show). Although these are preliminary results, they suggest that a moderate overexpression of *Dyrk1a* may not significantly change the proliferative behavior of cortical progenitor cells, at least in our *in vitro* conditions. Moreover it indicates that embryonic neural progenitors, like we have previously shown for adult neural progenitors (Ferron et al 2010), tolerate better a 50% increase of *Dyrk1a* than a 50% decrease. However, it has also been shown that acute over-expression of *Dyrk1a* in progenitors of the embryonic ventricular and subventricular zones inhibits their proliferation *in vivo* (Yabut et al., 2010). The apparent discrepancy between this work and our results could be due to differences in the overexpression levels of *Dyrk1a* and also to differences in the experimental approach used.

Table D3: *S100b* and *Aqp4* expression in different experimental models and associated growth phenotypes of neural progenitors.

		Dyrk1a	***S100b***	***Aqp4***	growth phenotype	Ref
Neurospheres	*Dyrk1a*$^{+/-}$	↓	↓	↓	reduced growth rate	this work
	BAC-*Dyrk1a*	↑	↑	=	unaltered growth rate	this work
	Ts1Cje	=	=	↑	reduced proliferation	Moldrich et al., 2009
	DS-hNPC	↑	↑	↑	reduced proliferation	Esposito et al., 2008
P0 cortex	*Dyrk1a*$^{+/-}$	↓	↓	↓		this work
	BAC-*Dyrk1a*	↑	↑	↑		this work
	Ts65Dn	↑	=	=		this work

Black arrows indicate primary gene dosage imbalances (intrinsic to the experimental model), gray arrows indicate differential expression of disomic genes, and = means no changes in gene expression. Differential expression was determined comparing each model to its wild type control. DS-hNPC: DS human neural progenitors.

Putting together our gene expression data and the studies on neural progenitors with the work published by other groups (Table D3), we could conclude the following: i) *Dyrk1a* dosage imbalance is sufficient to alter *S100b* but not *Aqp4* gene expression; ii) in the context of trisomy 21, some triplicated gene(s) other than *Dyrk1a* could down-regulate *S100b*, and compensate the *Dyrk1a*-dependent up-regulation of this gene; iii) *Aqp4* expression is not always directly related to *S100b* and *Dyrk1a* expression levels, but they seem to be always associated to proliferative defects of neural progenitors. This last point makes plausible that *Aqp4* up-regulation in trisomic progenitors represent a compensatory mechanism, as hypothesized by Moldrich and colleagues. However, although *Aqp4* knockout has been described to inhibit neurospheres proliferation (Kong et al., 2008), it is unknown whether *Aqp4* overexpression has the inverse effect on proliferating neural progenitors, thus rendering the "compensatory hypothesis" of Moldrich and Esposito a mere speculation.

A possible experiment to shade light on the specific contribution of *Dyrk1a* dosage to DS neural progenitor phenotypes is to cross Ts65Dn with *Dyrk1a*$^{+/-}$ mice, to normalize *Dyrk1a* dosage in a trisomic context, and analyze both the growth properties and the expression levels of *S100b* and *Aqp4* genes in embryonic neurosphere cultures prepared from the progeny of such crosses. The work of Moldrich and colleagues on Ts1Cje mice is not sufficient to clarify this point, given that *Dyrk1a* levels were normal in these mice despite de fact that *Dyrk1a* is in three

copies. This could be a false negative result of Moldrich's gene expression analysis or, alternatively, indicate that some compensatory event occurring in the trisomic neural progenitors reduces the levels of *Dyrk1a* to normal values.

4. Chromatin state of *S100b* and *Gfap* promoters in *Dyrk1a*$^{+/-}$ embryonic cortex and its association with gliogenesis

Demethylation of ***S100b*** promoter at CpG(-267) occurs in the mouse cerebral cortex between E11.5 ad E14.5, and has been associated with the onset of gliogenesis (Namihira et al., 2004). In agreement with the published data, we found that in the wild type cerebral cortex this key position was more methylated at E11.5, at the onset of neurogenesis, than at E14.5, when neural progenitors are switching their differentiation potential from neurogenic to gliogenic (Fig R30a). Interestingly, the CpG(-267) of *S100b* promoter was equally methylated in the cerebral cortex of *Dyrk1a*$^{+/+}$ and *Dyrk1a*$^{+/-}$ mice at E11.5 but not at E14.5, when specific demethylation of *S100b* promoter should have occurred (Fig R30a) (Namihira et al., 2004). This finding suggests that some mechanism associated to the demethylation of *S100b* promoter is probably altered in *Dyrk1a*$^{+/-}$ progenitors and that Dyrk1a could play a role in lineage differentiation by regulating the onset of glial gene expression in progenitors.

At P0, during the gliogenic phase of cortical development, the CpG(-267) was almost completely demethylated in our cortical samples, and again we did not observed differences in the methylation state of this position between genotypes (Fig R30a). This finding reinforces the idea

that the effect of *Dyrk1a* dose reduction on the methylation of *S100b* promoter specifically occurs in a defined time window of development that overlaps with the time window in which epigenetic changes controlling the neurogenic to gliogenic switch occur.

Demethylation of CpG(-267) in the embryonic cortex has been shown to coincide with a reduced binding of MeCP2 to the *S100b* promoter, and to an increased transcription of *S100b* gene. Therefore, MeCP2 is likely to mediate *S100b* transcriptional repression (Namihira et al., 2004). MeCP2 is known to physically impede TFs binding to the promoters and to recruit histone-modifying enzymes, including histone deacetylases (Lunyak et al., 2002). Indeed, the onset of *S100b* expression coincides with an increased acetylation of histones H3 and H4 in its promoters; event that requires both DNA demethylation and BMP2 stimulation (Namihira et al., 2004). In this work we have shown that the amounts of acetylated H4K16 in the *S100b* promoter is reduced in E14.5 *Dyrk1a*$^{+/-}$ cortices compared to the wild type situation (Fig R33). This result together with our DNA methylation data indicates that in the mutant condition, and at least at this developmental stage, the *S100b* gene is less prone to be activated than in the wild type condition. Indeed at E16.5, when we start to detect *S100b* transcripts in the mouse cerebral cortex, the expression of *S100b* gene is reduced in *Dyrk1a*$^{+/-}$ mice (data not shown).

Importantly, the impaired onset of *S100b* expression in *Dyrk1a*$^{+/-}$ mice is likely to explain the reduced number of S100b^{+} cells observed at postnatal stages (Fig R34). The observation that *Dyrk1a*$^{+/-}$ embryonic neurospheres differentiate less to S100b^{+} cells than wild type neurospheres do (Fig R28) further supports the idea that the decreased

numbers of S100b^{+} in *Dyrk1a*$^{+/-}$ postnatal cortices is the consequence of an altered gliogenic potential of the progenitors.

Epigenetic regulation of ***Gfap*** expression in the brain has been extensively studied and has been found to be crucial for the neurogenic to gliogenic switch (Takizawa et al., 2001; Fan et al., 2005; Shimozaki et al., 2005; Namihira et al., 2009). *Gfap* expression in the brain is induced during the gliogenic phase of neurodevelopment by STAT3, a key gliogenic TF (Nakashima 1999). During neurogenesis, methylation of the *Gfap* promoter at CpG(-1502), which is internal to the STAT3 site, impedes STAT3 binding to DNA and prevents *Gfap* expression. At the onset of gliogenesis, the STAT3 site gets demethylated, allowing *Gfap* expression, a crucial event in astroglial commitment of neural progenitors (Takizawa 2001). Very interestingly we have found that the STAT3 binding site of the *Gfap* promoter was significantly less methylated in *Dyrk1a*$^{+/-}$ cortices than in the wild types at E14.5, when neural progenitors are changing their potential from neurogenic to gliogenic (Fig R31a). This result points to an increased astrogliogenic potential of *Dyrk1a*$^{+/-}$ progenitors and correlates with other findings of our study: i) the increased expression of the *Gfap* gene in the mutant cortex at postnatal stages (Fig 13b); ii) the higher Gfap protein level in the cortex of adult mutant mice (Fig R40a-b), and iii) the increased number of Gfap^{+} astocytes in the adult mutant brains (Fig R41b-c). Changes in the methylation state of the *Gfap* promoter were not observed in P0 mutant cortices (Fig R31b). Therefore, similarly to *S100b*, changes in the methylation state of the *Gfap* promoter occurring in the mutant cortex at a precise time window, correlate with an altered expression of the gene and to an altered number of Gfap^{+} astrocytes later in development.

In the case of *Gfap*, contrarily to *S100b,* the decreased methylation of the promoter could not be confirmed in embryonic neurospheres because the STAT3 site was completely demethylated in the wild type condition (Fig R32b). Expression of *Gfap* is restricted to neural stem cells and astrocytes. Therefore, the most probable explanation for this result is that the epigenetic regulation of the gene is not the same in multipotent neurosphere cells than in committed progenitors that do not self-renew. Environmental differences between cortical progenitors *in vivo* and cortical progenitors in culture may also explain the differences in methylation observed in the case of *S100b* promoter. The CpG(+59) was in fact differently methylated between genotypes in neuropsheres but not in E14.5 cortex (Fig R30b and Fig R32a). Moreover, the overall methylation of CpG(-267) was much lower in embryonic neurospheres than in E14.5 cortex (5% and 50% respectively) (Fig R30a and Fig R32a), meaning that different epigenetic mechanisms regulate gene expression *in vivo* and *in vitro.*

The decreased methylation of *Gfap* promoter on one hand and the increased methylation of *S100b* promoter on the other hand, observed in *Dyrk1a*$^{+/-}$ embryonic cortex, indicate that the effects of *Dyrk1a* dose reduction in the epigenetic regulation of gene expression is gene specific. The different CpG content observed in the promoter regions of genes that were found up- or down- regulated in *Dyrk1a*$^{+/-}$ cerebral cortex in the array study suggest that global chromatin changes could contribute to the differential gene expression provoked by *Dyrk1a* dose reduction (Fig R12). To investigate this fascinating hypothesis, we are performing a *Methylated DNA ImmunoPrecipitation* (MeDIP) experiment to compare the methylome of *Dyrk1a*$^{+/+}$ and *Dyrk1a*$^{+/-}$ embryonic cortex. This study

will hopefully reveal whether changes in the CpG content of genes promoters indeed correlate with changes in DNA methylation.

Overall, our study suggests a role for Dyrk1a in the chromatin changes occurring in cortex development. Because epigenetic changes are crucial to determine the differentiation potential of neural progenitors, disturbances of these modifications are likely to contribute to the decreased potential of *Dyrk1a*$^{+/-}$ progenitor cells to differentiate into oligodendrocytes *in vitro* (Fig R28). More importantly, our findings suggest that changes in the chromatin state occurring in *Dyrk1a*$^{+/-}$ cerebral cortex at early developmental stages are likely to alter the postnatal and adult brain cellularity. Indeed, the observation that Dyrk1a expression is not detected in the *Corpus Callosum* of postnatal animals (Fig R2) is a strong indication that the different number of S100b^{+} cells that we have observed between wild type and mutant postnatal animals in this structure is the consequence of earlier events involving Dyrk1a. Experiments knocking down *Dyrk1a* with siRNA in wild type neural progenitors would definitively show whether or not the effect of *Dyrk1a* dose reduction in cell lineages differentiation is cell-autonomous.

Defects in the differentiation potential of neuronal progenitors derived from the brains of DS fetuses and Ts1Cje embryos have been reported (Esposito et al., 2008; Moldrich et al., 2009). Differentiation studies performed with neurosphere cultures derived from BAC-*Dyrk1a* embryos did not reveal any significant difference between the differentiation capacity of these progenitors and wild type progenitors (data non show). This result suggests that, contrarily to *Dyrk1a* dose reduction, *Dyrk1a* overexpression does not modify the differentiation potential of mouse cortical progenitors. It also indicates that genes in trisomy other than *DYRK1A* are responsible for the impaired

differentiation potential of trisomic progenitors (Esposito et al., 2008; Moldrich et al., 2009).

5. Dyrk1a and astrogliogenesis

Different evidences suggest that *Dyrk1a*$^{+/-}$ embryonic progenitors are more astrogliogenic than wild type progenitors. First, the already mentioned decreased methylation of the *Gfap* promoter in the STAT3 binding site indicates that *Dyrk1a*$^{+/-}$ progenitors are more prone to respond to environmental astrogliogenic cues. Second, *Dyrk1a*$^{+/-}$ embryonic neurospheres differentiate less into O4^{+} and S100b^{+} oligodendroglial cells, but the number of Sox9^{+} cells, which are cells committed to the glial lineage (both astroglial and oligodendroglial) is unaltered (Fig R27 and R28). Third, our microarray data point to an enhanced astrogliogenesis related to *Dyrk1a* dose reduction because key positive regulators of astrogliogenesis, like *Notch2* and the TFs *Nfia*, *Nfib*, *Sox4* and *Sox11* TFs were among the up-regulated genes in *Dyrk1a*$^{+/-}$ postnatal cortices (Table R1). Taking into account that developmental processes require a fine-tuned regulation of TFs, the 20 to 50% changes in the expression of gliogenic TFs observed between genotypes could account for relevant phenotypic consequences. Interestingly, Notch signaling pathway has been recently shown to promote the acquisition of astrogliogenic potential via the induction of *Nfia* expression in neural progenitors (Namihira et al., 2009). The up-regulation of both *Notch2* and *Nfia* indicates that *Dyrk1a* could be a regulator of the Notch pathway in the context of cortical gliogenesis. Because, Dyrk1a is a negative inhibitor of the Notch pathway (Fernandez-Martinez et al., 2009), the increased expression of *Nfia* in the

loss-of function mutants could be the result of having more Notch and a more activated Notch pathway.

If indeed *Dyrk1a* dose reduction affects the astrogliogenic potential of neural progenitors, and because all different astrocytic populations of the adult brain specify early in development (reviewed in Matyash and Kettenmann, 2010; Kimelberg et al., 2004; Emsley and Macklis, 2006), the number of astrocytes expressing Gfap in the adult brain should be higher in the mutants than in the wild types. As Gfap expression in astrocytes strongly varies according to the brain region and, within the telencephalic gray matter, the hippocampal astrocytes express high Gfap levels (reviewed in Emsley and Macklis, 2006) we have quantified the $Gfap^{+}$ astrocytes in this brain region to test our hypothesis. The increased number of $Gfap^{+}$ cells observed in the hippocampus of *Dyrk1a*$^{+/-}$ mice (Fig R41b-c) is in complete agreement with the hypothesis, which is supported by the fact that the levels of Gfap protein in the whole telencephalon of these mice (Fig R40a-b) is increased.

Mature astrocytes of the adult brain can change their morphology and increase the Gfap synthesis, as well as proliferate, in response to injury. For this reason, we cannot discard the possibility that the increased amounts of Gfap observed in adult *Dyrk1a*$^{+/-}$ brains was the consequence of an astrocytosis induced by stress. In fact, the reduced levels of Dyrk1a in adult brains could lead to an impaired cell function, either in neurons or in astrocytes where Dyrk1a is expressed (Martí et al., 2003; Wegiel et al., 2004), and activate stress-response mechanisms. It is worthy to mention in this context that *Dyrk1a* overexpression has been associated to neurodegeneration (reviewed in Wegiel et al., 2011). Although no clear symptoms of neurodegeneration have been observed in old *Dyrk1a*$^{+/-}$ mice (unpublished results of the laboratory), we cannot

exclude that neurodegenerative processes are occurring in this model. Astrocytosis can also be the consequence of the impaired myelination observed in the adult nervous system of *Dyrk1a*$^{+/-}$ mice that we next discuss. In fact, it has been described that, when myelination is reduced, astrocytosis occurs as a compensatory mechanism that enhances the transfer of cholesterol, required for myelin synthesis, from astrocytes to oligodendrocytes (Saher et al., 2005). Although both cellular stress and defective myelination may account for the increased number of Gfap^{+} cells in *Dyrk1a*$^{+/-}$ brains, the fact that Gfap protein levels are already increased in 2 week-old animals (data not shown), suggests that neurodevelopmental defects are more likely the cause of the observed phenotype. *In vitro* differentiation assays of *Dyrk1a*$^{+/+}$ and *Dyrk1a*$^{+/-}$ neural progenitors could help demonstrating whether Dyrk1a plays a role in astrocyte differentiation and shade light into the underlying molecular mechanisms.

6. Dyrk1a and oligodendrogenesis

The opposite effect of *Dyrk1a* dose reduction on the methylation state of *Gfap* and *S100b* promoters in the embryonic cortex was completely unpredicted. Previous studies described that both genes are analogously regulated during the neurogenic to gliogenic switch and that their de-repression determines the onset of astrogliogenesis *in vivo* (Takizawa et al., 2001; Namihira et al., 2004; 2009; Fan et al., 2005; Namihira et al., 2009). Thus our results uncouple for the first time the regulation of *S100b* and *Gfap* expression: the hypermethylation of *S100b* promoter at embryonic stages correlates with down-regulation of *S100b* gene and to the reduced number of S100b^{+} cells generated *in vitro* by neural progenitors and observed *in vivo* in *Dyrk1a*$^{+/-}$ postnatal cortex,

while hypomethylation of *Gfap* promoter associates to *Gfap* up-regulation in postnatal cortex and increased Gfap$^+$ astroglial cells in adult brain.

There are data in the literature showing that S100b$^+$ cells belong to the oligodendroglial lineage during development, and not to the astroglial lineage as has been assumed in all the works describing the epigenetic regulation of *S100b* gene (Takizawa et al., 2001; Namihira et al., 2004; 2009; Fan et al., 2005; Hirabayashi et al., 2009). Indeed none of the works describing the demethylation of *S100b* promoter during the neurogenic to gliogenic switch characterize the cell types expressing S100b (Takizawa et al., 2001; Namihira et al., 2004; 2009; Fan et al., 2005; Hirabayashi et al., 2009). It is always assumed in these works that, oligodendrocytes are generated from the ventral part of the forebrain and that gliogenesis in the developing cortex is primarily confined to astrocytes (Fan et al., 2005). However, it is now known that oligodendrocytes originate from both the ventral and the dorsal parts of the mouse telencephalon and, moreover, that most of the oligodendrocytes present in the adult brain have dorsal origins (Kessaris et al., 2006). The oligodendroglial identity of S100b$^+$ cells in the developing cortex has been described by two different groups and has been confirmed in this work by double immunolabelling experiments (Hachem et al., 2005; Deloulme et al., 2004; Vives et al., 2003 and Fig R29 in this work). During development, S100b expression in Ng2$^+$ oligodendroglial progenitors correlates with their transition from a fast dividing multipotent stage to a slow proliferating and morphological differentiated stage. S100b expression is then maintained all along oligodendroglial development, and progressively disappears in fully differentiated myelinating oligodendrocytes (Deloulme et al., 2004; Vives et al., 2003). The authors of these works propose that S100b promotes

the acquisition of a branched phenotype in differentiating oligodendrocytes, based on the following evidences: i) S100b associates with microtubules in cultured oligodendrocytes and ii) S100b plays a role in microtubules assembly/disassembly *in vitro,* in a calcium-dependent manner (Richter-Landsberg and Heinrich, 1995; Sorci et al., 1998; 2000). In the adult brain, S100b expression has been reported in slow proliferating $Ng2^{+}$ progenitors, which are responsible of oligodendrocyte turnover, as well as in mature peri-vascular astrocytes (Rickmann and Wolf, 1995; Deloulme et al., 2004; Hachem et al., 2005). Using the same *in vitro* differentiation protocol than ours, it has been shown that expression of S100b appears first in differentiating oligodendrocytes and later in mature astrocytes, further indicating that the onset of S100b expression correlates with the progression of neural progenitors to the oligodendroglial lineage (Deloulme et al., 2004). It is important to point out that the role of S100b is dispensable because: i) $S100b^{-/-}$ mice do not show evident defects in brain development or myelination (Nishiyama et al., 2002; Xiong et al., 2000); and ii) $S100b^{-/-}$ neural progenitors are able to generate $O4^{+}$ oligodendrocytes *in vitro*, although these cells are produced later in development and they have a less differentiated morphology (Deloulme et al, 2004).

According to the published data just mentioned, our results could be interpreted as follows: the impaired activation of *S100b* gene expression in $Dyrk1a^{+/-}$ progenitors leads to reduced number of cells expressing *S100b* in the developing cortex, which causes a defective maturation of the oligodendrocytes, due to the role of S100b in the progression of the oligodendroglial lineage (Deloulme et al., 2004). Indeed, the reduction in the mRNA levels of two myelin genes, *Mbp* and *Cnp,* in $Dyrk1a^{+/-}$ postnatal cortex, supports this hypothesis. Because $Dyrk1a^{+/+}$ and

Dyrk1a$^{+/-}$ adult cortices display the same number of Cc1^{+} mature oligodendrocytes, we can speculate that the defect in oligodendrocyte numbers during development is compensated in the adulthood. This finding is not surprising because the brain oligodendroglial population is very dynamic and new oligodendrocytes can be produced throughout life from Ng2^{+} progenitors. This cell population represents about 5% of total cells in the adult brain and, although maintained in a quiescent status, these cells are able to proliferate and differentiate into mature oligodendrocytes in response to stimuli (Rivers et al. 2008).

7. Dyrk1a and myelination

Despite the normal number of Cc1^{+} mature oligodendrocytes observed in the cortex of adult *Dyrk1a*$^{+/-}$ mice, the levels of the myelin protein Mbp were extremely reduced in the telencephalon of these mice (Fig R36 and R37). Our ultrastructural analysis of the *Corpus Callosum* indicated that the decrease in Mbp levels correlates with a reduction in the thickness of myelin sheaths (Fig R38c-d). This analysis also highlighted that *Dyrk1a*$^{+/-}$ *Corpus Callosum* lacks big-caliber myelinated axons, which likely contributes to the reduced average diameter and the increased density of the myelinated axons (Fig R38a-b, Table D4). The following two events could also contribute to the increased density of myelinated axons observed in the *Corpus Callosum* of *Dyrk1a*$^{+/-}$ mice: i) a significant reduction in the number of unmeylinated axons, which were not counted in our samples, and ii) the increased neuronal density observed in the cerebral cortex of this animals (Fotaki et al, 2002 and unpublished results from the laboratory).

Table D4: Myelin phenotype of adult *Dyrk1a*$^{+/-}$ mice

		Average diameter of myelinated axons	Myelin thickness	g-ratio	Density of myelinated axons
CNS	*Corpus Callosum*	↓	↓	↑[1]	↑
	Optic Nerve	=	↓	↑	=
PNS	Sciatic nerve	↓	↓	↑[1]	ND

All symbols indicate the phenotype of *Dyrk1a*$^{+/-}$ mice compared with the wild type littermates (n>2 per condition). Significance was determined by Student's T-test ($p<0.05$). The g-ratio was calculated by dividing the axon diameter by the fiber diameter. =, no change between genotypes; [1], trends that did not reach statistical significance ($p>0.05$ in the Student's T-test); ND, not determined.

Given that myelin thickness is proportional to axon diameter, we cannot exclude the possibility that the reduced average myelin thickness that we have observed is due to the reduced diameter of the axons instead of specific defects in myelination. The g-ratio is a parameter widely used to evaluate myelination and is calculated by dividing the axon diameter for the diameter of the fiber, which includes the axon and the myelinic sheath. This number tends to be constant (between 0.6 and 0.8) and increases when myelination in reduced (reviewed in Sherman and Brophy, 2005). In the *Corpus Callosum* of *Dyrk1a*$^{+/-}$ mice the overall g-ratio values did not highlight any statistically significant difference between genotypes, probably due to the lack of big diameter axons that biases the average axon diameter to low values. However, the reduction of myelin thickness within axons of similar diameter strongly indicates that g-ratio is increased within each group of axons and myelination is affected in the *Corpus Callosum* of mutant mice. Moreover, in the optic nerve of *Dyrk1a*$^{+/-}$ mice, where neither the average axon diameter nor the

axon density was affected, the axonal myelin thickness was also reduced and the overall g-ratio significantly increased (Fig R39a and Table D4). Axons of *Dyrk1a*$^{+/-}$ sciatic nerve, which belong to the PNS, also showed a significant decrease in myelin thickness (Fig R39b) that was associated to a reduced average axon diameter (Table D4). In this case the g-ratio was not significantly increased between genotypes, although a tendency was observed when analyzing groups of axons of similar diameters (Table D4). Other parameters, like the form factor, which is indicative of fiber roundness, were unaltered in mutants in the three nerve types analyzed. Although more samples should be studied to confirm our observations, these strongly suggest that myelination in *Dyrk1a*$^{+/-}$ mice is impaired in both the CNS and the PNS.

Dyrk1a dose reduction could affect the myelination process at several levels. One possibility is that Dyrk1a controls Mbp protein levels post-transcriptionally. The observation that in the adult cortex of *Dyrk1a*$^{+/-}$ mice, the decreased levels in Mbp protein do not correlate with a decrease in the levels of *Mbp* transcript (Fig R36) make plausible this hypothesis. Indeed altered post-transcriptional events affecting Mbp have already been associated to a defective myelination. This is for instance the case of *Quaking viable* (*qk*^{v}) mice in which an impaired nuclear export of *Mbp* transcripts leads to a reduced synthesis of the Mbp protein (Larocque et al., 2002).

Being Dyrk1a a protein kinase, it could regulate Mbp protein levels by phosphorylation. Indeed, phosphorylation of Mbp at several positions has been described, and it is likely that these phosphorylation events regulate myelin function (see Boggs 2006 for a review). Noteworthy, a Dyrk1a consensus phosphorylation site (RxxSP) is present at position

190 (RSGS^{190}P) of the Mbp amino acidic sequence (NP_001020422.1), which opens the possibility of Dyrk1a directly phosphorylating Mbp.

Another possibility is that low Mbp levels in the mutants are not the cause of the myelin phenotype but rather the consequence of a defect in myelination. Myelination is governed by a complex crosstalk between axons and myelin forming cells, oligodendrocytes in the CNS and Shwann cells in the PNS. The bilateral axonal-glial signaling is required both during development, when it determines which axons will be myelinated and the myelin thickness, and in the adulthood, when it maintains myelin and axonal integrity (reviewed in Nave and Trapp, 2008; Simons and Trajkovic, 2006). Several studies on mouse models helped to elucidate some of the signaling pathways involved in the axonal-glial communication in the CNS and in the PNS (see Taveggia et al., 2010 for a review). Interestingly, Dyrk1a regulates some of these pathways, like Notch, NGF and NFAT. Notch signaling, which is negatively regulated by Dyrk1a (Fernandez-Martinez et al., 2009), regulates myelination in both the CNS and PNS, but in completely different ways. In the CNS Notch inhibits oligodendrocytes differentiation (Wang et al., 1998) whereas in the PNS it promotes Shwann cells maturation although inhibiting the onset of myelinogenesis (Woodhoo et al., 2009). Similarly, NGF signaling, which is positively regulated by Dyrk1a (Kelly and Rahmani, 2005), promotes myelination in the PNS but inhibits it in the CNS (Chan et al., 2004). Finally, NFAT signaling has been identified as a positive regulator of myelination specifically in the PNS (Kao et al., 2009). Being Dyrk1a a negative regulator of NFAT signaling (Arron et al., 2006; Gwack et al., 2006), *Dyrk1a*$^{+/-}$ mice should present hypermyelination of peripheral nerves. However, the data we have so far show just the opposite result. The fact that the myelin

phenotype of *Dyrk1a*$^{+/-}$ mice affects both the PNS and the CNS points to the involvement of Dyrk1a in some process common to both systems. In these sense, phosphorylation by Dyrk1a of the intracellular domain of Notch, or of components of the NFG cascade, or of NFAT members are not likely the mechanisms underlying the myelin phenotype here reported.

Neuregulin1-typeIII (NRG1-III) is an axonal transmembrane protein that promotes myelination in the PNS and in the CNS (Brinkmann et al., 2008; Michailov et al., 2004; Nave and Salzer, 2006; Taveggia et al., 2008), although some authors suggest that NRG1-III signaling is dispensable for CNS myelination (Brinkmann et al., 2008). The extracellular domain of NRG1-III is cleaved by the ß-secretase BACE1 (Willem et al., 2006; Hu et al., 2006, 2008) or by ADAM proteases (Sagane et al., 2005, La Marca et al., 2011) in a process regulated by the metallopeptidase Nardilysin (NRD) (Ohno et al., 2009). Shed NRG1-III binds the Erb-B receptors on the glial surface to promote myelin gene expression via Akt-mTOR intracellular cascade (Goebbels et al., 2010; Flores et al., 2008). Loss of function mouse models of BACE1, NRG1-III and NRD show hypomyelination of the CNS and PNS (Willem et al., 2006; Hu et al., 2006, 2008; Michailov et al., 2004; Taveggia et al., 2008; Ohno et al., 2009). The myelin phenotype of *Dyrk1a*$^{+/-}$ mice resembles the one reported for these models, thus opening the intriguing possibility of Dyrk1a being involved in myelination through the NRG1-III pathway. The functional interaction of Dyrk1a with components of the NRG1-III signaling pathway should be tested to corroborate this interesting hypothesis.

Cytoskeleton remodeling in oligodendrocytes and Schwann cells is a key determinant for the formation of multilamellar myelin sheaths

(reviewed in Bauer et al., 2009 and in Sherman and Brophy, 2005. See also Wake et al., 2011; Rajasekharan et al., 2009 for recent evidences in this field). The involvement of Dyrk1a in cytoskeleton remodeling processes has been suggested by the following evidences: first, an RNAi screening performed in *Drosophila* identified Dyrk1a as a regulator of actin protrusions in CNS-derived cell lines (Liu et al., 2009b); and second, Dyrk1a regulates microtubules dynamics in growing axons by priming GSK3ß-mediated phosporylation of Map1b (Scales et al., 2009). Interestingly, the high expression of Map1b in premyelinating and actively myelinating oligodendrocytes, indicates an involvement of this specific microtubule associated protein in the cytoskeletal reorganization of myelin forming cells (Vouyiouklis and Brophy, 1993; Wu et al., 2001). Although the specific role of Dyrk1a in regulating the cytoskeleton dynamics of oligodendrocytes and Schwann cells has not been shown yet, the evidences here reported open the possibility that Dyrk1a plays a role in myelination by regulating the cytoskeletal remodeling of myelin forming cells.

The impaired gliogenesis observed *in vitro in* $Dyrk1a^{+/-}$ neurospheres and *in vivo* in $Dyrk1a^{+/-}$ postnatal cortices opens the possibility that although the number of oligodendrocytes is restored in adult $Dyrk1a^{+/-}$ brains, their functionality remains affected. The lack of any evident myelin phenotype in $S100b^{-/-}$ adult mice suggests that S100b, although playing a role in oligodendroglial differentiation, it is not involved in the myelination process (Deloulme et al., 2004). This evidence indicates that the reduced *S100b* expression observed in the cortex of $Dyrk1a^{+/-}$ mice is likely to correlate with the delayed oligodendrogenesis observed but not with the impaired myelination of the adult brain. A similar phenotype has been described for wa2 mice, in which EGFR

signaling is reduced (Luetteke et al., 1994). These mice, although displaying a delayed oligodendrogenesis during development, showed a normal number of oligodendroglial cells and a normal myelin phenotype in the adulthood (Aguirre et al., 2007). However, both *S100b*$^{-/-}$ and wa2 mice showed an impaired remyelination process after cuprazone-induced demyelination (Deloulme et al., 2004; Aguirre et al., 2007). These phenotypes suggest that a delayed developmental oligodendrogenesis, although compensated in the adulthood in normal conditions, can be reflected in a reduced capability of remyelination after injury (reviewed in Franklin and Ffrench-Constant, 2008; Taveggia et al., 2010). For this reason, it would be interesting to test whether the capability to remyelinate axons is impaired in *Dyrk1a*$^{+/-}$ brains.

Conclusions

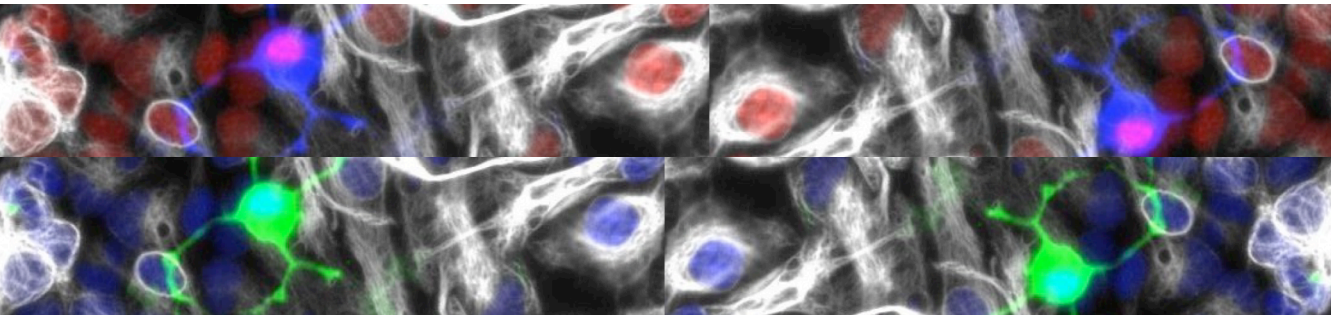

- *Dyrk1a* dose reduction leads to moderate changes in the expression of an important number of genes in the postnatal mouse cerebral cortex. These changes are stage specific and, in most cases, opposite to the changes occurring during normal cortical development. This suggests that the effect of *Dyrk1a* dose reduction on the transcriptome of the developing cerebral cortex is mainly the consequence of a delayed developmental gene expression program.

- The expression analysis of a subset of these genes in the postnatal cerebral cortex of a trisomic *Dyrk1a* transgenic mouse, suggested that most of the effects of *Dyrk1a* in cortical development are not dose dependent.

- No enrichment for a particular Gene Ontology category or for a transcription factor binding site was highlighted, by bioinformatic analysis, among the genes differentially expressed in *Dyrk1a*$^{+/-}$ postnatal cortices. The only difference that came up from this analysis was a different CpG content between the up- and down-regulated genes. These findings are in agreement with the idea of a delayed developmental gene expression program in the cortex of *Dyrk1a*$^{+/-}$ mice, and suggest that differences in DNA methylation may contribute to this delay.

- Embryonic cortical progenitor cells in culture show a reduced EGF- and FGF- dependent self-renewal potentials and decreased capability to differentiate into O4^{+} and S100b^{+} oligodendroglial cells.

- *Dyrk1a*$^{+/-}$ newborn mice have reduced numbers of S100b^{+} glial cells in their cerebral cortex suggesting that the oligodendrogenic potential of *Dyrk1a*$^{+/-}$ progenitors is also reduced *in vivo*.

- A specific position of *S100b* promoter shows increased DNA methylation and decreased K16H4 acetylation in *Dyrk1a*$^{+/-}$ embryonic cortical cells, which may confer to these cells a more inactive chromatin state than wild type cells. These differences in epigenetic modifications occur, *in vivo*, in a precise time window of cortical development (E14.5) and they could be at the basis of the altered number of S100b^{+} cells observed in the cortex of *Dyrk1a*$^{+/-}$ postnatal mice.

- The *Gfap* promoter of *Dyrk1a*$^{+/-}$ embryonic cortical cells shows decreased DNA methylation *in vivo* in a specific locus, whose demethylation is key for the onset of astrogliogenesis. This difference may confer *Dyrk1a*$^{+/-}$ progenitors an increased astrogliogenic potential, which is in agreement with the increased number of Gfap^{+} astrocytes of adult *Dyrk1a*$^{+/-}$ brains.

- The *Corpus Callosum* of *Dyrk1a*$^{+/-}$ adult mice shows decreased axonal myelin thickness but a normal number of mature oligodendrocytes. This evidence, together with the reduced Mbp protein level observed in *Dyrk1a*$^{+/-}$ adult cortices, indicates that normal levels of Dyrk1a are necessary for proper axonal myelination. This is supported by the reduced myelin thickness observed in the optic and sciatic nerves of adult *Dyrk1a*$^{+/-}$ mice.

Appendix

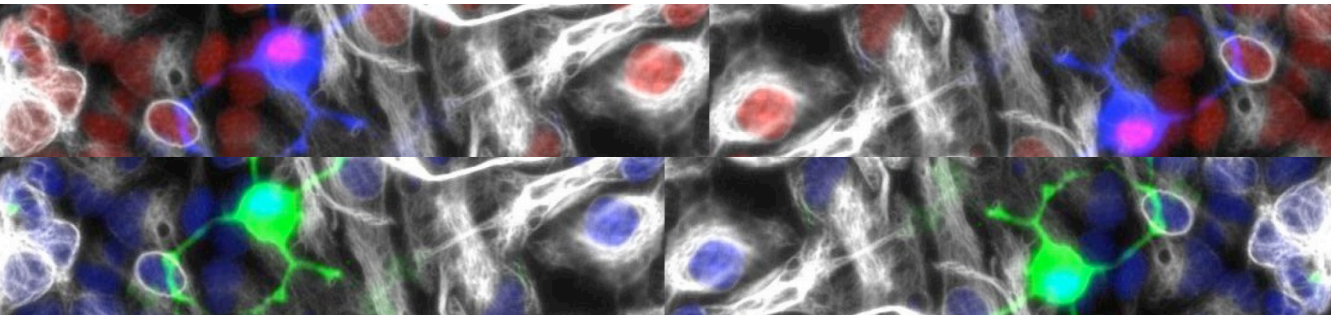

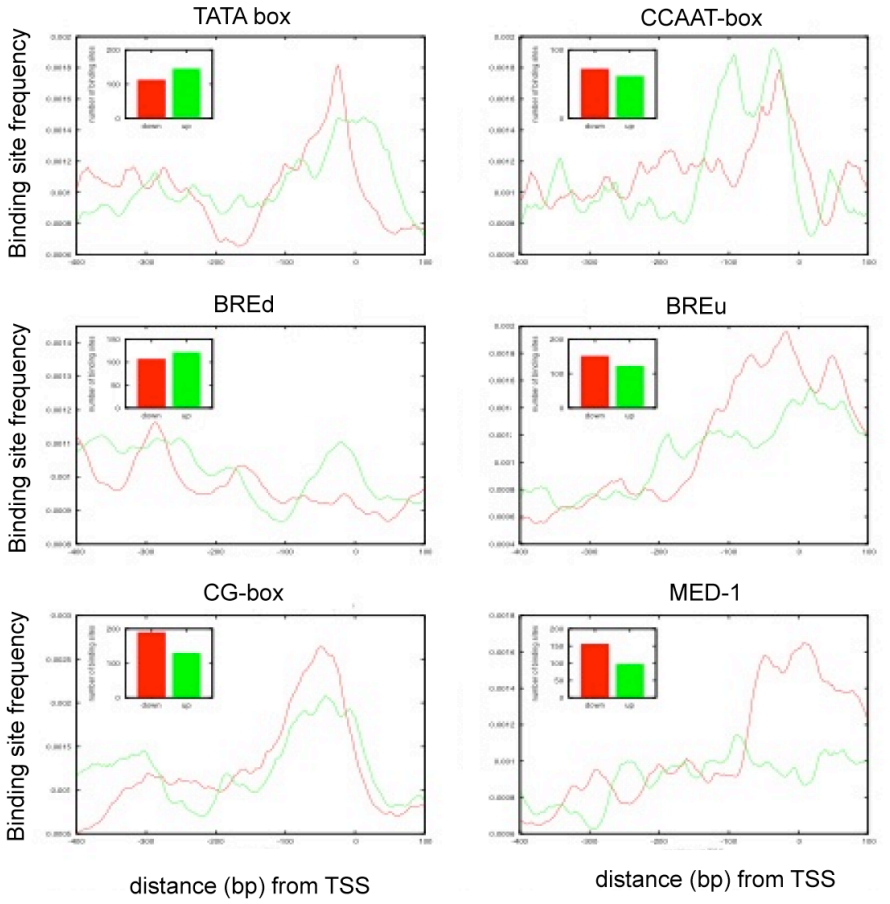

Fig A1: Frequencies and site distributions of different core promoter elements in the up- and down-regulated genes in *Dyrk1a*$^{+/-}$ P0 cortices. The distribution of each element around the transcription start site (TSS) is represented by green lines for the up-regulated genes and by red lines for the down-regulated ones. Insets show absolute numbers of sites in the range of -400bp to +100bp (considering position 0 the TSS). No statistical significance, determined by hypergeometric test, was obtained for any of the comparisons shown.

Fig A2: RE-1/NRSE consensus sequences. The canonical 21bp RE-1/NRSE motif (Chong et al., 1995; and Schoenherr and Anderson, 1995) is indicated as RE-1, the compressed and expanded variants described by Otto and colleagues (2007) as RE-1 (c) and RE-1 (e). All these three matrices were used in this work for DNA scanning.

Table A1: Top differentially expressed genes in the cerebral cortex of *Dyrk1a*$^{+/-}$ postnatal mice

P0- MvsWT					
	SYMBOL	logFC	t	P.Value	adj.P.Val
1424208_at	Ptger4	−0.976	−9.464	6.646e−08	2.106e−04
1439947_at	Cyp11a1	0.885	7.746	9.218e−07	1.000e−03
1446490_at	Ptbp2	0.771	7.604	1.164e−06	1.000e−03
1420955_at	Vsnl1	−0.627	−7.555	1.263e−06	1.000e−03
1435332_at	Htr7	−0.727	−7.228	2.188e−06	1.387e−03
1455469_at	Slc6a7	−0.799	−6.998	3.248e−06	1.567e−03
1456909_at	Gpi1	−0.804	−6.836	4.311e−06	1.567e−03
1458130_at	1110001A07Rik	0.944	6.776	4.790e−06	1.567e−03
1452763_at	Nipa1	−0.603	−6.727	5.224e−06	1.567e−03
1423405_at	Timp4	−0.841	−6.670	5.781e−06	1.567e−03
1439610_at	Rab27b	−0.698	−6.651	5.984e−06	1.567e−03
1433909_at		−0.721	−6.595	6.618e−06	1.567e−03
1427042_at	Mal2	−0.751	−6.589	6.679e−06	1.567e−03
1452598_at	Gins1	0.605	6.570	6.922e−06	1.567e−03
1416926_at	Trp53inp1	0.673	6.419	9.076e−06	1.912e−03
1456482_at	Pik3r3	0.749	6.385	9.652e−06	1.912e−03
1449172_a_at	Lin7b	−0.744	−6.309	1.109e−05	2.067e−03
1460601_at	Myrip	−0.625	−6.261	1.211e−05	2.132e−03
1441545_at	Zcchc11	0.541	6.111	1.599e−05	2.667e−03
1436990_s_at	Ndg2	−0.704	−6.024	1.881e−05	2.980e−03
1455304_at	Unc13c	−0.626	−5.954	2.144e−05	3.235e−03
1456307_s_at	Adcy7	−0.647	−5.916	2.302e−05	3.316e−03
1421312_a_at	Kifc2	−0.572	−5.876	2.482e−05	3.420e−03
1425090_s_at	Kcnc4	−0.607	−5.839	2.662e−05	3.478e−03
1447669_s_at	Gng4	−0.628	−5.814	2.790e−05	3.478e−03

P7- MvsWT					
	SYMBOL	logFC	t	P.Value	adj.P.Val
1427038_at	Penk1	−1.045	−7.586	1.200e−06	2.309e−03
1420994_at	B3gnt5	0.575	7.469	1.457e−06	2.309e−03
1417954_at	Sst	−1.000	−6.872	4.047e−06	4.275e−03
1428306_at	Ddit4	1.306	6.463	8.380e−06	6.639e−03
1436134_at	Scn2b	−0.714	−6.269	1.194e−05	6.824e−03
1424714_at	Aldoc	−0.643	−6.193	1.374e−05	6.824e−03
1424567_at	Tspan2	−0.770	−6.087	1.673e−05	6.824e−03
1457867_at	Sgpp2	−0.970	−6.071	1.723e−05	6.824e−03
450391_a_at	Mgll	−0.536	−5.839	2.660e−05	9.367e−03
1452346_at	B3gnt1	−0.557	−5.765	3.065e−05	9.714e−03
1452132_at	Tlcd1	−0.553	−5.658	3.760e−05	1.014e−02
1416926_at	Trp53inp1	0.592	5.647	3.841e−05	1.014e−02
1417970_at	Atp5s	−0.401	−5.514	4.964e−05	1.189e−02
1442258_at	Lonp2	0.425	5.485	5.251e−05	1.189e−02
1456482_at	Pik3r3	0.635	5.409	6.081e−05	1.264e−02
1434745_at	Ccnd2	0.499	5.360	6.697e−05	1.264e−02
1433802_at	Tmem151	−0.512	−5.353	6.779e−05	1.264e−02
459749_s_at	Fat4	0.532	5.244	8.405e−05	1.403e−02
1455190_at	Gng7	−0.494	−5.244	8.409e−05	1.403e−02
434437_x_at	Rrm2	0.710	5.174	9.640e−05	1.442e−02
441869_x_at	Auts2	0.521	5.164	9.851e−05	1.442e−02
1429372_at	Sox11	0.459	5.155	1.001e−04	1.442e−02
431569_a_at	Lypd1	−0.502	−5.010	1.336e−04	1.722e−02
420545_a_at	Chn1	−0.682	−5.007	1.344e−04	1.722e−02
1422756_at	Slc32a1	−0.594	−5.002	1.359e−04	1.722e−02

Results of the microarray-based gene expression comparison between mutant (M, *Dyrk1a*$^{+/-}$) and wild type (W, *Dyrk1a*$^{+/+}$) cerebral cortices, respectively, at postnatal day 0 (P0) and 7 (P7). Table reports the Affymetrix ID; the gene symbol; the fold change (FC) expression between genotypes expressed in log2 scale (LogFC); the moderated-t statistical test (t); the pValues obtained in the t test (pValue) and the adjusted pValues calculated according to the method described by Benjamini and Hochberg (adj-pVal) (Benjamini and Hochberg, 1995; Smyth, 2004).

Table A2: List of genes differentially expressed in the cerebral cortex of *Dyrk1a*$^{+/-}$ P0 and P7 mice

	P0-MvsW	P7-MvsW
Mbp	-0,91	-0,85
Thy1	-0,68	-0,50
Scn2b	-0,36	-0,71
Nrip3	-0,50	-0,41
Slc25a18	-0,69	-0,87
Slc7a10	-0,43	-0,52
Timp4	-0,84	-0,47
2900041A09	-0,42	-0,38
Rasgrp1	-0,37	-0,38
Ckmt1	-0,58	-0,47
Aadacl1	-0,53	-0,41
Rgs7bp	-0,40	-0,49
Tesc	-0,49	-0,51
Ramp1	-0,55	-0,49
Nrsn1	-0,41	-0,43
Ndg2	-0,70	-0,56
Rab27b	-0,70	-0,45
Mgll	-0,45	-0,54
9130213B05	-0,45	-0,49
Atp6v1g2	-0,45	-0,45
Rwdd2	-0,49	-0,51
Tmem151	-0,47	-0,51
Eno2	-0,33	-0,34
Penk1	-0,70	-1,05
Tlcd1	-0,46	-0,55
Gabpb2	-0,70	-0,54
Ptger4	-0,98	-0,48
Tspan17	-0,63	-0,46
Tspan2	-0,41	-0,77
Gng7	-0,39	-0,49
Aldoa	-0,48	-0,55
Ddit4	0,64	1,31
Tln2	-0,36	-0,50
Slc12a5	-0,46	-0,40
Mod1	-0,31	-0,45
Nefl	-0,46	-0,41
Olfm3	-0,65	-0,46
Slc36a1	-0,26	-0,34
Rit2	-0,43	-0,50
Htr1b	-0,59	-0,51
Tm7sf2	-0,42	-0,48
Slc7a4	-0,37	-0,54
Nrsn2	-0,42	-0,47
Slc32a1	-0,48	-0,59
Calb1	-0,51	-0,56
Pik3r3	0,75	0,63
Ccnd2	0,38	0,44
Rmnd5a	0,53	0,40
Trp53inp1	0,67	0,59
Smc4	0,46	0,40
Fat4	0,34	0,53
Bach2	0,36	0,49
Odz4	0,35	0,44
Lonp2	0,45	0,42
Nfib	0,59	0,68
Glcci1	0,51	0,60
Lmnb1	0,36	0,41
Sox4	0,48	0,42
Auts2	0,34	0,52
Sox11	0,30	0,46
AI426953	0,67	0,68

P0-MvsW and P7-MvsW indicates, respectively, the comparison between mutant (M, *Dyrk1a*$^{+/-}$) and wild type (W, *Dyrk1a*$^{+/+}$) cerebral cortices at postnatal day 0 (P0) and 7 (P7). Listed values correspond to the differences in gene expression obtained in the microarray experiment, expressed as log2 fold change (FC). Only genes that were differentially expressed with an adj-pValue<0.05 in both comparisons, are reported.

Table A3: List of most represented Gene Ontology (GO) categories in the set of up- and down- regulated genes in the cerebral cortex of *Dyrk1a*$^{+/-}$ postnatal mice

(a) P0-MvsW up

	GO_ID	Pvalue	ExpCount	Count	Term
MF	GO:0003723	0.000861	12.5	24	RNA binding
MF	GO:0003677	0.00183	35.1	51	DNA binding
MF	GO:0000166	0.00192	36	52	nucleotide binding
MF	GO:0003676	0.00293	11.3	21	nucleic acid binding
MF	GO:0004386	0.00317	2.69	8	helicase activity
MF	GO:0003682	0.00425	3.39	9	chromatin binding
MF	GO:0005524	0.00671	22.6	34	ATP binding
BP	GO:0043170	4.23e-07	96	129	macromolecule metabolic process
BP	GO:0044238	3.22e-06	108	138	primary metabolic process
BP	GO:0044237	5.68e-06	111	140	cellular metabolic process
BP	GO:0019219	7.16e-06	41.1	66	regulation of nucleic acid metabolic process
BP	GO:0006350	2.31e-05	41.6	65	transcription
BP	GO:0019222	7.97e-05	45.7	68	regulation of metabolic process
BP	GO:0006355	0.000157	37.9	58	regulation of transcription, DNA-dependent
BP	GO:0006397	0.000176	7.4	18	mRNA processing
BP	GO:0032774	0.000227	38.4	58	RNA biosynthetic process
BP	GO:0000279	0.000354	4.11	12	M phase
BP	GO:0007059	0.000677	1.29	6	chromosome segregation
BP	GO:0007001	0.000767	8.92	19	chromosome organization and biogenesis
BP	GO:0016070	0.00102	7.75	17	RNA metabolic process
BP	GO:0051301	0.00162	5.4	13	cell division
BP	GO:0007067	0.00191	3.64	10	mitosis
BP	GO:0050794	0.00265	65.9	84	regulation of cellular process
BP	GO:0006259	0.00331	3.29	9	DNA metabolic process
BP	GO:0006323	0.00461	8.1	16	DNA packaging
BP	GO:0000278	0.00468	4.7	11	mitotic cell cycle
BP	GO:0006281	0.00562	2.35	7	DNA repair
BP	GO:0007076	0.00583	0.47	3	mitotic chromosome condensation
BP	GO:0016568	0.00875	5.75	12	chromatin modification
BP	GO:0008380	0.00875	5.75	12	RNA splicing
CC	GO:0005634	1.2e-15	71.9	124	nucleus
CC	GO:0043227	9.48e-08	98.2	133	membrane-bound organelle
CC	GO:0005622	4.03e-07	133	163	intracellular
CC	GO:0031974	0.000206	14.3	28	membrane-enclosed lumen
CC	GO:0043229	0.00129	67.3	87	intracellular organelle
CC	GO:0005730	0.00139	2.4	8	nucleolus
CC	GO:0000228	0.00622	1.83	6	nuclear chromosome
CC	GO:0043228	0.0065	24.3	36	non-membrane-bound organelle
CC	GO:0044446	0.00798	42.1	56	intracellular organelle part
CC	GO:0031981	0.00986	11	19	nuclear lumen

(b) P7-MvsW up

	GO_ID	Pvalue	ExpCount	Count	Term
MF	GO:0003700	5.78e-05	2.36	10	transcription factor activity
MF	GO:0043565	0.0031	1.04	5	sequence-specific DNA binding
BP	GO:0045445	0.00215	0.0779	2	myoblast differentiation
BP	GO:0031323	0.0023	7.32	15	regulation of cellular metabolic process
BP	GO:0045449	0.00308	6.74	14	regulation of transcription
BP	GO:0048747	0.00525	0.117	2	muscle fiber development
BP	GO:0006139	0.00604	9.73	17	nucleic acid metabolic process
BP	GO:0048731	0.0066	4.98	11	system development
BP	GO:0008285	0.00705	0.409	3	negative regulation of cell proliferation
BP	GO:0030324	0.00726	0.136	2	lung development
BP	GO:0048637	0.00726	0.136	2	skeletal muscle development
BP	GO:0008283	0.00782	1.28	5	cell proliferation
BP	GO:0035295	0.00805	0.428	3	tube development

(c) P0-MvsW down

	GO_ID	Pvalue	ExpCount	Count	Term
MF	GO:0005509	5.64e-07	18.7	40	calcium ion binding
MF	GO:0005529	0.000704	1.34	6	sugar binding
MF	GO:0001584	0.000784	3.34	10	rhodopsin-like receptor activity
MF	GO:0008289	0.0023	9.75	19	lipid binding
MF	GO:0005248	0.00236	0.401	3	voltage-gated sodium channel activity
MF	GO:0004993	0.00236	0.401	3	serotonin receptor activity
MF	GO:0015291	0.00249	4.41	11	transporter activity
MF	GO:0015075	0.00536	13.5	23	ion transporter activity
MF	GO:0005262	0.00582	1.34	5	calcium channel activity
MF	GO:0030695	0.00656	8.41	16	GTPase regulator activity
MF	GO:0015268	0.00748	7.08	14	alpha-type channel activity
MF	GO:0015294	0.00782	0.935	4	solute:cation symporter activity
MF	GO:0005326	0.00849	0.534	3	neurotransmitter transporter activity
BP	GO:0007186	1.27e-06	10.7	27	G-protein coupled receptor signaling pathway
BP	GO:0006810	0.000519	45.5	65	transport
BP	GO:0005996	0.00073	2.27	8	monosaccharide metabolic process
BP	GO:0007154	0.000914	53.5	73	cell communication
BP	GO:0007242	0.00212	21.2	34	intracellular signaling cascade
BP	GO:0006865	0.00576	1.33	5	amino acid transport
BP	GO:0019320	0.00776	0.933	4	hexose catabolic process
BP	GO:0044275	0.00776	0.933	4	cellular carbohydrate catabolic process
BP	GO:0046164	0.00776	0.933	4	alcohol catabolic process
BP	GO:0048015	0.00776	0.933	4	phosphoinositide-mediated signaling
BP	GO:0006096	0.00776	0.933	4	glycolysis
BP	GO:0001662	0.00845	0.533	3	behavioral fear response
BP	GO:0051345	0.00845	0.533	3	positive regulation of hydrolase activity
BP	GO:0006006	0.00943	1.47	5	glucose metabolic process
BP	GO:0007600	0.00954	3.2	8	sensory perception
BP	GO:0051056	0.00954	3.2	8	regulation of small GTPase signal transd
CC	GO:0044425	1.57e-08	75.8	114	membrane part
CC	GO:0016021	1.3e-06	67.4	99	integral to membrane
CC	GO:0005886	0.000153	28.7	47	plasma membrane
CC	GO:0000267	0.00743	10	18	cell fraction
CC	GO:0009897	0.00778	0.934	4	external side of plasma membrane

(d) P7-MvsW down

	GO_ID	Pvalue	ExpCount	Count	Term
MF	GO:0005279	0.000253	0.368	4	amino acid-polyamine transporter activity
MF	GO:0015290	0.000545	1.52	7	electrochemical potential-driven transporters
MF	GO:0015293	0.00127	0.873	5	symporter activity
MF	GO:0005280	0.00209	0.0919	2	hydrogen:amino acid symporter activity
MF	GO:0004332	0.00209	0.0919	2	fructose-bisphosphate aldolase activity
MF	GO:0015187	0.00209	0.0919	2	glycine transporter activity
MF	GO:0005275	0.00216	0.597	4	amine transporter activity
MF	GO:0031420	0.0023	1.42	6	alkali metal ion binding
MF	GO:0008324	0.00316	3.72	10	cation transporter activity
MF	GO:0046943	0.00384	0.689	4	carboxylic acid transporter activity
MF	GO:0016830	0.00643	0.413	3	carbon-carbon lyase activity
BP	GO:0015672	0.000569	2.48	9	monovalent inorganic cation transport
BP	GO:0006865	0.000816	0.478	4	amino acid transport
BP	GO:0015980	0.00116	0.86	5	energy derivation by oxidation
BP	GO:0006811	0.00132	5.16	13	ion transport
BP	GO:0015849	0.00179	0.573	4	organic acid transport
BP	GO:0007613	0.00226	0.0956	2	memory
BP	GO:0015816	0.00226	0.0956	2	glycine transport
BP	GO:0045104	0.00226	0.0956	2	IF cytoskeleton organization and biogenesis
BP	GO:0019320	0.0032	0.335	3	hexose catabolic process
BP	GO:0044275	0.0032	0.335	3	cellular carbohydrate catabolic process
BP	GO:0046164	0.0032	0.335	3	alcohol catabolic process
BP	GO:0006096	0.0032	0.335	3	glycolysis
BP	GO:0051179	0.00557	19.6	30	localization
BP	GO:0048878	0.00609	1.72	6	chemical homeostasis
BP	GO:0006873	0.00909	1.34	5	cell ion homeostasis
CC	GO:0044444	0.00109	16.9	29	cytoplasmic part
CC	GO:0016021	0.00119	24.7	38	integral to membrane
CC	GO:0044425	0.0016	27.8	41	membrane part

GO analysis was performed on differentially expressed genes with adj-pVal<0.05. Tables report the most represented GO categories (or terms) in the set of up- (a and b) and down- (c and d) regulated genes at P0 (a and c) or P7 (b and d). GO terms belong to one of the three major annotations, based on the function of the genes included in each category: Molecular Function (MF), Biological Process (BP) or Cellular Component (CC) (first column). The GO_ID associated to each category is reported in the second column and the pValues indicating how significant is the enrichment of that category among the differentially expressed genes, is in the third column. pValues are calculated according to the number of genes counted for each term (fifth column) with respect to the number of expected genes falling in that category, assuming a random distribution (forth column). A description of each term is given in the last column.

Table A4: List of genes differentially expressed in *Dyrk1a*$^{+/-}$ cortices with one predicted RE-1 site in their promoter region

Down-regulated		Up-regulated	
Affy_ID	Gene symbol	Affy_ID	Gene symbol
1457984_at	Crh*	1438680_at	Auts2
1440148_at	Gpr6	1448205_at	Ccnb1-rs1
1449172_a_at	Lin7b	1429410_at	Eny2
1416713_at	2700055K07	1449244_at	Cdh2
1452090_a_at	Olfm3	1421065_at	Jak2
1418683_at	Lin7b	1457553_at	Cugbp2
1437341_x_at	Cnp1	1416488_at	Ccng2
1425090_s_at	Kcnc4	1443592_at	AA617406
1452763_at	Nipa1	1429707_at	Plaa
1420191_s_at	D16Bwg1494	1422886_a_at	Clk4
1417089_a_at	Ckmt1	1429857_at	Pou3f3
1426541_a_at	Endod1	1438739_at	Cnbp
1417943_at	Gng4	1430220_at	4833420G17
1449770_x_at	D16Bwg1494	1446088_at	9430081I23
1433556_at	Centa1	1452598_at	Gins1
1426785_s_at	Mgll	1456482_at	Pik3r3
1417504_at	Calb1*	1421190_at	Gabrb3
1448954_at	Nrip3		
1418212_at	Omg		
1436094_at	Vgf		
1427023_at	Phyhipl		
1416588_at	Ptprn		
1460343_at	Neurl		
1418588_at	Nrsn1		
1450693_at	Rgs17		
1441899_x_at	Bcan		
1423640_at	Synpr		
1447852_x_at	2900002H16		
1457412_at	Scn8a		
1435387_at	Slc2a13		
1452952_at	9030418K01		
1419358_at	Sorcs2		
1418149_at	Chga		
1452790_x_at	Ndufa3		
1452445_at	Slc41a2		
1437392_at	AW123113		
1428897_at	2610029I01		
1444026_at	AI593442		
1449147_at	Chst1		
1435297_at	Gja9		
1424474_a_at	Camkk2		
1417569_at	Ncald		
1417746_at	Cplx1		

Genes listed correspond to the differentially expressed genes at P0 (adj-pValue<0.05) with one predicted RE-1 site in the region of 4Kb

around the transcription start site (TSS). Matscan program was used for the scanning of promoter regions. Affymetrix ID (Affy_ID) and Gene symbols are reported for each gene in the first and second column respectively. Asterisks indicate validated Rest target genes according to Ballas et al., 2005 and Seth and Majzoub, 2001.

Table A5: Mouse reference genes evaluated by LDA

gene	average ct		ct variation %		
			P0 (MvsW)	P7 (MvsW)	W (P7vsP0)
ribosomal protein large P2 (rplp2)	30	*	1.3	1.0	3.7
glyceraldehyde-3-phosphate dehydrogenase (gapdh)	19	**	1.1	1.6	3.7
transferrin receptor (tfrc)	25		1.2	0.6	1.2
tata binding protein (tbp)	26		1.5	0,4	2.7
peptidylprolyl isomerase A (ppia)	20		0.8	1.2	2.5
polymerase (RNA) II (DNA directed) polypeptide A (polr2a)	25	**	1.2	1.4	1.4
monooxygenase activation protein, zeta polypeptide (ywhaz)	20	**	1.0	1.2	3.5
glucoronidase beta (gusb)	28	**	0.7	1.8	5.0
18s ribosomal RNA (18s)	8	*			
hypoxanthine guanine phosphoribosyl transferase (hprt1)	25		1.2	2,0	5.6
ubiquitine C (ubc)	22.5		1.3	1.2	0.9
beta-2 microglobuline (b2m)	25.5	**	2.0	3.1	3.5
phosphoglycerate kinase 1 (pgk1)	23	**	0,9	1.3	1.7
hydroxymethylbilane synthase (hbms)	26		1.2	1.2	1.5
importin 8 (ipo8)	26	**	0.8	1.0	1.3
actin-beta (actb)	17		1.2	0.4	1.4

Average ct (average ct) was calculated from all the samples analyzed, independently of their genotype and developmental stage (n=8). The standard deviations obtained for each comparison (P0-MvsW, P7-MvsW and W-P7vsP0), are expressed as percentage of the average ct (ct variation %). *indicates genes that were discarded because of its low or extremely high abundance. ** indicates genes whose variability was associated to genotypes. Marked in yellow are the genes that were chosen as reference for further expression analysis with LDA costumer cards.

Bibliography

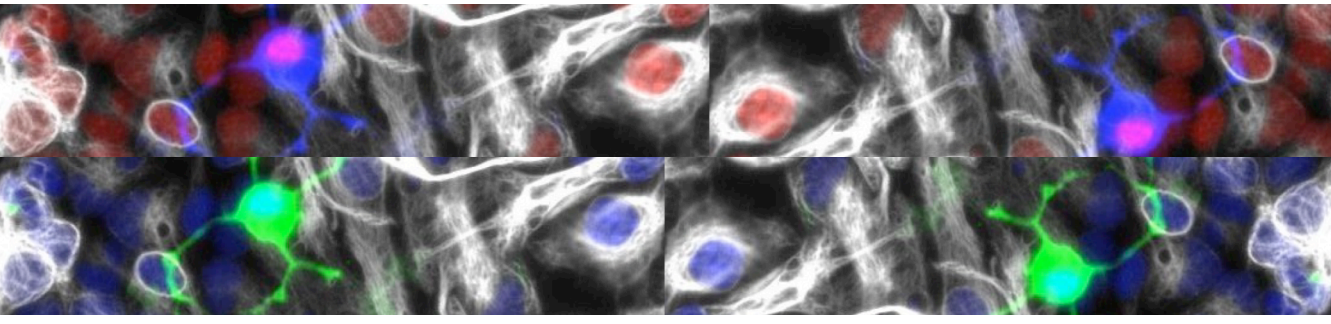

Aguirre A, Dupree JL, Mangin JM, Gallo V. (2007). A functional role for EGFR signaling in myelination and remyelination. Nat. Neurosci. 10:990–1002

Ahn KJ, Jeong HK, Choi HS, Ryoo SR, Kim YJ, Goo JS, Choi SY, Han JS, Ha I, Song WJ. (2006). DYRK1A BAC transgenic mice show altered synaptic plasticity with learning and memory defects. Neurobiol Dis. 22:463-72.

Alderton GK, Galbiati L, Griffith E, Surinya KH, Neitzel H, Jackson AP, Jeggo PA, O'Driscoll M. (2006). Regulation of mitotic entry by microcephalin and its overlap with ATR signalling. Nat Cell Biol. 8:725-33.

Aldridge K, Reeves RH, Olson LE, Richtsmeier JT. (2007). Differential effects of trisomy on brain shape and volume in related aneuploid mouse models. Am J Med Genet.143A:1060-70.

Alkuraya FS, Cai X, Emery C, Mochida GH, Al-Dosari MS, Felie JM, Hill RS, Barry BJ, Partlow JN, Gascon GG, Kentab A, Jan M, Shaheen R, Feng Y, Walsh CA. (2011). Human mutations in NDE1 cause extreme microcephaly with lissencephaly. Am J Hum Genet. 88:536-47.

Altafaj X, Dierssen M, Baamonde C, Martí E, Visa J, Guimerà J, Oset M, González JR, Flórez J, Fillat C, Estivill X. (2001). Neurodevelopmental delay, motor abnormalities and cognitive deficits in transgenic mice overexpressing Dyrk1A (minibrain), a murine model of Down's syndrome. Hum Mol Genet. 10:1915-23.

Altmann CR, Brivanlou AH (2001). Neural patterning in the vertebrate embryo. Int Rev Cytol. 203:447-482.

Alvarez M, Estivill X, de la Luna S. (2001). DYRK1A accumulates in splicing speckles through a novel targeting signal and induces speckle disassembly. J Cell Sci. 116:3099-107.

Alvarez, M. (2004). Localización subcelular de la proteína quinasa DYRK1A: compartimentos, señales y regulación (Doctoral Thesis, Universitat de Barcelona).

Alvarez, M., Altafaj, X., Aranda, S., and de la Luna, S. (2007). DYRK1A autophosphorylation on serine residue 520 modulates its kinase activity via 14-3-3 binding. Mol Biol Cell 18:1167-1178.

Amano K, Sago H, Uchikawa C, Suzuki T, Kotliarova SE, Nukina N, Epstein CJ, Yamakawa K. (2004). Dosage-dependent over-expression of genes in the trisomic region of Ts1Cje mouse model for Down syndrome. Hum Mol Genet. 13:1333-40.

Anderson SA, Eisenstat DD, Shi L, Rubenstein JL. (1997). Interneuron migration from basal forebrain to neocortex: dependence on Dlx genes. Science. 278:474-6.

Andreu-Agulló C, Morante-Redolat JM, Delgado AC, Fariñas I. (2009). Vascular niche factor PEDF modulates Notch-dependent stemness in the adult subependymal zone. Nat Neurosci. 12:1514-23.

Anthony, T. E., Klein, C., Fishell, G. & Heintz, N. (2004). Radial glia serve as neuronal progenitors in all regions of the central nervous system. Neuron 41: 881–890.

Anthony, T.E., Mason, H.A., Gridley, T., Fishell, G., and Heintz, N. (2005). Brain lipid-binding protein is a direct target of Notch signaling in radial glial cells. Genes Dev. 19:1028–1033.

Aranda S, Alvarez M, Turró S, Laguna A, de la Luna S. (2008). Sprouty2-mediated inhibition of fibroblast growth factor signaling is modulated by the protein kinase DYRK1A. Mol Cell Biol. 19:5899-911.

Aranda S, Laguna A, de la Luna S. (2011). DYRK family of protein kinases: evolutionary relationships, biochemical properties, and functional roles. FASEB J. 25:449-62.

Arqué G, Fotaki V, Fernández D, Martínez de Lagrán M, Arbonés ML, Dierssen M. (2008). Impaired spatial learning strategies and novel object recognition in mice haploinsufficient for the dual specificity tyrosine-regulated kinase-1A (Dyrk1A). PLoS One. 3:e2575.

Arron JR, Winslow MM, Polleri A, Chang CP, Wu H, Gao X, Neilson JR, Chen L, Heit JJ, Kim SK, Yamasaki N, Miyakawa T, Francke U, Graef IA, Crabtree GR. (2006). NFATdysregulation by increased dosage of DSCR1 and DYRK1A on chromosome 21. Nature. 441:595-600.

Artavanis-Tsakonas S, Rand MD, Lake RJ. (1999). Notch signaling: cell fate control and signal integration in development. Science. 284:770-6.

Ashburner M, Ball CA, Blake JA, Botstein D, Butler H, Cherry JM, Davis AP, Dolinski K, Dwight SS, Eppig JT, Harris MA, Hill DP, Issel-Tarver L, Kasarskis A, Lewis S, Matese JC, Richardson JE, Ringwald M, Rubin GM, Sherlock G. (2000). Gene ontology: tool for the unification of biology. The Gene Ontology Consortium. Nat Genet. 25:25-9.

Bakircioglu M, Carvalho OP, Khurshid M, Cox JJ, Tuysuz B, Barak T, Yilmaz S, Caglayan O, Dincer A, Nicholas AK, Quarrell O, Springell K, Karbani G, Malik S, Gannon C, Sheridan E, Crosier M, Lisgo SN, Lindsay S, Bilguvar K, Gergely F, Gunel M, Woods CG. (2011). The essential role of centrosomal NDE1 in human cerebral cortex neurogenesis. Am J Hum Genet. 88:523-35.

Ballas N, Battaglioli E, Atouf F, Andres ME, Chenoweth J, Anderson ME, Burger C, Moniwa M, Davie JR, Bowers WJ, Federoff HJ, Rose DW, Rosenfeld MG, Brehm P, Mandel G. (2001). Regulation of neuronal traits by a novel transcriptional complex. Neuron. 31:353-65.

Ballas N, Grunseich C, Lu DD, Speh JC, Mandel G. (2005). REST and its corepressors mediate plasticity of neuronal gene chromatin throughout neurogenesis. Cell. 121:645-57.

Ballas N, Mandel G. (2005). The many faces of REST oversee epigenetic programming of neuronal genes. Curr Opin Neurobiol. 15:500-6.

Barnabé-Heider F, Wasylnka JA, Fernandes KJ, Porsche C, Sendtner M, Kaplan DR, Miller FD. (2005). Evidence that embryonic neurons regulate the onset of cortical gliogenesis via cardiotrophin-1. Neuron. 48:253-65.

Baron W, Hoekstra D. (2010). On the biogenesis of myelin membranes: sorting, trafficking and cell polarity. FEBS Lett. 584:1760-70.

Barres BA, Raff MC. (194). Control of oligodendrocyte number in the developing rat optic nerve. Neuron.12:935-42.

Bauer NG, Richter-Landsberg C, Ffrench-Constant C. (2009). Role of the oligodendroglial cytoskeleton in differentiation and myelination. Glia. 57:1691-705.

Baxter LL, Moran TH, Richtsmeier JT, Troncoso J, Reeves RH. (2000). Discovery

and genetic localization of Down syndrome cerebellar phenotypes using the Ts65Dn mouse. Hum Mol Genet. 9:195-202.

Bayer SA, Altman J (1991). *Neocortical Development.* New York Raven Press.

Becker W, Joost HG. (1999). Structural and functional characteristics of Dyrk, a novel subfamily of protein kinases with dual specificity. Prog Nucleic Acid Res Mol Biol. 62:1-17.

Belichenko PV, Masliah E, Kleschevnikov AM, Villar AJ, Epstein CJ, Salehi A, Mobley WC. (2004). Synaptic structural abnormalities in the Ts65Dn mouse model of Down Syndrome. J Comp Neurol. 480:281-98.

Benavides-Piccione R, Ballesteros-Yáñez I, de Lagrán MM, Elston G, Estivill X, Fillat C, Defelipe J, Dierssen M. (2004). On dendrites in Down syndrome and DS murine models: a spiny way to learn. Prog Neurobiol. 74:111-26.

Benavides-Piccione R, Dierssen M, Ballesteros-Yáñez I, Martínez de Lagrán M, Arbonés ML, Fotaki V, DeFelipe J, Elston GN. (2005). Alterations in the phenotype of neocortical pyramidal cells in the Dyrk1A+/- mouse. Neurobiol Dis. 20:115-22.

Benjamini Y. and Hochberg Y. (1995). Controlling the false discovery rate: A practical and powerful approach to multiple testing. Journal of the Royal Statistical Society B, 57:289–300.

Bentires-Alj M, Kontaridis MI, Neel BG. (2006). Stops along the RAS pathway in human genetic disease. Nat Med. 12:283-5.

Bentivoglio M, Mazzarello P. (1999). The history of radial glia. Brain Res Bull. 49:305-15.

Bergsland M, Werme M, Malewicz M, Perlmann T, Muhr J. (2006). The establishment of neuronal properties is controlled by Sox4 and Sox11. Genes Dev. 20:3475-86.

Bertrand N, Castro DS, Guillemot F. (2002). Proneural genes and the specification of neural cell types. Nat Rev Neurosci. 7:517-30.

Bhat V, Girimaji SC, Mohan G, Arvinda HR, Singhmar P, Duvvari MR, Kumar A. (2011). Mutations in WDR62, encoding a centrosomal and nuclear protein, in Indian primary microcephaly families with cortical malformations. Clin Genet. 80:532-40.

Bilgüvar K, Oztürk AK, Louvi A, Kwan KY, Choi M, Tatli B, Yalnizoğlu D, Tüysüz B, Cağlayan AO, Gökben S, Kaymakçalan H, Barak T, Bakircioğlu M, Yasuno K, Ho W, Sanders S, Zhu Y, Yilmaz S, Dinçer A, Johnson MH, Bronen RA, Koçer N, Per H, Mane S, Pamir MN, Yalçinkaya C, Kumandaş S, Topçu M, Ozmen M, Sestan N, Lifton RP,State MW, Günel M. (2010). Whole-exome sequencing identifies recessive WDR62 mutations in severe brain malformations. Nature. 467:207-10.

Blanco E, Messeguer X, Smith TF, Guigó R. (2006). Transcription factor map alignmentof promoter regions. PLoS Comput Biol. 2:e49.

Boggs JM. (2006). Myelin basic protein: a multifunctional protein. Cell Mol Life Sci. 63:1945-61.

Bond J, Roberts E, Mochida GH, Hampshire DJ, Scott S, Askham JM, Springell K, Mahadevan M, Crow YJ, Markham AF, Walsh CA, Woods CG. (2002). ASPM is a major determinant of cerebral cortical size. Nat Genet. 32:316-20.

Bond J, Roberts E, Springell K, Lizarraga SB, Scott S, Higgins J, Hampshire DJ, Morrison EE, Leal GF, Silva EO, Costa SM, Baralle D, Raponi M, Karbani G, Rashid Y, Jafri H, Bennett C, Corry P, Walsh CA, Woods CG. (2005). A centrosomal mechanism involving CDK5RAP2 and CENPJ controls brain size. Nat Genet. 37:353-5. Erratum in: Nat Genet. (2005) 37:555.

Bonni A, Sun Y, Nadal-Vicens M, Bhatt A, Frank DA, Rozovsky I, Stahl N, Yancopoulos GD, Greenberg ME. (1997). Regulation of gliogenesis in the central nervous system by the JAK-STAT signaling pathway. Science. 278:477-83.

Borello U, Pierani A. (2010). Patterning the cerebral cortex: traveling with morphogens. Curr Opin Genet Dev. 20:408-15.

Boulder Committee (1970). Embryonic vertebrate central nervous system: revised terminology. Anat. Rec.166, 257–261

Branchi I, Bichler Z, Minghetti L, Delabar JM, Malchiodi-Albedi F, Gonzalez MC, Chettouh Z, Nicolini A, Chabert C, Smith DJ, Rubin EM, Migliore-Samour D, Alleva E. (2004). Transgenic mouse in vivo library of human Down syndrome critical region 1: association between DYRK1A overexpression, brain development abnormalities, and cell cycle protein alteration. J Neuropathol Exp Neurol. 63:429-40.

Branner A, Stein RB, Normann RA. (2001). Selective stimulation of cat sciatic nerve using an array of varying-length microelectrodes. J Neurophysiol. 85:1585-94.

Brinkmann BG, Agarwal A, Sereda MW, Garratt AN, Müller T, Wende H, Stassart RM, Nawaz S, Humml C, Velanac V, Radyushkin K, Goebbels S, Fischer TM, Franklin RJ, Lai C, Ehrenreich H, Birchmeier C, Schwab MH, Nave KA. (2008). Neuregulin-1/ErbB signaling serves distinct functions in myelination of the peripheral and central nervous system. Neuron. 28:581-95.

Bruce AW, Donaldson IJ, Wood IC, Yerbury SA, Sadowski MI, Chapman M, Göttgens B, Buckley NJ. (2004). Genome-wide analysis of repressor element 1 silencing transcription factor/neuron-restrictive silencing factor (REST/NRSF) target genes. Proc Natl Acad Sci U S A. 101:10458-63.

Bruce AW, López-Contreras AJ, Flicek P, Down TA, Dhami P, Dillon SC, Koch CM, Langford CF, Dunham I, Andrews RM, Vetrie D. (2009). Functional diversity for REST (NRSF) is defined by in vivo binding affinity hierarchies at the DNA sequence level. Genome Res. 19:994-1005.

Buratti, E., De Conti, L., Stuani, C., Romano, M., Baralle, M., and Baralle, F. (2010). Nuclear factor TDP-43 can affect selected microRNA levels. FEBS J 277:2268-2281.

Cai L, Hayes NL, Takahashi T, Caviness VS Jr, Nowakowski RS. (2002). Size distribution of retrovirally marked lineages matches prediction from population measurements of cell cycle behavior. J Neurosci Res. 69:731-44.

Canzonetta C, Mulligan C, Deutsch S, Ruf S, O'Doherty A, Lyle R, Borel C, Lin-Marq N, Delom F, Groet J, Schnappauf F, De Vita S, Averill S, Priestley JV, Martin JE, Shipley J, Denyer G, Epstein CJ, Fillat C, Estivill X, Tybulewicz VL, Fisher EM, Antonarakis SE, Nizetic D. (2008). DYRK1A-dosage imbalance perturbs NRSF/REST levels, deregulating pluripotency and embryonic stem cell fate in Down syndrome. Am J Hum Genet. 83:388-400.

Casaccia-Bonnefil P, Tikoo R, Kiyokawa H, Friedrich V Jr, Chao MV, Koff A. (1997). Oligodendrocyte precursor differentiation is perturbed in the absence of the cyclin-dependent kinase inhibitor p27Kip1. Genes Dev. 11:2335-46.

Caviness VS Jr, Takahashi T, Nowakowski RS. (1995). Numbers, time and neocortical neuronogenesis: a general developmental and evolutionary model. Trends Neurosci. 18:379-83.

Chakrabarti L, Galdzicki Z, Haydar TF. (2007). Defects in embryonic neurogenesis and initial synapse formation in the forebrain of the Ts65Dn mouse model of Down syndrome. J Neurosci. 27:11483-95.

Chan JR, Watkins TA, Cosgaya JM, Zhang C, Chen L, Reichardt LF, Shooter EM, Barres BA. (2004). NGF controls axonal receptivity to myelination by Schwann cells or oligodendrocytes. Neuron. 43:183-91.

Chandran S, Kato H, Gerreli D, Compston A, Svendsen CN, Allen ND. (2003). FGF-dependent generation of oligodendrocytes by a hedgehog-independent pathway. Development. 130:6599-609.

Chang HS, Lin CH, Yang CH, Yen MS, Lai CR, Chen YR, Liang YJ, Yu WC. (2007). Increased expression of Dyrk1a in HPV16 immortalized keratinocytes enable evasion of apoptosis. Int J Cancer. 120:2377-85.

Chawla A, Barak Y, Nagy L, Liao D, Tontonoz P, Evans RM. (2001). PPAR-gamma dependent and independent effects on macrophage-gene expression in lipid metabolism and inflammation. Nat Med. 7:48-52.

Chen B, Schaevitz LR, McConnell SK. (2005). Fezl regulates the differentiation and axon targeting of layer 5 subcortical projection neurons in cerebral cortex. Proc Natl Acad Sci USA. 102:17184-9.

Chettouh Z, Croquette MF, Delobel B, Gilgenkrants S, Leonard C, Maunoury C, Prieur M, Rethoré MO, Sinet PM, Chery M, et al. (1995). Molecular mapping of 21 features associated with partial monosomy 21: involvement of the APP-SOD1 region. Am J Hum Genet. 57:62-71.

Chew LJ, Gallo V. (2009). The Yin and Yang of Sox proteins: Activation and repression in development and disease. J Neurosci Res. 87:277-87.

Choi BH, Kim RC. (1985). Expression of glial fibrillary acidic protein by immature oligodendroglia and its implications. J Neuroimmunol. 8:215-35.

Choi BH, Lapham LW. (1978). Radial glia in the human fetal cerebrum: a combined Golgi, immunofluorescent and electron microscopic study. *Brain Res.* 148:295–311.

Chong JA, Tapia-Ramírez J, Kim S, Toledo-Aral JJ, Zheng Y, Boutros MC, Altshuller YM, Frohman MA, Kraner SD, Mandel G. (1995). REST: a mammalian silencer protein that restricts sodium channel gene expression to neurons. Cell. 24:949-57.

Conlon RA, Reaume AG, Rossant J (1995): Notch1 is required for the coordinate segmentation of somites. Development, 121:1533-1545.

Contestabile A, Fila T, Bartesaghi R, Ciani E. (2009). Cell cycle elongation impairs proliferation of cerebellar granule cell precursors in the Ts65Dn mouse, an animal model for Down syndrome. Brain Pathol. 19:224-37.

Contestabile A, Fila T, Ceccarelli C, Bonasoni P, Bonapace L, Santini D, Bartesaghi R, Ciani E. (2007). Cell cycle alteration and decreased cell proliferation in the

hippocampal dentate gyrus and in the neocortical germinal matrix of fetuses with Down syndrome and in Ts65Dn mice. Hippocampus. 17:665-78.
Cooper DN, Ball EV, Mort M. (2010). Chromosomal distribution of disease genes in the human genome. Genet Test Mol Biomarkers. 14:441-6.
Costa MR, Bucholz O, Schroeder T, Götz M. (2009). Late origin of glia-restricted progenitors in the developing mouse cerebral cortex. Cereb Cortex. 19 Suppl 1:135-43.
Cox DR, Smith SA, Epstein LB, Epstein CJ. (1984). Mouse trisomy 16 as an animal model of human trisomy 21 (Down syndrome): production of viable trisomy 16 diploid mouse chimeras. Dev Biol. 101:416-24.
Coyle JT, Oster-Granite ML, Gearhart JD. (1986). The neurobiologic consequences of Down syndrome. Brain Res Bull. 16:773-87.
Cross SH, Meehan RR, Nan X, Bird A. (1997). A component of the transcriptional repressor MeCP1 shares a motif with DNA methyltransferase and HRX proteins. Nat Genet. 16:256-9.
Da Costa Martins PA, Salic K, Gladka MM, Armand AS, Leptidis S, el Azzouzi H, Hansen A, Coenen-de Roo CJ, Bierhuizen MF, van der Nagel R, van Kuik J, de Weger R, de Bruin A, Condorelli G, Arbones ML, Eschenhagen T, De Windt LJ. (2010). MicroRNA-199b targets the nuclear kinase Dyrk1a in an auto-amplification loop promoting calcineurin/NFAT signalling. Nat Cell Biol. 12:1220-7.
Dauphinot L, Lyle R, Rivals I, Dang MT, Moldrich RX, Golfier G, Ettwiller L, Toyama K, Rossier J, Personnaz L, Antonarakis SE, Epstein CJ, Sinet PM, Potier MC. (2005). The cerebellar transcriptome during postnatal development of the Ts1Cje mouse, a segmental trisomy model for Down syndrome. Hum Mol Genet. 14:373-84.
Davisson MT, Schmidt C, Akeson EC. (1990). Segmental trisomy of murine chromosome 16: a new model system for studying Down syndrome. Prog Clin Biol Res. 360:263-80.
Davisson MT, Schmidt C, Reeves RH, Irving NG, Akeson EC, Harris BS, Bronson RT. (1993). Segmental trisomy as a mouse model for Down syndrome. Prog Clin Biol Res. 384:117-33.
Dawson, M.R., Polito, A., Levine, J.M. & Reynolds, R. (2003). NG2-expressing glial progenitor cells: an abundant and widespread population of cycling cells in the adult rat CNS. Mol. Cell. Neurosci. 24:476–488.
Delabar JM, Theophile D, Rahmani Z, Chettouh Z, Blouin JL, Prieur M, Noel B, Sinet PM. (1993). Molecular mapping of twenty-four features of Down syndrome on chromosome 21. Eur J Hum Genet. 2:114-24.
Delaunay D, Heydon K, Cumano A, Schwab MH, Thomas JL, Suter U, Nave KA, Zalc B, Spassky N. (2008). Early neuronal and glial fate restriction of embryonic neural stem cells. J Neurosci. 28:2551-62.
Deloulme JC, Raponi E, Gentil BJ, Bertacchi N, Marks A, Labourdette G, Baudier J. (2004). Nuclear expression of S100B in oligodendrocyte progenitor cells correlates with differentiation toward the oligodendroglial lineage and modulates oligodendrocytes maturation. Mol Cell Neurosci. 27:453-65.
Deneen B, Ho R, Lukaszewicz A, Hochstim CJ, Gronostajski RM, Anderson DJ.

(2006). The transcription factor NFIA controls the onset of gliogenesis in the developing spinal cord. Neuron. 52:953-68.
Dewald LE, Rodriguez JP, Levine JM. (2011). The RE1 binding protein REST regulates oligodendrocyte differentiation. J Neurosci. 31:3470-83.
Doe CQ, Skeath JB. (1996). Neurogenesis in the insect central nervous system. Curr Opin Neurobiol. 6:18-24.
Donato R, Sorci G, Riuzzi F, Arcuri C, Bianchi R, Brozzi F, Tubaro C, Giambanco I. (2009). S100B's double life: intracellular regulator and extracellularsignal. Biochim Biophys Acta. 1793:1008-22.
Dowjat WK, Adayev T, Kuchna I, Nowicki K, Palminiello S, Hwang YW, Wegiel J. (2007). Trisomy-driven overexpression of DYRK1A kinase in the brain of subjects with Down syndrome. Neurosci Lett. 413:77-81.
Durand B, Fero ML, Roberts JM, Raff MC. (1998). p27Kip1 alters the response of cells to mitogen and is part of a cell-intrinsic timer that arrests the cell cycle and initiates differentiation. Curr Biol. 8:431-40.
Durand B, Gao FB, Raff M. (1997). Accumulation of the cyclin-dependent kinase inhibitor p27/Kip1 and the timing of oligodendrocyte differentiation. EMBO J. 16:306-17.
Emsley JG, Macklis JD. (2006). Astroglial heterogeneity closely reflects the neuronal-defined anatomy of the adult murine CNS. Neuron Glia Biol. 2:175-186.
Erez A, Chaussepied M, Castiel A, Colaizzo-Anas T, Aplan PD, Ginsberg D, Izraeli S. (2008). The mitotic checkpoint gene, SIL is regulated by E2F1. Int J Cancer. 123:1721-5.
Esposito G, Imitola J, Lu J, De Filippis D, Scuderi C, Ganesh VS, Folkerth R, Hecht J, Shin S, Iuvone T, Chesnut J, Steardo L, Sheen V. (2008). Genomic and functional profiling of human Down syndrome neural progenitors implicates S100B and aquaporin 4 in cell injury. Hum Mol Genet. 17:440-57.
Fan G, Martinowich K, Chin MH, He F, Fouse SD, Hutnick L, Hattori D, Ge W, Shen Y, Wu H, ten Hoeve J, Shuai K, Sun YE. (2005). DNA methylation controls the timing of astrogliogenesis through regulation of JAK-STAT signaling. Development. 132:3345-56.
Fancy SP, Baranzini SE, Zhao C, Yuk DI, Irvine KA, Kaing S, Sanai N, Franklin RJ, Rowitch DH. (2009). Dysregulation of the Wnt pathway inhibits timely myelination and remyelination in the mammalian CNS. Genes Dev. 23:1571-85.
Feng Y, Walsh CA. (2004). Mitotic spindle regulation by Nde1 controls cerebral cortical size. Neuron. 44:279-93.
Fernández E, Cuenca N, De Juan J. (1991). A useful programme in BASIC for axonal morphometry with introduction of new cytoskeletal parameters. J Neurosc Methods. 39:271-89.
Fernandez-Martinez J, Vela EM, Tora-Ponsioen M, Ocaña OH, Nieto MA, Galceran J. (2009). Attenuation of Notch signalling by the Down-syndrome-associated kinase DYRK1A. J Cell Sci. 122:1574-83.
Ferrer I, Barrachina M, Puig B, Martínez de Lagrán M, Martí E, Avila J, Dierssen M. (2005). Constitutive Dyrk1A is abnormally expressed in Alzheimer disease, Down syndrome, Pick disease, and related transgenic models. Neurobiol Dis.

20:392-400.
Ferron SR, Andreu-Agullo C, Mira H, Sanchez P, Marques-Torrejon MA, Farinas I. (2007). A combined ex/in vivo assay to detect effects of exogenously added factors in neural stem cells. Nat Protoc. 2:849-859.
Ferron SR, Pozo N, Laguna A, Aranda S, Porlan E, Moreno M, Fillat C, de la Luna S, Sánchez P, Arbonés ML, Fariñas I. (2010). Regulated segregation of kinase Dyrk1A during asymmetric neural stem cell division is critical for EGFR-mediated biased signaling. Cell Stem Cell. 7:367-79.
Flores AI, Narayanan SP, Morse EN, Shick HE, Yin X, Kidd G, Avila RL, Kirschner DA, Macklin WB. (2008). Constitutively active Akt induces enhanced myelination in the CNS. J Neurosci. 28:7174-83.
Fotaki V, Dierssen M, Alcántara S, Martínez S, Martí E, Casas C, Visa J, Soriano E, Estivill X, Arbonés ML. (2002). Dyrk1A haploinsufficiency affects viability and causes developmental delay and abnormal brain morphology in mice. Mol Cell Biol. 22:6636-47.
Fotaki V, Martínez De Lagrán M, Estivill X, Arbonés M, Dierssen M. (2004). Haploinsufficiency of Dyrk1A in mice leads to specific alterations in the development and regulation of motor activity. Behav Neurosci. 118:815-21.
Franklin RJ, Ffrench-Constant C. (2008). Remyelination in the CNS: from biology to therapy. Nat Rev Neurosci. 9:839-55.
Frantz GD, Weimann JM, Levin ME, McConnell SK. (1994). Otx1 and Otx2 define layers and regions in developing cerebral cortex and cerebellum. J Neurosci. 14:5725–5740l
Frederiksen K, McKay RD. (1988). Proliferation and differentiation of rat neuroepithelial precursor cells in vivo. J Neurosci. 8:1144-51.
Freese JL, Pino D, Pleasure SJ. (2010). Wnt signaling in development and disease. Neurobiol Dis. 38:148-53.
Gaiano N, Fishell G. (2002). The role of notch in promoting glial and neural stem cell fates. Annu Rev Neurosci. 25:471-90.
Gauthier AS, Furstoss O, Araki T, Chan R, Neel BG, Kaplan DR, Miller FD. (2007). Control of CNS cell-fate decisions by SHP-2 and its dysregulation in Noonan syndrome. Neuron. 54:245-62.
Ge, W., Martinowich, K., Wu, X., He, F., Miyamoto, A., Fan, G., Weinmaster, G., and Sun, Y.E. (2002). Notch signaling promotes astrogliogenesis via direct CSL-mediated glial gene activation. J. Neurosci. Res. 69:848–860.
Gearhart JD, Singer HS, Moran TH, Tiemeyer M, Oster-Granite ML, Coyle JT. (1986). Mouse chimeras composed of trisomy 16 and normal (2N) cells: preliminary studies. Brain Res Bull. 16:815-24.
Genoud S, Lappe-Siefke C, Goebbels S, Radtke F, Aguet M, Scherer SS, Suter U, Nave KA, Mantei N. (2002). Notch1 control of oligodendrocyte differentiation in the spinal cord. J Cell Biol. 158:709-18.
Ghiani C, Gallo V. (2001). Inhibition of cyclin E-cyclin-dependent kinase 2 complex formation and activity is associated with cell cycle arrest and withdrawal in oligodendrocyte progenitor cells. J Neurosci. 21:1274-82.
Givogri MI, Costa RM, Schonmann V, Silva AJ, Campagnoni AT, Bongarzone ER. (2002). Central nervous system myelination in mice with deficient expression of

Notch1 receptor. J Neurosci Res. 67:309-20.
Goebbels S, Oltrogge JH, Kemper R, Heilmann I, Bormuth I, Wolfer S, Wichert SP, Möbius W, Liu X, Lappe-Siefke C, Rossner MJ, Groszer M, Suter U, Frahm J, Boretius S, Nave KA. (2010). Elevated phosphatidylinositol 3,4,5-trisphosphate in glia triggers cell-autonomous membrane wrapping and myelination. J Neurosci. 30:8953-64.
Götz M, Hartfuss E, Malatesta P. (2002). Radial glial cells as neuronal precursors: a new perspective on the correlation of morphology and lineage restriction in the developing cerebral cortex of mice. Brain Res Bull. 57:777-88.
Graef IA, Wang F, Charron F, Chen L, Neilson J, Tessier-Lavigne M, Crabtree GR. (2003). Neurotrophins and netrins require calcineurin/NFAT signaling to stimulate outgrowth of embryonic axons. Cell. 113:657-70.
Grandbarbe L, Bouissac J, Rand M, Hrabé de Angelis M, Artavanis-Tsakonas S, Mohier E. (2003). Delta-Notch signaling controls the generation of neurons/glia from neural stem cells in a stepwise process. Development. 130:1391-402.
Griffith E, Walker S, Martin CA, Vagnarelli P, Stiff T, Vernay B, Al Sanna N, Saggar A, Hamel B, Earnshaw WC, Jeggo PA, Jackson AP, O'Driscoll M. (2008). Mutations in pericentrin cause Seckel syndrome with defective ATR-dependent DNA damage signaling. Nat Genet. 40:232-6.
Gross RE, Mehler MF, Mabie PC, Zang Z, Santschi L, Kessler JA. (1996). Bone morphogenetic proteins promote astroglial lineage commitment by mammalian subventricular zone progenitor cells. Neuron. 17:595-606.
Guernsey DL, Jiang H, Hussin J, Arnold M, Bouyakdan K, Perry S, Babineau-Sturk T, Beis J, Dumas N, Evans SC, Ferguson M, Matsuoka M, Macgillivray C, Nightingale M, Patry L, Rideout AL, Thomas A, Orr A, Hoffmann I, Michaud JL, Awadalla P, Meek DC, Ludman M, Samuels ME. (2010). Mutations in centrosomal protein CEP152 in primary microcephaly families linked to MCPH4. Am J Hum Genet. 87:40-51.
Guillemot F. (2005). Cellular and molecular control of neurogenesis in the mammalian telencephalon. Curr Opin Cell Biol. 17:639-47.
Guimera J, Casas C, Estivill X, Pritchard M. (1999). Human minibrain homologue (MNBH/DYRK1): characterization, alternative splicing, differential tissue expression, and overexpression in Down syndrome. Genomics. 57:407-18.
Guimerá J, Casas C, Pucharcòs C, Solans A, Domènech A, Planas AM, Ashley J, Lovett M, Estivill X, Pritchard MA. (1996). A human homologue of Drosophila minibrain (MNB) is expressed in the neuronal regions affected in Down syndrome and maps to the critical region. Hum Mol Genet. 5:1305-10.
Guo X, Williams JG, Schug TT, Li X. (2010). DYRK1A and DYRK3 promote cell survival through phosphorylation and activation of SIRT1. J Biol Chem. 285:13223-32.
Guy GR, Jackson RA, Yusoff P, Chow SY. (2009). Sprouty proteins: modified modulators, matchmakers or missing links? J Endocrinol. 203:191-202.
Gwack Y, Sharma S, Nardone J, Tanasa B, Iuga A, Srikanth S, Okamura H, Bolton D, Feske S, Hogan PG, Rao A. (2006). A genome-wide Drosophila RNAi screen identifies DYRK-family kinases as regulators of NFAT. Nature. 441:646-50.
Hachem S, Aguirre A, Vives V, Marks A, Gallo V, Legraverend C. (2005). Spatial

and temporal expression of S100B in cells of oligodendrocyte lineage. Glia. 51:81-97.

Hajós F, Woodhams PL, Bascó E, Csillag A, Balázs R. (1981). Proliferation of astroglia in the embryonic mouse forebrain as revealed by simultaneous immunocytochemistry and autoradiography. Acta Morphol Acad Sci Hung. 29:361-4.

Hämmerle B, Elizalde C, Galceran J, Becker W, Tejedor FJ. (2003). The MNB/DYRK1A protein kinase: neurobiological functions and Down syndrome implications. J Neural Transm Suppl. 67:129-37.

Hämmerle B, Elizalde C, Tejedor FJ. (2008). The spatio-temporal and subcellular expression of the candidate Down syndrome gene Mnb/Dyrk1A in the developing mouse brain suggests distinct sequential roles in neuronal development. Eur J Neurosci. 27:1061-74.

Hämmerle B, Ulin E, Guimera J, Becker W, Guillemot F, Tejedor FJ. (2011). Transient expression of Mnb/Dyrk1a couples cell cycle exit and differentiation of neuronal precursors by inducing p27KIP1 expression and suppressing NOTCH signaling. Development. 138:2543-54.

Hämmerle B., Vera-Samper E., Speicher S., Arencibia R., Martinez S., and Tejedor F.J. (2002). Mnb/Dyrk1A is transiently expressed and asymmetrically segregated in neural progenitor cells at the transition to neurogenic divisions. Dev Biol 246:259-273.

Hartfuss E, Galli R, Heins N, Götz M. (2001). Characterization of CNS precursor subtypes and radial glia. Dev Biol. 229:15-30.

Haubensak W, Attardo A, Denk W, Huttner WB. (2004). Neurons arise in the basal neuroepithelium of the early mammalian telencephalon: a major site of neurogenesis. *Proc. Natl. Acad. Sci. USA* 101:3196–201

He Y, Dupree J, Wang J, Sandoval J, Li J, Liu H, Shi Y, Nave KA, Casaccia-Bonnefil P. (2007). The transcription factor Yin Yang 1 is essential for oligodendrocyte progenitor differentiation. Neuron. 55:217-30.

Himpel S, Panzer P, Eirmbter K, Czajkowska H, Sayed M, Packman LC, Blundell T, Kentrup H, Grötzinger J, Joost HG, Becker W. (2001). Identification of the autophosphorylation sites and characterization of their effects in the protein kinase DYRK1A. Biochem J. 359:497-505.

Himpel S, Tegge W, Frank R, Leder S, Joost HG, Becker W. (2000). Specificity determinants of substrate recognition by the protein kinase DYRK1A. J Biol Chem. 275:2431-8.

Hirabayashi Y, Gotoh Y. (2010). Epigenetic control of neural precursor cell fate during development. Nat Rev Neurosci. 11:377-88.

Hirabayashi Y, Gotoh Y. (2005). Stage-dependent fate determination of neural precursor cells in mouse forebrain. Neurosci Res. 51:331-6.

Hirabayashi Y, Itoh Y, Tabata H, Nakajima K, Akiyama T, Masuyama N, Gotoh Y. (2004). The Wnt/beta-catenin pathway directs neuronal differentiation of cortical neural precursor cells. Development. 131:2791-801.

Hirabayashi Y, Suzki N, Tsuboi M, Endo TA, Toyoda T, Shinga J, Koseki H, Vidal M, Gotoh Y. (2009). Polycomb limits the neurogenic competence of neural precursor cells to promote astrogenic fate transition. Neuron. 63:600-13.

Hirano M, Goldman JE. (1988). Gliogenesis in rat spinal cord: evidence for origin of astrocytes and oligodendrocytes from radial precursors. J Neurosci Res. 21:155-67.

Hirata H, Yoshiura S, Ohtsuka T, Bessho Y, Harada T, Yoshikawa K, Kageyama R. (2002). Oscillatory expression of the bHLH factor Hes1 regulated by a negative feedback loop. Science. 298:840-3.

Hochstim C, Deneen B, Lukaszewicz A, Zhou Q, Anderson DJ. (2008). Identification of positionally distinct astrocyte subtypes whose identities are specified by a homeodomain code. Cell. 133:510-22.

Hogan, B., Costantini, F., and Lacy, E. (1986). Manipulating the Mouse Embryo (Cold Spring Harbor).

Hogan PG, Chen L, Nardone J, Rao A. (2003). Transcriptional regulation by calcium, calcineurin, and NFAT. Genes Dev. 2003 17:2205-32.

Honjo T. (1996). The shortest path from the surface to the nucleus: RBP-J kappa/Su(H) transcription factor. Genes Cells. 1:1-9.

Hsieh J, Nakashima K, Kuwabara T, Mejia E, Gage FH. (2004). Histone deacetylase inhibition-mediated neuronal differentiation of multipotent adult neural progenitor cells. Proc Natl Acad Sci U S A. 101:16659-64.

Hu QD, Ang BT, Karsak M, Hu WP, Cui XY, Duka T, Takeda Y, Chia W, Sankar N, Ng YK, Ling EA, Maciag T, Small D, Trifonova R, Kopan R, Okano H, Nakafuku M, Chiba S, Hirai H, Aster JC, Schachner M, Pallen CJ, Watanabe K, Xiao ZC. (2003). F3/contactin acts as a functional ligand for Notch during oligodendrocyte maturation. Cell. 115:163-75.

Hu X, He W, Diaconu C, Tang X, Kidd GJ, Macklin WB, Trapp BD, Yan R. (2008). Genetic deletion of BACE1 in mice affects remyelination of sciatic nerves. FASEB J. 22:2970-80.

Hu X, Hicks CW, He W, Wong P, Macklin WB, Trapp BD, Yan R. (2006). Bace1 modulates myelination in the central and peripheral nervous system. Nat Neurosci. 9:1520-5.

Huang JK, Jarjour AA, Nait Oumesmar B, Kerninon C, Williams A, Krezel W, Kagechika H, Bauer J, Zhao C, Evercooren AB, Chambon P, Ffrench-Constant C,Franklin RJ. (2011). Retinoid X receptor gamma signaling accelerates CNS remyelination. Nat Neurosci. 14:45-53.

Ichikawa M, Shiga T, Hirata Y. (1983), Spatial and temporal pattern of postnatal proliferation of glial cells in the parietal cortex of the rat. *Brain Res.* 285:181–87

Impey S, McCorkle SR, Cha-Molstad H, Dwyer JM, Yochum GS, Boss JM, McWeeney S, Dunn JJ, Mandel G, Goodman RH. (2004). Defining the CREB regulon: a genome-wide analysis of transcription factor regulatory regions. Cell. 119:1041-54.

Ingram WJ, McCue KI, Tran TH, Hallahan AR, Wainwright BJ. (2008). Sonic Hedgehog regulates Hes1 through a novel mechanism that is independent of canonical Notch pathway signalling. Oncogene. 27:1489-500.

Insausti AM, Megías M, Crespo D, Cruz-Orive LM, Dierssen M, Vallina IF, Insausti R, Flórez J. (1998). Hippocampal volume and neuronal number in Ts65Dn mice: a murine model of Down syndrome. Neurosci Lett. 253:175-8.

Irizarry, R.A., Hobbs B., Collin F., Beazer-Barclay Y.D., Antonellis K.J., Scherf U.,

and Speed T.P. (2003). Exploration, normalization, and summaries of high density oligonucleotide array probe level data. Biostatistics, 4:249–264.

Iwata T, Hevner RF. (2009). Fibroblast growth factor signaling in development of the cerebral cortex. Dev Growth Differ. 51:299-323.

Jackson AP, Eastwood H, Bell SM, Adu J, Toomes C, Carr IM, Roberts E, Hampshire DJ, Crow YJ, Mighell AJ, Karbani G, Jafri H, Rashid Y, Mueller RF, Markham AF, Woods CG. (2002). Identification of microcephalin, a protein implicated in determining the size of the human brain. Am J Hum Genet. 71:136-42.

Jessell TM. (2000). Neuronal specification in the spinal cord: inductive signals and transcriptional codes. Nat Rev Genet. 1:20-9.

Johnson R, Samuel J, Ng CK, Jauch R, Stanton LW, Wood IC. (2009). Evolution of the vertebrate gene regulatory network controlled by the transcriptional repressor REST. Mol Biol Evol. 2009 26:1491-507.

Josselyn SA. (2005). What's right with my mouse model? New insights into the molecular and cellular basis of cognition from mouse models of Rubinstein-Taybi Syndrome. Learn Mem. 12:80-3.

Kageyama R, Ohtsuka T, Kobayashi T. (2007). The Hes gene family: repressors and oscillators that orchestrate embryogenesis. Development. 134:1243-51.

Kamakura, S., Oishi, K., Yoshimatsu, T., Nakafuku, M., Masuyama, N., and Gotoh, Y. (2004). Hes binding to STAT3 mediates crosstalk between Notch and JAK-STAT signalling. Nat. Cell Biol. 6:547–554.

Kao SC, Wu H, Xie J, Chang CP, Ranish JA, Graef IA, Crabtree GR. (2009). Calcineurin/NFAT signaling is required for neuregulin-regulated Schwann cell differentiation. Science. 323:651-4.

Kato H, Taniguchi Y, Kurooka H, Minoguchi S, Sakai T, Nomura-Okazaki S, Tamura K, Honjo T. (1997). Involvement of RBP-J in biological functions of mouse Notch1 and its derivatives. Development. 124:4133-41.

Kawaguchi D, Yoshimatsu T, Hozumi K, Gotoh Y. (2008). Selection of differentiating cells by different levels of delta-like 1 among neural precursor cells in the developing mouse telencephalon. Development. 135:3849-58.

Kelly PA, Rahmani Z. (2005). DYRK1A enhances the mitogen-activated protein kinasecascade in PC12 cells by forming a complex with Ras, B-Raf, and MEK1. Mol BiolCell. 16:3562-73.

Kentrup H, Becker W, Heukelbach J, Wilmes A, Schürmann A, Huppertz C, Kainulainen H, Joost HG. (1996). Dyrk, a dual specificity protein kinase with unique structural features whose activity is dependent on tyrosine residues between subdomains VII and VIII. J Biol Chem. 271:3488-95.

Kessaris N, Fogarty M, Iannarelli P, Grist M, Wegner M, Richardson WD. (2006). Competing waves of oligodendrocytes in the forebrain and postnatal elimination of an embryonic lineage. Nat Neurosci. 9:173-9.

Kessaris N, Jamen F, Rubin LL, Richardson WD. (2004). Cooperation between sonic hedgehog and fibroblast growth factor/MAPK signalling pathways in neocortical precursors. Development. 131:1289-98.

Kim H, Kim S, Chung AY, Bae YK, Hibi M, Lim CS, Park HC. (2008). Notch-regulated perineurium development from zebrafish spinal cord. Neurosci Lett.

448:240-4.
Kim MY, Jeong BC, Lee JH, Kee HJ, Kook H, Kim NS, Kim YH, Kim JK, Ahn KY, Kim KK. (2006). A repressor complex, AP4 transcription factor and geminin, negatively regulates expression of target genes in nonneuronal cells. Proc Natl Acad Sci U S A. 103:13074-9.
Kimelberg HK. (2004). The problem of astrocyte identity. Neurochem Int. 45:191-202.
Kimura R, Kamino K, Yamamoto M, Nuripa A, Kida T, Kazui H, Hashimoto R, Tanaka T, Kudo T, Yamagata H, Tabara Y, Miki T, Akatsu H, Kosaka K, Funakoshi E, Nishitomi K, Sakaguchi G, Kato A, Hattori H, Uema T, Takeda M. (2007). The DYRK1A gene, encoded in chromosome 21 Down syndrome critical region, bridges between beta-amyloid production and tau phosphorylation in Alzheimer disease. Hum Mol Genet. 16:15-23.
Kohyama J, Kojima T, Takatsuka E, Yamashita T, Namiki J, Hsieh J, Gage FH, Namihira M, Okano H, Sawamoto K, Nakashima K. (2008). Epigenetic regulation of neural cell differentiation plasticity in the adult mammalian brain. Proc Natl Acad Sci U S A. 105:18012-7.
Kong H, Fan Y, Xie J, Ding J, Sha L, Shi X, Sun X, Hu G. (2008). AQP4 knockout impairs proliferation, migration and neuronal differentiation of adult neural stem cells. J Cell Sci. 121:4029-36.
Konno D, Shioi G, Shitamukai A, Mori A, Kiyonari H, Miyata T, Matsuzaki F. (2008). Neuroepithelial progenitors undergo LGN-dependent planar divisions to maintain self-renewability during mammalian neurogenesis. *Nat.Cell Biol.* 10:93–101
Kopan R, Ilagan MX. (2009). The canonical Notch signaling pathway: unfolding the activation mechanism. Cell. 137:216-33.
Kousar R, Hassan MJ, Khan B, Basit S, Mahmood S, Mir A, Ahmad W, Ansar M. (2011). Mutations in WDR62 gene in Pakistani families with autosomal recessive primary microcephaly. BMC Neurol. 11:119.
Kraner SD, Chong JA, Tsay HJ, Mandel G. (1992). Silencing the type II sodium channel gene: a model for neural-specific gene regulation. Neuron. 9:37-44.
Krey G, Braissant O, L'Horset F, Kalkhoven E, Perroud M, Parker MG, Wahli W. (1997). Fatty acids, eicosanoids, and hypolipidemic agents identified as ligands of peroxisome proliferator-activated receptors by coactivator-dependent receptor ligand assay. Mol Endocrinol. 11:779-91.
Kriegstein A, Alvarez-Buylla A. (2009). The glial nature of embryonic and adult neural stem cells. Annu Rev Neurosci.32:149-84.
Kriegstein A, Noctor S, Martínez-Cerdeño V. (2006). Patterns of neural stem and progenitor cell division may underlie evolutionary cortical expansion. Nat Rev Neurosci. 11:883-90.
Kuhn C, Frank D, Will R, Jaschinski C, Frauen R, Katus HA, Frey N. (2009). DYRK1A is a novel negative regulator of cardiomyocyte hypertrophy. J Biol Chem. 284:17320-7.
Kumar RA. (2009). STIL on my small brain: a new gene for microcephaly. Clin Genet. 76:501-2.
Kurt MA, Davies DC, Kidd M, Dierssen M, Flórez J. (2000). Synaptic deficit in the temporal cortex of partial trisomy 16 (Ts65Dn) mice. Brain Res. 8585:191-7.

Kurt MA, Kafa MI, Dierssen M, Davies DC. (2004). Deficits of neuronal density in CA1 and synaptic density in the dentate gyrus, CA3 and CA1, in a mouse model of Down syndrome. Brain Res.1022:101-9.

Kuwahara A, Hirabayashi Y, Knoepfler PS, Taketo MM, Sakai J, Kodama T, Gotoh Y. (2010). Wnt signaling and its downstream target N-myc regulate basal progenitors in the developing neocortex. Development. 137:1035-44.

La Marca R, Cerri F, Horiuchi K, Bachi A, Feltri ML, Wrabetz L, Blobel CP, Quattrini A, Salzer JL, Taveggia C. (2011). TACE (ADAM17) inhibits Schwann cell myelination. Nat Neurosci. 14:857-65.

Laguna A, Aranda S, Barallobre MJ, Barhoum R, Fernández E, Fotaki V, Delabar JM, de la Luna S, de la Villa P, Arbonés ML. (2008). The protein kinase DYRK1A regulates caspase-9-mediated apoptosis during retina development. Dev Cell.15:841-53.

Larocque D, Pilotte J, Chen T, Cloutier F, Massie B, Pedraza L, Couture R, Lasko P, Almazan G, Richard S. (2002). Nuclear retention of MBP mRNAs in the quaking viable mice. Neuron. 36:815-29.

Leingartner A, Richards LJ, Dyck RH, Akazawa C, O'Leary DD. (2003). Cloning and cortical expression of rat Emx2 and adenovirus-mediated overexpression to assess its regulation of area-specific targeting of thalamocortical axons. Cereb Cortex. 13:648-60

Lejeune J, Gauthier M, Turpin R. (1959). Etude des chromosomes somatiques de neuf enfants mongoliens. C R Acad Sci Paris 248:1721 –1722.

Lejeune J, Turpin R, Gautier M. (1958/1959). Le mongolisme. Premier exemple d'aberration autosomique humaine. Annales Génétique Par is 1:41 – 49

Lemmon MA, Schlessinger J. (2010). Cell signaling by receptor tyrosine kinases. Cell. 141:1117-34.

Leone DP, Srinivasan K, Chen B, Alcamo E, McConnell SK. (2008). The determination of projection neuron identity in the developing cerebral cortex. Curr Opin Neurobiol. 18:28-35.

Lepagnol-Bestel AM, Zvara A, Maussion G, Quignon F, Ngimbous B, Ramoz N, Imbeaud S, Loe-Mie Y, Benihoud K, Agier N, Salin PA, Cardona A, Khung-Savatovsky S, Kallunki P, Delabar JM, Puskas LG, Delacroix H, Aggerbeck L, Delezoide AL, Delattre O, Gorwood P, Moalic JM, Simonneau M. (2009). DYRK1A interacts with the REST/NRSF-SWI/SNF chromatin remodelling complex to deregulate gene clusters involved in the neuronal phenotypic traits of Down syndrome. Hum Mol Genet. 18:1405-14.

Levison SW, Goldman JE. (1993). Both oligodendrocytes and astrocytes develop from progenitors in the subventricular zone of postnatal rat forebrain. Neuron 10:201–12.

Levitt, P.; Cooper, M. L.; Rakic, P. (1981). Coexistence of neuronal and glial precursor cells in the cerebral ventricular zone of the fetal monkey: An ultrastructural immunoperoxidase analysis. J. Neurosci. 1:27–39.

Lewis JD, Meehan RR, Henzel WJ, Maurer-Fogy I, Jeppesen P, Klein F, Bird A. (1992). Purification, sequence, and cellular localization of a novel chromosomal protein that binds to methylated DNA. Cell. 69:905-14.

Li H, Lu Y, Smith HK, Richardson WD. (2007). Olig1 and Sox10 interact

synergistically to drive myelin basic protein transcription in oligodendrocytes. J Neurosci. 27:14375-82.

Li HS, Wang D, Shen Q, Schonemann MD, Gorski JA, Jones KR, Temple S, Jan LY, Jan YN. (2003). Inactivation of Numb and Numblike in embryonic dorsal forebrain impairs neurogenesis and disrupts cortical morphogenesis. Neuron. 40:1105-18.

Li W, Cogswell CA, LoTurco JJ. (1998). Neuronal differentiation of precursors in the neocortical ventricular zone is triggered by BMP. J Neurosci. 18:8853-62

Li, D., Jackson, R.A., Yusoff, P., and Guy, G.R. (2010). The direct association of Sprouty-related protein with an EVH1 domain (SPRED) 1 or SPRED2 with DYRK1A modifies substrate/kinase interactions. J Biol Chem. 85:35374-85.

Ligon KL, Fancy SP, Franklin RJ, Rowitch DH. (2006). Olig gene function in CNS development and disease. Glia. 54:1-10.

Lin SY, Rai R, Li K, Xu ZX, Elledge SJ. (2005). BRIT1/MCPH1 is a DNA damage responsive protein that regulates the Brca1-Chk1 pathway, implicating checkpoint dysfunction in microcephaly. Proc Natl Acad Sci U S A. 102:15105-9.

Liu A, Li J, Marin-Husstege M, Kageyama R, Fan Y, Gelinas C, Casaccia-Bonnefil P. (2006). A molecular insight of Hes5-dependent inhibition of myelin gene expression: old partners and new players. EMBO J. 25:4833-42.

Liu H, Hu Q, D'ercole AJ, Ye P. (2009a). Histone deacetylase 11 regulates oligodendrocyte-specific gene expression and cell development in OL-1 oligodendroglia cells. Glia. 57:1-12.

Liu T, Sims D, Baum B. (2009b). Parallel RNAi screens across different cell lines identify generic and cell type-specific regulators of actin organization and cell morphology. Genome Biol. 10:R26.

Lochhead PA, Sibbet G, Morrice N, Cleghon V. (2005). Activation-loop autophosphorylation is mediated by a novel transitional intermediate form of DYRKs. Cell. 2005 121:925-36.

Lockstone HE, Harris LW, Swatton JE, Wayland MT, Holland AJ, Bahn S. (2007). Gene expression profiling in the adult Down syndrome brain. Genomics. 90:647-60.

Lorenzi HA, Reeves RH. (2006). Hippocampal hypocellularity in the Ts65Dn mouse originates early in development. Brain Res. 1104:153-9.

Louvi A, Artavanis-Tsakonas S. (2006). Notch signalling in vertebrate neural development. Nat Rev Neurosci. 7:93-102.

Lu M, Zheng L, Han B, Wang L, Wang P, Liu H, Sun X. (2011). REST regulates DYRK1A transcription in a negative feedback loop. J Biol Chem. 286:10755-63.

Lu QR, Sun T, Zhu Z, Ma N, Garcia M, Stiles CD, Rowitch DH (2002). Common developmental requirement for Olig function indicates a motor neuron/oligodendrocyte connection. *Cell,* 109:75-86.

Lu QR, Yuk D, Alberta JA, Zhu Z, Pawlitzky I, Chan J, McMahon AP, Stiles CD, Rowitch DH. (2000). Sonic hedgehog regulated oligodendrocyte lineage genes encoding bHLH proteins in the mammalian central nervous system. Neuron. 25:317-29.

Luetteke NC, Phillips HK, Qiu TH, Copeland NG, Earp HS, Jenkins NA, Lee DC. (1994). The mouse waved-2 phenotype results from a point mutation in the EGF

receptor tyrosine kinase. Genes Dev. 8:399-413.
Lukaszewicz A, Savatier P, Cortay V, Kennedy H, Dehay C. (2002). Contrasting effects of basic fibroblast growth factor and neurotrophin 3 on cell cycle kinetics of mouse cortical stem cells. J Neurosci. 22:6610-6622.
Lunyak VV, Burgess R, Prefontaine GG, Nelson C, Sze SH, Chenoweth J, Schwartz P, Pevzner PA, Glass C, Mandel G, Rosenfeld MG. (2002). Corepressor-dependent silencing of chromosomal regions encoding neuronal genes. Science. 298:1747-52.
Lyssiotis CA, Walker J, Wu C, Kondo T, Schultz PG, Wu X. (2007). Inhibition of histone deacetylase activity induces developmental plasticity in oligodendrocyte precursor cells. Proc Natl Acad Sci U S A. 104:14982-7.
Mabie PC, Mehler MF, Kessler JA. (1999). Multiple roles of bone morphogenetic protein signaling in the regulation of cortical cell number and phenotype. J Neurosci. 19:7077-88.
Maenz B, Hekerman P, Vela EM, Galceran J, Becker W. (2008). Characterization of the human DYRK1A promoter and its regulation by the transcription factor E2F1. BMC Mol Biol. 9:30.
Magini J. (1888). Nouvelles recherches histologiques sur le cerveau du foetus. *Arch. Ital. Biol.* 10:384–87
Malatesta P, Hartfuss E, Götz M. (2000). Isolation of radial glial cells by fluorescent-activated cell sorting reveals a neuronal lineage. Development. 127:253-63.
Mao J, Maye P, Kogerman P, Tejedor FJ, Toftgard R, Xie W, Wu G, Wu D. (2002). Regulation of Gli1 transcriptional activity in the nucleus by Dyrk1. J Biol Chem. 277:35156-61.
Mao L, Zabel C, Herrmann M, Nolden T, Mertes F, Magnol L, Chabert C, Hartl D, Herault Y, Delabar JM, Manke T, Himmelbauer H, Klose J. (2007). Proteomic shifts in embryonic stem cells with gene dose modifications suggest the presence of balancer proteins in protein regulatory networks. PLoS One. 2:e1218.
Mares V, Bruckner G. (1978). Postnatal formation of non-neuronal cells in the rat occipital cerebrum: an autoradiographic study of the time and space pattern of cell division. *J. Comp. Neurol.* 177:519–28
Marín O, Rubenstein JL. (2001). A long, remarkable journey: tangential migration in the telencephalon. Nat Rev Neurosci. 2:780-90.
Marín O, Rubenstein JL. (2003). Cell migration in the forebrain. Annu Rev Neurosci. 26:441-83
Marin-Husstege M, Muggironi M, Liu A, Casaccia-Bonnefil P. (2002). Histone deacetylase activity is necessary for oligodendrocyte lineage progression. J Neurosci. 22:10333-45.
Marin-Padilla M. (1971). Early prenatal ontogenesis of the cerebral cortex (neocortex) of the cat (Felis domestica). A Golgi study. I. The primordial neocortical organization. Z Anat Entwicklungsgesch. 134:117-45.
Martí E, Altafaj X, Dierssen M, de la Luna S, Fotaki V, Alvarez M, Pérez-Riba M, Ferrer I, Estivill X. (2003). Dyrk1A expression pattern supports specific roles of this kinase in the adult central nervous system. Brain Res. 964:250-63.
Martin D, Tawadros T, Meylan L, Abderrahmani A, Condorelli DF, Waeber G,

Haefliger JA. (2003). Critical role of the transcriptional repressor neuron-restrictive silencer factor in the specific control of connexin36 in insulin-producing cell lines. J Biol Chem. 278:53082-9.

Martinez de Lagran M, Bortolozzi A, Millan O, Gispert JD, Gonzalez JR, Arbones ML, Artigas F, Dierssen M. (2007). Dopaminergic deficiency in mice with reduced levels of the dual-specificity tyrosine-phosphorylated and regulated kinase 1A, Dyrk1A(+/-). Genes Brain Behav. 6:569-78.

Mason JM, Morrison DJ, Basson MA, Licht JD. (2006). Sprouty proteins: multifaceted negative-feedback regulators of receptor tyrosine kinase signaling. Trends Cell Biol. 16:45-54.

Matsumoto N, Ohashi H, Tsukahara M, Kim KC, Soeda E, Niikawa N. (1997). Possible narrowed assignment of the loci of monosomy 21-associated microcephaly and intrauterine growth retardation to a 1.2-Mb segment at 21q22.2. Am J Hum Genet. 60:997-9.

Matsuo R, Ochiai W, Nakashima K, Taga T. (2001). A new expression cloning strategy for isolation of substrate-specific kinases by using phosphorylation site-specific antibody. J Immunol Methods. 247:141-51.

Matyash V, Kettenmann H. (2010). Heterogeneity in astrocyte morphology and physiology. Brain Res Rev. 63:2-10.

Matys V, Kel-Margoulis OV, Fricke E, Liebich I, Land S, Barre-Dirrie A, Reuter I, Chekmenev D, Krull M, Hornischer K, Voss N, Stegmaier P, Lewicki-Potapov B,

Maue RA, Kraner SD, Goodman RH, Mandel G. (1990). Neuron-specific expression of the rat brain type II sodium channel gene is directed by upstream regulatory elements. Neuron. 4:223-31.

Meissner A, Mikkelsen TS, Gu H, Wernig M, Hanna J, Sivachenko A, Zhang X, Bernstein BE, Nusbaum C, Jaffe DB, Gnirke A, Jaenisch R, Lander ES. (2008). Genome-scale DNA methylation maps of pluripotent and differentiated cells. Nature. 454:766-70.

Mekki-Dauriac S, Agius E, Kan P, Cochard P. (2002). Bone morphogenetic proteins negatively control oligodendrocyte precursor specification in the chick spinal cord. Development. 129:5117-30.

Menn B, García-Verdugo JM, Yaschine C, Gonzalez-Perez O, Rowitch D, Alvarez-Buylla A. (2006). Origin of oligodendrocytes in the subventricular zone of the adult brain. J. Neurosci. 26:7907–18

Michailov GV, Sereda MW, Brinkmann BG, Fischer TM, Haug B, Birchmeier C, Role L, Lai C, Schwab MH, Nave KA. (2004). Axonal neuregulin-1 regulates myelin sheath thickness. Science. 304:700-3.

Mieda M, Haga T, Saffen DW. (1997). Expression of the rat m4 muscarinic acetylcholine receptor gene is regulated by the neuron-restrictive silencer element/repressor element 1. J Biol Chem. 272:5854-60.

Misson JP, Takahashi T, Caviness VS Jr. (1991). Ontogeny of radial and other astroglial cells in murine cerebral cortex. *Glia* 4:138–48

Miyata T, Kawaguchi A, Okano H, Ogawa M. (2001). Asymmetric inheritance of radial glial fibers by cortical neurons. Neuron. 31:727-41.

Miyata T, Kawaguchi A, Saito K, Kawano M, Muto T, Ogawa M. (2004). Asymmetric production of surface dividing and non-surface-dividing cortical progenitor cells.

Development 131:3133–45
Mohn F, Weber M, Rebhan M, Roloff TC, Richter J, Stadler MB, Bibel M, Schübeler D. (2008). Lineage-specific polycomb targets and de novo DNA methylation define restriction and potential of neuronal progenitors. Mol Cell. 30:755-66.
Moldrich RX, Dauphinot L, Laffaire J, Vitalis T, Hérault Y, Beart PM, Rossier J, Vivien D, Gehrig C, Antonarakis SE, Lyle R, Potier MC. (2009). Proliferation deficits and gene expression dysregulation in Down's syndrome (Ts1Cje) neural progenitor cells cultured from neurospheres. J Neurosci Res. 87:3143-52.
Molkentin JD. (2004). Calcineurin-NFAT signaling regulates the cardiac hypertrophic response in coordination with the MAPKs. Cardiovasc Res. 63:467-75.
Møller RS, Kübart S, Hoeltzenbein M, Heye B, Vogel I, Hansen CP, Menzel C, Ullmann R, Tommerup N, Ropers HH, Tümer Z, Kalscheuer VM. (2008). Truncation of the Down syndrome candidate gene DYRK1A in two unrelated patients with microcephaly. Am J Hum Genet. 82:1165-70.
Morest DK. (1970). A study of neurogenesis in the forebrain of opossum pouch young. *Z. Anat. Entwickl.*130:265–305
Mori N, Schoenherr C, Vandenbergh DJ, Anderson DJ. (1992). A common silencer element in the SCG10 and type II Na+ channel genes binds a factor present in nonneuronal cells but not in neuronal cells. Neuron. 9:45-54.
Morin X, Jaouen F, Durbec P. (2007). Control of planar divisions by the G-protein regulator LGN maintains progenitors in the chick neuroepithelium. *Nat. Neurosci.* 10:1440–48
Morrow T, Song MR, Ghosh A. (2001). Sequential specification of neurons and glia by developmentally regulated extracellular factors. Development. 128:3585-94.
Murakami N, Bolton D, Hwang YW. (2009). Dyrk1A binds to multiple endocytic proteins required for formation of clathrin-coated vesicles. Biochemistry. 48:9297-305.
Nait-Oumesmar B, Decker L, Lachapelle F, Avellana-Adalid V, Bachelin C, Van Evercooren AB. (1999). Progenitor cells of the adult mouse subventricular zone proliferate, migrate and differentiate into oligodendrocytes after demyelination. Eur J Neurosci. 11:4357-66.
Nakashima K, Taga T. (2002). Mechanisms underlying cytokine-mediated cell-fate regulation in the nervous system. Mol Neurobiol. 25:233-44.
Nakashima K, Yanagisawa M, Arakawa H, Taga T. (1999). Astrocyte differentiation mediated by LIF in cooperation with BMP2. FEBS Lett. 457:43-6.
Namihira M, Kohyama J, Semi K, Sanosaka T, Deneen B, Taga T, Nakashima K. (2009). Committed neuronal precursors confer astrocytic potential on residual neural precursor cells. Dev Cell. 16:245-55.
Namihira M, Nakashima K, Taga T. (2004). Developmental stage dependent regulation of DNA methylation and chromatin modification in a immature astrocyte specific gene promoter. FEBS Lett. 572:184-8.
Nan X, Campoy FJ, Bird A. (1997). MeCP2 is a transcriptional repressor with abundant binding sites in genomic chromatin. Cell. 88:471-81.
Nave KA, Salzer JL. (2006). Axonal regulation of myelination by neuregulin 1. Curr Opin Neurobiol. 16:492-500.

Nave KA, Trapp BD. (2008). Axon-glial signaling and the glial support of axon function. Annu Rev Neurosci. 31:535-61.

Nery S, Wichterle H, Fishell G. (2001). Sonic hedgehog contributes to oligodendrocyte specification in the mammalian forebrain. Development. 128:527-40.

Nguyen L, Besson A, Heng JI, Schuurmans C, Teboul L, Parras C, Philpott A,Roberts JM, Guillemot F. (2006). p27kip1 independently promotes neuronal differentiation and migration in the cerebral cortex. Genes Dev. 20:1511-24.

Nieto M, Monuki ES, Tang H, Imitola J, Haubst N, Khoury SJ, Cunningham J, Gotz M, Walsh CA. (2004). Expression of Cux-1 and Cux-2 in the subventricular zone and upper layers II-IV of the cerebral cortex. J Comp Neurol. 479:168–180.

Nieto M, Schuurmans C, Britz O, Guillemot F. (2001). Neural bHLH genes control the neuronal versus glial fate decision in cortical progenitors. Neuron. 29:401-13.

Nishiyama H, Knopfel T, Endo S, Itohara S. (2002). Glial protein S100B modulates long-term neuronal synaptic plasticity. Proc Natl Acad Sci U S A. 99:4037-42.

Noctor SC, Flint AC, Weissman TA, Dammerman RS, Kriegstein AR. (2001). Neurons derived from radial glial cells establish radial units in neocortex. Nature. 409:714-20.

Noctor SC, Martínez-Cerdeño V, Ivic L, Kriegstein AR. (2004). Cortical neurons arise in symmetric and asymmetric division zones and migrate through specific phases. Nat Neurosci. 7:136-44.

Noctor SC, Martínez-Cerdeño V, Kriegstein AR. (2007). Contribution of intermediate progenitor cells to cortical histogenesis. Arch Neurol. 64:639-42.

Noctor SC, Martínez-Cerdeño V, Kriegstein AR. (2008). Distinct behaviors of neural stem and progenitor cells underlie cortical neurogenesis. J Comp Neurol. 508:28-44.

O'Doherty A, Ruf S, Mulligan C, Hildreth V, Errington ML, Cooke S, Sesay A, Modino S, Vanes L, Hernandez D, Linehan JM, Sharpe PT, Brandner S, Bliss TV, Henderson DJ, Nizetic D, Tybulewicz VL, Fisher EM. (2005). An aneuploid mouse strain carrying human chromosome 21 with Down syndrome phenotypes. Science. 309:2033-7.

Ohno M, Hiraoka Y, Matsuoka T, Tomimoto H, Takao K, Miyakawa T, Oshima N, Kiyonari H, Kimura T, Kita T, Nishi E. (2009). Nardilysin regulates axonal maturation and myelination in the central and peripheral nervous system. Nat Neurosci. 12:1506-13.

Ohnuma S, Philpott A, Wang K, Holt CE, Harris WA. (1999). p27Xic1, a Cdk inhibitor, promotes the determination of glial cells in Xenopus retina. Cell. 99:499-510.

Okui M, Ide T, Morita K, Funakoshi E, Ito F, Ogita K, Yoneda Y, Kudoh J, Shimizu N. (1999). High-level expression of the Mnb/Dyrk1A gene in brain and heart during rat early development. Genomics. 62:165-71.

Olson LE, Roper RJ, Baxter LL, Carlson EJ, Epstein CJ, Reeves RH. (2004). Down syndrome mouse models Ts65Dn, Ts1Cje, and Ms1Cje/Ts65Dn exhibit variable severity of cerebellar phenotypes. 230:581-9.

Otto SJ, McCorkle SR, Hover J, Conaco C, Han JJ, Impey S, Yochum GS, Dunn JJ, Goodman RH, Mandel G. (2007). A new binding motif for the transcriptional

repressor REST uncovers large gene networks devoted to neuronal functions. J Neurosci. 27:6729-39.
Park HC, Appel B. (2003). Delta-Notch signaling regulates oligodendrocyte specification. Development. 130:3747-55.
Park J, Oh Y, Chung KC. (2009). Two key genes closely implicated with the neuropathological characteristics in Down syndrome: DYRK1A and RCAN1. BMB Rep. 42:6-15.
Park J, Oh Y, Yoo L, Jung MS, Song WJ, Lee SH, Seo H, Chung KC. (2010). Dyrk1A phosphorylates p53 and inhibits proliferation of embryonic neuronal cells. J Biol Chem. 285:31895-906.
Parras CM, Hunt C, Sugimori M, Nakafuku M, Rowitch D, Guillemot F. (2007). The proneural gene Mash1 specifies an early population of telencephalic oligodendrocytes. J Neurosci. 27:4233-42.
Patterson D. (2009). Molecular genetic analysis of Down syndrome. Hum Genet. 126:195-214.
Petersen PH, Tang H, Zou K, Zhong W. (2006). The enigma of the numb-Notch relationship during mammalian embryogenesis. Dev Neurosci. 28:156-68.
Petersen PH, Zou K, Hwang JK, Jan YN, Zhong W. (2002). Progenitor cell maintenance requires numb and numblike during mouse neurogenesis. Nature. 419:929-34.
Petersen PH, Zou K, Krauss S, Zhong W. (2004). Continuing role for mouse Numb and Numbl in maintaining progenitor cells during cortical neurogenesis. Nat Neurosci. 7:803-11.
Pfaff KL, Straub CT, Chiang K, Bear DM, Zhou Y, Zon LI. (2007). The zebra fish cassiopeia mutant reveals that SIL is required for mitotic spindle organization. Mol Cell Biol. 27:5887-97.
Pfaffl MW. (2001). A new mathematical model for relative quantification in real-time RT-PCR. Nucleic Acids Res. 29:e45.
Pierani A, Wassef M (2009). Cerebral cortex development: from progenitors patterning to neocortical size during evolution. Dev Growth Differ. 51:325-342.
Pierfelice T, Alberi L, Gaiano N. (2011). Notch in the vertebrate nervous system: an old dog with new tricks. Neuron. 69:840-55.
Piper M, Barry G, Hawkins J, Mason S, Lindwall C, Little E, Sarkar A, Smith AG, Moldrich RX, Boyle GM, Tole S, Gronostajski RM, Bailey TL, Richards LJ. (2010). NFIA controls telencephalic progenitor cell differentiation through repression of the Notch effector Hes1. J Neurosci. 30:9127-39.
Portales-Casamar E, Thongjuea S, Kwon AT, Arenillas D, Zhao X, Valen E, Yusuf D, Lenhard B, Wasserman WW, Sandelin A. (2010). JASPAR 2010: the greatly expanded open-access database of transcription factor binding profiles. Nucleic Acids Res. 38:D105-10.
Potier MC, Rivals I, Mercier G, Ettwiller L, Moldrich RX, Laffaire J, Personnaz L, Rossier J, Dauphinot L. (2006). Transcriptional disruptions in Down syndrome: a case study in the Ts1Cje mouse cerebellum during post-natal development. J Neurochem. 97 Suppl 1:104-9.
Powell LM, Jarman AP. (2008). Context dependence of proneural bHLH proteins. Curr Opin Genet Dev. 18:411-7.

Prada I, Marchaland J, Podini P, Magrassi L, D'Alessandro R, Bezzi P, Meldolesi J. (2011). REST/NRSF governs the expression of dense-core vesicle gliosecretion in astrocytes. J Cell Biol. 193:537-49.

Pritchard M, Reeves RH, Dierssen M, Patterson D, Gardiner KJ. (2008). Down syndrome and the genes of human chromosome 21: current knowledge and future potentials. Report on the Expert workshop on the biology of chromosome 21 genes: towards gene-phenotype correlations in Down syndrome. Cytogenet Genome Res. 121:67-77.

Puelles L, Kuwana E, Puelles E, Bulfone A, Shimamura K, Keleher J, Smiga S, Rubenstein JL. (2000). Pallial and subpallial derivatives in the embryonic chick and mouse telencephalon, traced by the expression of the genes Dlx-2, Emx-1, Nkx-2.1, Pax-6, and Tbr-1. J Comp Neurol. 424:409-38.

Qi Y, Cai J, Wu Y, Wu R, Lee J, Fu H, Rao M, Sussel L, Rubenstein J, Qiu M. (2001). Control of oligodendrocyte differentiation by the Nkx2.2 homeodomain transcription factor. Development. 128:2723-33.

Qian X, Shen Q, Goderie SK, He W, Capela A, Davis AA, Temple S. (2000). Timing of CNS cell generation: a programmed sequence of neuron and glial cell production from isolated murine cortical stem cells. Neuron. 28:69-80.

Rachidi, M., and Lopes, C. (2007). Mental retardation in Down syndrome: from gene dosage imbalance to molecular and cellular mechanisms. Neurosci Res. 59, 349-369.

Rahmani Z, Blouin JL, Créau-Goldberg N, Watkins PC, Mattei JF, Poissonnier M, Prieur M, Chettouh Z, Nicole A, Aurias A, et al. (1990). Down syndrome critical region around D21S55 on proximal 21q22.3. Am J Med Genet Suppl. 7:98-103.

Rajasekharan S, Baker KA, Horn KE, Jarjour AA, Antel JP, Kennedy TE. (2009). Netrin 1 and Dcc regulate oligodendrocyte process branching and membrane extension via Fyn and RhoA. Development. 136:415-26.

Rakic P, Ayoub AE, Breunig JJ, Dominguez MH (2009). Decision by division: making cortical maps. Trends Neurosci. 32:291-301.

Rakic P. (1988). Specification of cerebral cortical areas. *Science* 241:170–76

Rakic P. (1995). A small step for the cell, a giant leap for mankind: a hypothesis of neocortical expansion during evolution. Trends Neurosci. 18:383-8.

Rakic P. (1971a). Guidance of neurons migrating to the fetal monkey neocortex. Brain Res. 33:471-6.

Rakic P. (1971b). Neuron-glia relationship during granule cell migration in developing cerebellar cortex. A Golgi and electronmicroscopic study in Macacus Rhesus. J Comp Neurol. 141:283-312.

Rakic P. (1974). Neurons in rhesus monkey visual cortex: systematic relation between time of origin and eventual disposition. Science. 183:425-7.

Rakic, P. (1978). Neuronal migration and contact guidance in the primate telencephalon. Postgrad. Med. J. 1:25–40.

Raponi E, Agenes F, Delphin C, Assard N, Baudier J, Legraverend C, Deloulme JC. (2007). S100B expression defines a state in which GFAP-expressing cells lose their neural stem cell potential and acquire a more mature developmental stage. Glia. 55:165-77.

Rasin MR, Gazula VR, Breunig JJ, Kwan KY, Johnson MB, et al. (2007). Numb and

Numbl are required for maintenance of cadherin-based adhesion and polarity of neural progenitors. *Nat. Neurosci.* 10:819–27

Rasin MR, Gazula VR, Breunig JJ, Kwan KY, Johnson MB, Liu-Chen S, Li HS, Jan LY, Jan YN, Rakic P, Sestan N. (2007). Numb and Numbl are required for maintenance of cadherin-based adhesion and polarity of neural progenitors. Nat Neurosci. 10:819-27.

Reeves RH, Irving NG, Moran TH, Wohn A, Kitt C, Sisodia SS, Schmidt C, Bronson

RT, Davisson MT. (1995). A mouse model for Down syndrome exhibits learning and behaviour deficits. Nat Genet. 11:177-84.

Retzius G. (1894). Die Neuroglia des Gehirns beim Menschen und bei S¨augetieren. *Biol. Unters.* 6:1–24

Richardson WD, Kessaris N, Pringle N. (2006). Oligodendrocyte wars. Nat Rev Neurosci. 7:11-8.

Richter-Landsberg C, Heinrich M. (1995). S-100 immunoreactivity in rat brain glial cultures is associated with both astrocytes and oligodendrocytes. J Neurosci Res. 42:657-65.

Rickmann M, Wolff JR. (1995). S100 immunoreactivity in a subpopulation of oligodendrocytes and Ranvier's nodes of adult rat brain. Neurosci Lett. 186:13-6.

Riethoven JJ. (2010). Regulatory regions in DNA: promoters, enhancers, silencers, and insulators. Methods Mol Biol. 674:33-42.

Rivers LE, Young KM, Rizzi M, Jamen F, Psachoulia K, Wade A, Kessaris N, Richardson WD. (2008). PDGFRA/NG2 glia generate myelinating oligodendrocytes and piriform projection neurons in adult mice. Nat. Neurosci. 11:1392–401

Ronan A, Fagan K, Christie L, Conroy J, Nowak NJ, Turner G. (2007). Familial 4.3 Mb duplication of 21q22 sheds new light on the Down syndrome critical region. J Med Genet. 44:448-51.

Ross SE, Greenberg ME, Stiles CD (2003). Basic helix–loop–helix factors in cortical development. Neuron. 39:13-25.

Roubertoux PL, Carlier M. (2010). Mouse models of cognitive disabilities in trisomy 21 (Down syndrome). Am J Med Genet C Semin Med Genet. 154C:400-16.

Rowitch DH, Kriegstein AR. (2010). Developmental genetics of vertebrate glial-cell specification. Nature. 468:214-22.

Sagane K, Hayakawa K, Kai J, Hirohashi T, Takahashi E, Miyamoto N, Ino M, Oki T, Yamazaki K, Nagasu T. (2005). Ataxia and peripheral nerve hypomyelination in ADAM22-deficient mice. BMC Neurosci. 6:33.

Sago H, Carlson EJ, Smith DJ, Kilbridge J, Rubin EM, Mobley WC, Epstein CJ, Huang TT. (1998). Ts1Cje, a partial trisomy 16 mouse model for Down syndrome, exhibits learning and behavioral abnormalities. Proc Natl Acad Sci U S A. 95:6256-61.

Saher G, Brügger B, Lappe-Siefke C, Möbius W, Tozawa R, Wehr MC, Wieland F, Ishibashi S, Nave KA. (2005). High cholesterol level is essential for myelin membrane growth. Nat Neurosci. 8:468-75.

Salichs E, Ledda A, Mularoni L, Albà MM, de la Luna S. (2009). Genome-wide analysis of histidine repeats reveals their role in the localization of human proteins to the nuclear speckles compartment. PLoS Genet. 5:e1000397.

Samanta J, Kessler JA. (2004). Interactions between ID and OLIG proteins mediate the inhibitory effects of BMP4 on oligodendroglial differentiation. Development. 131:4131-42.

Sato D, Kawara H, Shimokawa O, Harada N, Tonoki H, Takahashi N, Imai Y, Kimura H, Matsumoto N, Ariga T, Niikawa N, Yoshiura K. (2008). A girl with Down syndrome and partial trisomy for 21pter-q22.13: a clue to narrow the Down syndrome critical region. Am J Med Genet A. 146A:124-7.

Sauvageot CM, Stiles CD. (2002). Molecular mechanisms controlling cortical gliogenesis. Curr Opin Neurobiol. 12:244-9.

Saxel H, Kel AE, Wingender E. (2006). TRANSFAC and its module TRANSCompel: transcriptional gene regulation in eukaryotes. Nucleic Acids Res. 34:D108-10.

Scales TM, Lin S, Kraus M, Goold RG, Gordon-Weeks PR. (2009). Nonprimed and DYRK1A-primed GSK3 beta-phosphorylation sites on MAP1B regulate microtubule dynamics in growing axons. J Cell Sci. 122:2424-35.

Schmechel DE, Rakic P. (1979). A Golgi study of radial glial cells in developing monkey telencephalon: morphogenesis and transformation into astrocytes. *Anat. Embryol.* 156:115–52

Schmechel, D. E. & Rakic, P. (1979). Arrested proliferation of radial glial cells during midgestation in rhesus monkey. Nature 277, 303–305.

Schmid, R.S., McGrath, B., Berechid, B.E., Boyles, B., Marchionni, M., Sestan, N., and Anton, E.S. (2003). Neuregulin 1-erbB2 signaling is required for the establishment of radial glia and their transformation into astrocytes in cerebral cortex. Proc. Natl. Acad. Sci. USA 100, 4251–4256.

Schoenherr CJ, Anderson DJ. (1995). The neuron-restrictive silencer factor (NRSF): a coordinate repressor of multiple neuron-specific genes. Science. 267:1360-3.

Schulz RA, Yutzey KE. (2004). Calcineurin signaling and NFAT activation in cardiovascular and skeletal muscle development. Dev Biol. 266:1-16.

Seifert A, Allan LA, Clarke PR. (2008). DYRK1A phosphorylates caspase 9 at an inhibitory site and is potently inhibited in human cells by harmine. FEBS J. 275:6268-80.

Seifert A, Clarke PR. (2009). p38alpha- and DYRK1A-dependent phosphorylation of caspase-9 at an inhibitory site in response to hyperosmotic stress. Cell Signal. 21:1626-33.

Selkoe D, Kopan R. (2003). Notch and Presenilin: regulated intramembrane proteolysis links development and degeneration. Annu Rev Neurosci. 26:565-97.

Sestan N, Artavanis-Tsakonas S, Rakic P. (1999). Contact-dependent inhibition of cortical neurite growth mediated by notch signaling. Science. 286:741-6.

Seth KA, Majzoub JA. (2001). Repressor element silencing transcription factor/neuron-restrictive silencing factor (REST/NRSF) can act as an enhancer as well as a repressor of corticotropin-releasing hormone gene transcription. J Biol Chem. 276:13917-23.

Setoguchi H, Namihira M, Kohyama J, Asano H, Sanosaka T, Nakashima K. (2006). Methyl-CpG binding proteins are involved in restricting differentiation plasticity in neurons. J Neurosci Res. 84:969-79.

Shen Q, Zhong W, Jan YN, Temple S. (2002). Asymmetric Numb distribution is critical for asymmetric cell division of mouse cerebral cortical stem cells and neuroblasts. Development. 129:4843-53.

Shen S, Casaccia-Bonnefil P. (2008). Post-translational modifications of nucleosomal histones in oligodendrocyte lineage cells in development and disease. J Mol Neurosci. 35:13-22.

Sherman DL, Brophy PJ. (2005). Mechanisms of axon ensheathment and myelin growth. Nat Rev Neurosci. 6:683-90.

Shield JP. (2000). Neonatal diabetes: new insights into aetiology and implications. Horm Res. 53 Suppl 1:7-11.

Shimizu T, Kagawa T, Wada T, Muroyama Y, Takada S, Ikenaka K. (2005). Wnt signaling controls the timing of oligodendrocyte development in the spinal cord. Dev Biol. 282:397-410.

Shimojo H, Ohtsuka T, Kageyama R. (2008). Oscillations in notch signaling regulate maintenance of neural progenitors. Neuron. 58:52-64.

Shimojo M, Paquette AJ, Anderson DJ, Hersh LB. (1999). Protein kinase A regulates cholinergic gene expression in PC12 cells: REST4 silences the silencing activity of neuron-restrictive silencer factor/REST. Mol Cell Biol. 19:6788-95.

Shimokawa T, Tostar U, Lauth M, Palaniswamy R, Kasper M, Toftgård R, Zaphiropoulos PG. (2008). Novel human glioma-associated oncogene 1 (GLI1) splice variants reveal distinct mechanisms in the terminal transduction of the hedgehog signal. J Biol Chem. 283:14345-54.

Shimozaki K, Namihira M, Nakashima K, Taga T. (2005). Stage- and site-specific DNA demethylation during neural cell development from embryonic stem cells. J Neurochem. 93:432-9.

Shirasaki R, Pfaff SL. (2002). Transcriptional codes and the control of neuronal identity. Annu Rev Neurosci. 25:251-81.

Simons M, Trajkovic K. (2006). Neuron-glia communication in the control of oligodendrocyte function and myelin biogenesis. J Cell Sci. 119:4381-9.

Smith DJ, Zhu Y, Zhang J, Cheng JF, Rubin EM. (1995). Construction of a panel of transgenic mice containing a contiguous 2-Mb set of YAC/P1 clones from human chromosome 21q22.2. Genomics. 7:425-34

Smyth GK. (2004). Linear models and empirical bayes methods for assessing differential expression in microarray experiments. Statistical applications in genetics and molecular biology, 3.

Solecki DJ, Liu XL, Tomoda T, Fang Y, Hatten ME. (2001). Activated Notch2 signaling inhibits differentiation of cerebellar granule neuron precursors by maintaining proliferation. Neuron. 30:557-68.

Sorci G, Agneletti AL, Bianchi R, Donato R. (1998). Association of S100B with intermediate filaments and microtubules in glial cells. Biochim Biophys Acta. 1998 1448:277-89.

Sorci G, Agneletti AL, Donato R. (2000). Effects of S100A1 and S100B on microtubule stability. An in vitro study using triton-cytoskeletons from astrocyte and myoblast cell lines. Neuroscience. 99:773-83.

Sorkin A, von Zastrow M. (2009). Endocytosis and signalling: intertwining molecular

networks. Nat Rev Mol Cell Biol. 10:609-22.
Stolt CC, Lommes P, Sock E, Chaboissier MC, Schedl A, Wegner M. (2003). The Sox9 transcription factor determines glial fate choice in the developing spinal cord. Genes Dev. 17:1677-89.
Stolt CC, Schlierf A, Lommes P, Hillgärtner S, Werner T, Kosian T, Sock E, Kessaris N, Richardson WD, Lefebvre V, Wegner M. (2006). SoxD proteins influence multiple stages of oligodendrocyte development and modulate SoxE protein function. Dev Cell. 11:697-709.
Stolt CC, Wegner M. (2010). SoxE function in vertebrate nervous system development. Int J Biochem Cell Biol. 42:437-40.
Sun Y, Nadal-Vicens M, Misono S, Lin MZ, Zubiaga A, Hua X, Fan G, Greenberg ME. (2001). Neurogenin promotes neurogenesis and inhibits glial differentiation by independent mechanisms. Cell. 104:365-76.
Sun Y, Goderie SK, Temple S. (2005a). Asymmetric distribution of EGFR receptor during mitosis generates diverse CNS progenitor cells. Neuron. 45:873-86.
Sun YM, Greenway DJ, Johnson R, Street M, Belyaev ND, Deuchars J, Bee T, Wilde S, Buckley NJ. (2005b). Distinct profiles of REST interactions with its target genes at different stages of neuronal development. Mol Biol Cell. 16:5630-8. Erratum in: Mol Biol Cell. (2006).17:1494 .
Takahashi T, Goto T, Miyama S, Nowakowski RS, Caviness VS Jr (1999). Sequence of neuron origin and neocortical laminar fate: relation to cell cycle of origin in the developing murine cerebral wall. J Neurosci.19:10357-10371.
Takizawa T, Nakashima K, Namihira M, Ochiai W, Uemura A, Yanagisawa M, Fujita N, Nakao M, Taga T. (2001). DNA methylation is a critical cell-intrinsic determinant of astrocyte differentiation in the fetal brain. Dev Cell. 1:749-58.
Tamamaki N, Nakamura K, Okamoto K, Kaneko T. (2001). Radial glia is a progenitor of neocortical neurons in the developing cerebral cortex. Neurosci Res. 41:51-60.
Tang XM, Beesley JS, Grinspan JB, Seth P, Kamholz J, Cambi F. (1999). Cell cycle arrest induced by ectopic expression of p27 is not sufficient to promote oligodendrocyte differentiation. J Cell Biochem. 76:270-9.
Tarabykin V, Stoykova A, Usman N, Gruss P. (2001). Cortical upper layer neurons derive from the subventricular zone as indicated by Svet1 gene expression. Development. 128:1983–1993.
Taveggia C, Feltri ML, Wrabetz L. (2010). Signals to promote myelin formation and repair. Nat Rev Neurol. 6:276-87.
Taveggia C, Thaker P, Petrylak A, Caporaso GL, Toews A, Falls DL, Einheber S, Salzer JL. (2008). Type III neuregulin-1 promotes oligodendrocyte myelination. Glia. 56:284-93.
Tejedor F, Zhu XR, Kaltenbach E, Ackermann A, Baumann A, Canal I, Heisenberg M, Fischbach KF, Pongs O. (1995). minibrain: a new protein kinase family involved in postembryonic neurogenesis in Drosophila. Neuron. 14:287-301.
Tejedor FJ, Hämmerle B. (2011). MNB/DYRK1A as a multiple regulator of neuronal development. FEBS J. 278:223-35.
Tikoo R, Osterhout DJ, Casaccia-Bonnefil P, Seth P, Koff A, Chao MV. (1998). Ectopic expression of p27Kip1 in oligodendrocyte progenitor cells results in cell-

cycle growth arrest. J Neurobiol. 36:431-40.
Vallstedt A, Klos JM, Ericson J. (2005). Multiple dorsoventral origins of oligodendrocyte generation in the spinal cord and hindbrain. Neuron. 45:55-67.
Van Bon BW, Hoischen A, Hehir-Kwa J, de Brouwer AP, Ruivenkamp C, Gijsbers AC, Marcelis CL, de Leeuw N, Veltman JA, Brunner HG, de Vries BB. (2011). Intragenic deletion in DYRK1A leads to mental retardation and primary microcephaly. Clin Genet. 79:296-9.
Vaquero A. (2009). The conserved role of sirtuins in chromatin regulation. Int J Dev Biol. 53:303-22.
Vives V, Alonso G, Solal AC, Joubert D, Legraverend C. (2003). Visualization of S100B-positive neurons and glia in the central nervous system of EGFP transgenic mice. J Comp Neurol. 457:404-19.
Voigt, T. (1989). Development of glial cells in the cerebral wall of ferrets: Direct tracing of their transformation from radialglia into astrocytes.J. Comp. Neurol. 289:74 – 88.
Vouyiouklis DA, Brophy PJ. (1993) Microtubule-associated protein MAP1B expression precedes the morphological differentiation of oligodendrocytes. J Neurosci Res. 35:257-67.
Voyvodic JT. (1989). Target size regulates calibre and myelination of sympathetic axons. Nature. 342:430-3.
Wake H, Lee PR, Fields RD. (2011). Control of local protein synthesis and initial events in myelination by action potentials. Science. 333:1647-51.
Wall DS, Mears AJ, McNeill B, Mazerolle C, Thurig S, Wang Y, Kageyama R, Wallace VA. (2009). Progenitor cell proliferation in the retina is dependent on Notch-independent Sonic hedgehog/Hes1 activity. J Cell Biol. 184:101-12.
Walton EL, Francastel C, Velasco G. (2011). Maintenance of DNA methylation: Dnmt3b joins the dance. Epigenetics. 6:11.
Wang DD, Bordey A. (2008). The astrocyte odyssey. Prog Neurobiol. 86:342-67.
Wang S, Sdrulla AD, DiSibio G, Bush G, Nofziger D, Hicks C, Weinmaster G, Barres BA. (1998). Notch receptor activation inhibits oligodendrocyte differentiation. Neuron. 21:63-75.
Wang S, Sdrulla AD, diSibio G, Bush G, Nofziger D, Hicks C, Weinmaster G, Barres BA. (1998). Notch receptor activation inhibits oligodendrocyte differentiation. Neuron. 21:63-75.
Warren N, Caric D, Pratt T, Clausen JA, Asavaritikrai P, Mason JO, Hill RE, Price DJ (1999). The transcription factor, Pax6, is required for cell proliferation and differentiation in the developing cerebral cortex. Cereb Cortex. 9:627-635.
Watt F, Molloy PL. (1988). Cytosine methylation prevents binding to DNA of a HeLa cell transcription factor required for optimal expression of the adenovirus major late promoter. Genes Dev. 2:1136-43.
Wegiel J, Dowjat K, Kaczmarski W, Kuchna I, Nowicki K, Frackowiak J, Mazur Kolecka B, Wegiel J, Silverman WP, Reisberg B, Deleon M, Wisniewski T, Gong CX, Liu F, Adayev T, Chen-Hwang MC, Hwang YW. (2008). The role of overexpressed DYRK1A protein in the early onset of neurofibrillary degeneration in Down syndrome. Acta Neuropathol. 116:391-407.
Wegiel J, Gong CX, Hwang YW. (2011). The role of DYRK1A in neurodegenerative

diseases. FEBS J. 278:236-45.
Wegiel J, Kuchna I, Nowicki K, Frackowiak J, Dowjat K, Silverman WP, Reisberg B, DeLeon M, Wisniewski T, Adayev T, Chen-Hwang MC, Hwang YW. (2004). Cell type- and brain structure-specific patterns of distribution of minibrain kinase in human brain. Brain Res. 1010:69-80.
Wei Q, Miskimins WK, Miskimins R. (2005). Stage-specific expression of myelin basic protein in oligodendrocytes involves Nkx2.2-mediated repression that is relieved by the Sp1 transcription factor. J Biol Chem. 280:16284-94.
Wichterle H, Turnbull DH, Nery S, Fishell G, Alvarez-Buylla A. (2001). In utero fate mapping reveals distinct migratory pathways and fates of neurons born in the mammalian basal forebrain. Development. 128:3759-71.
Wiechmann S, Czajkowska H, de Graaf K, Grötzinger J, Joost HG, Becker W. (2003). Unusual function of the activation loop in the protein kinase DYRK1A. Bioche Biophys Res Commun. 302:403-8.
Willem M, Garratt AN, Novak B, Citron M, Kaufmann S, Rittger A, DeStrooper B, Saftig P, Birchmeier C, Haass C. (2006). Control of peripheral nerve myelination by the beta-secretase BACE1. Science. 314:664-6.
Willems M, Geneviève D, Borck G, Baumann C, Baujat G, Bieth E, Edery P, Farra C, Gerard M, Héron D, Leheup B, Le Merrer M, Lyonnet S, Martin-Coignard D, Mathieu M, Thauvin-Robinet C, Verloes A, Colleaux L, Munnich A, Cormier-Daire V. (2010). Molecular analysis of pericentrin gene (PCNT) in a series of 24 Seckel/microcephalic osteodysplastic primordial dwarfism type II (MOPD II) families. J Med Genet. 47:797-802.
Wiseman FK, Alford KA, Tybulewicz VL, Fisher EM. (2009). Down syndrome recent progress and future prospects. Hum Mol Genet. 18:R75-83.
Woodhoo A, Alonso MB, Droggiti A, Turmaine M, D'Antonio M, Parkinson DB, Wilton DK, Al-Shawi R, Simons P, Shen J, Guillemot F, Radtke F, Meijer D, Feltri ML, Wrabetz L, Mirsky R, Jessen KR. (2009). Notch controls embryonic Schwann cell differentiation, postnatal myelination and adult plasticity. Nat Neurosci. 12:839-47.
Wu HY, Dawson MR, Reynolds R, Hardy RJ. (2001). Expression of QKI proteins and MAP1B identifies actively myelinating oligodendrocytes in adult rat brain. Mol Cell Neurosci. 17:292-302.
Wu SX, Goebbels S, Nakamura K, Nakamura K, Kometani K, Minato N, Kaneko T, Nave KA, Tamamaki N. (2005). Pyramidal neurons of upper cortical layers generated by NEX-positive progenitor cells in the subventricular zone. Proc Natl Acad Sci U S A. 102:17172-7.
Xiong Z, O'Hanlon D, Becker LE, Roder J, MacDonald JF, Marks A. (2000). Enhanced calcium transients in glial cells in neonatal cerebellar cultures derived from S100B null mice. Exp Cell Res. 257:281-9.
Xu X, Lee J, Stern DF. (2004). Microcephalin is a DNA damage response protein involved in regulation of CHK1 and BRCA1. J Biol Chem. 279:34091-4.
Yabut O, Domogauer J, D'Arcangelo G. (2010). Dyrk1A overexpression inhibits proliferation and induces premature neuronal differentiation of neural progenitor cells. J Neurosci. 30:4004-14.
Yang EJ, Ahn YS, Chung KC. (2001). Protein kinase Dyrk1 activates cAMP

response element-binding protein during neuronal differentiation in hippocampal progenitor cells. J Biol Chem. 276:39819-24.

Ye F, Chen Y, Hoang T, Montgomery RL, Zhao XH, Bu H, Hu T, Taketo MM, van Es JH, Clevers H, Hsieh J, Bassel-Duby R, Olson EN, Lu QR. (2009). HDAC1 and HDAC2 regulate oligodendrocyte differentiation by disrupting the beta-catenin-TCF interaction. Nat Neurosci. 12:829-38.

Yoon K, Gaiano N. (2005). Notch signaling in the mammalian central nervous system: insights from mouse mutants. Nat Neurosci. 8:709-15. Erratum in: Nat Neurosci. (2005). 8:1411.

Yoon K, Nery S, Rutlin ML, Radtke F, Fishell G, Gaiano N. (2004). Fibroblast growth factor receptor signaling promotes radial glial identity and interacts with Notch1 signaling in telencephalic progenitors. J Neurosci. 24:9497-9506.

Yu H, Pardoll D, Jove R. (2009). STATs in cancer inflammation and immunity: a leading role for STAT3. Nat Rev Cancer. 9:798-809.

Yu TW, Mochida GH, Tischfield DJ, Sgaier SK, Flores-Sarnat L, Sergi CM, Topçu M, McDonald MT, Barry BJ, Felie JM, Sunu C, Dobyns WB, Folkerth RD, Barkovich AJ, Walsh CA. (2010). Mutations in WDR62, encoding a centrosome associated protein, cause microcephaly with simplified gyri and abnormal cortical architecture. Nat Genet. 42:1015-20.

Yung SY, Gokhan S, Jurcsak J, Molero AE, Abrajano JJ, Mehler MF. (2002). Differential modulation of BMP signaling promotes the elaboration of cerebral cortical GABAergic neurons or oligodendrocytes from a common sonic hedgehog-responsive ventral forebrain progenitor species. Proc Natl Acad Sci U S A. 99:16273-8.

Zembrzycki A, Griesel G, Stoykova A, Mansouri A (2007). Genetic interplay between the transcription factors Sp8 and Emx2 in the patterning of the forebrain. Neural Dev. 2:8.

Zhong W, Jiang MM, Schonemann MD, Meneses JJ, Pedersen RA, Jan LY, Jan YN (2000). Mouse numb is an essential gene involved in cortical neurogenesis. Proc Natl Acad Sci USA. 97:6844-6849

Zhong WM, Feder JN, Jiang MM, Jan LY, Jan YN. (1996). Asymmetric localization of a mammalian numb homolog during mouse cortical neurogenesis. *Neuron* 17:43–53

Zhong X, Liu L, Zhao A, Pfeifer GP, Xu X. (2005). The abnormal spindle-like, microcephaly-associated (ASPM) gene encodes a centrosomal protein. Cell Cycle. 4:1227-9.

Zhou CJ, Borello U, Rubenstein JL, Pleasure SJ. (2006). Neuronal production and precursor proliferation defects in the neocortex of mice with loss of function in the canonical Wnt signaling pathway. Neuroscience. 142:1119-31.

Acknowledgments

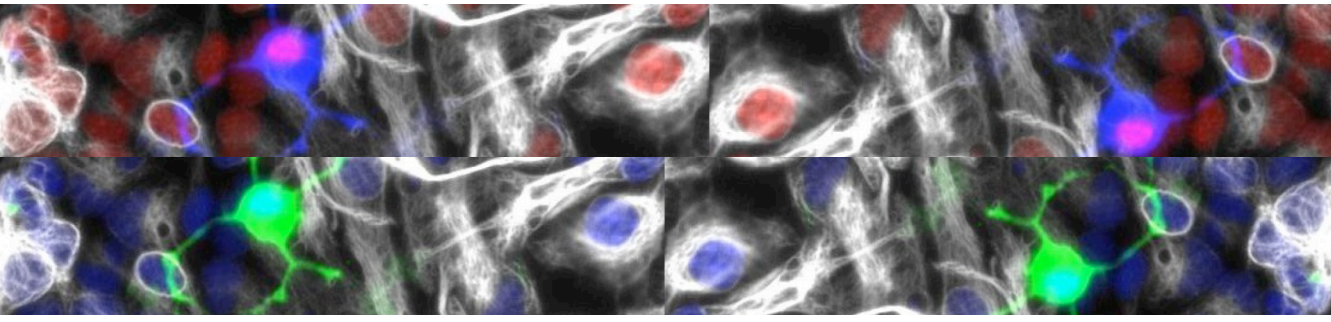

Quien me lo decía que acabaría escribiendo este apartado en un aeropuerto, no podía esperarme nada más simbólico..

Gracias a todos los que me han acompañado hasta aquí. Mariona, increíble, lo he conseguido sin ir a yoga como me decías! Gracias por haber creído en mi en estos años, por haberme enseñado desde la independencia en el trabajo hasta la santa calidad de la paciencia, y sobre todo por haber sido una jefa honesta y humana. Mariajo, eres una guía en el trabajo y en la vida, por tu actitud positiva y por tener valores sin tener dogmas. Cuando de pequeña me preguntaban a quien querría parecer decía Rita Levi Montalcini, hoy diría MJ y si dudar! Soni, me encanta tu energía fresca y tu practicidad, eres un pilar del equipo. Silvia, gracias por tus consejos farmacológicos, y Juan por aportar un cromosoma Y al lab..ya veras que es muy bonita esta familia! Como olvidar nuestro pasado. Ari, has sido una buena maestra y una buena compañera. Si me hubieras tocado de amigo invisible te hubiera regalado un timer de minutos libres, para pasar más momentos juntas Erikita, echo de menos tu infinita paciencia y tu cariño en mis días negros, gracias por haber sido siempre tan presente. SDL lab, nuestra dulce mitad!…Ali, has estado allí cuando lloraba por un western, y sobre todo cuando lo hacía por tener muletas y no tener piso! Chiari, sei la persona che piú mi ha messo alla prova nella vita. Con nessuno sono riuscita ad essere cosí vicina e cosí lontana. Mi hai aiutata a conoscermi… forza, che siamo nel buon cammino! Gracias a Susana, por estos debates científicos tan buenos, por darnos tantos estímulos, y por estos vinitos en el barrio.. eres increíble! Y Esteban, Julia, Uli, Silvi, Salix, Sergi…habéis contribuido a crear un ambiente de trabajo sereno y estimulante, sois un sol.. Me olvido alguien? Kriszty como podría? Te siento cada vez mas cercana y me encanta pensar que sigua

así!...nuestro grupito de ladies es un punto de referencia muy importante. Monica, vaya suerte fue coincidir en Berlín, y Viki tu energía es única, me encantas.

Thanks to all my collaborators, to Cedric Notredame, for your points of view; to Ionas Erb, the bioinformatician and the best teacher of tango of my life, thanks for decipher my ideas better that I do; a todo el lab de Mario Fraga en Oviedo, por haberme abierto al mundo de la epigenética y haberme hecho sentir en casa; a Mireia Moreno del lab de Isabel Fariñas, por haberme trasmitido todo lo imaginable sobre las neuroesferas y por el amor con que lo hacía; a Eduardo Fernández por los análisis de TEM; a Fatima Núñez del servicio de microarray del Vall d'Hebron; a M. Carme Ruiz, Israel Ortega and Alex Sánchez de la Universidad de Barcelona, por el análisis de los microarray; to the components of my thesis committe (Cristina Pujades, Eulalia Martí y James Sharpe) for the positive feedbacks I have received from you; y finalmente a los ratoncitos, que nos dan mucho no lo olvidemos..

Agradezco mi actitud de meterme siempre nuevos obstáculos, porque me ha hecho encontrar personas increíbles que en estos años han alimentado el aspecto humano de mi vida. El curso de Inglés me ha regalado Mariana, Oscar, Roser, Gari y Susana, con que acabamos compartiendo muchos mas bailes, ideologías y marisco que idioma anglosajón! Nunca lo olvidaré. En un curso de cocina me apareció Tommaso. Vaya suerte encontrarte, y tener tantas visiones y tantas chinas en común! Con el baile africano Agostino hizo su aparición en mi vida y con el Paco, las hermanas Trapp, los Oh-Peta! Me encanta este grupito de músicos-artistas que hace parte de mi vida y mantiene vivo mi lado no científico! E ovviamente in tutto il gruppetto, Vale, Pacca, Mirko avete un ruolo speciale. Siete il ponte tra il mio presente e tutte le fasi del

mio passato. Sapere che ci siete e mi conocete è una sicurezza! Jara, Alessa, Luci, Jelena, Xavi, Anna, me encanta soñar con vosotros y imaginar un futuro sostenible… lo conseguiremos! Luego, por tocar percusiones, me apareció la BandSambant y con ella emociones, crisis de la vida y una nueva familia catalana! Sonia, me reí cuando me dijiste que la banda me cambiaria la vida…si que tenías razón, y me encanta! Y finalmente, surgió BIOcomuniCA'T y todo un mundo nuevo, gracias chicos por compartir este sueño!

Casita Bobila...cuanta historia con todos lo que han aportado su experiencia de vida en este piso. El equipo del principio es inolvidable: el pequeño Raoni que acogí en muletas, la Fra y Martin. Fra, sai che se sono qua é in gran parte grazie a te. Sei stata un appoggio unico. Ho impresso come fosse ieri il nostro pianto di fronte al mare. Senza parlare ma in sintonia completa. Ti volgio bene da morire! Martino, pues no se, sin ti no se que haría, en serio…y mira que no comunicamos bien…imaginas si lo hiciéramos! Gracias por estar, siempre.

Isa me encanta ir al grano de todo contigo, quiero tenerte en el barrio otra vez! Guille.. si no me recogías de la calle que hubiera sido de mi?? Tu y toda tu familia habéis contribuido un montón a mi sobrevivencia al principio de esta aventura, nunca lo olvidaré! La Vane y la Marisa, los francofonos tan fantásticos, la Saccinto e Tommaso..bueno, todos me habéis dado mucho chicos! Y los granadinos, chicos no olvideis que me habéis atrapado para siempre en la península ibérica! Debo, quien diría que acaba mi tesis contigo al lado! Que bonito ha sido!

Se sono arriva qua lo devo a due cose: i regaz e Pesaro. I regaz perché hanno alimentato le mie inquietudini scientifiche e umane e mi hanno spinta oltre le colonne d'Ercole di via Zamboni. Sono stati anni

indimenticabili tra scienza, amori, spritz, Caterina insulina e Simone glucagone..incredible. Pesaro perchè mi ha permesso sperimentare con la consapevolezza che qualcuno mi voleva bene sempre e comunque. É fondamentale sapere che ogni Natale ci rivediamo ed è sempre come non essere mai partita: il panettone della Noe, Villa Fastigi on fire, Diota e la sua alta cucina, la Maci e la salsiccia, la Mara e….Mara? dove sei?, il cotto di Fiori, la soffitta di Maurino, le labbra di Checcone, la garanzia che Goffi c'é, Pivi che è capace di farmi sentire che mi é sempre vicino, e *dulcis in fundo* la Vali e la Sere. Vali, sei un fiume in piena, mi piaci, sto bene con te, mi sento capita e ti stimo un bel pó. Voglio che sia sempre cosí! Sere, sei tante cose per me che non so dove classificarti. Grazie per integrarmi sempre nelle vostre vita e non farmi MAI sentire lontana e sola, e per avere avuto con me una pazienza unica. Sei importantísima. Luca, mi hai accompagnata per un bel pezzo di questo cammino e hai sempre accettato la mia vita. Mi hai insegnato molto, non lo dimentico.

Family, so che nonostante tutto, il giorno che mi vedrete discutere questa tesi sarete orgogliosi di me. E io lo saró di voi per avermi dato questa voglia di guardare sempre oltre la siepe –che a volte ci fa soffrire ma non possiamo evitarlo- e per darmi amore attraverso la fiducia e la libertá. Sono stata fortunata ad avervi, vi voglio bene! Sissi, sei ancora l'unica persona al mondo che sarebbe capace si trascinarmi in qualunque posto. Alimenti la mia mente e il mio cuore con ogni tuo gesto, sei fondamentale. Nonna, a te che sei un esempio e una forza, a tutti i cugini e zii che hanno creduto in me,

A chi appartiene alla mia storia, lo zio Ameris,

A chi appartiene al mio futuro, il piccolo Goffi.

Elisa